UNIVERSITÀ
DI PAVIA

PhD IN BIOMEDICAL SCIENCES

DEPARTMENT OF BRAIN AND BEHAVIORAL SCIENCES

UNIT OF NEUROPHYSIOLOGY

CHONDRODYSPLASIAS CAUSED BY DEFECTS IN GLYCOSAMINOGLYCAN BIOSYNTHESIS: DEEP PHENOTYPING AND THERAPEUTIC APPROACHES USING *IN VITRO* AND *IN VIVO* MODELS

PhD Tutor: **Prof. Antonio Rossi**

PhD dissertation of

Chiara Gramegna Tota

a.a. 2021/2022

CONTENTS

LIST OF ABBREVIATIONS

ACG1B = Achondrogenesis type 1B

AO2 = Atelosteogenesis type 2

APS = adenosine 5'-phosphosulfate

BMP = bone morphogenetic protein

CANT1 = calcium activated nucleotidase 1

COMP = cartilage oligomeric matrix protein

CS = chondroitin sulfate

DBDQ1 = Desbuquois dysplasia type 1

DS = dermatan sulfate

DTD = Diastrophic dysplasia

DTDST = diastrophic dysplasia sulfate transporter

ECM = cartilage extracellular matrix

EGF = epidermal growth factor

FGF= fibroblast growth factor

GAG = glycosaminoglycan

Gal = galactose

GalNAc = N-acetylgalactosamine

GlcNAC = N-acetylglucosamine

GlcUA = glucuronic acid

HA = hyaluronic acid

HPLC = high performance/pressure liquid chromatography.

HS = heparan sulfate

IdoUA = iduronic acid

Ihh = Indian Hedgehog

KS = keratan sulfate

LP = link protein

MEM = minimal essential medium

NAC = N-acetyl-L-cisteine

PAPS = 3'-phosphoadenosine 5'-phosphosulfate

PAPSS = PAPS synthase

PAPST = PAPS transporter

PCR = polymerase chain reaction

PG = proteoglycan

PTHrP = parathyroid hormone-related protein

rMED = Recessive multiple epiphyseal dysplasia

SLC26A2 = solute carrier family 26 member 2

SLRP = small leucine-rich proteoglycan

Xyl = xylose

TEM = transmission electron microscopy

TGFβ = transforming growth factor β

VEGF = vascular endothelial growth factor

CHAPTER I

Cartilage and chondrodysplasias

1. The cartilage

Cartilage is a specialized form of connective tissue belonging to the supporting skeletal connective tissues. It is composed of a single type of specialized cells, called chondrocytes, embedded in an abundant extracellular matrix (ECM), composed of collagen and elastic fibres surrounded by an amorphous matrix rich in proteoglycans (PG) and hyaluronic acid (HA) [1].
The structural features of its matrix make cartilage ideal for a variety of mechanical and protective roles, both during the different stages of development and the maintenance of adult skeleton. For example, in the respiratory system, ears and nose, cartilage provides support for softer tissues, while in the joints, because of its flexibility and lubricated surface, it provides a wear-resistant surface that facilitates bone movements. Finally, it is involved in the development and growth of long bones, both during foetal life and after birth [2].
Differently from the other connective tissues, cartilage lacks vascular network and innervation; therefore, chondrocytes take oxygen and nutrients for their maintenance by diffusion from the perichondrium. This layer of dense vascularized and innervated connective tissue surrounds cartilage, forming an interface between it and other tissues. The perichondrium is formed during chondrogenesis, through differentiation of the most superficial cells that form the mesenchymal cell cluster providing chondrocytes or osteoblasts. The perichondrium is not present in the articular cartilage and it plays a role in cartilage growth and repair.
The avascular character, low cellular density and reduced proliferative activity of chondrocytes makes cartilage unable to regenerate upon injury or degeneration [2].
There are three types of cartilage based on the composition of the extracellular matrix and in particular on the relative abundance of amorphous substance and fibres: hyaline cartilage, fibrocartilage and elastic cartilage.
Hyaline cartilage is the most abundant cartilage type in the body. It is characterized by a high amount of amorphous substance, rich in PG. Hyaline cartilage is a highly hydrated tissue (the water content can reach 80%) conferring resistance to pressure shocks. The fibrillar component of hyaline cartilage consist in collagen, mainly type II, associated with types XI and IX, all synthesized by chondrocytes. Chondrocytes are present alone or in isogenic groups within the extracellular matrix [1].
In the embryo, hyaline cartilage forms a large part of the skeleton, providing templates for bone that develop through the endochondral ossification process. In the adult, cartilage distribution

is more restricted and it is present in costal cartilages, tracheal rings, most of the laryngeal cartilages, bronchi, nose and in the joints with the function of mechanical support. In joints, where it is called articular cartilage, it plays an additional role providing a smooth, lubricated surface to facilitate pain-free joint movements [2, 3].

Articular cartilage is the highly specialized form of connective tissue composed of four zones differing for ECM composition, organization of collagen fibres, distribution and morphology of chondrocytes [3].

The superficial zone protects deeper layers from shear stresses. It is mainly composed of collagen fibres (primarily type II and IX collagen) with small diameters and densely packed parallel to the joint surface; the chondrocytes, surrounded by collagen, have flattened shape and are arranged parallel to the surface. The middle zone, connecting the adjacent zones anatomically and functionally, contains the highest PG concentration among all zones. It is characterized by round shaped chondrocytes at low density, and abundant type II collagen fibrils. Although the middle zone provides initial support during joint movement, the deep zone is primarily responsible for resisting compressive forces. These functional properties are due to collagen fibrils with a larger diameter and arranged perpendicularly to the articular surface. In the deep zone chondrocytes are elongated and typically arranged in short column, perpendicularly to the joint surface [4].

The viscoelastic property of articular cartilage determines resistance to loading and compressive forces. When load is applied, a tensile force is generated by collagen and proteoglycans on the cartilage surface causing fluid phase leaking from the ECM, generating a frictional drag [5]. When the compressive load is removed, fluid flows back into the tissue relieving the cartilage deformation. The low permeability of cartilage tissues prevents that fluid is quickly squeezed out of the matrix [3].

Fibrocartilage constitutes the intervertebral discs, temporomandibular joint discs, pubic symphysis and the meniscus of the knee. It represents an intermediate between dense fibrous connective tissue, such as tendon and ligaments, and hyaline cartilage, combining the tensile strength and durability of tendon with resistance to compression of cartilage. Its matrix is characterized of a small amount of amorphous substance, consisting of a variable amount of proteoglycans and numerous collagen fibres, arranged in parallel bundles, conferring the characteristic fibrous appearance to the matrix. The orientation depends on the mechanical stimuli acting on fibrocartilage, since the collagen bundles take a direction parallel to that of the applied forces. Chondrocytes, alone or in groups, are dispersed in the matrix and are arranged in short, parallel rows between collagen fibre bundles. Differently from hyaline

cartilage, rich in type II collagen, fibrocartilage is mainly composed of type I collagen, although the exact ratio can vary in tissues. For example, in the temporomandibular joint discs almost type I collagen is present, with trace of type II collagen, while in knee meniscus there is an heterogeneous distribution of type I and type II collagens [6]. Fibrocartilage forms from dense connective tissue rich in fibroblasts, some of which differentiate into chondrocytes. Thus, a mixture of chondrocytes and fibroblasts is characteristic of mature fibrocartilage. Unlike other types of cartilage, fibrocartilage lacks the perichondrium [1].

Elastic cartilage is mainly present in ear lobe, in epiglottis and in some area of the trachea. Its matrix is characterized by a small amount of proteoglycans and chondrocytes, but contains an abundant network of elastic fibres and type II collagen fibrils, accounting for the elastic properties. Thus, its main function is to support the shape and flexibility of organs [1].

1.1. The skeletal development

The skeleton provides structural support to the body, allowing controlled postures and movements and protects vital organs. In humans, bone formation begins during the embryonic period, between the sixth and seventh weeks of gestation, and continues until puberty [7]. Bone formation occurs through two different processes depending on the bone elements: the axial skeleton, the appendicular skeleton and the skull base form via endochondral ossification, while the flat bones of the skull, most of the cranial bones, and the clavicles via intramembranous ossification [8].

Both these processes begin from a mesenchymal tissue precursor, that directly differentiate in osteoblast forming new bone tissue in intramembranous ossification or differentiate in chondrocytes forming a cartilage template, which is then replaced by bone, in endochondral ossification [9].

There are some metabolic and morphogenetic differences between the two ossification processes, but similar expression patterns of genes involved in cell differentiation suggest strong similarities in the regulation of bone formation [10].

1.1.1. Intramembranous ossification

Intramembranous ossification begins with the aggregation of a large group of multipotent mesenchymal cells into dense homogeneous condensation. The ossification occurs when these cells, surrounded by a highly vascularized area of the embryonic connective tissue, start proliferate and migrate outward expanding these condensations, defining the early shape of the developing bone [10].

Some of the mesenchymal cells differentiate into capillaries, while others proliferate and differentiate in osteogenic cells that, in presence of specific regulatory signal, differentiate in specialized cells called osteoblasts. Osteoblasts group into clusters, forming ossification centres, surrounded by the periosteum and start synthesizing and secreting unmineralized matrix, called osteoid, which bind calcium. Thus, the matrix rapidly mineralize and calcify, forming bone trabeculae that entrap osteoblasts resulting in the differentiation of these cells to osteocytes, and blood vessels that will form the future hematopoietic bone marrow. Mesenchymal cells on the surface of the bone, forming the periosteum continue to differentiate into osteoblasts. As osteoblasts continue to secrete osteoid surrounding blood vessels, the trabeculae increase in size and number, forming a strong and well-organized cortical bone [9, 11].

1.1.2. Endochondral ossification

Endochondral ossification is a complex process in which new bone develops by replacing hyaline cartilage, which serves as a template. During foetal life, most of the skeleton is formed through endochondral ossification but this process continues until the end of the puberty, allowing long bones and body growth.

Bone formation begins, as in intramembranous ossification, with the condensation of mesenchymal cells, forming clusters of cells favoured by the expression of adhesion molecules. Differently from what occurs in intramembranous bone formation, these cells differentiate in chondrocytes. Chondrocytes start reproducing rapidly and secreting the characteristic cartilage matrix, rich in type II collagen and aggrecan, enlarging the cartilage template [12, 13]. The expression of these markers distinguishes differentiating chondrocytes from undifferentiated mesenchymal cells, at the periphery of the condensation centre, which will form the perichondrium.

Meanwhile inner cells change their phenotype from proliferating to hypertrophic chondrocytes becoming bigger and starting producing type X collagen [14].

Hypertrophic chondrocytes play an important regulatory role directing the differentiation of perichondrial cells in osteoblasts that start producing around the cartilaginous core a mineralized structure, called bone collar. This results in the apoptosis of the hypertrophic chondrocytes since nutrients can no longer reach them.

Hypertrophic chondrocytes also produce the vascular endothelial growth factor (VEGF) and other factors, inducing the invasion of blood vessels fundamental for attracting osteoclasts that will degrade the ECM surrounding cells, and bringing osteoblast progenitor and hematopoietic

cells from the perichondrium [15]. Thus, activated osteoclasts degrade cartilage extracellular matrix, while osteoblast progenitors differentiate in osteoblasts producing type I collagen and guiding cartilage mineralization. At the same time, hematopoietic cells, together with blood vessels form the bone marrow. All these events lead to the formation of the primary ossification centre, in the diaphyseal region of the bone, while in the perichondrium, osteoblasts create a bone collar around the cartilage template. While bone is replacing cartilage in the diaphysis, chondrocytes continues to proliferate at the extremities of the bone, increasing bone length. The primary ossification centre, expand during the foetal life replacing the cartilage template. After birth, in the epiphyseal region of the long bones the formation of the secondary ossification centre occurs entrapping a portion of cartilage between the two ossification centres, in the metaphyseal area. Therefore, the proliferative areas become this cartilage portion, called growth plates, that grows until the end of puberty providing longitudinal growth of long bones **(Figure 1.1)** [13, 14].

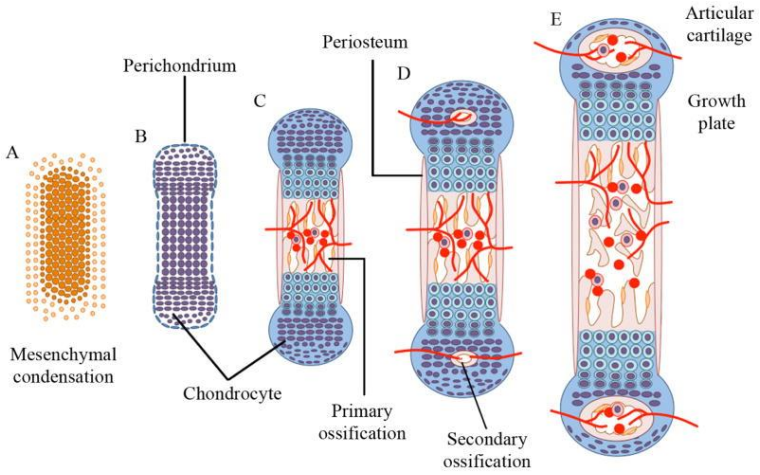

Figure 1.1: Schematic representation of endochondral ossification process. (A) Endochondral ossification starts with the formation of mesenchymal condensation and **(B)** mesenchymal cells differentiate in chondrocytes that proliferate forming an avascular cartilage template for new bone, surrounded by the perichondrium. **(C)** In the centre of the cartilage template chondrocytes undergo hypertrophy and promote the vascular invasion and formation of the primary ossification centre. (D) After birth the secondary ossification centre is formed. **(E)** Growth plate is entrapped between the two centres of ossification allowing bone growth. *(Adapted from Usami et al. 2016)* [8].

1.1.3. The growth plate

The growth plate is a well-organized cartilage area in the metaphysis of the bone, between the secondary ossification centres and the diaphysis. This structure is composed of chondrocytes at different stage of differentiation and for this reason are divided into four zones. The first zone, near to the secondary ossification centre, is the resting zone, where chondrocytes are small and

relatively inactive, functioning as a reservoir of chondrocyte progenitors. The second is the proliferative zone where chondrocytes replicate at high rate and produce a large amount of type II collagen and aggrecan. Here cells present a clonal expansion and are aligned in column parallel to the longitudinal axis of the bone, thus guiding the growth [8, 16]. Chondrocytes leaving the proliferative zone become pre-hypertrophic, typical cells of the third pre-hypertrophic zone. They undergo growth arrest, producing type X collagen and Indian Hedgehog (Ihh). The last is the hypertrophic zone where cells terminally differentiate in hypertrophic chondrocytes. During the hypertrophic process, chondrocytes undergo changes in their phenotype increasing about sixfold to tenfold their height and volume, making an important contribution to longitudinal growth [17]. Moreover, hypertrophic chondrocytes remain metabolically active even if their cellular density is reduced due to the increase of cellular volume [18]; on the other hand, the volume of extracellular matrix is reduced [19]. Hypertrophic chondrocytes finally undergo apoptosis or transdifferentiate in osteoblasts [20, 21], completing the hypertrophic process **(Figure 1.2)**. Hypertrophic chondrocytes express some proteinases including MMP13, MMP9, ADAMTS, cathepsin and calpain allowing the degradation of ECM surrounding cells. Matrix degradation is an important process required for volume expansion of hypertrophic chondrocytes and vascular invasion [22]. At the end of the hypertrophic zone, blood vessels invasion and, concurrently, bone deposition by osteoblasts allow skeletal growth [18]. In humans, the growth plate become thinner with age and is replaced by bone at the end of puberty.

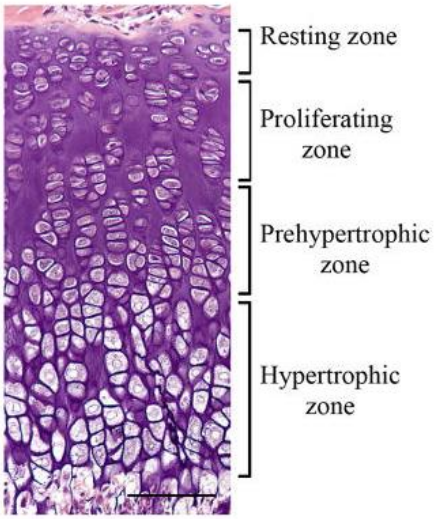

Figure 1.2: Growth plate structure. Histological section of cartilage growth plate stained with hematoxylin and eosin. Growth plate is organized in four different zones in which chondrocytes present different features: resting zone, proliferating zone, pre-hypertrophic zone and hypertrophic zone. *(Adapted from Usami et al. 2016)* [8].

Several signalling molecules are involved in regulating the growth plate [18]. Among these, the Indian hedgehog protein (Ihh), an important regulator in bone development, coordinates the proliferation and differentiation of chondrocytes, and osteoblast differentiation [23]. Ihh is synthesized by chondrocytes leaving the proliferative zone (pre-hypertrophic chondrocytes) and early hypertrophic chondrocytes. Ihh binds its receptor, Patched-1 leading to activation of gene expression. In particular, it triggers chondrocyte proliferation, and perichondrial cells and early proliferating chondrocytes to synthesize parathyroid hormone-related peptide (PTHrP).

Both Ihh and PTHrP control the decision of chondrocytes to leave the proliferative pool through a feedback loop [13]. In fact, PTHrP acts on chondrocytes in the proliferative zone to keep them proliferating and delaying their hypertrophy, thus inhibiting the synthesis of Ihh. When chondrocytes are no longer stimulated by PTHrP, they stop proliferating and start synthesizing Ihh, which in turn stimulates PTHrP production at the ends of long bones [23]. Ihh also stimulates osteoblast differentiation in the perichondrium close to the hypertrophic zone and the deposition of mineralized extracellular matrix.

Another important regulatory pathway is transforming growth factor β (TGFβ) signalling, that mainly inhibits chondrocytes hypertrophy. In particular, TGFβ2 mediates Ihh signalling while TGFβ1 stimulates non-apoptotic physiological death [24]. These factors act on perichondrium cells and proliferating chondrocytes of the growth plate due to the expression on the cell membrane of the specific receptors, TGFβR1 and TGFβR2 [20].

Most importantly, TGFβ together with the bone morphogenetic protein (BMP), another member of the TGFβ superfamily, stimulates the expression and maintenance of SOX9, a master transcriptional regulator of chondrogenesis [20].

BMP and his receptors are expressed in proliferating chondrocytes, hypertrophic chondrocytes, and perichondrium cells. BMP is crucial for endochondral bone formation since it stimulates cartilage condensation and regulates growth plate chondrocyte proliferation and differentiation [20]. In particular, BMP signalling stimulates resting chondrocytes to proliferate. Moreover by inducing hypertrophic differentiation, it plays an antagonist role to the TGFβ pathway acting independently to Ihh/PTHrP signalling [25].

Antagonist of BMP signalling is the fibroblast growth factor (FGF) pathway, inhibiting chondrocytes proliferation and promoting hypertrophy and vascular invasion. Most important members of the FGF family in the growth plate are FGF9 and FGF18, which have redundant function [20]. Interestingly, FGF18 has a biphasic effect, promoting chondrocyte proliferation and hypertrophy in early gestation and inhibiting them in late gestation [20, 26].

WNT signalling is well known to regulate chondrocyte differentiation and cartilage development [27]. In the growth plate, WNT acts through two different pathways: a canonical pathway allowing β-catenin to translocate to the nucleus and activate gene expression and a non-canonical pathway including planar cell-polarity (PCP). Through WNT canonical pathway, β-catenin antagonizes SOX9 activity, regulating chondrocyte differentiation. On the other hand, non-canonical WNT signalling inhibits canonical one, promoting chondrocytes differentiation and column formation by growth plate chondrocytes [20].

The last important transcription factor in the growth plate is Runx2 as it drives the differentiation of proliferating chondrocytes into hypertrophic chondrocytes. Moreover, Runx2 is expressed in the late condensation stage of chondrogenesis and therefore its expression is decreased in proliferating chondrocytes, while it increases in pre-hypertrophic and hypertrophic chondrocytes. It is also highly expressed in perichondral cells and osteoblasts, as it is essential for bone ECM mineralization [70].

1.2. The chondrocytes

Chondrocytes are the only cell type in cartilage. These cells normally shows a typical rounded or polygonal shape, but can also have flattened or discoid form in peripheral areas, such as at the articular surface of joints.

In adult cartilage, chondrocytes have a low proliferative activity, but they are particularly active in macromolecule synthesis. Thus, chondrocytes show typical features of metabolically active cells such as the presence of a prominent nucleus, a particularly developed RER and Golgi apparatus, and a high number of ribosomes. Moreover they also present glycogen granules and primary cilium [28]. These characteristics correlate with the main function of chondrocytes: production and turnover of all the components of the cartilage extracellular matrix, such as collagens, glycoproteins, PGs and hyaluronic acid. In fact, chondrocytes also play an important role in the degradation of matrix macromolecules, through the synthesis of enzymes, such as collagenases, proteinases and cathepsins. These anabolic and catabolic functions therefore make them responsible for regulating cartilage growth and homeostasis [29].

Chondrocytes also present different function dependent on cell location. First, they have a supporting role due to the presence of cartilage tissue in different part of the skeleton. Moreover, the other major function of chondrocytes is in skeletal growth, during embryonic development and endochondral ossification [28].

Being in a non-vascularized tissue, chondrocytes carry out all the exchanges of nutrients and waste products by diffusion through the matrix. Therefore, their metabolism occurs in low

oxygen tension and most part of cell's energy comes from glycolysis, further demonstrated by the small number of mitochondria present in cells that are so biosynthetically active [28].
As part of connective tissue lineage, chondrocytes differentiate from mesenchymal stem cells through a process whose molecular events are not completely known. This process begins when aggregation of mesenchymal cells occurs, mediated by adhesion molecules, particularly N-CAM and N-cadherin [30]. The cells then begin their chondrogenic differentiation, induced by the expression of fibroblast growth factor 2 (FGF-2) and express tissue-specific molecules. In this way, the so-called chondrification centers (or protochondral blastema) are formed and the synthesis of extracellular matrix begins, a function which is accentuated during differentiation. The production of intercellular substance therefore leads the cells to isolate themselves in cartilaginous lacunae, in which they reach the terminal differentiation. A key role in the chondrocyte differentiation process is played by the transcription factor Sox9 that, together with Sox5 and Sox6, induces the synthesis of aggrecan and type II collagen, an isoform expressed in immature chondrocytes. Due to the relevance of Sox9, its expression is finely regulated [31]. Another factor involved in the late phases of differentiation and in the proliferation of chondrocytes is Runx2 a transcription factor that induces the expression of extracellular matrix molecules such as type X collagen [32].

1.3. The extracellular matrix

The extracellular matrix (ECM) is a well-organized network of molecules contributing to the formation of a three-dimensional scaffold in which cells can grow and differentiate [33]. Cells, in fact, through their surface receptors, can interact with the macromolecules of the ECM by integrating extracellular signals, which can influence cellular functions and behaviour [33]. Thus, a variation in the matrix composition can modify the structure and the biomechanical properties of the tissue. This phenomenon can occur physiologically during development, but can also contribute to the onset of various pathological conditions [33].
The cartilaginous ECM consists of fibres immersed in an amorphous matrix. The amorphous component is mainly composed of proteoglycans (PG), hyaluronic acid (HA) and glycoproteins, which attract abundant amounts of water **(Figure 1.3)**. The peculiar hydration of the ECM confers a semi-rigid structure, which makes cartilage an excellent pressure shock absorber [1].
The fibrillar component is made up of different collagen types, specifically type II and XI (in less amount), as well as other types of fibres, such as elastic fibres. Collagen makes cartilage remarkably resistant to tensile forces, while the elastic fibres contribute to the flexibility and

deformability of the tissue [34]. Type IX collagen, can interact with other collagen fibrils and bind other ECM molecules [35, 36]. Fibril formation and stability are regulated by ECM proteins such as decorin, biglycan, fibromodulin and lumican, belonging to the small leucine rich repeat proteoglycan family (SLRPs), thrombospondin and matrilins.

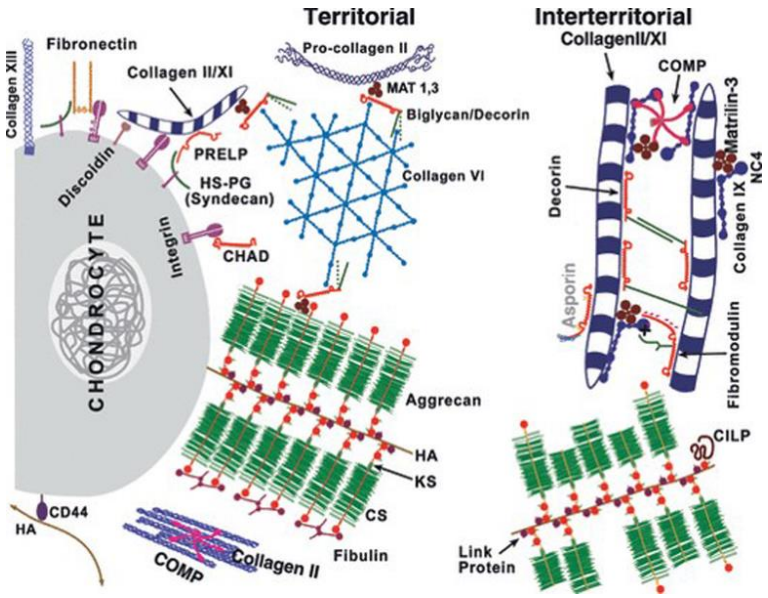

Figure 1.3: Schematic overview of cartilage extracellular matrix. The main cartilage components are collagens and proteoglycans that may organise in different large multi-molecular assemblies in different cartilage regions defining the physical and mechanical properties of this tissue. *(Adapted from Heinegard 2009)* [37].

1.3.1. Proteoglycans

Proteoglycans are a heterogeneous family of macromolecules that can be found in the ECM of different tissues, on the cell membrane or more rarely inside cells. They are composed of a core protein to which glycosaminoglycan (GAG) chains are covalently attached through an oligosaccharide linker **(Figure 1.4)**. GAG chains may vary in number, composition and size in different proteoglycans [38, 39].

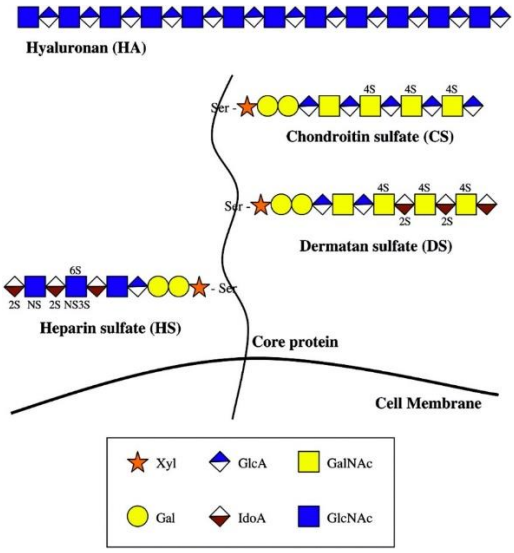

Figure 1.4: Proteoglycan and glycosaminoglycan structure.
PGs are composed of a core protein to which GAGs are covalently attached. GAGs are linear oligosaccharide chains composed of repeated disaccharide units that can be highly sulphated. *(Adapted from Taylor et al. 2006)* [40].

According to the size and properties of the core protein and to the GAG composition and location, PG can be divided in different classes, suggesting the enormous structural variability and functional flexibility of these molecules. The first class includes the modular PGs, divided into the subfamily of hyalectans and of nonhyaluronan-binding PGs [41]. Hyalectans are a group of PGs that electrostatically interact with hyaluronic acid through their N-terminal domain and with lectins through the C-terminal domain. This group includes aggrecan, versican, neurocan, and brevican. The nonhyaluronan-binding PGs are not able to bind HA, but they interact with other basement membrane components and cell-surface adhesion receptors. This group includes perlecan, agrin and leprecan [42].

The second class includes the small leucine-rich proteoglycans (SLRPs), characterized by a relatively small core protein with a central leucine-rich domain (Leu) flanked by two cysteine-rich regions (Cys) [43]. Decorin, biglycan, fibromodulin and lumican are member of this class. Finally, the third class includes cell-surface associated PGs, which are able to modulate the function of several extracellular ligands [44]. These are divided in syndecans and glypicans. Syndecans present a short hydrophobic transmembrane domain that links the large extracellular domain, containing GAGs, to the small intracellular cytoplasmic portion [43], while glypicans bind the cell membrane with a glycosylphosphatidylinositol anchor [42].

GAGs are linear polysaccharides chains, composed of repeated disaccharide units, mainly composed of an uronic acid, in particular glucuronic acid (GlcUA) or iduronic acid (IdoUA) and an amino sugar, N-acetylgalactosamine (GalNAc) or N-acetylglucosamine (GlcNAc) [43].

Thanks to the different combinations and repetitions of these disaccharides, very heterogeneous molecules can be formed in terms of both size (10-50 kDa) and biochemical features. They can also be sulfated and are therefore characterized by a high number of negative charges due to the presence of sulfate groups in addition to carboxyl groups [45].

Based on the sulfation level, GAGs are divided into two families: sulfated GAGs, including chondroitin sulfate (CS), dermatan sulfate (DS), keratan sulfate (KS), heparan sulfate (HS) and non-sulfated GAGs including mainly hyaluronic acid [39].

Chondroitin sulfate, the main sulfated GAG in cartilage, is composed of repeated disaccharide units of GlcUA and GalNAc, linked by a β(1-3) glycosidic bond. CS disaccharides are usually sulfated in C-4 or C-6 position on GalNAc residues, forming chondroitin sulfate A and C, respectively, both present in cartilage. Moreover, they are rarely disulfated in position C-2 of GlcUA and C-6 of GalNAc (D unit) or in position C-4 and C-6 of GalNAc (E unit) [39, 46]. CS is an important structural component of the cartilage ECM, but it also plays an important role in the development and function of the nervous system. CS is present in the skin, kidneys and aorta [47].

Dermatan sulfate is obtained by epimerization of GlcUA residues of CS chains in IdoUA, forming a repeated disaccharide unit with GalNAc residues, linked by α(1-3) glycosidic bonds. DS can be monosulfated in C-4 or C-6 of GalNAc residues, or disulfated in C-4 and C-6 of GalNAc and in C-2 of IdoUA and C-4 of GalNAc, even if rarely [46]. DS is present in skin, blood vessels, tendons, and heart valves [39].

Heparan sulfate is composed of repeated GlcUAβ1-4GlcNAc disaccharide. During the biosynthesis, these residues can be modified by epimerization of GlcUA to IdoUA, or by deacetylation and sulfation of GlcNAc, forming glucosamine sulfate ($GlcNSO_3$). Sulfation can occur in C-2 of GlcUA or IdoUA and in C-6 or C-3 of GlcNAc [39]. HS is a ubiquitous component of cell surface and extracellular matrix. HS may bind different core proteins; the amount and structure of HS are strictly dependent on the developmental stage and the cell type [39, 48].

CS, DS and HS bind the PG core protein on serine residues through a tetrasaccharide linker, composed of one xylose (Xyl), two galactoses (Gal) and a glucuronic acid. There is no specific consensus sequence, but usually a glycine is found at the C-terminal end of serine and, in addition, two acid amino acids are present [39, 43].

Keratan sulfate is characterized by a peculiar disaccharide unit composed of galactose (Gal) and GlcNAc, linked by β(1-4) glycosidic bonds. Its sulfate content is extremely heterogeneous; disaccharides can be unsulfated, monosulfated in C-6 of GlcNAc, or disulfated in C-6 of both

GlcNAc and Gal residues. There are two forms of KS which differ for the link with the PG core protein, that occurs through a N-glycosylation bonds to asparagine residues or O-glycosylation bonds to serine or threonine residues forming KSI and KSII, respectively [43]; KSI consists of about 50 disaccharide units and is longer than KSII which is composed of 22-30 disaccharide units [49]. KS is mainly expressed in the cornea, cartilage, bone, but is also present in the central nervous system [39].

Hyaluronic acid is a long linear polysaccharide composed of disaccharide units of GlcUA and GlcNAc, linked by β(1-3) glycosidic bonds, that can reach a molecular weight of 10^7 Da [50]. Unlike the other GAGs, HA is a non-sulfated polysaccharide and it does not bind a core protein. Thanks to its ability to interact with a large number of ECM molecules, it contributes to the maintenance of mechanical properties of cartilage [51]. It also binds CD44, HA-mediated motility receptor (RHAMM) [52] and Toll-like receptors [53] being involved in angiogenesis [54] and inflammatory response [55]. Further differences between HA and other GAGs concern its biosynthesis. In fact, GAG synthesis usually occurs in the Golgi apparatus, while HA synthesis occurs in the inner surface of the cell membrane and HA is directly released in the ECM [39]. This molecule is found in all connective, epithelial and neural tissues, but also in others, such as the vitreous humor of eye and synovial fluid of joints [39, 56].

1.3.2. Proteoglycans biosynthesis

PG biosynthesis is a complex process involving several enzymes and transporters. This process can be divided in four main steps: core protein biosynthesis, GAG biosynthesis (including tetrasaccharide linker synthesis and subsequent chain elongation), GAG sulfation, and secretion of newly synthesized PGs **(Figure 1.5)** [38].

Core protein synthesis occurs in the rough endoplasmic reticulum where first modifications, such as N-glycosylation, take place [38]. Once synthesized the protein moves to the Golgi apparatus where GAG biosynthesis occurs.

Chondroitin sulfate, dermatan sulfate and heparan sulfate are attached to serine residues of the core protein through a tetrasaccharide linker, composed of one xylose (Xyl), two Gal, and one GlcUA. Each of these sugars is added by a specific glycosyltransferase, which uses a specific UDP-sugar as a donor substrate [39].

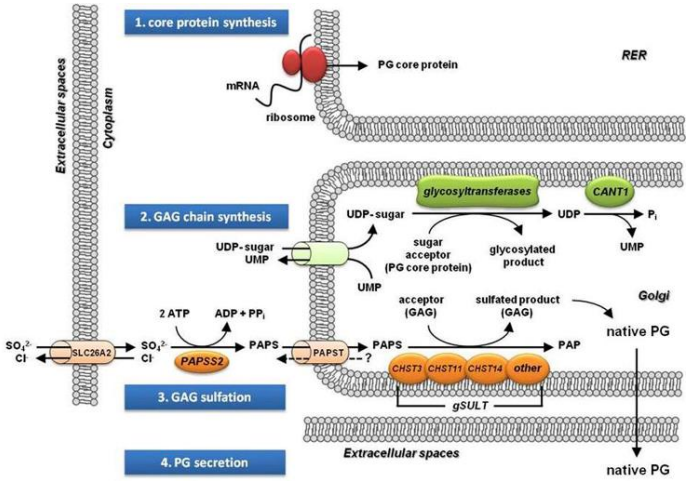

Figure 5: **Schematic representation of proteoglycan biosynthesis.**
PG core protein is synthesized in the ER lumen and then it moves to Golgi, where synthesis and sulfation of GAG occurs. Once synthesized PGs can be secreted in the ECM. [39].

The xylose residue is bound to serine residues by β-xylosyltransferases (XylT) encoded by the XYLT1 or XYLT2 genes, which use UDP-Xyl as substrate. This binding occurs in the cis-Golgi, while the binding of the other sugars occurs in the medial and trans-Golgi [57, 58]. Two galactose are transferred from UDP-Gal to the growing GAG chain by β1,4-galactosyltransferase-I (GalT-I) and β1,3-galactosyltransferase-II (GalT-II), which are respectively encoded by B4GALT7 and B3GALT6 genes. B3GALT3 encodes for β1,3-glucuronosyltransferase-I (GlcAT-I) which catalyses the transfer of GlcUA from UDP-GlcUA to the second Gal [59, 60]. The tetrasaccharide link region can undergo some modifications such as 2-O-phosphorylation of Xyl residues, catalyzed by GAG-Xyl kinase or sulfation at C-6 on the first Gal and at C-4 and C-6 on the second Gal [59]. The phosphorylation can be transient and together with sulfation can regulate the activity of GalT-I and GlcAT-I determining GAGs sorting and role [38, 39]. When the linker region synthesis is complete, GAG synthesis goes on with the polymerization of specific disaccharide units of GAG [59, 61]. In particular, in the synthesis of CS, the first sugar of the disaccharide unit, GalNAc, is transferred by β1,4-N-acetylgalactosaminetransferase-I (CSGalNAcT-I). The chondroitin synthase family is composed of six different members: four chondroitin synthases (ChSy1-4), a chondroitin-polymerizing factor (ChPF), and two chondroitin N-acetylgalactosaminetransferases (CSGalNAcT-I and CSGalNAcT-II) [45, 57, 62, 63]. Different sulfotransferases catalyse the sulfation of disaccharides units. Three sulfotransferases specific for C-4 sulfation of GalNAc have been identified: chondroitin-4-O-sulfotransferases 1, 2 and 3 (C4ST1-3); while only one for the C-6 sulfation of GalNAc, chondroitin-6-O-sulfotransferase (C6ST). These units can be further sulfated by GalNAc-4-O-sulfate-6-O-sulfotransferase

(GalNAc4S-6ST), which is responsible for the sulfation of GalNAc disulfate, and by uronosyl-2-O-sulfotransferase (UST), which is responsible for the sulfation of C-2 of GlcUA [64]. Another important modification catalyzed by specific enzymes called epimerases such as dermatan sulfate epimerase (DSE), is the epimerization of the C-5 position of GlcUA residues of the CS in IdoUA, thus producing DS. In addition, DS can be then sulfated by dermatan-4-O-sulfotransferase (D4ST) and UST [59]. Epimerization and sulfation occur during GAG synthesis or just before PG secretion [38, 39].

HS polymerization starts with the addition of a GlcNAc to the tetrasaccharide linker catalyzed by α1,4-N-acetylglucosaminyltransferase-I (GlcNAcT-I). Subsequently, HS-β1,4-glucuronyltransferase-II (HS-GlcAT-II) and α1,4-N-acetylglucosaminyltransferase-II (GlcNAcT-II) transfer GlcUA and GlcNAc from UDP-GlcUA and UDP-GlcNAc to the HS chain [59]. HS undergoes a large number of modifications such as deacetylation of GlcNAc residues by N-deacetylase, epimerization of GlcUA in IdoUA by HS-glucuronyl-C5-epimerase, and sulfations at C-2 of uronic acid and C-3 and C-6 of GlcN catalyzed by HS-2-O-sulfotransferase, HS-3-O-sulfotransferase and HS-6-O-sulfotransferase, respectively [59]. Furthermore, an extracellular HS-6-O-endosulfatase removes the sulfate group from 6-O-sulfated GlcNS in HS chain modifying its structure to regulate some biological events such as cell signalling, tumour growth and angiogenesis [65].

The first sugar of KS, D-GalNAc, is linked to the core protein on asparagine residues by a N-glycosidic bond or on serine or threonine residues by a O-glycosidic bond, and its synthesis goes on with the addition of N-acetyllactosamine [38], a disaccharide unit composed of Gal and GlcNAc. Sulfation on the KS chain is catalyzed by two sulfotransferases: GlcNAc-6-O-sulfotransferase and galactose-6-O-sulfotransferase [65]. GlcNAc-6-O-sulfation occurs only on the nonreducing terminal, while Gal sulfation also on internal Gal near the sulfated GlcNAc [39]. Interestingly sulfation on the nonreducing terminal Gal may block KS chain polymerization regulating chain length [38, 39].

The synthesis of hyaluronic acid occurs at the inner surface of the plasma membrane and follows a different mechanism compared to the other GAGs. It is mediated by three transmembrane isoenzymes, named HA synthases 1, 2 and 3 (HAS1, HAS2 and HAS3), which produce different HA isoforms of different lengths and molecular weights [38]. They catalyse the transfer of GlcUA and GlcNAC from UDP-GlcUA and UDP- GlcNAC. HASs present a double catalytic domain that allows them to bind both UDP-GlcUA and UDP-GlcNAc.

GAG sulfation is an important step in PGs biosynthesis and occurs in the Golgi apparatus. GAGs are sulfated by specific sulfotransferases that catalyse the transfer of sulfate groups from

the universal sulfate donor, the 3'-phosphoadenosine 5'-phosphosulfate (PAPS), to the sugars of GAG chains. The maintenance of PAPS concentration is important for sulfotransferase reactions and a continuous uptake and activation of inorganic sulfate is necessary [66].

Intracellular sulfate mainly depends on the extracellular uptake, and only a small amount comes from the degradation of sulfated molecules or from the catabolism of sulfur-containing amino acids, such as cysteine. The transport of inorganic sulfate occurs through a sulphate/chloride antiporter called SLC26A2 or diastrophic dysplasia sulfate transporter (DTDST) [67].

Once in cells inorganic sulfate is activated to PAPS by two sequential reactions. First, inorganic sulfate reacts with ATP to form adenosine 5'-phosphosulfate (APS) and pyrophosphate (PPi) by the action of ATP sulfurylase; then the reaction of APS with ATP, catalyzed by APS kinase, results in the production of PAPS and adenosine diphosphate (ADP). In humans, ATP sulfurylase and APS kinase form the C-terminal and the N-terminal domains of a single bifunctional enzyme, called PAPS synthase (PAPSS). There are two isoforms of this enzyme with different cellular localization: PAPSS1, mainly present in the nucleus and PAPSS2 in the cytosol [68, 69]. Although the two proteins present 77% homology, PAPSS2 has a 10- to 15-fold higher catalytic activity than PAPSS1 [70].

After its synthesis, PAPS is transported in Golgi apparatus, where sulfotransferase reaction occurs. This occurs through two specific PAPS antiporters, named PAPST1 and PAPST2, which exchange PAPS with phosphoadenosine phosphate (PAP) or adenosine monophosphate (AMP) molecule [71]. Sulfotransferase reactions produce phosphoadenosine phosphate (PAP), as a byproduct, which is rapidly degraded in AMP and phosphate by a Golgi-resident phosphoadenosine phosphate phosphatase (gPAPP), preventing the inhibition of sulfotransferases by their by-product [72].

Newly synthesized PGs are then secreted in the ECM through secretory vesicles. PGs can follow different secretion pathways and their sorting seems to depend on the type of GAG chains, their binding site or other regions of the core protein [73, 74].

1.3.3. Cartilage proteoglycans and their function

Proteoglycans are fundamental component of cartilage ECM conferring structural and physical properties to this tissue.

Among the PGs of cartilage matrix, the most representative is aggrecan. It is composed of a core protein of about 200 kDa, on which about 100 CS and 60 KS chains are linked, as well as various N- and O-linked oligosaccharides [75]. Aggrecan core protein includes three highly conserved globular domains (G1, G2, G3) connected by less conserved linear domains **(Figure**

1.6). At the N-terminal portion there is the G1 domain composed of three disulphide-bonded domains. Two of these (B and B' domains) interact with HA, while the third domains (A domain) stabilises the interaction through link protein (LP) [76]. The G1 domain may be glycosylated by N-linked oligosaccharides or KS [77]. Between the G1 and G2 domains, there is the short interglobular domain (IGD) that is more sensitive to proteinases than globular domains. This domain may be glycosylated by N-linked and O-linked oligosaccharides or KS [76]. G2 domain is composed of disulphide-bonded B and B' domains that do not interact with HA, even if they are similar to those in G1 domain; thus the functional role of the G2 is not yet known. Between the G2 and G3 domains is the GAG attachment region [64], composed of a KS-rich and CS-rich domains.

The KS-rich domain contains a six amino acids repeated sequence and about 30 KS are O-linked to serine residues [75].

In the CS-rich domain about 100 CS are bounded to the core protein where dipeptides composed of serine and glycine are regularly repeated and divided by acid and hydrophobic residues [75].

At the C-terminal portion of the core protein there is the G3 domain composed of several disulphide-bonded domains with homology to the epidermal growth factor (EGF), c-type lectin and complement regulatory protein (CRP) [76]. This domain is crucial for GAG attachment and secretion of aggrecan [75].

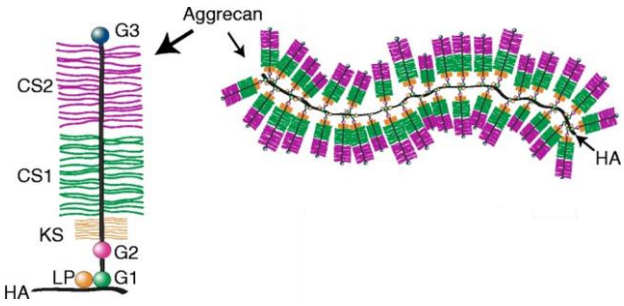

Figure 1.6: Schematic representation of aggrecan structure and proteoglycan aggregate.
Aggrecan is composed of three globular domains (G1, G2 and G3) and a GAG attachment region, where CS and KS are linked. Through the G1 domain, aggrecan binds HA forming huge aggregates maintaining cartilage stability. (*Adapted from Roughley et al. 2014*) [78].

Aggrecan has large but highly variable dimensions, since the dimensions of the core protein and linked GAG chains can vary, both in number and in length. Furthermore, aggrecan has the ability to organize itself into aggregates composed of a variable number of molecules, which can reach thousands, interacting with hyaluronic acid and link protein [38] conferring matrix stability to cartilage.

Aggrecan is important in maintaining the osmotic pressure providing the ability to resist to compressive loads [76]. In fact, the highly negative charges that characterize the sulfated GAGs of aggrecan, attract the positive ions inside tissue such as sodium and calcium, creating a gradient between the ion concentration inside cartilage and in the surrounding environment. The osmotic imbalance and the limited diffusion of aggrecan due to its large size, cause incoming of water inside tissue and causes an expansion of the ECM. This imparts tension to collagen fibre network, until a condition of equilibrium is reached when the swelling pressure, caused by the entry of water, is counterbalanced by the tension of collagen fibre network [79]. When a compressive load is applied, water goes out from the tissue and the concentration of aggrecan increase; this allows water coming back after load removal **(Figure 1.7)**.
Moreover, aggrecan inhibits hydroxyapatite deposition since calcium is used as counter ion for sulfate, reducing the amount of free calcium ions that allows mineral deposition [76].
With aging aggrecan structure can vary in size, sulfation and GAG chains, for example a decreased CS content, an increased KS content [38] and a different ratio of C-4 and C-6 sulfation has been observed [80]. Moreover, in aged cartilage a decrease in total amount of aggrecan has been described [38]. This can influence the characteristics of the tissue, leading to a decrease in the negative charge of the molecule and consequently altering its ability to absorb pressure shocks.

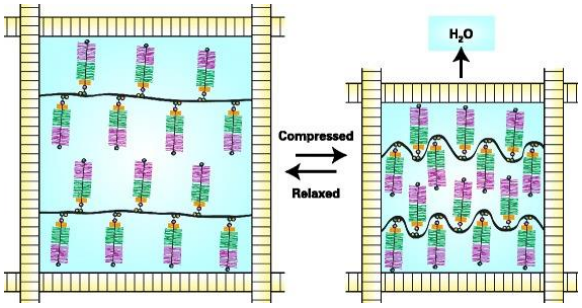

Figure 1.7: Schematic representation of proteoglycans function in cartilage.
Highly negative charged PGs bind counter ions such as Na^+ and Ca^+, allowing the incoming of water in cartilage. When a load force is applied, water goes out from the tissue giving to cartilage its compressive ability. *(Adapted from Roughley et al. 2014)* [78].

Decorin and biglycan are members of SLRPs class and they are composed of a core protein of about 40 kDa and one or two GAG chains, respectively. The GAG type is dependent on tissue where decorin and biglycan are expressed. In fact, in skin they contain DS while in cartilage and bone CS chains, even if biglycan can contain DS in articular cartilage.

Decorin and biglycan interact with their N-terminal domain with various types of collagens, during fibril formation and regulate its assembly determining the rate and the late stage of this process [37]. They can also bind other ECM molecules such as matrilins and may interact with growth factor. In particular, decorin binds transforming growth factor β (TGF-β) and biglycan binds bone morphogenetic protein-4 (BMP-4) regulating cartilage metabolism [38].
Fibromodulin is another member of SLRPs class present in cartilage. It contains one or two KS chains bounded through N-glycosidic bond to its core protein and its N-terminal portion contains nine sulfated tyrosine residues that form a cluster with other acid amino acids providing a polyanionic domain. This domain can bind growth factors such as FGF-2, interleukin 10 (IL-10) and Oncostatin M, releasing them after cartilage degradation [37, 81]. Moreover, through its leucine rich repeat region fibromodulin binds collagen fibrils [37].

1.3.4. Cartilage collagens

Collagen is the most abundant structural protein in all animal's connective tissues. Thanks to its insoluble fibres, it forms a flexible but not very extensible structure, with great mechanical resistance that can interact with the other macromolecules of the extracellular matrix.
There are 28 different types of tissue-specific collagen composed of at least 46 distinct polypeptide chains and many other proteins contain collagenous domains [82].
Collagen present a structural motif characterized by three parallel polypeptide chains that associate to form a triple helix. The triple helix structure makes the molecule resistant to the action of most proteases, but it can be degraded by specific enzymes, such as metalloproteases [83]. In the amino acid sequence, glycine, proline and 4-hydroxyproline prevail. In smaller quantities uncommon amino acids such as, 3-hydroxyproline and 5-hydroxylysine, that results through post-translational modifications are also present.
Three collagen types are mainly present in cartilage tissue: type II, IX and XI.
The most abundant is the fibrillar type II collagen, a homotrimer composed of three α1(II) chains, encoded by the COL2A1 gene [84]. Type II and type XI collagen co-polymerize with type IX collagen to form a heteropolymeric fibrillar framework consisting of central filaments of type XI collagen surrounded by type II collagen fibrils and a superficial layer of type IX collagen. This structure promotes the interactions with other ECM components, including mainly PGs. This dense network of collagen, stabilized by cross-links, confers the peculiar cartilage stiffness and tensile strength [35, 85]. In addition to its structural function, type II collagen is an important extracellular signalling molecule that can regulate chondrocyte

proliferation, metabolism, and differentiation [85]. Its relevance in cartilage is demonstrated by chondrodysplasias caused by mutations in COL2A1 [86].

Type XI collagen is another fibrillar collagen abundant in cartilage. It is a heterotrimer composed of three different α chains (α1, α2, α3). The first two chains are encoded by the COL11A1 and COL11A2 genes, while the α3 chain is encoded by the same gene as the α1 chain of type II collagen, the COL2A1 gene, and differs from it for post-translational modifications [84]. It represents 10% of total collagen in foetal cartilage, while in adult cartilage it decreases to about 3% [85]. Interestingly, type XI collagen is more concentrated in fibrils of pericellular cartilage region and it presents binding sites with high-affinity for heparan sulfate [87].

Type IX collagen is a heterotrimer composed of three different α1(IX), α2(IX), α3(IX) chains encoded by COL9A1, COL9A2 and COL9A3 genes [84]. It is one of the Fibril-associated collagen with interrupted triple helix (FACIT). These are small collagens characterized by an interruption in the triple helix domain, making the fibrillar structure more flexible. Furthermore, they are unable to form fibrils on their own, but require the presence of other fibrillar collagen molecules. In fact, collagen IX is present on the surface of collagen II/XI fibrils and it can regulate interactions between collagen fibril themselves or other ECM molecules, increasing mechanical stability of collagen network and providing an equilibrium with osmotic swelling caused by PGs [35, 36].

Type VI collagen is a heterotrimer composed mainly of three different α-chains, α1(VI), α2(VI), and α3(VI), which are encoded by the genes COL6A1, COL6A2, and COL6A3. Recently, 3 other subunit of type VI collagen, having high homology with the α3(VI) chain, (α4(VI), α5(VI), and α6(VI) chains encoded by the COL6A4, COL6A5, and COL6A6 genes), have been founded [85]. Collagen VI trimer can assemble to form dimers, tetramers or filamentous network around chondrocytes [35]. Moreover, type VI collagen, that is a non fibrillar collagen, does not bind directly to fibrillar collagens, but interacts with them through decorin, biglycan, fibronectin, perlecan and heparin. Thus, type VI collagen has been hypothesized to play an essential role in mediating cell-matrix interactions as well as intermolecular interactions in various tissues [88], maintaining tissue integrity creating cell-matrix and matrix-matrix interactions [85, 89].

Another non fibrillar collagen is type X collagen, a homotrimer composed of three identical α1(X) chains, encoded by the COL10A1[84]. In physiological conditions, it is synthesized by the hypertrophic chondrocytes of the growth plate during the endochondral ossification process and it forms a hexagonal network in the pericellular matrix retaining the correct type and

amount of ECM molecules. Being present in the growth plate and binding calcium ions at the beginning of the calcification process, it is considered a marker of terminal chondrocyte differentiation [90]. Point mutations of the COL10A1 gene cause Schmid type metaphyseal chondrodysplasia, impairing endochondral ossification in the metaphyseal growth plate [85, 91].

1.3.5. Other cartilage extracellular matrix proteins

Within cartilage extracellular matrix, in addition to collagen and PGs, also proteins are present such as matrilin, cartilage oligomeric matrix protein (COMP) and fibronectin.

Matrilins are a family of four multimeric proteins, whose subunits interact through the C-terminal portion. In cartilage matrix, tissue-specific matrilins are predominantly found: type 1, abundant in the tracheal cartilage, and type 3, in articular cartilage. They are composed of one or two von Willebrand factor A domains, an epidermal growth factor-like motif and a C-terminal coiled-coil domain allowing the homo- and hetero-oligomerization [84]. Matrilins may interact with different ECM molecules through the von Willebrand factor A domains, acting as adapters between these macromolecules in the organization of the matrix. In fact, these proteins can be found associated with collagen fibres, but is also capable of covalent binding to aggrecan. They present also high affinity for decorin and biglycan, which are bounded to collagen type VI. Thus in cartilage, matrilins are interconnected on one side to type VI collagen via decorin or biglycan, and on the other hand to type II collagen [37]. Moreover, they can also bind type IX collagen and cartilage oligomeric matrix protein (COMP).

COMP or thrombospondin 5 is a pentameric protein composed of five equal subunits. They are linked to each other through N-terminal coiled-coil domain, stabilized by disulphide bonds. A COMP subunit contains EGF-like, thrombospondin type 3 repeats and a C-terminal globular domain, that is responsible for the interactions with other components of the ECM, in particular collagen, matrilin and fibronectin [84]. COMP is in fact important for maintaining the integrity of the matrix, and intervenes in the organization of collagen fibrils. It can bind five collagen molecules at the same time with the consequence of rapidly approaching them, facilitating their interaction and the formation of fibres. For this reason, it can promote the growth of cartilage and its regeneration [92].

Fibronectin is a protein expressed in the extracellular matrix of various tissues. It is composed of two subunits covalently linked by disulfide bonds at the C-terminal portion. There are numerous forms of this protein, resulting from tissue-specific alternative splicing of the same gene [93]. Through the different domains, they can bind collagen, heparin, fibrin and cells,

interacting with integrin receptors or with syndecan GAGs [33]. Fibronectin therefore acts as an adhesion molecule between the components of the extracellular matrix, contributing to its integrity [94].

1.3.6. Extracellular matrix homeostasis and quality control

Extracellular matrix is a complex, highly organized network of protein, whose composition and quality determines biochemical and biomechanical properties of cartilaginous tissue. Chondrocytes, being the only cell type in cartilage, are responsible for the synthesis and maintenance of the ECM, made mainly of collagens, proteoglycans and glycoproteins.

The endoplasmic reticulum is the largest organelle in chondrocytes since it functions as the place of protein synthesis and folding and as the starting point of the protein secretory pathway. Proteins and proteoglycans are synthesized in the ribosomes at the RER, and once released into the lumen of the ER they undergo post-translational modifications, usually fundamental for correct protein folding and function. Resident ER molecular chaperons mediate protein folding, also providing a quality control system, since they retain newly folded proteins until they get the correct conformation. As soon as proteins reach the native conformation, they are released and secreted into the ECM [95].

Being so synthetically active, chondrocytes are particularly susceptible to ER stress that can result from different factors such as hypoxia, viral infections, nutrient deprivation, but also mutations in cartilage proteins, causing defects in protein folding, trafficking and resulting in protein aggregates to accumulate in the ER. In response to ER stress, cells have developed a highly conserved protective mechanism, known as unfolded protein response (UPR) that decrease or halts cellular protein synthesis, increases the production of chaperones or degrade protein aggregates to restore cell homeostasis [95].

UPR is triggered by the activation of Bip (binding immunoglobulin protein), a lumen resident chaperon, that dissociate from the sensor protein IRE-1 (inositol-requiring enzyme 1), the transcription factor ATF6 (activating transcription factor 6) and PERK (protein kinase-RNA-like endoplasmic reticulum kinase), activating them **(Figure 1.8)**. These three proteins activate three different signalling pathways with the ultimate aim of decreasing protein translation and degrading misfolded proteins or if stress cannot be overcome promoting cell death [96].

First, the transmembrane ER protein PERK is activated by oligomerization and autophosphorylation. It acts as a kinase on eIF2α (eukaryotic translation initiation factor 2A), resulting in translational attenuation, thereby reducing the total protein load in the ER to prevent further accumulation of unfolded proteins. Due to the preferred translation of mRNAs with

short open reading frames in the 5'-UTRs, the amount of the transcription factor ATF4 (Activating Transcription Factor 4) increases. ATF4 up-regulates the expression of UPR genes involved in amino acid metabolism, antioxidant response, folding, and regulation of autophagy and apoptosis [97].

The transmembrane ER protein ATF6 is transported to the Golgi apparatus where it is cleaved by two proteases resulting in the release of the ATF6 cytoplasmic domain. It translocates to the nucleus where acts as a transcription factor and induces the expression of UPR genes encoding for additional chaperones and initiators of ER-associated degradation (ERAD) or autophagy [97].

The transmembrane ER protein IRE1 oligomerizes and is activated by autophosphorylation. With its RNase cytosolic domain, induces the splicing of the transcription factor X-box-binding protein 1 (XBP1). Spliced XBP1 in turn activates gene expression of folding proteins and components of the quality control mechanisms in the ER, including the activation of ERAD.

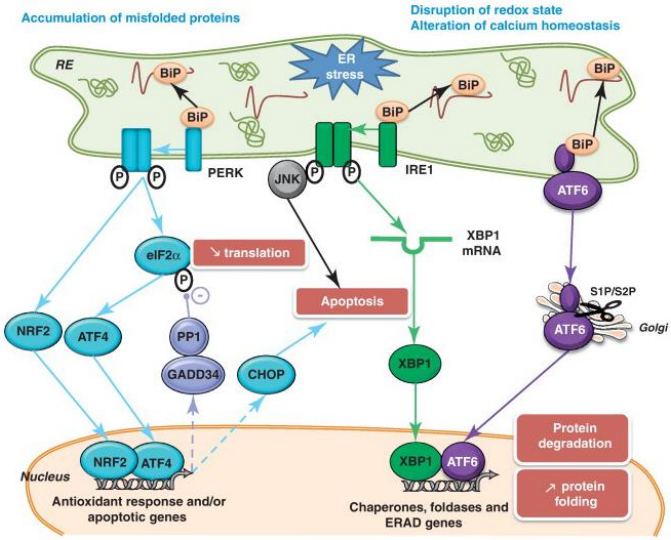

Figure 1.8: Schematic representation of the unfolded protein response pathway (UPR). In presence of ER stress caused by the accumulation of misfolded or unfolded protein, BiP activates three UPR transducers. PERK, activated by dimerization and autophosphorylation, phosphorylates eIF2α that induces the selective translation of ATF4, resulting in the transcription of genes involved in amino acid metabolism, antioxidant response, folding, and regulation of autophagy and apoptosis. IRE1, activated by oligomerization and autophosphorylation, induces the splicing of the transcription factor XBP1 that in turn activates gene expression of folding proteins and components of the quality control mechanisms in the ER, including ERAD. The third is the transcription factor ATF6 that once activated translocates to the nucleus where it induces the expression of genes encoding for additional chaperones and initiators of ERAD or autophagy. (*Adapted from Flamment et al. 2012*) [98].

The induction of ER stress with the activation of the UPR pathway has been described in different skeletal diseases with similar clinical features caused by mutations in genes encoding for different cartilage ECM proteins, such as COMP, matrilin-3 or type II and X collagen. For example, ER accumulation of mutant type X collagen results in metaphyseal chondrodysplasia type Schmid (MCDS), while type II collagen mutations resulting in ER protein aggregation has been reported in spondyloepiphyseal dysplasia (SED) [96].

There are two different mechanisms to degrade misfolded or unfolded proteins activated by the UPR: endoplasmic reticulum-associated degradation (ERAD) and autophagy (ER-phagy).

The first strategy is the major degradation pathway and facilitates proteasome-dependent degradation. ERAD complex includes different proteins involved in different steps of the degradation process, first of all identifying non-native proteins by detecting some structural defects such as exposed hydrophobic regions, unpaired cysteine residues or immature glycans. Protein are then retrotranslocated to the cytosol, where the ubiquitin-proteasome system (UPS) is located. Ubiquitination requires a cascade of enzymes including E1, ubiquitin-activating enzyme, E2, ubiquitin-conjugating enzyme and E3, ubiquitin ligase. These reactions produce a polyubiquitinated protein, which is identified and degraded by the proteasome [99, 100].

ER-phagy consists in the selective elimination of specific fragments of the ER with aggregated protein inside. These structures are sequestered into autophagosomes and broken down via the lysosomal machinery. ER-phagy receptors concentrate proteins in an ER subdomain via interaction with LC3 (microtubule-associated protein light chain 3) or GABARAP (GABAA receptor-associated protein) in the growing autophagic membrane, the phagophore. ER-phagy substrates are then enclosed in a double-membrane-bound autophagosome, which fuses with the lysosome [95].

To date different ER transmembrane proteins have been identified as ER-phagy receptors, mediating the turnover of ER domain in specific cellular conditions. In particular, FAM134B and reticulon 3 (RTN3) mediate the degradation of ER sheets and tubules, respectively, in response to nutrient starvation. The ER protein SEC62 is as a receptor for the ER-phagy mediated recovery from ER stresses [101].

Golgi apparatus also plays an important role in cartilage proteostasis since the majority of post-translational modifications and the sorting of ECM proteins occurs in this organelle.

Newly synthesized proteins exit the ER and are transported by specific carriers COPII-coated through the ER-Golgi intermediate compartment (ERGIC) to the Golgi where the modifications occur. In particular, proteins enter in the cis-Golgi and moves to the trans-Golgi, undergoing post-translational modifications catalyzed by Golgi specific enzymes, such as glycosylation,

sulfation, phosphorylation and proteolytic processing. Other vesicles, COPI-coated, mediate the retrograde trafficking recycling Golgi-resident enzymes and other membrane proteins, in order to maintain Golgi homeostasis, or recycling ER protein, including chaperones, back to the ER. Once the trans-Golgi network has been reached, proteins are transported in the extracellular space to the final destination [102].

The Golgi apparatus coordinates the post-translational modification, that impact on the secretion and assembly of matrix components and guide the proteolytic processing of these molecules prior to secretion. The importance of Golgi organisation and function in the synthesis of matrix molecules is exemplified by its role in the biosynthesis of PGs, highly glycosylated fundamental component of cartilaginous ECM [102].

The sequential nature of GAG assembly is reflected in the compartmentalization of Golgi enzymes. Chain initiation begins with the addition of xylose to specific residues in the core protein that occurs in the ERGIC and/or cis-Golgi. The core tetrasaccharide is then assembled in the cis-medial Golgi, while chain elongation and modification take place in the medial-trans Golgi. Also the other modifications are compartmentalized, since sulfation at the C6 and C4 positions in N-acetylgalactosamine occurs in the trans-Golgi, while, epimerisation occurs specifically in the late trans-Golgi. This strict organisation ensures efficient glycan assembly and regulate the nature or quantity of GAG chains that are produced. The compartmentalisation of enzymes within cisternae also supports the formation of functional enzyme complexes to facilitate efficient substrate transfer between enzymes [102].

When Golgi is overloaded, Golgi stress, an autoregulatory pathway, which augments Golgi function, occurs. Golgi stress has not been well characterized as ER stress but recent studies revealed the importance of some regulatory mechanisms **(Figure 1.9)**.

In particular, the activation of the transcription factor E 3, TFE3, which in normal conditions is phosphorylated and retained in the cytosol. In case of altered Golgi homeostasis it is dephosphorylated and translocated to the nucleus where it interacts with an enhancer element called Golgi apparatus stress response element (GASE), resulting in transcriptional activation of genes encoding for Golgi structural proteins, such as GM130 (Golgi matrix protein 130) and giantin, glycosylation enzymes and components of vesicular transport.

Two less known pathways involves the ER chaperone HSP47 (heat shock protein 47), whose expression prevents cells from Golgi stress-induced apoptosis and CREB-ARF4. ARF4 (ADP Ribosylation Factor 4) is a member of the small GTPase family localized in the Golgi membrane, where it regulates Golgi-to-ER vesicular transport that is inhibited upon Golgi stress. CREB (cAMP response element-binding protein) is a transcription factor resident in the

ER membrane as a transmembrane protein. In presence of Golgi stress it is activated by proteolysis, causing the release of its cytoplasmic domain that translocates to the nucleus where it upregulates the transcription of ARF4 gene, resulting in Golgi stress-induced apoptosis and Golgi disruption [97].

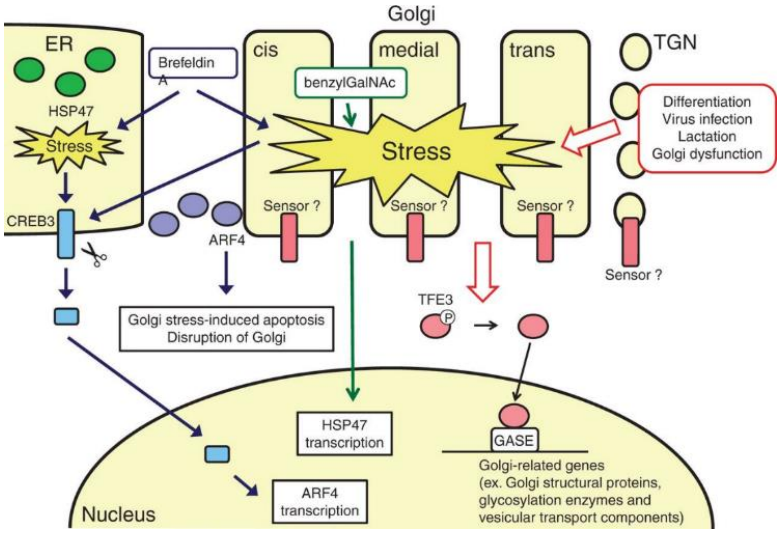

Figure 1.9: Schematic representation of Golgi stress response.
Several pathways regulate the Golgi stress response, the homeostatic mechanism that augments Golgi functions in response to its insufficiency. The TFE3 pathway, activated by dephosphorylation of TFE3, cause the translocation of this transcription factor to the nucleus where it binds the enhancer element GASE, stimulating the expression of genes encoding for Golgi structural proteins, glycosylation enzymes and vesicular transport components. The pathway of the transcription factor CREB that once activated by proteolysis translocates to the nucleus where it stimulates the transcription of ARF4, resulting apoptosis activation. The less known is the HSP47 pathway, that has anti-apoptotic role. (*Adapted from Sasaki and Yoshida 2015)* [97].

Due to the fundamental role of the Golgi in synthesis and maintenance of the ECM, several skeletal disorders are caused by mutations in Golgi proteins, such as Golgi enzymes or proteins involved in Golgi trafficking, resulting in matrix defects. In fact, chondrocytes, characterized by high rates of ECM protein synthesis, may be particularly susceptible to stress when Golgi processing is inefficient. For example, mutations in the gene *TRIP11* encoding for the golgin GMAP210 (Golgi microtubule-associated protein 210) causes structural and functional defects of the Golgi apparatus, resulting in achondrogenesis 1A (ACG1A), a skeletal disorders associated with Golgi fragmentation and defective trafficking [103]. Another example is the bone disorder gerodermia osteodysplastica (GO), caused by mutations in the trans-Golgi protein GORAB, involved in COPI trafficking, which results in reduced recycling of trans-

Golgi enzymes and defective glycanation of matrix protein such as decorin and biglycan [104]. Another nonlethal skeletal dysplasia characterized by altered transport between ER and Golgi is the Dyggve-Melchior-Clausen syndrome, caused by mutation in the gene *DYM*, encoding for dymeclin, a protein involved in vesicular trafficking to and from the Golgi [105]. Lastly, there is the Saul-Wilson syndrome that is caused by mutation in COG4 protein, a subunit of the oligomeric Golgi complex (COG) involved in intracellular vesicular transport, which results in delayed anterograde vesicular trafficking from the ER to the Golgi and accelerated retrograde vesicular recycling from the Golgi to the ER [106].

Intracellular protein quality system are also tightly regulated in the Golgi apparatus, which is involved in three main different intracellular degradation processes.

Endosome and Golgi-associated degradation (EGAD), which is similar to ERAD, operated via the proteasome, endosome and lysosome. Golgi apparatus-related degradation (GARD) regulates Golgi morphology during excessive Golgi stress and consists in the degradation of the cis-Golgi protein GM130 by the proteasome localized to the Golgi apparatus. Excessive Golgi stress induces irreversible apoptosis and cell death. If Golgi stress is relieved, Golgi morphology is maintained. Golgi membrane-associated degradation (GOMED) is a non-canonical degradation pathway that mediates extensive proteolysis to compensate for deficient canonical autophagy and involves autophagosome formation from the Golgi [107].

Lysosomes are fundamental organelles for degradation and recycling of extracellular matrix components. Extracellular materials can be transported to lysosomes for degradation through phagocytosis, while intracellular proteins and polysaccharides, unfolded or misfolded proteins and even whole organelles, are transported to be degraded or recycled to the plasma membrane by the mechanism called autophagy. During autophagy, damaged proteins or dysfunctional organelles are surrounded by double membrane vesicles, the autophagosomes, which then fuse with the lysosome and are digested by lysosomal hydrolases, resulting in the final release of amino acids and monosaccharides [108, 109].

Apart from their degradative roles, lysosomes also have an important role in the regulation of multiple cellular functions participating in intracellular nutrient sensing and in cellular homeostatic maintenance. For example, when cells are starved, they initiate the process of autophagy and increase the capacity of the lysosome by the lysosomal stress response, which has not been well characterized as the ER stress response. The kinase complex mTORC1 (mammalian target of rapamycin complex 1) is a key regulator of autophagy initiation as well as the lysosome stress response. In normal conditions, it is localized on lysosome membrane and phosphorylates the autophagy regulator ULK1, resulting in autophagy suppression.

Furthermore, mTORC1 also suppresses the transcription of autophagy genes, as well as of lysosomal genes, by inhibiting the transcription factor EB (TFEB) and the transcription factor E3 (TFE3), which are master regulator of lysosome biogenesis. Phosphorylated TFEB and TFE3 are retained in the cytoplasm as an inactive form by binding to 14-3-3 protein [110]. Under stress condition, which can also be caused by drugs or pathogens, mTORC1-TFEB/TFE3 signalling pathway is activated to promote lysosome biogenesis. mTORC1 dissociates from the lysosome and calcium is released through calcium permeable channels into the cytosol, where it activates the cytosolic phosphatase calcineurin. Activated calcineurin dephosphorylate TFEB/TFE3, which translocate to the nucleus where it binds the enhancer element CLEAR (coordinated lysosomal expression and regulation), and activates transcription of genes related to the lysosome biogenesis and autophagy. Subsequently, there is an increase of lysosome-related genes that lead to the possible restoration of these stressed organelles [97, 108].

Inter-organelle signalling might affect organelle stress responses, so lysosomal stress pathway can also be connected to other stress response pathway, such as ER-stress, which causes increase of lysosomal size, lysosome membrane permeabilization and lysosomal repositioning. Moreover, it inhibits autophagic flux and causes the nuclear translocation of TFEB and TFE3. Furthermore, the lysosome resident protein mTORC1 contributes to ER stress, and cell life and death by regulating expression levels of ER stress response genes [108].

The TFEB/TFE3 pathway of the lysosome stress response is closely related to various diseases such as lysosomal storage diseases (LSD) [97]. The cellular pathogenesis of the diseases is complex, since a progressive accumulation of primary substrates within lysosomes induces a generalized lysosomal dysfunction, which in turn leads to the accumulation of a variety of secondary storage products that eventually contribute to disease manifestation [101]. Among LSD, there is a subfamily named Mucopolysaccharidosis (MPS) caused by inherited defects in the catabolism of GAG including some skeletal disorders (group XXVII in the classification of skeletal disorders) [111].

2. Skeletal dysplasias

Skeletal dysplasias are a huge and heterogeneous group of genetic diseases that mainly affect cartilage and bone. Even if each disorder is relatively rare, the birth incidence of overall these disorders is almost 1/5000 [112].

Nowadays 461 disorders have been characterized and classified in 42 different groups, based on radiographic features, clinical course and molecular criteria [66, 113].

Skeletal dysplasias show a wide range of severity from very mild phenotypes, compatible with life, to foetal and neonatal lethality [113].

Moreover, beyond the skeletal phenotype, these disorders can be associated with neurologic, auditory, visual, cardiac, pulmonary, and renal complications since the causative genes might also have functional roles in tissues other than the skeleton [112].

In fact, 437 disease-causing genes involved in a broad range of cell biologic processes have been identified. These genes encode not only for tissue-specific proteins that are essential for the formation and maintenance of bone and cartilage, but also for proteins that have a more ubiquitous role such as regulating gene transcription, cell division, or intracellular transport [113]. In particular genes involved in skeletal dysplasias encode for ECM proteins, enzymes, cellular transporters, transcription factors, signal transducers, channel proteins, chaperones, cytoplasmic proteins, cilia, proteins involved in cell cycle, and chromatin modifying enzymes [66].

2.1 Desbuquois dysplasia

Desbuquois dysplasia (DBQD) is a severe autosomal recessive chondrodysplasia, belonging to the skeletal diseases characterized by multiple joint dislocations (XX group) [113]. It's a rare chondrodysplasia first described by Desbuquois et al. in 1966 [114], with the prevalence of 1 to 1,000,000 birth in worldwide population.

Patients affected by DBQD present severe growth retardation, which affects both the prenatal and postnatal ages, short stature, joint laxity, short extremities, and progressive scoliosis with consequent orthopaedic complications and ambulatory difficulties. Furthermore, it is also associated with characteristic facial dysmorphic features including flat round face, mid-face hypoplasia, short nose, microstomia, and microretrognathia [115].

There are some peculiar radiological features, fundamental for the diagnosis of the pathology, such as advanced ossification of the carpus and tarsus, progressive kyphoscoliosis and brevity of the long bones compared to the trunk with a particular deformity of the femoral head, called

"Swedish key". Other radiological features found in 90% or more of the patients are the flat acetabular roof, proximal fibular overgrowth, and elevated greater trochanter **(Figure 10)** [116]. The finding of specific radiological features could be useful to make a correct clinical diagnosis since Desbuquois dysplasia present some phenotypical aspect in common with other dysplasias including pseudodiastrophic dysplasia, diastrophic dysplasia, Catel-Manzke syndrome, and Larsen syndrome [116].

Furthermore, some specific hand anomalies are characteristic of patient affected by DBQD, such as an additional ossification centre, distal to the second metacarpal, the bifid distal phalanx of the thumb, phalange dislocations and the “delta phalanx”, an extra phalanx that causes the medial deviation of the last phalanx of the thumb **(Figure 1.10)** [117].

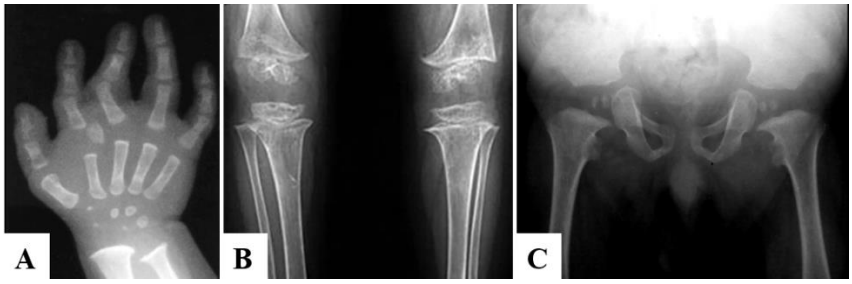

Figure 1.10: Radiological features of Desbuquois dysplasia type 1.
X-ray of patients with typical features of Desbuquois dysplasia type 1: **(A)** hand with advanced carpal ossification and delta phalanx, **(B)** metaphyseal irregularities of knee and horizontal acetabular roofs and **(C)** the “Swedish key” appearance of the proximal femur. *(Adapted from Huber et al. 2009)* [118].

Since DBDQ is clinically and phenotypically very heterogeneous and since the presence of the typical hand anomalies has been observed in one third to one half of DBDQ patients, two forms have been classified based on the presence or absence of this typical feature in Desbuquois dysplasia type 1 (DBQD1) and type 2 (DBQD2), respectively [119].

In addition, another milder variant of DBQD, named the Kim variant, characterized by almost normal appearing hands in infancy, but significant radiographic changes, including short metacarpals, elongated phalanges, and remarkably advanced carpal bone age has been described [118, 120].

DBDQ1 is caused by mutations in *CANT1* gene that encodes for a calcium-activated nucleotidase 1 (CANT1), a Golgi protein whose physiological role has not been completely elucidated. The pathology displays a high lethality rate of more than 33%, due to respiratory failure [115] or cardiopulmonary complications caused by thorax hypoplasia [121]. Different *CANT1* gene mutations have been identified in homozygous or compound heterozygous state including missense and nonsense mutations. Among them, the most frequent are Arg300Cys or

Arg300His substitutions in the apyrase domain. The genetic alterations co-segregate with the pathology and patients present different skeletal anomalies, due to an alteration of GAG glycosylation, depending on the mutation [115, 122].

Desbuquois dysplasia type 2 is caused by mutations in the *XYLT1* gene encoding for the enzyme xylosyltransferase 1 [117], involved in the earliest step of glycosaminoglycan synthesis. *XYLT1* mutations lead to a complete or partial loss of function of XYLT1 causing an impaired PG biosynthesis [123].

2.1.1. The calcium activated nucleotidase 1 (CANT1)

CANT1 is a calcium-activated nucleotidase located in the endoplasmic reticulum and in Golgi apparatus. This enzyme preferentially catalyses the hydrolysis of uridine diphosphate (UDP) to uridine monophosphate (UMP) and phosphate [124]. Alternatively, it can hydrolyse guanosine diphosphate (GDP) and uridine triphosphate (UTP), with lower affinity [125].

CANT1 is a member of the apyrase family and is homologous to apyrases present in the saliva of blood-sucking arthropods. They use apyrases to feed, hydrolysing extracellular nucleotides, such as adenosine diphosphate (ADP) that is a potent platelet activator, in order to inhibit haemostasis in their hosts [117, 126].

Two forms of CANT1 protein, a membrane-bound, present in ER and Golgi apparatus, and a soluble secreted form [124, 125] have been identified in humans. Both forms show high activity when dimers are assembled and their activity could be modulated by calcium concentration [127].

The *CANT1* gene is located on chromosome 17. It consists of five exons resulting in three different transcripts. One of these encodes for CANT1, a protein of 401 amino acids containing eight nucleotidase conserved regions (NCR) [127]. A lot of missense and nonsense mutations in *CANT1* gene, including a large deletion encompassing the 5' UTR region and exon 1, linked to Desbuquois dysplasia have been identified. All mutations are located in the NCR7-encoding region, which is highly conserved among related apyrases. Within the NCR7 domain there is a pentapetide composed of five positively and negatively charged amino acids alternately organized forming four salt bridges, involved in the catalytic site of CANT1 [122]. Mutations in this domain causing amino acid substitution lead to decreased enzyme activity. However, children with nonsense mutations also have cardiorespiratory abnormalities, leading to early death [122].

Since Desbuquois dysplasia share some phenotypic features with Diastrophic dysplasia and Larsen syndrome, both characterized by altered PG biosynthesis, it has been suggested that

CANT1 may play a role in PG metabolism. This was also confirmed by studies on fibroblasts of Desbuquois dysplasia patients, presenting reduced PG synthesis and GAGs with reduced size. Moreover, due to the nature of its substrate and its cellular localization, several studies have focused on the activity of CANT1 enzyme, in order to completely elucidate its role in proteoglycan biosynthesis [124].

In the Golgi apparatus, CANT1 hydrolyses UDP, a by-product of glycosyltransferase reaction, preventing their inhibition. Moreover, UDP hydrolysis produces phosphate and UMP that ensures the correct functioning of the UMP/UDP-sugars antiporters and the entry of the latter into the Golgi apparatus. Once in the Golgi, UDP-sugars become the substrate of glycosyltransferases, enzymes responsible for the synthesis of GAGs **(Figure 1.11)** [117].

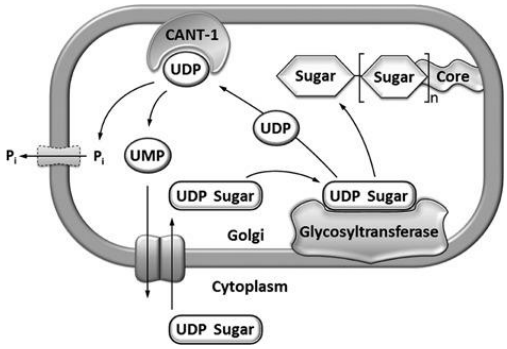

Figure 1.11: Schematic representation of CANT1 role in proteoglycan biosynthesis.
UDP sugars are transported into the lumen of the Golgi apparatus, where sugars are transferred by specific glycosyltransferases to the growing GAG chains. CANT1 hydrolyses UDP, a by-product of glycosyltransferase reactions, in UMP and phosphate (Pi). Thanks to UDP hydrolysis, glycosyltransferase reactions are not inhibited by the product and UMP is exchanged with cytosolic UDP-sugars through an antiporter exchanger. *(Adapted from Nizon et al. 2012)* [119].

Thus, impairment of CANT1 may cause increased UDP levels in Golgi apparatus, resulting in the inhibition of glycosyltransferase reactions and, reduced UMP levels, that affects UDP-sugar uptake in the Golgi, resulting in reduced PG synthesis [119].

In addition to its role in glycosylation reactions, an involvement of CANT1 in protein folding and quality control has been demonstrated in neuroblastoma cell lines [128]. The existence of the soluble form of CANT1 in the extracellular environment, where also signalling nucleotides such as UDP and UDP-sugars are present, suggests a modulating function of cellular responses to extracellular signalling by the interaction of UDP with specific pyrimidinergic receptors of the P2Y family [129].

Therefore, CANT1 seems to have different functions depending on the cell type, but it has been observed that mutations causing a total or partial loss of the enzyme's catalytic activity *in vivo*

have phenotypic consequences mainly on the skeletal system, as in DBQD1, although CANT1 is a ubiquitous enzyme [117].

2.1.2. The *Cant1*$^{-/-}$ mouse

Bone or cartilage tissue biopsies from patients affected by DBQD1 are rarely available, thus to further study the physiological functions of CANT1 and the pathogenic mechanism of DBQD1, a *Cant1* knock-out mouse was generated by the excision of exons 3 and 4 of the *Cant1* gene, encoding for the active site of the enzyme. The homozygous knock-out (*Cant1*$^{-/-}$) mice have been validated as an animal model of DBQD1 since they recapitulate the chondrodysplastic phenotype observed in DBQD1 patients **(Figure 1.12)** [117].

In fact, *Cant1*$^{-/-}$ mice present growth retardation and reduced size compared to age matched wild-types. Moreover, X-ray analysis show moderate thoracic kyphosis and the presence of the "delta phalanx", the typical hand anomaly described in DBQD1 patients [117].

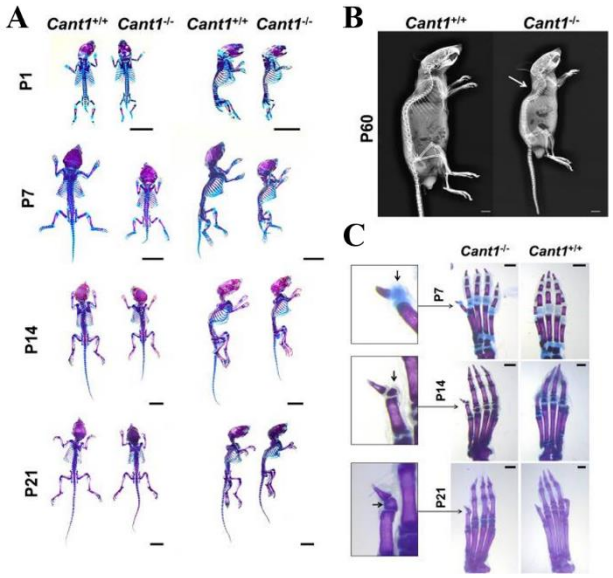

Figure 1.12: Skeletal phenotype of *Cant1* knock-out (*Cant1*$^{-/-}$) mouse compared to wild-type (*Cant1*$^{+/+}$).
The *Cant1*$^{-/-}$ mouse is a knock-out mouse generated by the excision of exons 3 and 4 of the *Cant1* gene. It recapitulates the chondrodysplastic phenotype of DBQD1 patients presenting **(A)** reduced size and growth retardation, **(B)** a moderate thoracic kyphosis and **(C)** the typical hand anomaly "delta phalanx". (*Adapted from Paganini et al. 2018*) [117].

Morphometric analysis of three representative long bones (tibia, ilium and femur) of *Cant1*$^{-/-}$ mouse, confirmed growth retardation and suggested that deletion of the CANT1 gene leads to defects in the endochondral ossification process. In fact, in the tibial growth plate, the proliferative zone present a reduced area, despite the increased proliferation of chondrocytes

observed in the first two weeks of life. This is partly counterbalanced by increased cell apoptosis that occurs in the first week. The hypertrophic zone of the growth plate is also reduced, probably due to a defect in the terminal differentiation of the chondrocytes [117].

Defects in chondrocyte homeostasis confirm the impaired endochondral ossification process accounting for the reduced size of long bones.

Reduced PG synthesis, analyzed in primary chondrocyte cultures from rib cartilage of *Cant1*$^{-/-}$ and wild-type mice, was observed in *Cant1*$^{-/-}$ chondrocytes. These data were confirmed *in vivo* since a reduced amount of GAGs was detected in cartilage of *Cant1*$^{-/-}$ mice compared to wild-type ones [117].

Further *in vitro* experiments demonstrated GAG oversulfation and reduced hydrodynamic size in *Cant1*$^{-/-}$ chondrocytes compared to those extracted from wild-type cells [117].

The reduced PG biosynthesis is a further confirmation of the phenotypic similarity of the *Cant1*$^{-/-}$ mouse with human DBQD1, in which these alterations have been identified in patient fibroblasts [117, 119].

Overall these data demonstrated that *Cant1*$^{-/-}$ mouse is a good model to better understand the pathogenesis of DBQD1 and provide a final evidence of CANT1 involvement in PG biosynthesis in cartilage.

2.2. Diastrophic dysplasia

Diastrophic dysplasia (DTD) is a severe but usually nonlethal osteochondrodysplasia belonging to the sulfation disorder group (IV group) [113].

The prevalence of this disease is around 1:100,000 births in worldwide population, but interestingly in the Finnish population, the prevalence is higher, reaching 1:33,000 births because of a founder effect [130].

The disorder was first described in 1960 by Lamy and Maroteaux [131] with the term "diastrophic dwarfism", which refers to the deformities, such as the twisted and bent shape bones [131].

Patients affected by diastrophic dysplasia present short stature, with a mean adult height of 136 cm for males and 129 cm for females [132], due to short trunk and severe short limbs, but a normal size head. In addition, distinctive features are bilateral clubfoot, cleft palate, characteristic hand deformities, deformities of the external ear and progressive kyphoscoliosis of the spine **(Figure 1.13)** [133].

Fingers are short and the abduction of the thumb, named "hitchhiker's thumb", is a peculiar feature of DTD patients. In addition, also toes are generally contracted and the first toe can

show the same characteristic anomalies of the hand. These typical hand and foot deformities can be observed since the fifteenth or sixteenth weeks of gestation **(Figure 1.13)** [134].

In the first period of life, diastrophic dysplasia involves not only the skeleton, but also tendons, ligaments and joint capsules, which are more tense and shorter than normal, resulting in joint stiffness and reduced joint mobility [135].

Diastrophic dysplasia is a progressive disease. In young adults, degenerative arthrosis of the hip is quite common, causing pain and an anterior tilting of pelvis [136]. Additionally, the spine may develop excessive lumbar lordosis, thoracolumbar kyphosis, and scoliosis [137]. Moreover, brachydactyly, ulnar deviation, phalangeal synostosis, and ankylosis of fingers may cause significant disability. In addition to the skeletal abnormalities, mild muscle hypoplasia of the thighs and legs is quite common [138].

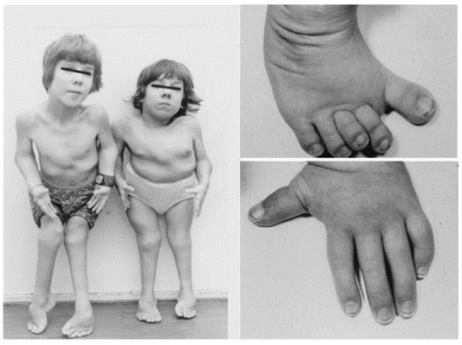

Figure 1.13: Patients affected by diastrophic dysplasia.
DTD patients show growth retardation, short stature, kyphoscoliosis, painful osteoarthrosis and abduction of the thumb, named “hitchhiker's thumb”.

In some cases, severe cervical kyphosis can lead to spinal cord compression [139], while mental development and intellect are not affected. Hearing and vision defects are rarely observed, although the tendency to myopia is quite frequent [140].

Over the years, a wide variability in phenotypic expression of diastrophic dysplasia has been observed, which can results in very severe conditions or mild forms of the disease, even within the same family. Consequently, the influence of other genetic or epigenetic factors on the phenotype has been hypothesized [141].

To date, there are no curative therapies for diastrophic dysplasia, but only symptomatic therapies aimed at improving life quality of patients. In fact, they have difficulties in moving and carrying out normal daily activities, not only due to reduced stature, deformation of the limbs and degeneration affecting the spine and joints, but also to the pain associated with these problems [142]. Furthermore, cartilage defects can cause complications in the respiratory tract,

auditory system and palate, leading to alterations in respiratory capacity and communication difficulties. Orthopaedic problems are treated with physiotherapy in order to reduce pain and maintain joint mobility, but often surgery is required. They are performed at young age due to the early onset of degeneration and to stem the pathology progression as much as possible, but quite often they have to be repeated several times [143].

Diastrophic dysplasia is caused by mutations in the *SLC26A2* gene that encodes for a sulfate/chloride antiporter present on the cell membrane, named SLC26A2 or diastrophic dysplasia sulfate transporter (DTDST). Mutations in *SLC26A2* gene are associated with other three skeletal diseases with different severity, forming a wide spectrum of clinical phenotype [144].

2.2.1 Other skeletal dysplasia associated with *SLC26A2* mutations

Mutations in the *SLC26A2* gene are related to the onset of four different forms of chondrodysplasia in humans including in order of decreasing severity achondrogenesis type 1B, atelosteogenesis type 2, diastrophic dysplasia and recessive multiple epiphyseal dysplasia [145].

Achondrogenesis type 1B (ACG1B) is the most severe form of SLC26A2 chondrodysplasias, lethal before or shortly after birth. The cause of prenatal death is unknown while in the live-born foetuses, death is due to respiratory failure. The term "achondrogenesis" (Greek for “not producing cartilage”) refers to the lack of cartilage formation that characterizes this group of pathologies. Foetuses affected by ACG1B appear abnormal immediately at birth. The excess of soft tissue in relation to the skeleton of reduced dimensions, give the new born a hydropic appearance and determine a disproportion between the almost normal-size head and the markedly reduced body length. The face appears flat, the neck rather short, the thorax narrow and the abdomen prominent. The limbs are markedly shortened with inturning of the hands and feet, similar to what occurs in DTD; in addition, the fingers and toes are short [146].

Atelosteogenesis type 2 (AO2) is a chondrodysplasia with intermediate severity between ACG1B and DTD. Affected foetuses present short limbs, abduction of feet, and the “hitchhiker's thumb”, typical of DTD patients. The disease is generally lethal at birth or shortly thereafter because of pulmonary hypoplasia due to the small rib cage [147]. The radiological features are similar to those found in DTD patients, with the addition, however, of a peculiar thinning of the distal humerus [148]. Before the first description of the pathology in 1987 by Sillence, it has been considered as a severe or lethal form of DTD, due to the many phenotypic similarities [149].

Recessive multiple epiphyseal dysplasia (rMED or EDMA4) is the mildest form of chondrodysplasias caused by mutations in *SLC26A2* gene. Patients affected by rMED shares only a few phenotypic features with DTD, such as clubfoot and hip dysplasia at birth. At the same time, they present normal stature and do not show cleft palate, spinal deformity, and "hitchhiker's thumb". During puberty, they develop hip pain and mild hand and feet deformations, as well as multiple epiphyseal dysplasia with double-layered patella on lateral knee [150].

The classification of the different chondrodysplasias associated with mutations of *SLC26A2* gene occurs mainly on a clinical and phenotypic basis; in fact, a molecular classification would not be possible since all disorders are determined by mutations in the same gene. Furthermore, the phenotypic spectrum of these chondrodysplasias is highly variable and a continuous gradient of severity can be observed starting from very severe forms (ACG1B) to relatively benign conditions (rMED) [151]. Genotype-phenotype correlations can be identified, but the phenotypic severity of the disease is not only due the *SLC26A2* mutations, since relevant phenotypic differences have been observed in patients presenting the same mutation [152].

2.2.2. Pathogenesis of SLC26A2 disorders

As mentioned above, functional impairment of the SLC26A2 transporter can lead to the onset of four chondrodysplasias, causing changes in the composition, architecture and mechanical properties of cartilage extracellular matrix. In particular, impaired function of the SLC26A2 transporter causes a reduced uptake of sulfate in chondrocytes. The intracellular sulfate pool mainly comes from uptake of circulating sulfate that occurs through tissue specific carrier proteins, present on the cell membrane. Sulfate transporters have been identified in the intestinal epithelium, renal tubular epithelium, hepatocytes and fibroblasts [153]. Specifically, due to its negative charge, extracellular sulfate is transported to the cytoplasm through specific anion transporters, such as sulfate/chloride antiporter and sodium/sulfate symporter [154, 155].

Among the different sulphate transporters, the diastrophic dysplasia sulfate transporter (DTDST) also defined SLC26A2 (solute carrier family 26 member 2), is a sulfate/chloride antiporter expressed in different tissues **(Figure 1.14)** [144].

In human, plasma concentration of sulfate is maintained at approximately 250–400 μM, by intestinal absorption and by kidneys, which filter sulfate in the glomerulus and then reabsorb it in the proximal tubule [154, 156]. Sulfate plasma concentration may vary according to several physiological conditions such as age [157] or diseases [158]. For example during pregnancy

[159], plasma level of sulfate increase while it decrease in some neurological diseases such as Alzheimer's, Parkinson's or moto neuron disease [160].

Alternatively, intracellular sulfate comes in small amount from the catabolism of sulfur-containing amino acids, such as cysteine and methionine, and other thiols or from the degradation of sulfated molecules through sulfatases **(Figure 1.14)** [66].

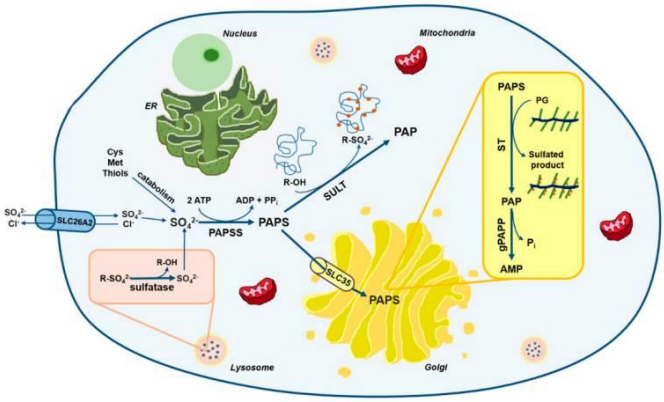

Figure 1.14: Schematic representation of sulfate metabolism in cells.
Intracellular sulfate level mainly depends on extracellular uptake through membrane transporters such as SLC26A2. In addition, a small amount of sulfate may come from the metabolism of sulfur-containing amino acids and thiols or from sulfatases in lysosomes. Once in cell, sulfate is activated to PAPS, the universal sulfate donor, by PAPS synthase II. PAPS moves to Golgi through different transporters, such as the solute carrier family 35B2 and B3 (SLC35B2 and SLC35B3), where it is used for macromolecular sulfation, especially GAGs, catalyzed by sulfotransferases (STs) [66].

The intracellular pool of sulfate in chondrocytes, mainly comes from the extracellular environment and only a small amount from the intracellular catabolism of thiols [154]. For this reason, a reduced intracellular sulfate content is found in cartilage of patients with diastrophic dysplasia, which cause the undersulfation of proteoglycans [161].

This leads to an impairment of the composition, architecture, signalling and mechanical properties of the cartilaginous ECM, since this tissue is particularly rich in PGs, which under normal conditions are highly sulfated. This condition results in the onset of chondrodysplastic phenotypes that exhibit a high degree of variability associated with residual sulfate transporter function. In fact, there is a correlation between the extent of PG undersulfation and different clinical phenotypes [152].

Patient's cartilage presents a reduced ECM volume, which corresponds to an increase in cell density. Furthermore, the lack of sulfated PGs leads to a reduced recall of water into the tissue and to collagen fibres unmasking [162].

These data demonstrate that SLC26A2 is the main sulfate transporter in chondrocytes. However, it is still not well understood why only cartilage tissue shows impairments associated

with the presence of *SLC26A2* mutations, while other PG-rich tissues such as the cornea show no abnormalities. This probably occurs because other cell types might use other sulfate sources or express different sulfate transporters on the cell membrane. For example in DTD patient renal tubular secretion and absorption are normal since these process depend by the presence of other transporters such as SLC13A1 and SLC26A1, as demonstrated by normal plasma and urine levels of sulfate [154].

The degree of functional impairment of SLC26A2 are related to mutations with different consequences on the protein; a strong correlation between the clinical phenotype of SLC26A2 chondrodysplasias and the level of residual transport function has been demonstrated [163]. In fact, individuals with achondrogenesis 1B have null mutations on both SLC26A2 alleles, while heterozygotes for a null mutation and a partial loss of function mutation result in either atelosteogenesis type 2 or DTD; finally the milder, recessive multiple epiphyseal dysplasia phenotype is homozygous for partial loss of function mutations [150, 163].

2.2.3. The sulphate/chloride antiporter SLC26A2

The *SLC26A2* gene coding sequence is organized into two exons, separated by an intron of approximately 1.6 kb and encodes for a protein of 739 amino acids [144]. The structure and function of this transporter has been clarified thanks to the homology of SLC26A2 with Sat-1 or SLC26A1, a sulfate transporter present in rat hepatocytes [164]. Thus, the presence of twelve transmembrane domains and a hydrophobic domain in the C-terminal cytoplasmic portion, probably associated with the plasma membrane, has been inferred **(Figure 1.15)** [144].

SLC26A2 is a cell membrane transporter expressed in many tissues [165]; however, the main phenotypic consequences of its functional impairment are limited to bone and joints [166], in which a high sulfate requirement is fundamental for the production of highly sulphated PGs of the cartilage ECM.

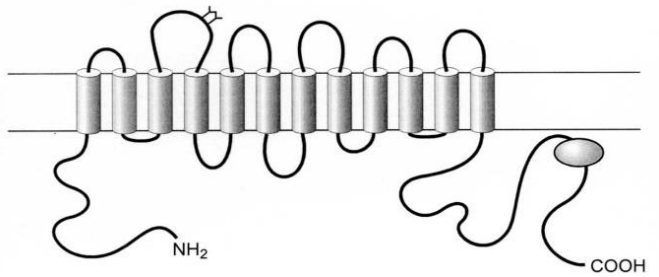

Figure 1.15: Schematic representation of the SLC26A2 transporter.
Sulfate/chloride antiporter SLC26A2 is a cell membrane transporter composed of twelve transmembrane domains and a C-terminal hydrophobic membrane-associated domain [165].

2.2.4 The dtd mouse

The homozygous mutant mouse, named dtd mouse, is an animal model of human DTD.
The transgenic mouse was generated by homologous recombination in embryonic stem cells. To obtain the A386V amino acid substitution in the transmembrane domain of the DTDST, a C1184T transition was introduced via site-directed mutagenesis into a cloned fragment of exon 3. This missense mutation was already found at the homozygous state in a patient with diastrophic dysplasia [161].
The knock-in mouse, homozygous for the mutation, recapitulate the peculiar features of the DTD phenotype in human, presenting growth retardation, which leads to a reduced length of the long bones, thoracic kyphosis that causes deformities of the rib cage, bite overclosure and hip dysplasia **(Figure 1.16)** [161].

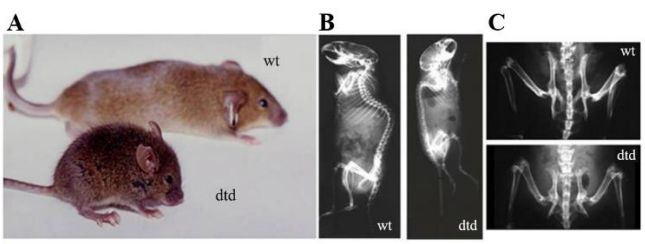

Figure 1.16: Morphological phenotype of dtd mouse compared to wild-type. The dtd mouse is a knock-in mouse harbouring the A386V substitution. It shows typical features of patients with DTD such as **(A)** short stature, growth retardation, **(B)** kyphosis and **(C)** hip dysplasia. (*Adapted from Forlino et al. 2005*) [161].

Undersulfation of PG from dtd cartilage has been demonstrated at different ages. Even if there is a progressive increase in PG sulfation with aging, the alterations in cartilage are collective and a partial recovery of sulfation is not able to restore the pathological phenotype. PG undersulfation is caused by reduced sulfate uptake that has been observed in dtd chondrocytes, osteoblasts and fibroblasts cultures [161].
The overall architecture of the growth plate at birth and during the first 3 weeks of age is normal, with the presence of well-defined resting, proliferative and hypertrophic zones, even if chondrocytes of dtd mice present reduced and more variable size compared with wild-type cells. Disorganization of the growth plate is marked in adults, explaining the postnatal component of growth failure [161]. The formation of the secondary ossification centre shows a delay in mutant animals, indicating chondrocytes differentiation impairment. This hypothesis is further confirmed by reduced cell proliferation and apoptosis in the proliferative and hypertrophic

zones respectively of dtd mice growth plate. These data, together with the finding of reduced chondrocyte proliferation *in vitro*, suggest that reduced bone growth might be due to reduced chondrocyte proliferation and/or incomplete differentiation [161].

Moreover dtd mouse show an osteopenic phenotype. The indirect effect of abnormal cartilage on bone has been excluded, since PG undersulfation in dtd mice lead to an alteration in bone ECM causing an increase in osteoclasts resorption and reduction in osteoblast activity. Thus, the osteopenic phenotype is due to a primary bone defect [167].

In conclusion, the dtd mouse, recapitulating the skeletal phenotype of DTD patients, has been validated as a model to elucidate the pathogenesis of SLC26A2 disorders and to study potential pharmacological treatment for diastrophic dysplasia.

3. *In vitro* models

Generation and characterization of *in vivo* models has fundamental importance in the study of skeletal diseases, in order to deeply investigate their pathogenesis and development. In fact, the analysis of genetically modified animals provides a powerful method to study the role of gene products *in vivo*. However, given the complexity of animal models, specific molecular aspects of bone and cartilage biology have been investigated *in vitro* using primary cell cultures and tumour or immortalized cell lines. The use of *in vitro* models has various advantages, since they are easier to manipulate, allow a tight control of the chemical and physical environment, are less expensive, and mostly reduce the use of laboratory animals.

3.1. Primary cell cultures

Primary cell cultures are directly isolated from animal model tissues or human biopsies and cultured *in vitro*. They are a powerful tool to investigate specific aspects of a pathology. The use of cell cultures to study chondrocyte activity in both normal and pathological conditions represent a well-defined but sometimes not appropriate approach. This is partly due to the low cellularity of the cartilage tissue, which limits the supply of chondrocytes for research purposes. Furthermore, if cartilage is of human origin, regulatory and ethical issues arise regarding the collection and use of human tissues. However, the main drawback of using primary chondrocyte cultures is the phenotype instability with increased time in culture [168]. Indeed, these cells tend to de-differentiate as demonstrated by the progressive reduction of the expression levels of the main chondrocyte markers (type II and type IX collagen, COMP) with passage in culture. In particular, they change from a round to a flattened fibroblast-like shape, and start to synthesise type I collagen instead of the cartilage-specific type II [169].

For this reason, different culture systems have been studied to maintain the chondrocyte phenotype. Among these the high density aggregate culture methods [170] or the use of co-culture of chondrocytes with mesenchymal stem cells [171]. However, even if these methods reduce the de-differentiation of primary chondrocytes, they do not guarantee the complete maintenance of their phenotype [170]. Thus, the use of three-dimensional gel culture systems have been introduced, with the aim of favouring the re-differentiation of de-differentiated chondrocytes; among these, gels containing hyaluronic acid [156], agarose [157], alginate [158], and a combination of alginate and collagen [159] have been described. These culture systems stabilize the cell phenotype, as demonstrated by the maintenance of the chondrocyte morphology and the high expression of type II collagen and PGs, mainly aggrecan. However,

none of these culture systems is able to overcome the limitation in cell supply, since cells do not proliferate [172].

3.2. Cell lines

To overcome the limits of primary cell culture described above and study the biomolecular mechanisms underlying chondrogenesis in pathophysiological conditions, also different cell lines can be used. In general, the term "cell line" identifies a well-defined population of cells, which can be maintained in culture for a long period, preserving their functional and phenotypic stability. Generally, cell lines are clonal, meaning that the entire population originate from a single common ancestor cell that gives rise to a transformed cell population with an unlimited proliferative capacity. This characteristic may be due to an immortalization process performed in the laboratory or to the fact that the cell line derives from an animal or human tumorigenic source, establishing a tumour cell line. The use of cell lines has several advantages, as they are homogeneous cells, with well-defined characteristics, are easier to culture and they grow vigorously. Furthermore, the use of cell lines guarantees high reproducibile experiments.
Among the tumour cell lines, a valid *in vitro* model is represented by ATDC5 cells, isolated from murine teratocarcinoma fibroblastic cells. These cells easily proliferate, maintaining an undifferentiated state during expansion. In this way, it is possible to obtain a huge number of cells to set up *in vitro* culture systems that reproduce chondrocyte condensation during *in vivo* chondrogenesis [173]. Furthermore, the ATDC5 cell line reproduces all the chondrogenic differentiation steps that occurs during the endochondral ossification process [174]. This is demonstrated, in the early differentiation stage, by the secretion of type II collagen, aggrecan and other ECM components. Subsequently, in the late stage of differentiation, these cells reach the hypertrophic phenotype, as demonstrated by the increase of type X collagen production, followed by extracellular matrix mineralization [173]. Due to these properties, ATDC5 cells have been used as an *in vitro* model for numerous studies, with the aim of investigating molecular defects of several pathological conditions affecting bone and cartilage tissue, such as, for example, aggrecanopathies [175].

Another chondrogenic cell line is the one derived from the Swarm rat chondrosarcoma (RCS). RCS tumour cells produce several macromolecules of hyaline cartilage ECM, including aggrecan, type II and type IX collagen, link protein, hyaluronic acid, COMP, and fibronectin. This cell line has been used to study the cartilage ECM, in particular to deeply investigate aspects related to the biosynthesis, organization and interaction of its components [176, 177].

Furthermore, it has been used for the isolation and analysis of cartilage molecules, such as metalloproteases [178] and CD-RAP (Cartilage-derived retinoic acid-sensitive protein) [179].

3.3. Immortalized cell lines

To obtain a surrogate model for the study of cartilage tissue biology, which preserve the chondrocytic phenotype, immortalized chondrocytes, derived from human controls or wild-type mice have been generated [168]. Immortalized cell lines consist of artificially manipulated cells that to proliferate indefinitely over time.

To date, several immortalization strategies are known. The most used techniques involve the cell transfection with viral oncogenes, oncoproteins or the enzyme telomerase (TERT), which catalyses the synthesis of telomeric DNA starting from an RNA template [180]. Viral oncogenes can inhibit the cellular senescence process by inactivating the tumour suppressors p53 and pRb, the retinoblastoma protein. These two proteins are fundamental in cell cycle control, as they regulate the balance between proliferation and apoptosis. When these are inhibited, pro-apoptotic pathways are not activated, resulting in constitutive activation of the cell cycle and unlimited cell proliferation [181]. On the other hand, transfection with TERT, an enzyme physiologically absent or poorly expressed in primary cells, blocks cellular senescence by preventing the shortening of telomeres in the chromosomes, extending cell life [180].

There are several methods of gene transfer used to introduce viral genes and proteins into cells. The most used are plasmid transfection or transduction with viral vectors. Plasmid transfection is an easier method, which allows to obtain a stable cell immortalization.

The most common transduction approaches involve the use of viral vectors such as lentiviral and retroviral vectors. Lentiviral vectors derived from the Human Immunodeficiency Virus (HIV) can be used for efficient immortalization of dividing and non-dividing cells, which maintain cell differentiation even after the procedure. Retroviral vectors, such as Moloney Murine Leukemia Virus (Mo-MLV) derived vectors, have the main advantage of stable integration of the immortalization gene, which is also efficiently transmitted to the progeny, without activation of the immune response [182].

One of the most used viral vectors is the Simian Vacuolating Virus 40 (SV40), consisting of two proteins, the small T antigen (ST) and the large T antigen (LT). The latter is essential, as it is able to interact with p53, inhibiting its pathway and to pRb, hindering its binding to the transcription factor E2F, important in the progression of the cell cycle. Furthermore, LT is able to interact with TERT, leading to the formation of genetically stable cells [180]. Another frequently used viral vector is the Human Papilloma Virus (HPV), a small DNA virus. In

particular, the E6 oncoprotein, which causes telomerase enzyme activation and speed up p53 degradation by the proteasome, and the E7 oncoprotein, which inactivate pRb, preventing its binding to E2F, are used. Finally, a further approach involves the use of oncogenes of myc family, which include the c-myc, N-myc, L-myc and B-myc genes. The c-myc oncogene can be used for immortalization alone, or in association with other oncoproteins or TERT [180].

Immortalized chondrocyte lines generated through these different strategies have been characterized with the aim of evaluating whether, in addition to providing a huge cell number they show a stable chondrocyte phenotype. The data available suggest that these cells maintain the chondrogenic differentiation, as demonstrated by the expression of type II collagen and PGs [183]. However, the phenotype stability can often be affected by the physicochemical conditions, such as temperature, humidity and CO_2 levels or by the culture system used, whether monolayer or 3D and in the latter case, also by the biomaterial used as scaffold [168, 184, 185].

Immortalized cell lines can be further modified, by knocking down specific genes through RNA interference or gene editing. This approach is also used for other *in vitro* models, such as ATDC5 cells and Swarm rat chondrosarcoma cells illustrated above, in order to evaluate the involvement of specific gene products in pathological mechanisms of cartilage. Nonetheless, this approach has some limitations, since it requires further sub-culturing to obtain genetically modified clonal lines, with the risk of non-specific off-target effects [172].

A strategy to overcome the problems related to gene knock-down or knock-out may be to immortalize chondrocytes from mouse models of genetic skeletal disorders. This would provide a simple and well characterized *in vitro* model to study alterations in ECM protein synthesis and assembly, and putative skeletal diseases pathways [172].

CHAPTER II

Research objectives

Skeletal dysplasias are a huge heterogeneous group of genetic diseases that mainly affect cartilage and bone. They are caused by mutations in different genes important for skeleton development, maintenance and turn-over including extracellular matrix proteins, enzymes, cellular transporters, transcription factors, signal transducers, channel proteins, chaperones, cytoplasmic proteins, cilia, proteins involved in cell cycle, and chromatin modifying enzymes. Since skeletal dysplasias are rare diseases affecting a small number of patients, skeletal tissue biopsies are rarely available, making difficult the elucidation of their molecular basis that nowadays are poorly understood.

Therefore, different *in vivo* and *in vitro* models have been developed in order to study the biology of cartilage in normal and pathological conditions. Analysis of genetically modified mice and/or zebrafishes provides a strong approach to elucidate the role of gene products *in vivo*. However, due to the complexity of the animal model, *in vitro* studies are a powerful tool to investigate specific aspects of cartilage biology. Moreover, the use of *in vitro* models allows to reduce the number of sacrificed animals, according to the principle of the Three Rs (https://www.nc3rs.org.uk/), and the time for the experiments.

Among cartilage ECM components, proteoglycans are the most abundant and fundamental proteins. They play several roles maintaining cartilage physical and mechanical properties; moreover, PGs can bind growth factors regulating chondrocyte proliferation and differentiation. Alteration in PG synthesis, due to mutations in genes encoding for the core proteins or enzymes and other proteins involved in this complex process, lead to the onset of genetic diseases most of them affecting cartilage.

In this work, two different chondrodysplasias, in which proteoglycan synthesis is impaired, has been studied: Desbuquois dysplasia type 1 (DBQD1) and diastrophic dysplasia (DTD). In both disorders, PG glycosylation is affected at different levels: in DBQD1 GAG synthesis is impaired, while in DTD GAG sulfation is reduced. Our knowledge about the two disorders is different; the molecular basis of DBQD1, whose causative gene *CANT1* has been discovered in 2009 [122], are still far from complete. Conversely, our molecular understanding of DTD, whose causative gene *SLC26A2* has been identified in 1994 [165], allows the identification of potential therapeutic approaches.

Thus, in this work different *in vivo* and *in vitro* models, including primary and immortalized chondrocytes and two mouse models, have been used to pursue the following objectives:

I. the study of CANT1 role in PG processing and organelle homeostasis to clarify its involvement in Desbuquois dysplasia type 1 pathogenesis, using the *Cant1*$^{-/-}$ mouse, an animal model for the human disorder;

II. the validation of immortalized *Cant1*$^{-/-}$ chondrocytes as an *in vitro* model to study specific aspects of CANT1 role in PG biosynthesis;

III. the evaluation of a postnatal treatment with N-acetylcysteine in a mouse model of DTD to develop a new pharmacological treatment for this disease.

CHAPTER III: Characterization of proteoglycan processing and Golgi homeostasis in a *Cant1* knock-out mouse

1. Aim of the work

Desbuquois dysplasia type 1 is a rare recessive chondrodysplasia caused by mutations in *CANT1* gene, encoding for a calcium-activated nucleotidase 1 of the Golgi apparatus [122].

To study the physiological role of CANT1 and to clarify its involvement in DBQD1 pathogenesis, an animal model for the human disorder, the *Cant1* knock-out mouse (*Cant1*$^{-/-}$) was generated and characterized [117].

Using the animal model, the role of CANT1 in PG biosynthesis was recently demonstrated, since reduced PG synthesis and oversulfated GAGs, with reduced hydrodynamic size, were observed in chondrocytes and cartilage from mutant animals [117]. Moreover, mutant chondrocytes in both primary cultures and cartilage showed dilated ER cisternae full of electrondense materials **(Figure 3.1)**, suggesting delayed protein secretion and the presence of ER stress with the activation of the unfolded protein response (UPR) pathways. This hypothesis was not confirmed since the expression of the markers of canonical ER stress and UPR including Bip and ATF4 were normal and the spliced form of Xbp1 was not present [117].

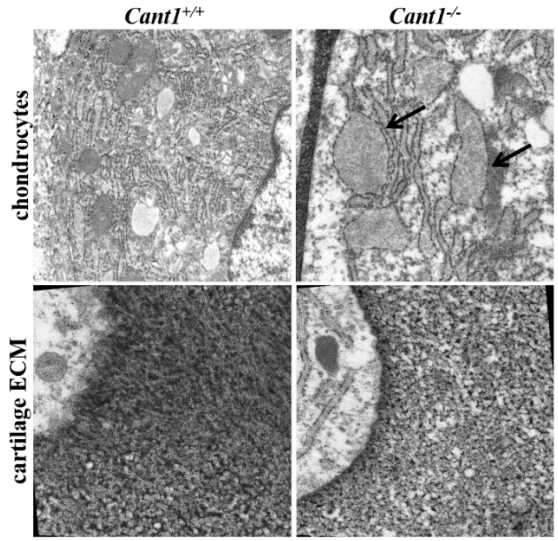

Figure 3.1: ER enlargement in *Cant1*$^{-/-}$ chondrocytes.
Transmission electron microscopy (T.E.M.) analysis of *Cant1*$^{-/-}$ and *Cant1*$^{+/+}$ cartilage. *Cant1*$^{-/-}$ chondrocytes showed huge vacuoles and ER enlargement with the accumulation of electrondense material. *Cant1*$^{-/-}$ cartilage showed a less dense ECM compared to *Cant1*$^{+/+}$ [117].

These observations suggested that the ER enlargement was not due to ER stress, but more likely to the impaired GAG synthesis in the Golgi.

Based on these observations and hypothesis the aims of this work were:

I. to further characterize the defect in PG biosynthesis by analysing the kinetics of PG secretion and the intracellular processing of aggrecan;

II. to study the homeostasis of other organelles involved in chondrocyte proteostasis, in particular the Golgi apparatus by analysing the activation of its potential stress pathways, since CANT1 is mainly a Golgi protein and GAG synthesis occurs in this organelle.

2. Results

2.1. Analysis of proteoglycan secretion in *Cant1*$^{-/-}$ chondrocytes

The defects observed in PG synthesis linked to GAG quantity, oversulfation and hydrodynamic size and the ER enlargement observed in *Cant1*$^{-/-}$ chondrocytes suggested to further study their metabolism, considering PG secretion in the extracellular space by a pulse chase experiment. Primary chondrocytes extracted from the ribs of *Cant1*$^{-/-}$ and wild-type (*Cant1*$^{+/+}$) mice were incubated with ^{35}S-sulfate for 2 hours. At the end of the incubation, the medium was replaced with medium containing an excess of cold sulfate and cells were harvested at different time points: 0.5, 2.5 and 5 hours. The percentage of ^{35}S-labelled PGs in the medium to total labelled PGs (in medium and cell layer) was measured for each time point. Results demonstrated a significant reduction in PG secretion in *Cant1*$^{-/-}$ chondrocytes compared with *Cant1*$^{+/+}$ cells **(Figure 3.2)**.

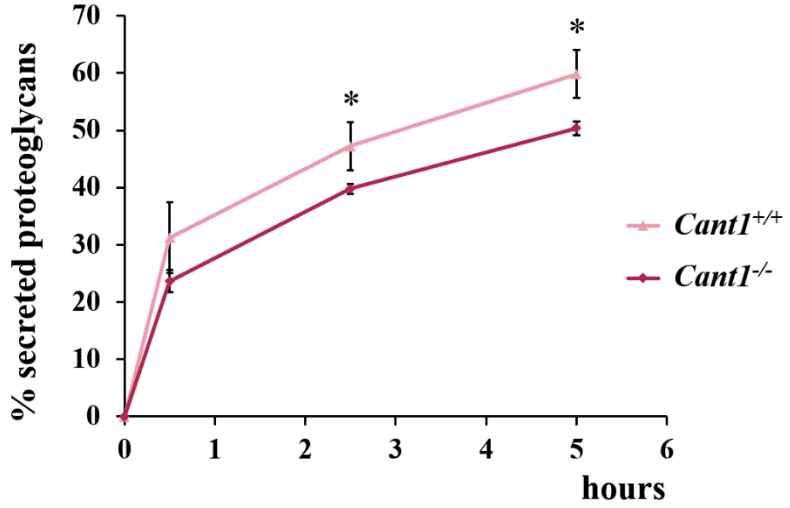

Figure 3.2: Proteoglycan secretion is reduced in *Cant1*$^{-/-}$ chondrocytes.
PG secretion was analyzed by a pulse chase experiment. Chondrocytes were metabolically labelled with ^{35}S-sulfate for 2 hour, and then the medium was replaced with medium containing cold sulfate. Cells were harvested after 0.5, 2.5, 5 hours, and the percentage of ^{35}S-PGs in the medium to labelled PG in medium and cell layer was measured. *Cant1*$^{-/-}$ chondrocytes showed a delayed PG secretion compared with *Cant1*$^{+/+}$ cells. Data are reported as mean ± standard deviation. Significance among samples was analyzed by Student's t-test; * $p < 0.05$. n = 3

2.2. Analysis of total protein secretion in *Cant1*$^{-/-}$ chondrocytes

The reduced PG secretion observed in *Cant1*$^{-/-}$ chondrocytes suggested a possible impairment of the secretion of all proteins synthesized by these cells. For this reason, total protein secretion was studied in primary cultures of chondrocytes extracted from the ribs of *Cant1*$^{-/-}$ and *Cant1*$^{+/+}$ mice. In a pulse chase experiment, chondrocytes were incubated with medium containing a mixture of [^{35}S]-cysteine and [^{35}S]-methionine (Express ^{35}S Protein Labeling Mix). After 1 hour incubation, the medium was replaced with medium containing an excess of cold cysteine and methionine and cells were harvested at different time points: 1, 2.5, 5 and 8 hours. The percentage of ^{35}S-labeled proteins secreted in the medium to the total (medium and cell layer) was then measured for each time point. However, no differences in total protein secretion were observed in *Cant1*$^{-/-}$ chondrocytes compared to *Cant1*$^{+/+}$ chondrocytes **(Figure 3.3)**.

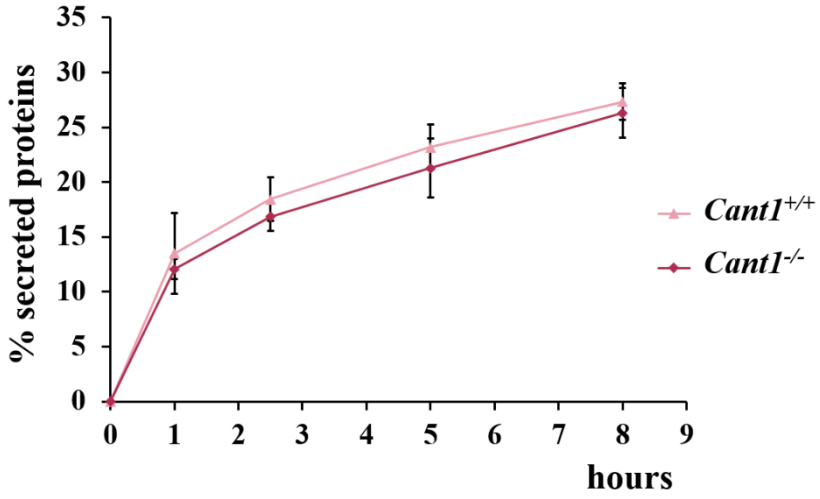

Figure 3.3: Total protein secretion is not impaired in *Cant1*$^{-/-}$ chondrocytes.
Total protein secretion was analyzed by a pulse chase experiment. Chondrocytes were labelled with [^{35}S] Express Protein Labeling Mix, and then the medium was replaced with medium containing cold cysteine and methionine. Cells were harvested after 1, 2.5, 5 and 8 hours, and the percentage of ^{35}S-protein secreted in the medium to the total (medium and cell layer) was measured. Total protein secretion was not delayed in *Cant1*$^{-/-}$ chondrocytes compared with *Cant1*$^{+/+}$ cells. Data are reported as mean ± standard deviation. Significance among samples was analyzed by Student's t-test; n = 3.

2.3. Analysis of aggrecan processing in *Cant1*$^{-/-}$ chondrocytes

To further characterize the defect in PG secretion, the processing of aggrecan, the most expressed PG in cartilage, was analyzed by Western blots of cell lysates from *Cant1*$^{-/-}$ and

Cant1$^{+/+}$ chondrocytes **(Figure 3.4 A)**. Densitometric analysis of the aggrecan band, normalized to actin, demonstrated that the intracellular level of this PG was significantly higher in *Cant1*$^{-/-}$ chondrocytes compared to *Cant1*$^{+/+}$ cells ($p = 0.005$) **(Figure 3.4 B)**, suggesting the accumulation of this molecule in mutant cells.

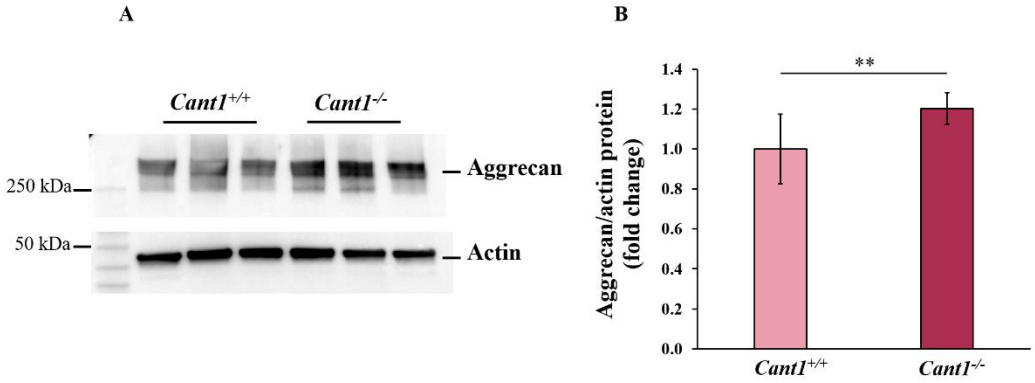

Figure 3.4: Intracellular aggrecan level is increased in *Cant1*$^{-/-}$ chondrocytes.
(A) Cell lysates from *Cant1*$^{-/-}$ and *Cant1*$^{+/+}$ chondrocytes were analyzed by Western blot, using a specific antibody against the aggrecan core protein. **(B)** Densitometric quantification of the bands demonstrated a significantly higher level of aggrecan in *Cant1*$^{-/-}$ chondrocytes compared to *Cant1*$^{+/+}$ cells. The aggrecan band was normalized to the Actin band. The band intensity of *Cant1*$^{+/+}$ samples was set to one and the expression of *Cant1*$^{-/-}$ samples was reported as a fold change. Data are reported as mean ± standard deviation of three independent experiments. Significance among samples was analyzed by Student's t-test; ** $p < 0.01$; n = 3.

Moreover, since GAG synthesis is a fundamental step in aggrecan post-translational processing, its glycosylation was investigated by Western blot analysis. Cell layer and medium proteins of primary *Cant1*$^{-/-}$ and *Cant1*$^{+/+}$ chondrocytes were splitted into two aliquots, one digested with the chondroitinase ABC to unmask the epitope of the specific antibody by removing the GAGs linked to the aggrecan core and one undigested. Then samples were analyzed by Western blot, comparing the aliquot digested with chondroitinase ABC with the undigested one.

An approximately 245 kDa band, corresponding to aggrecan core protein, was observed in medium samples, both *Cant1*$^{-/-}$ and *Cant1*$^{+/+}$, digested with chondroitinase ABC, while no band was observed in all undigested samples **(Figure 3.5 A)**. This result demonstrated that only glycanated aggrecan is secreted by *Cant1*$^{-/-}$ chondrocytes, as in *Cant1*$^{+/+}$ cells, despite the defect in GAG synthesis.

In *Cant1*$^{-/-}$ and *Cant1*$^{+/+}$ cell layer samples a band corresponding to aggrecan core protein was observed in both digested and undigested aliquots **(Figure 3.5 B)**. Densitometric analysis of

both aliquots demonstrated similar aggrecan band intensity, suggesting that aggrecan inside mutant (*Cant1*$^{-/-}$) and wild-type cells was in the unglycanated form and that, once glycanated, it was immediately secreted in the extracellular space.

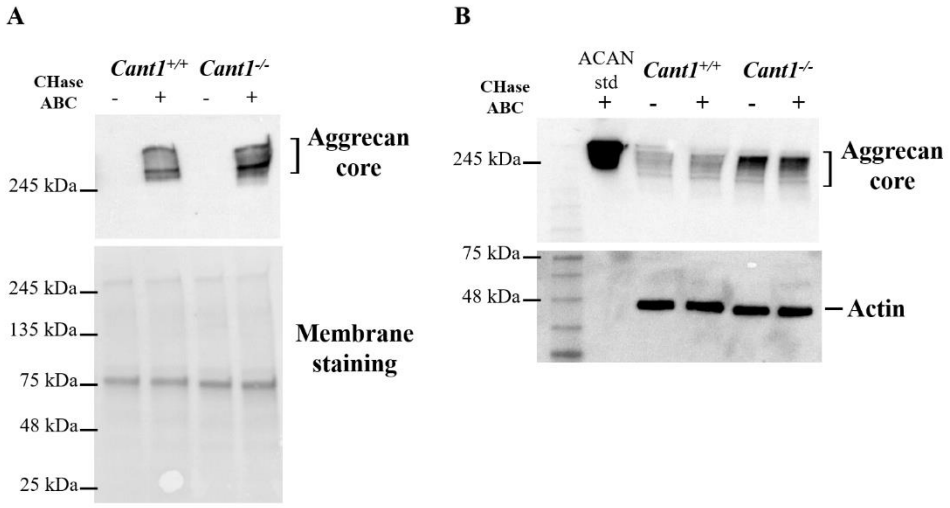

Figure 3.5: Only glycanated aggrecan is secreted in *Cant1*$^{-/-}$ and *Cant1*$^{+/+}$ chondrocytes.
Medium **(A)** and cell layer **(B)** proteins from *Cant1*$^{-/-}$ and *Cant1*$^{+/+}$ chondrocytes were analyzed by Western blot, using a specific antibody against the aggrecan core protein. Each sample was splitted into two aliquots, one digested with chondroitinase ABC (CHase ABC) and the other undigested. As loading controls total protein staining and an Actin antibody were used for medium and cell layer samples, respectively. **(A)** In *Cant1*$^{-/-}$ and *Cant1*$^{+/+}$ medium samples, the band corresponding to aggrecan core protein was observed only in aliquots digested with chondroitinase ABC, demonstrating that only glycanated aggrecan was secreted. **(B)** In *Cant1*$^{-/-}$ and *Cant1*$^{+/+}$ cell layer samples a band in both digested and undigested aliquots was observed; since the two bands had similar intensity, most aggecan inside cells was in the unglycanated form. Data are representative of three independent experiments. ACAN std = aggrecan core standard.

2.4. Analysis of Golgi homeostasis in *Cant1*$^{-/-}$ chondrocytes

The presence of morphological alterations of the endoplasmic reticulum, without activation of the UPR pathways, suggested to analyse other potential cellular stress conditions. In particular, we focused on Golgi homeostasis based on the observations that: i) there is a tight crosstalk between ER and Golgi, ii) CANT1 is mainly a Golgi protein and iii) GAG synthesis occurs in this organelle.

Golgi homeostasis and morphology were investigated analysing the expression of the Golgi structural proteins GM130 and Golgin-97, cis and trans Golgi markers respectively.

Chondrocytes cell lysates of *Cant1*$^{-/-}$ and *Cant1*$^{+/+}$ cells were analyzed by Western blot using specific GM130 and Golgin-97 antibodies **(Figure 3.6 A)**. Densitometric analysis of the bands

demonstrated a significant increase of GM130 expression in *Cant1*$^{-/-}$ chondrocytes compared with *Cant1*$^{+/+}$ cells ($p = 0.038$) **(Figure 3.6 B)**. An increase of Golgin-97 expression in *Cant1*$^{-/-}$ chondrocytes compared with *Cant1*$^{+/+}$ cells was observed even if the difference was not significant ($p = 0.22$) **(Figure 3.6 C)**.

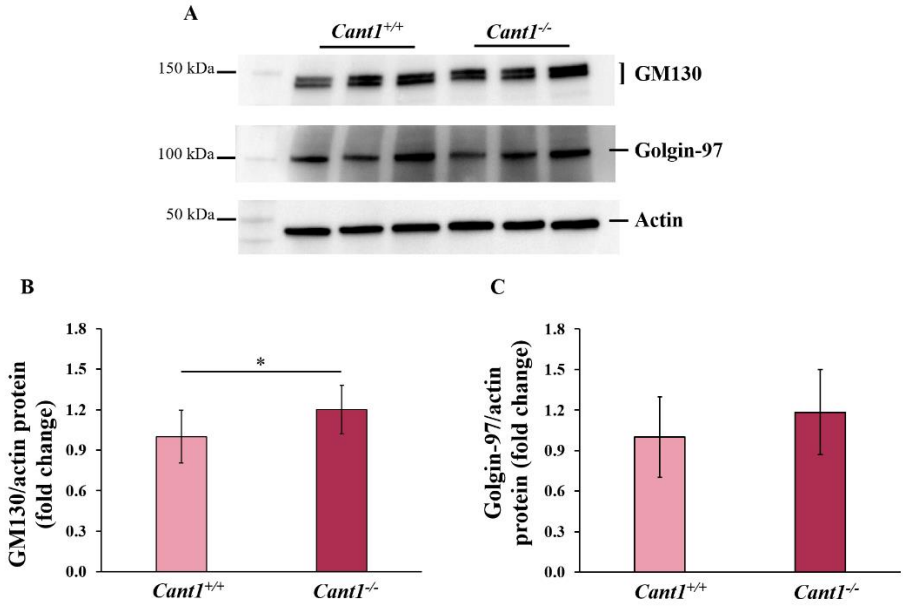

Figure 3.6: Expression of Golgi marker was higher in *Cant1*$^{-/-}$ chondrocytes.
(A) Western blot analysis of GM130 and Golgin-97, cis and trans Golgi marker respectively, was performed in *Cant1*$^{-/-}$ and *Cant1*$^{+/+}$ chondrocyte cell lysates. Densitometric quantification of the bands demonstrated a significantly increased expression of GM130 **(B)** in *Cant1*$^{-/-}$ chondrocytes compared to *Cant1*$^{+/+}$ cells, while an increase of Golgin-97 expression, even if not significant, was observed in *Cant1*$^{-/-}$ chondrocytes **(C)**. The GM130 and Golgin-97 bands were normalized to the Actin band. The band intensity of *Cant1*$^{+/+}$ samples was set to one and the expression of *Cant1*$^{-/-}$ samples was reported as fold change. Data are reported as mean ± standard deviation of three independent experiments. Significance among samples was analyzed by Student's t-test; * $p < 0.05$; n = 3.

In order to confirm these data, the expression of the two Golgi markers was also studied by confocal microscopy **(Figure 3.7 A)**. Quantification of the integrated fluorescence intensity demonstrated a significant increase of both GM130 **(Figure 3.7 B)** and Golgin-97 **(Figure 3.7 C)** expression in *Cant1*$^{-/-}$ chondrocytes compared to *Cant1*$^{+/+}$ cells ($p = 0.009$ and $p = 0.04$, respectively).

Moreover, quantification of the area of GM130 **(Figure 3.7 D)** and Golgin-97 **(Figure 3.7 E)** fluorescence demonstrated a significant increase of the cis and trans Golgi dimensions in *Cant1*$^{-/-}$ chondrocytes compared with *Cant1*$^{+/+}$ cells ($p = 0.0007$ and $p = 0.002$, respectively).

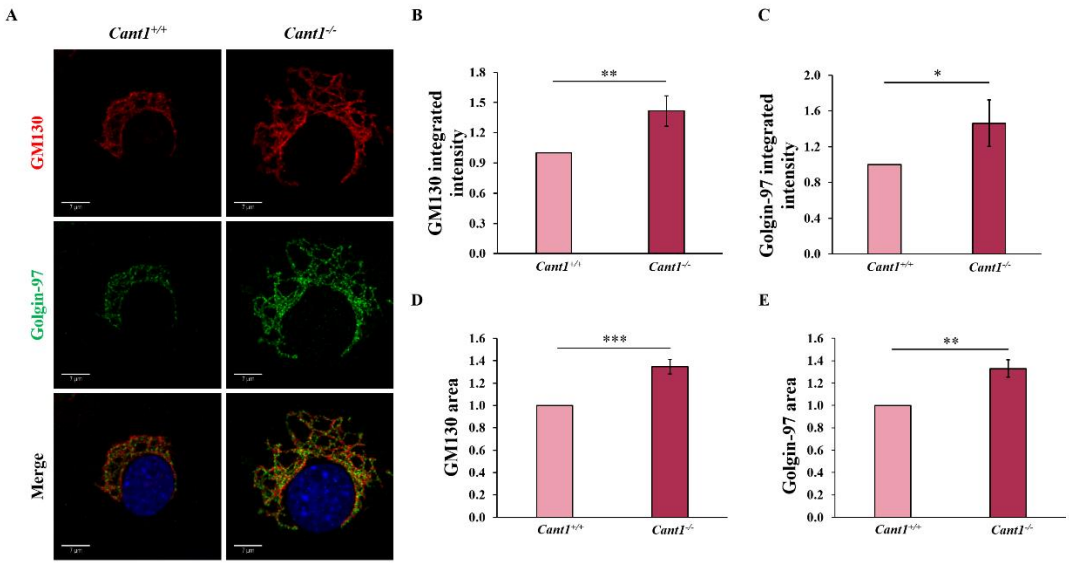

Figure 3.7: Expression of Golgi marker was higher in *Cant1*$^{-/-}$ chondrocytes.
(A) Immunofluorescence confocal microscopy of the cis and trans Golgi markers, GM130 and Golgin-97, was performed in *Cant1*$^{-/-}$ and *Cant1*$^{+/+}$ chondrocytes. Cells were double stained with antibodies against GM130 and Golgin-97. Quantification of the red (GM130) and green (Golgin-97) fluorescence demonstrated a significantly higher expression of GM130 **(B)** and Golgin-97 **(C)**, respectively in *Cant1*$^{-/-}$ chondrocytes compared with *Cant1*$^{+/+}$ cells. The green and red fluorescence in *Cant1*$^{+/+}$ cells was set to one and the expression of *Cant1*$^{-/-}$ samples was reported as fold change. Quantification of the red and green fluorescence area demonstrated a significant increase of the cis **(D)** and trans **(E)** Golgi dimensions, respectively in *Cant1*$^{-/-}$ chondrocytes compared with *Cant1*$^{+/+}$ cells. The green and red fluorescence area in *Cant1*$^{+/+}$ cells was set to one and the expression of *Cant1*$^{-/-}$ samples was reported as fold change. Data are reported as mean ± standard deviation of three independent experiments. Significance among samples was analyzed by Student's t-test; * $p < 0.05$, *** $p < 0.001$; n = 3. Scale bars 7 μm.

Overall this data, demonstrated that Golgi structure was altered in *Cant1*$^{-/-}$ chondrocytes, thus, Golgi homeostasis was investigated. To date, the molecular mechanisms of the Golgi stress response are poorly known; among them, activation and translocation into the nucleus of the transcription factor E3 (TFE3) has recently been described. Moreover, TFE3 activation is related to various cellular stress conditions. In normal conditions, TFE3 localizes in the cytosol and in presence of altered Golgi homeostasis, it is activated by dephosphorylation and translocates to nucleus, where it increases the expression of Golgi structural proteins, glycosylation enzymes and vesicular transport components.

In order to investigate the activation of TFE3 pathway, its localization in primary *Cant1*$^{-/-}$ and *Cant1*$^{+/+}$chondrocytes was analyzed by Western blot. Subcellular fractionation of chondrocyte cell lysates was performed to separate the cytosolic fraction, where the phosphorylated and inactive form of TFE3 is present, from the nuclear one, where TFE3 is active as a transcription factor. Then Western blot analysis of proteins from the total cell lysate, the cytosolic and the

nuclear fraction of *Cant1*$^{-/-}$ and *Cant1*$^{+/+}$chondrocytes was performed using an antibody against TFE3 **(Figure 3.8 A)**. Densitometric analysis demonstrated that the protein level of TFE3 in the *Cant1*$^{-/-}$ nuclear fractions was significantly increased compared to the *Cant1*$^{+/+}$ ones (p = 0.01), suggesting the activation of this transcription factor **(Figure 3.8 B)**. Conversely there were no differences in TFE3 protein level in the cytosolic fraction **(Figure 3.8 C)** and the total cell lysate **(Figure 3.8 D)** of *Cant1*$^{-/-}$ and *Cant1*$^{+/+}$chondrocytes. Since no difference in TFE3 expression in the total cell lysate of *Cant1*$^{-/-}$ and *Cant1*$^{+/+}$ cells was observed, the significant TFE3 increase in the nuclear fraction of mutant chondrocytes was due to its activation and not to its overexpression.

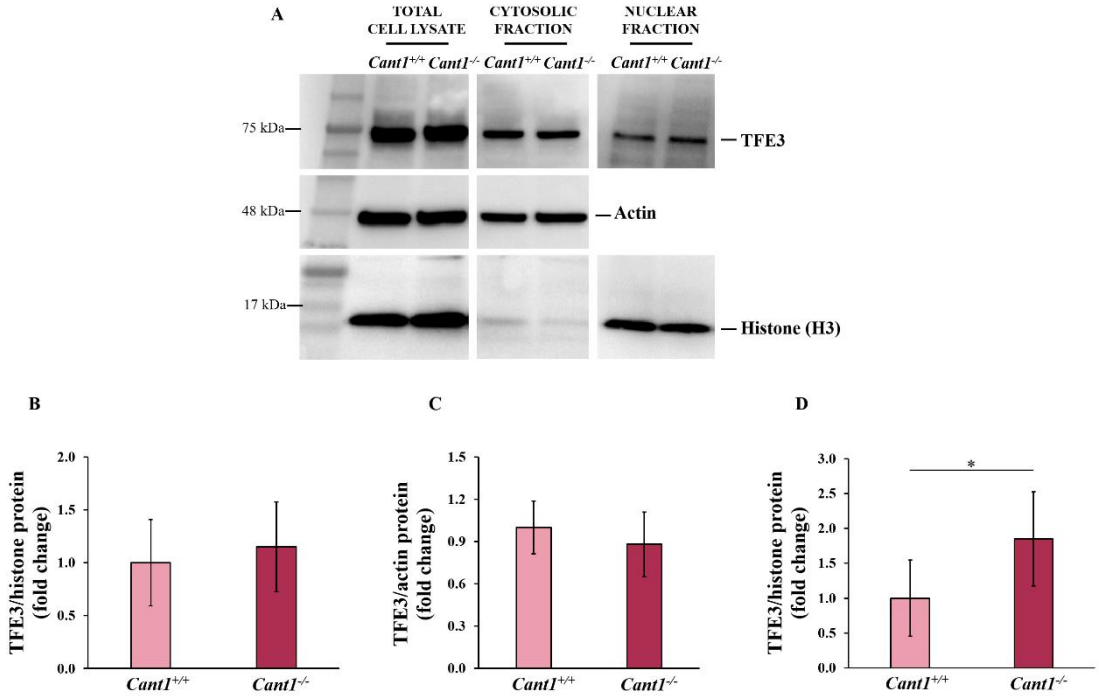

Figure 3.8: TFE3 pathway was activated in *Cant1*$^{-/-}$ chondrocytes.
(A) Western blot analysis of subcellular distribution of TFE3 was performed on protein extracted from the total cell lysate, cytosolic fraction and nuclear fraction. The subcellular fractionations were probed with antibodies against Histone H3, a nuclear marker and Actin, a cytosolic marker. Densitometric analysis of the bands demonstrated a significantly higher level of TFE3 in the nuclear fraction **(B)** of *Cant1*$^{-/-}$ chondrocytes compared to *Cant1*$^{+/+}$ cells, even if no differences were observed in the total lysate **(C)** and in the cytosolic fraction **(D)**. The TFE3 band was normalized to the Histone H3 band for the total lysate and nuclear fraction samples, while to the Actin band for the cytosolic fraction samples. The band intensity of *Cant1*$^{+/+}$ samples was set to one and the expression of *Cant1*$^{-/-}$ samples was reported as fold change. Data are reported as mean ± standard deviation of three independent experiments. Significance among samples was analyzed by Student's t-test; * $p < 0.05$; Representative images of n = 3 biological replicates.

To confirm the activation of TFE3 pathway, confocal analysis of *Cant1*$^{-/-}$ and *Cant1*$^{+/+}$ chondrocytes was performed using specific antibodies against TFE3, in order to study its subcellular distribution **(Figure 3.9 A)**. Quantification of TFE3 fluorescence in the nucleus of both *Cant1*$^{-/-}$ and *Cant1*$^{+/+}$ chondrocytes demonstrated that there is a significant increased level of TFE3 in the nucleus of *Cant1*$^{-/-}$ chondrocytes compared with *Cant1*$^{+/+}$ cells (p = 0.03). Moreover, in mutant and wild-type chondrocytes the nuclear TFE3 levels was significantly lower compared to a positive control made by chondrocytes treated for 6 hours with 5 µM monensin, a Golgi stress inducer **(Figure 3.9 B)**.

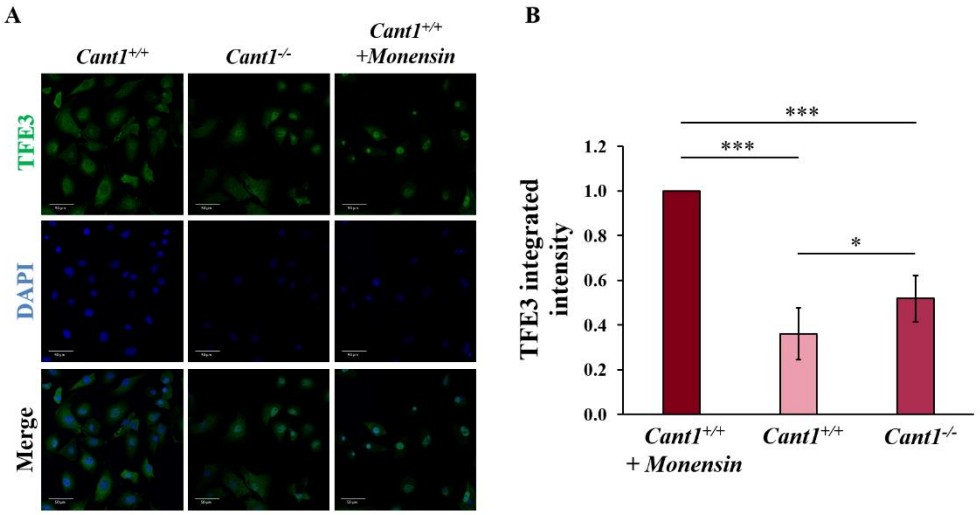

Figure 3.9: TFE3 pathway is activated in *Cant1*$^{-/-}$ chondrocytes.
(A) Cells were double stained with a TFE3 antibody and with DAPI and confocal microscopy analysis of the subcellular distribution of TFE3 in *Cant1*$^{-/-}$ and *Cant1*$^{+/+}$ chondrocytes was performed. **(B)** Quantification of the nuclear green fluorescence demonstrated a significant nuclear translocation increase of TFE3 in *Cant1*$^{-/-}$ chondrocytes compared with *Cant1*$^{+/+}$ cells. *Cant1*$^{+/+}$ cells treated with 5 µM monensin for 6 hour were used as positive control. The green fluorescence in nuclei of the positive control was set to one and the expression of *Cant1*$^{-/-}$ and *Cant1*$^{+/+}$ samples was reported as fold change. Data are reported as mean ± standard deviation of three independent experiments. Significance among samples was analyzed by Student's t-test; * $p < 0.05$, *** $p < 0.001$; n = 3. Scale bars 50 µm.

To further confirm the nuclear translocation of TFE3 in mutant cells, immunofluorescence analysis was also performed after cells incubation for 20 hours with 1 mM p-nitrophenyl β-D-xylopiranoside (β-D-xyloside), an enhancer of GAG synthesis **(Figure 3.10 A)**. Also in this culture condition, a significant increased nuclear translocation of TFE3 in *Cant1*$^{-/-}$ chondrocytes compared with *Cant1*$^{+/+}$ cells was observed (p = 0.024), as already detected in basal conditions. Moreover, a significant lower level of TFE3 was detected in the nucleus of both *Cant1*$^{-/-}$ and *Cant1*$^{+/+}$ chondrocytes compared to the positive control **(Figure 3.10 B)**.

Together these results demonstrated the activation of TFE3 pathway in *Cant1*$^{-/-}$ chondrocytes.

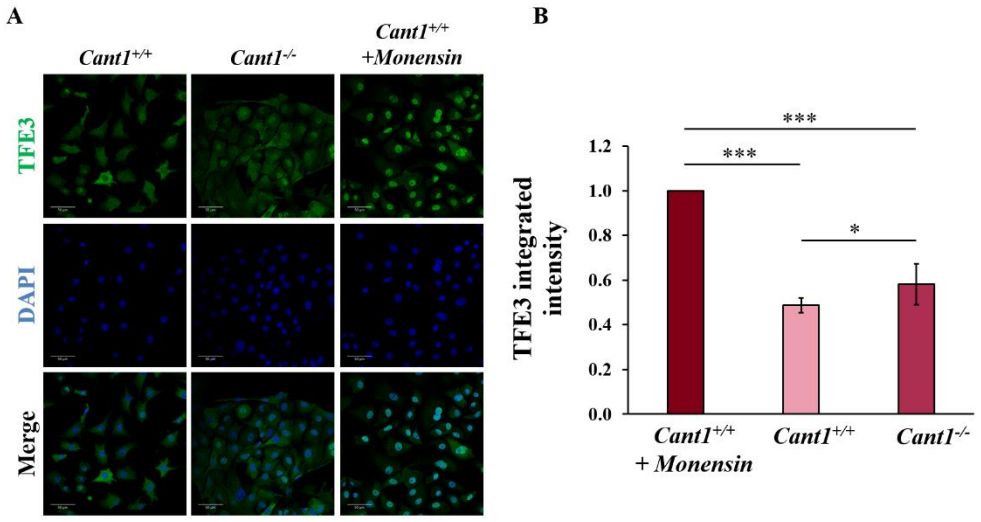

Figure 3.10: TFE3 pathway is activated in *Cant1*$^{-/-}$ chondrocytes after incubation with p-nitrophenyl β-D-xylopiranoside.
(A) *Cant1*$^{-/-}$ and *Cant1*$^{+/+}$ chondrocytes were treated with 1 mM β-D-xyloside for 20 hours and cells were analyzed by confocal microscopy after double staining with a TFE3 antibody and DAPI.
(B) Quantification of the green fluorescence in the nucleus demonstrated a significant increased nuclear translocation of TFE3 in *Cant1*$^{-/-}$ chondrocytes compared with *Cant1*$^{+/+}$ cells. *Cant1*$^{+/+}$ cells treated with 5 µM monensin for 6 hour were used as positive control. The green fluorescence in the nuclei of the positive control was set to one and the expression of *Cant1*$^{-/-}$ and *Cant1*$^{+/+}$ samples was reported as fold change. Data are reported as mean ± standard deviation of three independent experiments. Significance among samples was analyzed by Student's t-test; * $p < 0.05$, *** $p < 0.001$; n = 3. Scale bars 50 µm.

2.5. Analysis of lysosomal activation in *Cant1*$^{-/-}$ chondrocytes

To further study the homeostasis of organelles involved in cellular proteostasis, lysosome analysis was performed studying the expression of the lysosomal marker LAMP1 (lysosome-associated membrane protein 1) in Western blots of lysates from primary *Cant1*$^{-/-}$ and *Cant1*$^{+/+}$chondrocytes **(Figure 3.11 A)**. Densitometric analysis of the bands demonstrated a significant decreased expression of LAMP1 in *Cant1*$^{-/-}$ chondrocytes compared to *Cant1*$^{+/+}$ cells ($p = 0.022$) **(Figure 3.11 B)**.

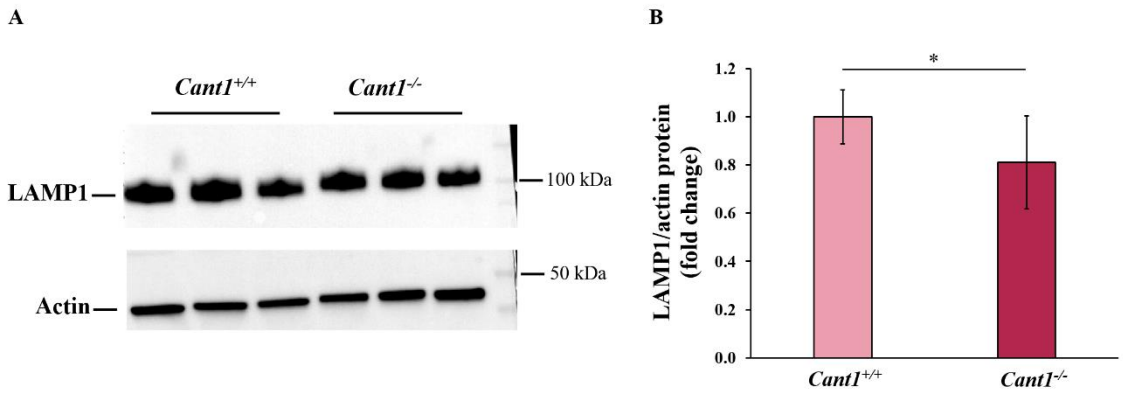

Figure 3.11: Expression of LAMP1 was decreased in *Cant1*$^{-/-}$ chondrocytes.
(A) Western blot analysis of LAMP1 was performed in *Cant1*$^{-/-}$ and *Cant1*$^{+/+}$ chondrocytes. Densitometric analysis demonstrated a significant decreased level of LAMP1 in *Cant1*$^{-/-}$ chondrocytes compared with *Cant1*$^{+/+}$ cells **(B)**. LAMP1 was normalized to the Actin band. LAMP1 level in *Cant1*$^{+/+}$ samples was set to one and the expression of *Cant1*$^{-/-}$ samples was reported as fold change. Data are reported as mean ± standard deviation of three independent experiments. Significance among samples was analyzed by Student's t-test; * $p < 0.05$; n = 3.

To confirm these data, the expression of LAMP1 in *Cant1*$^{-/-}$ and *Cant1*$^{+/+}$ chondrocytes was also analyzed by immunofluorescence microscopy **(Figure 3.12 A)**. Quantification of the integrated intensity demonstrated a significant decreased expression of LAMP1 in *Cant1*$^{-/-}$ chondrocytes compared to *Cant1*$^{+/+}$ cells ($p = 0.011$) **(Figure 3.12 B)**.

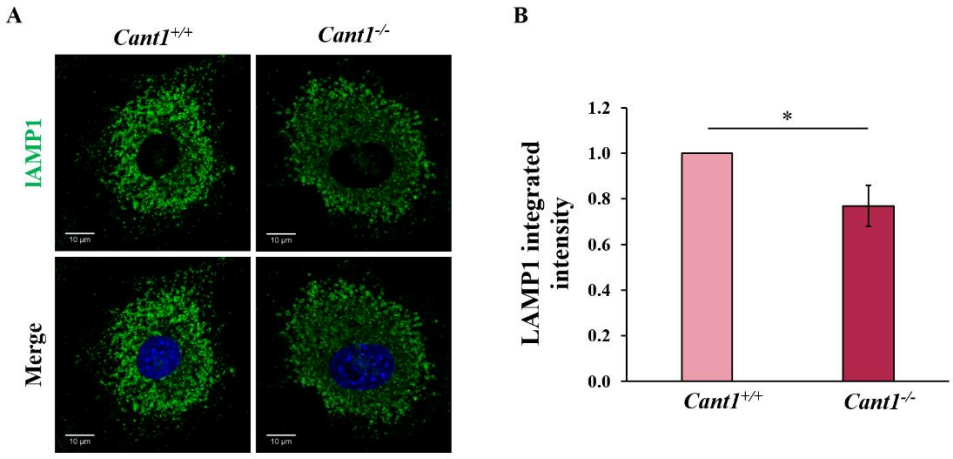

Figure 3.12: Expression of LAMP1 was decreased in *Cant1*$^{-/-}$ chondrocytes.
(A) Confocal microscopy analysis of the lysosomal marker LAMP1 was performed in *Cant1*$^{-/-}$ and *Cant1*$^{+/+}$ chondrocytes. Cells were stained with a LAMP1 antibody. **(B)** Quantification of the green fluorescence demonstrated a significant decreased expression of LAMP1 in *Cant1*$^{-/-}$ chondrocytes compared with *Cant1*$^{+/+}$ cells. The green fluorescence in *Cant1*$^{+/+}$ cells was set to one and the expression of *Cant1*$^{-/-}$ samples was reported as fold change. Data are reported as mean ± standard deviation of three independent experiments. Significance among samples was analyzed by Student's t-test; * $p < 0.05$; n = 3. Scale bars 10 µm.

3. Discussion

Desbuquois dysplasia type 1 (DBDQ1) is a rare recessive chondrodysplasia caused by mutations in *CANT1* gene, encoding for calcium-activated nucleotidase 1 of the Golgi apparatus.

To define the physiological role of CANT1 and better understand the pathophysiology of DBQD1, a mouse model for the disease, the *Cant1* knock-out (*Cant1*$^{-/-}$) mouse, was generated and validated. The mutant mouse recapitulated the chondrodysplastic phenotype of DBQD1 patients presenting reduced size, growth retardation and typical hand anomalies such as the "delta phalanx" [117].

Using the animal model, the role of CANT1 in proteoglycan biosynthesis was demonstrated, since reduced PG synthesis and oversulfated GAGs, with reduced hydrodynamic size, were observed in chondrocytes and cartilage from mutant (*Cant1*$^{-/-}$) animals. Reduced PG synthesis was already observed in fibroblast cultures from patients affected by DBDQ1, confirming also at the biochemical level that the *Cant1*$^{-/-}$ mouse was reminiscent of the human disorder [117].

Moreover, as already reported in fibroblast from patients, mutant mice chondrocytes, in both primary cultures and cartilage, showed dilated ER cisternae full of electrondense materials, suggesting potential protein retention and delayed secretion [117].

To further characterize the defect in PG biosynthesis, in this work, the kinetics of PG secretion was investigated, in chondrocytes extracted from the cartilage of *Cant1*$^{-/-}$ and wild-type mice. With a pulse chase experiment, in which PG were metabolically labelled with ^{35}S-sulfate, the ratio between PGs secreted in the medium and total PGs (medium and cell-layer) was measured at different time points. The data demonstrated a significant reduction in PG secretion in *Cant1*$^{-/-}$ chondrocytes compared to *Cant1*$^{+/+}$ cells, confirming our hypothesis.

To further characterize the defect in PG secretion, the processing of aggrecan, the most expressed PG in cartilage ECM, was analyzed by Western blot of cell lysates from *Cant1*$^{-/-}$ and *Cant1*$^{+/+}$ chondrocytes. The data demonstrated that the intracellular level of aggrecan was significantly higher in *Cant1*$^{-/-}$ chondrocytes compared to *Cant1*$^{+/+}$ cells, confirming the defect already observed in PG secretion and suggesting the retention of this molecule in mutant cells.

The delay in PG secretion suggested to check a potential delay in protein secretion. This process was analyzed in *Cant1*$^{-/-}$ and *Cant1*$^{+/+}$ chondrocytes by a pulse chase experiment using ^{35}S Express Protein Labeling mix. The hypothesis was not confirmed since no differences between mutant and wild-type samples were observed.

Overall these data, suggested that the delayed PG secretion was probably related to impaired glycosylation in Golgi, a process in which CANT1 is involved.

All these observations suggested to further study aggrecan glycosylation, since GAG synthesis is a fundamental step in its post-translational processing. In fact, it has been reported that defects in PG glycosylation may lead to the secretion of unglycanated PG species: in a patient with a progeria-like syndrome and signs of Ehlers-Danlos syndrome, the defect in galactosyltransferase I, that catalyses the second glycosyl transfer reaction in the assembly of the dermatan sulfate growing chain, results in the secretion of an unglycanated core protein [186]. Moreover, in other skeletal dysplasias such as the gerodermia osteodysplastica and the Saul-Wilson syndrome, defects in decorin glycanation, related to an altered Golgi-dependent glycosylation, have been reported [104, 106]. Thus, proteins extracted from medium and cell-layer of primary *Cant1*$^{-/-}$ and *Cant1*$^{+/+}$ chondrocytes, were analyzed by Western blot using a specific antibody, which recognizes an epitope on the aggrecan core protein. Results demonstrated that, despite the defects observed in GAG synthesis, only glycanated aggrecan was secreted by *Cant1*$^{-/-}$ chondrocytes, as in *Cant1*$^{+/+}$ cells. Moreover, aggrecan inside cells was mostly in the unglycanated form and, once glycanated, it was immediately secreted in the extracellular space.

As previously observed, the presence of morphological alterations of the endoplasmic reticulum in *Cant1*$^{-/-}$ chondrocytes was not associated to the presence of ER stress and activation of the canonical UPR pathways since the expression of the specific markers of canonical ER stress and UPR, including Bip and ATF4 was normal and the spliced form of Xbp1 was not present [117].

Alterations in the structure of the ER without the activation of ER stress pathways, have also been described in other skeletal dysplasias such as Achondrogenesis 1A or the Dyggve-Melchior-Clausen syndrome, as a consequence of defects in Golgi microtubule-associated protein 210 (GMAP-210) and dymeclin, both Golgi proteins involved in intracellular trafficking [103, 105].

Thus, we focused our attention on this organelle since there is a close cross-talk between the Golgi and the ER, CANT1 is mainly a Golgi protein and GAG synthesis occurs in this organelle. Therefore, Golgi homeostasis and morphology were investigated analysing the expression of two Golgi structural proteins GM130 and Golgin-97, cis and trans Golgi markers, respectively. Western blot analysis of proteins extracted from *Cant1*$^{-/-}$ and *Cant1*$^{+/+}$ chondrocytes demonstrated an increase of the expression of the two Golgi markers, even if only GM130 expression was significant. These data were confirmed by confocal microscopy analysis: the

quantification of red (GM130) and green (Golgin-97) fluorescence demonstrated a significant increase of the expression of the two Golgi markers in *Cant1*$^{-/-}$ chondrocytes. Moreover, the fluorescence area of the two signals was measured and the results demonstrated a significant increase of this parameter for both markers, suggesting a 30-35% increase of the cis and trans Golgi in mutant chondrocytes. Despite this, the Golgi architecture was not altered in mutant chondrocytes since there was no Golgi fragmentation and no collapsed stacks. This result was also confirmed by the observation that there was no colocalization between the Golgi cis and trans signals.

However, the overexpression of the Golgi markers and the increase of Golgi dimension suggested the presence of altered Golgi homeostasis in *Cant1*$^{-/-}$ chondrocytes. To date, the molecular pathways of the Golgi stress are still poorly known, in contrast to those of the ER stress. Golgi stress, as well as ER stress, activates different autoregulatory homeostatic mechanisms, with the aim of increasing organelle function in response to cellular needs, such as the increased load of proteins that need to be modified after translation [97]. Several pathways involved in Golgi stress have recently been proposed.

The TFE3 pathway regulates the general functions of the Golgi apparatus, the pathway linked to PG glycosylation and sulfation, essential in the biosynthesis of PGs, the cAMP response element-binding protein 3 (CREB3) pathway stimulates apoptosis, while the heat shock protein 47 (HSP47) pathway has an anti-apoptotic function [187].

In particular, the TFE3 pathway was analyzed due to the increased expression of the Golgi markers observed in mutant chondrocytes and its involvement in several Golgi functions, including the glycosylation process and vesicular transport [187].

In normal condition, TFE3 is present in the cytosol in the phosphorylated and inactive form and can be activated, in different cell stress conditions, including the accumulation of incorrectly glycosylated PGs within the Golgi [188]. When dephosphorylated, TFE3 translocates to the nucleus, where, after binding to enhancer elements, it activates the expression of different genes depending on the type of cellular stress.

In particular, when Golgi homeostasis is altered, TFE3 in the nucleus binds the Golgi apparatus stress response element (GASE), activating the transcription of genes encoding for Golgi structural proteins (such as GM130 or giantin), glycosylation enzymes and components of vesicle transport [188].

Therefore, the activation of this pathway was investigated analysing the localization of TFE3 in *Cant1*$^{-/-}$ and *Cant1*$^{+/+}$ by Western blot. Subcellular fractionation of chondrocyte cell lysates was performed to separate the cytosolic fraction, where the phosphorylated and inactive form

of TFE3 is present, from the nuclear one, where TFE3 is active as a transcription factor. Western blot analysis showed a significant higher level of TFE3 in the nuclear fraction of mutant chondrocytes compared to wild-types, suggesting the activation of this transcription factor. Conversely, there were no differences in TFE3 protein level in the cytosolic fraction and the total cell lysate of *Cant1*$^{-/-}$ and *Cant1*$^{+/+}$chondrocytes demonstrating that the significant TFE3 increase in the nuclear fraction of mutant chondrocytes was due to its activation and not to its overexpression.

To confirm the activation of TFE3 pathway, confocal microscopy analysis of *Cant1*$^{-/-}$ and *Cant1*$^{+/+}$ chondrocytes was performed, in order to study its subcellular distribution. For this experiment, wild-type cells treated with 5 μM monensin, a Golgi stress inducer for the TFE3 pathway, were used as positive control. Monensin is a ionophore that antiports Na^+ and H^+, which neutralizes the Golgi pH causing a reduced activity of Golgi proteins, that require an acid environment. Treatment with monensin results in functional impairment of Golgi enzymes; moreover, the Golgi becomes swollen and expanded because of the influx of water and the accumulation of secretory proteins [188].

Quantification of fluorescence integrated intensity confirmed the significant nuclear translocation of TFE3 in mutant chondrocytes, confirming the activation of this pathway. However, TFE3 activation was significantly lower in the nucleus of both mutant and wild-type chondrocytes, compared to the positive control, in agreement with the observation that the morphology of the Golgi was not dramatically altered.

Lastly, to further confirm TFE3 nuclear translocation in mutant cells, immunofluorescence analysis was also performed after incubation of cells for 20 hours with 1 mM p-nitrophenyl β-D-xylopiranoside (β-D-xyloside), an enhancer of GAG synthesis that, as other xylosides, causes Golgi fragmentation and the activation of TFE3 pathway [188]. Results confirmed what already observed in basal conditions, a significant nuclear translocation of TFE3 in mutant chondrocytes, demonstrating the activation of the Golgi stress response.

These data suggested that the increased expression of the two Golgi markers, GM130 and Golgin-97, in mutant cells might be linked to the activation of the TFE3 pathway which increases the expression of genes encoding for Golgi structural proteins [188], in order to enhance its function.

To further study the homeostasis of the organelles involved in chondrocyte proteostasis, lysosomal activation was analyzed studying the expression of the lysosomal marker LAMP1 (lysosome-associated membrane protein 1) by Western blot and immunofluorescence. Results

demonstrated a significant decreased expression of LAMP1 in mutant chondrocytes, suggesting a lower lysosomal activation in *Cant1*$^{-/-}$ cells.

In the literature, TFE3 has been described as a promoter of lysosomal activation. In fact, once activated and translocated to the nucleus, TFE3 can bind the coordinated lysosomal expression and regulation (CLEAR) motifs, activating genes associated with lysosomal biogenesis and autophagy [189, 190]. However, this occurs during starvation or ER stress, different conditions from those occurring in *Cant1*$^{-/-}$ chondrocytes. In fact, two different pathways of TFE3 activation have been described in different cell stress situations. Starvation or ER stress cause the activation of TFE3 through dephosphorylation on Ser321, resulting in the increased expression of genes associated with lysosomal biogenesis and autophagy [189]. Conversely Golgi stress causes the activation of TFE3 through the dephosporilation on Ser108, resulting in the enhanced expression of genes involved in the regulation of Golgi function [188].

In conclusion, in this work the analysis of PG metabolism in *Cant1*$^{-/-}$ chondrocytes was completed, demonstrating a reduced PG secretion, confirmed by the accumulation of aggrecan inside mutant cells. However, the delayed PG secretion was not associated with a delay in total protein secretion, but it was probably related to impaired PG glycosylation in the Golgi. Although *Cant1*$^{-/-}$ chondrocytes synthesize shorter and oversulfated GAGs compared to wild-type cells [117], it has been demonstrated that only glycanated aggrecan is secreted by *Cant1*$^{-/-}$ chondrocytes, as in wild-type cells. Alteration in the structure of the ER, without activation of ER stress, suggested that the ER enlargement might be due to impaired GAG synthesis in the Golgi. Thus, the studies on Golgi homeostasis demonstrated an increase of the cis and trans Golgi dimensions and an overexpression of Golgi structural proteins GM130 and Golgin-97 in mutant chondrocytes, suggesting alteration in Golgi homeostasis. Thus, by analysing TFE3 nuclear localization, the activation of one of the three putative Golgi stress response pathways was demonstrated. To date, Golgi stress represents a still partially unexplored field. The study of molecular pathways underlying Golgi stress could lead to increasing knowledge of the molecular basis of diseases, such as Desbuquois dysplasia type 1, paving the way for development of new therapies.

4. Materials and Methods

4.1. The *Cant1*$^{-/-}$ mouse model

The mouse model of Desbuquois dysplasia type 1, previously generated in the laboratory of Prof. A. Rossi, is a knock-out mouse for the *Cant1* gene obtained by excision of exons 3 and 4, encoding for the active site of the enzyme [117]. In this work, wild-type (*Cant1*$^{+/+}$) and homozygous *Cant1* knock-out mice (*Cant1*$^{-/-}$), with a C57B1/6Jx129/SV background, were used. To discriminate mutant from wild-type animals, mice were genotyped by polymerase chain reaction (PCR) using genomic DNA extracted from mouse tail clips.
Animals were bred with free access to water and standard pelleted food. Care and use of animals for the work described in this thesis complied with relevant animal welfare institutional guidelines and protocols were approved by the Animal Care and Use Committee of the University of Pavia and the Ministry of Health.

4.2. Extraction of rib chondrocytes

Cant1$^{-/-}$ and *Cant1*$^{+/+}$ chondrocytes were extracted from rib cartilage of 4 days old mice. Mice were sacrificed and their thoracic cage was harvested and digested with 2 mg/ml collagenase type II (Invitrogen) in Dulbecco's modified Eagle's medium (DMEM, Sigma) at 37°C for 90 minutes, to remove intercostal muscles. Then, cartilages were dissected from each rib, using the dissecting microscope, and digested with 2 mg/ml collagenase type II in DMEM with 10% foetal bovine serum (FBS, Euroclone) at 37°C overnight. Released chondrocytes were plated and cultured in DMEM with 10% FBS and antibiotics at 37°C in a humidified atmosphere containing 5% CO_2.

4.3. Analysis of proteoglycan secretion

Proteoglycan secretion was analyzed by a pulse chase experiment. *Cant1*$^{-/-}$ and *Cant1*$^{+/+}$ primary chondrocytes were plated in 24-well plates at a cell density of 50 kcells/well in DMEM 10% FBS. After 24 hours, the medium was discarded and chondrocytes were labelled with 30 µCi/well of ^{35}S-sulphate (PerkinElmer) for 2 hours in Minimum Essential Medium (MEM, Sigma) without FBS at 37°C in 5% CO_2. At the end of the labelling period, the medium was removed, cells were incubated in MEM without FBS containing 5 mM cold sulfate for different chase times: 0, 0.5, 2.5 and 5 hours, as previously described [191]. At each time point, cell layer and medium were collected separately. To each medium sample, an equal volume of 0.2 M sodium acetate, pH 5.8, containing 2% Triton X-100, 8 M guanidinium chloride and protease

inhibitors (4 mM EDTA, 10 mM benzamidine and 2 mM N-ethylmalemide (NEM) was added. Each cell layer sample was scraped in 0.1 M sodium acetate, pH 5.8, containing 2% Triton X-100, 4 M guanidinium chloride and protease inhibitors. PD MiniTrap G-25 columns (GE Healthcare) were used to remove ^{35}S-sulfate from both medium and cell layer samples, separately. To equilibrate columns and elute samples, 50 mM sodium acetate, pH 6.0, containing 4 M guanidinium chloride and 0.5% Triton X-100 was used. In each gel filtration, the first filtered fraction V_0, containing the proteoglycans, was collected and ^{35}S-radioactivity was measured by scintillation counting. For each time point, the percentage of ^{35}S-radioactivity in the medium to the total counts (medium and cell layer) was measured.

4.4. Analysis of total protein secretion

Total protein secretion was analyzed in primary cultures of *Cant1*$^{-/-}$ and *Cant1*$^{+/+}$ chondrocytes by a pulse-chase experiment. Chondrocytes were plated in 24 well-plates at a cell density of 50 kcell/well in DMEM 10% FBS. After 24 hours, the medium was discarded and replaced with DMEM without FBS containing 90,5 µCi/ml of EXPRESS^{35}S Protein Labeling Mix (PerkinElmer) containing both (^{35}S-L-methionine and ^{35}S-L-cysteine) and cells were incubated at 37°C in 5% CO_2 for 1 hour. At the end of the labelling period, the medium was replaced with DMEM without FBS containing an excess of cold cysteine and methionine and cell were incubated at 37°C in 5% CO_2 for different chase time: 1, 2.5, 5 and 8 hours. At each time point, medium was collected in an eppendorf containing 10 mg/ml albumin in PBS and 10x protease inhibitors (40 mM EDTA, 0.1 M benzamidine and 20 mM NEM). Then RIPA Buffer (150 mM sodium chloride, 1% IGEPAL CA-630, 0.5% deoxycholate, 0.1% SDS, 50 mM Tris, pH 8.0, containing 10 mM benzamidine, 2 mM NEM, 4 mM EDTA) was added to cells and the cell lysate was collected in an eppendorf containing 10 mg/ml albumin in PBS. Medium and cell layer proteins were precipitated in 10% trichloroacetic acid (TCA) on ice for 30 minutes, samples were centrifuged at 12,000 rpm for 10 minutes at 4°C and the pellet was washed with acetone. The pellet was solubilized in 100 mM Tris-HCl, pH 6.8, containing 2% SDS at 50°C overnight and radioactivity was then measured by liquid scintillation counting. For each time interval, the percentage of radioactivity in the medium to the total (medium and cell layer) was measured.

4.5. Sample preparation for Western blot

4.5.1 Aggrecan extraction

Chondrocytes were plated in 60 mm diameter petri dishes at a cell density of 1,500 kcell/petri in DMEM with 10% FBS and incubated at 37°C in 5% CO_2. Two days after seeding, cells were incubated in DMEM without FBS at 37°C in 5% CO_2 for 24 hours. The medium was then harvested, centrifuged at 2,000 rpm for 10 minutes and the supernatant was ultrafiltered with Amicon Ultra 4mL Centrifugal Filter unit (10 kDa cut-off, Merck Millipore), at 4200 x g for 10 minutes. The Centrifugal Filter unit was then washed with 0.1 M ammonium acetate, pH 7.35, centrifuged at 4200 x g for 10 minutes and the concentrated retained solution was recovered in an Eppendorf tube. The cell layer was scraped in PBS, centrifuged at 12,000 x g for 5 minutes at 4 °C and the pellet was resuspended in RIPA lysis buffer and solubilized with 3 cycles of freezing and thawing. Lysates were then centrifuged at 12,000 x g for 5 minutes at 4 °C and the supernatant was diluted with 0.1 M ammonium acetate, pH 7.35. Samples were ultrafiltered with Amicon Ultra 0.5mL Centrifugal Filter unit (10 kDa cut-off, Merk Millipore) at 9000 x g for 10 minutes. To recover the concentrated retained solution, the Filter Unit was placed upside down in a new collection tube and centrifuged at 10,000 x g for 5 minutes. The cell layer and medium samples were lyophilized. Samples were then resuspended in 0.1 M ammonium acetate pH 7.35 and divided into two aliquots: one aliquot was digested with 40 mU of chondroitinase ABC (Seikagaku) in 0.1 M ammonium acetate pH 7.35 (Chase ABC digested aliquot), while only 0.1 M ammonium acetate pH 7.35 was added to the other aliquot (Chase ABC not digested aliquot) and all samples were incubated overnight at 37°C. Samples were then lyophilized, resuspended in electrophoresis sample buffer (62.5 mM Tris-HCl, 2% SDS, 10% glycerol, 0.01% bromophenol blue) containing 5% β-mercaptoethanol and denatured at 90°C for 10 minutes. Once cooled, vortexed and spinned, samples were analyzed by Western blot.

4.5.2. Total protein extraction

Cant1$^{-/-}$ and *Cant1*$^{+/+}$ chondrocytes were plated in a 60 mm diameter petri dish in DMEM with 10% FBS at a cell density 1,500 kcell/petri and incubated at 37°C in 5% CO_2. After 3 days, cells were scraped in PBS and centrifuged at 12,000 x g for 5 minutes at 4°C. The pellet was resuspended in RIPA lysis buffer supplemented with protease inhibitors (1 mM phenylmethylsulfonyl fluoride (PMSF) and 2 mM $NaVO_3$) and solubilized with 3 cycles of freezing and thawing. The protein content was measured by BCA Protein Assay (Thermofisher), using Bovine Serum Albumin (BSA, Thermofisher) as standard. A volume of 4x sample buffer (250 mM Tris-HCl, 8 % SDS, 40% glycerol and 0.04% bromophenol blue) was added to reach the 1x final concentration and samples were reduced by addition of β-

mercaptoethanol to 5% final concentration. Finally, samples were denatured at 90°C for 10 minutes. Samples were then analyzed by Western blot.

4.5.3. Subcellular fractionation

Cant1$^{-/-}$ and *Cant1*$^{+/+}$ chondrocytes were plated in a 60 mm diameter petri dish in DMEM with 10% FBS at a cell density of 1,500 kcell/petri and incubated at 37°C in 5% CO_2. After 2 days, cells were scraped in PBS and centrifuged at 12,000 x g for 5 minutes at 4°C. Pellets were resuspended in NP-40 Lysis buffer (10 mM Tris, pH 7.9, 140 mM potassium chloride, 5 mM magnesium chloride, 0.5% IGEPAL CA-630 and protease inhibitors) and incubated on ice for 15 minutes. Samples were then centrifuged at 1000 x g for 5 minutes at 4°C and the supernatant, representing the cytosolic fraction, was recovered in an Eppendorf tube. The pellet was washed with NP-40 Lysis buffer and centrifuged at 1000 x g for 5 minutes at 4°C; then the pellet was sonicated in Triton Lysis buffer (100 mM Tris-HCl, pH 7.4, 0.5% Triton X-100 and 0.5% SDS), centrifuged at 12,000 x g for 5 minutes at 4°C and the supernatant thus obtained, representing the nuclear fraction, was recovered in an eppendorf tube. The protein content was measured by the BCA protein assay. Sample buffer 4x to reach the final concentration of 1x and 5% β-mercaptoethanol were added to the cytosolic and nuclear fractions and samples were then denatured at 90°C for 10 minutes. Samples were then analyzed by Western blot.

4.6. Western blot analysis

The same protein amount from each samples (15-20 μg), obtained as previously described, was analyzed by SDS-PAGE on 4-15% polyacrylamide gradient gels (Mini-PROTEAN TGX Stain-Free Protein Gel, BioRad). Proteins were then transferred from the gel to a polyvinylidene difluoride (PVDF) membrane (Amersham) at 100 V for 2 hours on ice in Transfer buffer (20 mM Tris, 50 mM glycine and 20% (v/v) methanol). Membranes were blocked in 5% BSA, 0.05% Tween-20 in TBS (20 mM Tris, pH 7.5, 500 mM NaCl) for 2 hours at room temperature, except for the LAMP1 Western blot membrane that was blocked in 5% Milk (BioRad) in TBS 0.1% Tween 20 (TBS-T) for 2 hours at room temperature. After washing with TBS-T, membranes were incubated with specific primary antibodies: anti-aggrecan (1:500, rabbit monoclonal antibody, Merck Millipore), anti-GM130 (1:1000, mouse monoclonal antibody, BD Biosciences), anti-Golgin-97 (1:1000, rabbit monoclonal antibody, Cell Signaling), anti-TFE3 (1:1000, rabbit monoclonal antibody, Sigma), anti-histone H3 (1:3000, rabbit monoclonal antibody, Cell Signaling), anti-actin (1:5000, mouse monoclonal antibody, Merck Millipore) and anti-LAMP1 (1:1000, rabbit monoclonal antibody, Abcam) in blocking solution

overnight at 4°C. The appropriate HRP secondary antibodies, anti-rabbit (Cell Signaling) or anti-mouse (Cell Signaling), was added at the dilution of 1:2000 in 5% BSA, 0.05% Tween-20 in TBS for 1 hour at room temperature. The signal was detected by ECL Western blotting detection reagent (Cyanagen) and images were acquired by Image Quant LAS 4000 instrument (GE Healthcare) using ImageQuant LAS 4000 software. Densitometric analysis was performed using ImageJ software. The signal of aggrecan (for cell layer samples), GM130, Golgin-97, TFE3 in the cytosolic fraction and LAMP1 bands was normalized to the signal of the actin band, while the signal of TFE3 in the total cell lysate and in the nuclear fraction was normalized to the signal of the histone H3 band, as a loading control. For normalization of medium samples, before the blocking step, the membrane was stained with the Swift Membrane Stain (G-Biosciences) and scanned with ImageQuant LAS 4000; the signal of the aggrecan band was normalized to the absorbance of the lane after membrane staining. For each gel, the intensity of the wild-type band was set to one and the expression of mutant samples was reported as fold change.

4.7. Immunofluorescence analysis

For immunofluorescence analysis, 10,000 chondrocytes were plated on sterile glass coverslips in a 24 well-plate in DMEM with 10% FBS and incubated at 37°C in 5% CO_2. After 3 days, the medium was removed and cells were then fixed in 4% formaldehyde in PBS (Fixative Solution, Invitrogen) for 10 minutes at room temperature. For TFE3 immunofluorescence analysis, a positive control was made treating some wild-type samples with 5 μM monensin, for 6 hours before fixation. For TFE3, GM130 and Golgin-97 immunofluorescence analysis, cells were then washed 3 times in PBS, permeabilized with 0.3% Triton X-100 in PBS for 10 minutes at room temperature and incubated in blocking solution (1.5% BSA in PBS) for 2 hours at room temperature. For LAMP1 immunofluorescence analysis, cells were washed 3 times in PBS and incubated in blocking solution (0.5% BSA, 0.05% Saponin, 50 mM NH_4Cl, 0.02% NaN_3, 15 mM glycin, pH 7.3 in PBS) for 2 hours at room temperature. Cells were then incubated with the specific primary antibody: anti-GM130 conjugated with Alexa Fluor 647 (1:100, mouse monoclonal antibody, BD Bioscience), anti-Golgin-97 (1:200, rabbit monoclonal antibody, Cell Signaling), anti-TFE3 (1:1200, rabbit monoclonal antibody, Sigma), anti-LAMP1 (1:200, rabbit monoclonal antibody, Abcam) in blocking solution overnight at 4°C. The following day, cells were washed 3 times in PBS and incubated, protected from light for 2 hours at room temperature with the appropriate secondary antibody: anti-rabbit conjugated with

Alexa Fluor 488 (Immunological Sciences) diluted 1:2000 in blocking solution. Nuclei were then counterstained with 4′,6-diamidino-2-phenylindole (DAPI, Sigma) for 3 min at room temperature. Samples were analyzed by Leica SP8 high-resolution confocal microscope (Leica), equipped with a 63x oil immersion objective, at Centro Grandi Strumenti of the University of Pavia. Fluorescence integrated intensity and area per cell were measured by ImageJ software. The fluorescence intensity of GM130, Golgin-97 and LAMP1 in wild-type was set to one and the expression of mutant samples was reported as fold change. The fluorescence intensity of TFE3 in the nuclei of the positive control was set to one and the expression of wild-type and mutant samples was reported as a fold change.

4.8. Statistical analysis

Statistical analysis was performed by Microsoft Excel software. All values are reported as mean ± standard deviation. Statistical difference between different groups was evaluated using Student's t-test and a p-value < 0.05 was considered statistically significant.

CHAPTER IV: Phenotypic characterization of immortalized chondrocytes from a Desbuquois dysplasia type 1 mouse model: a tool for studying defects in glycosaminoglycan biosynthesis

1. Aim of the work

Since cartilage and bone biopsies a rarely available, the use of *in vivo* models is essential to elucidate the molecular basis and the pathogenetic mechanisms of the disease.
Using the mouse model for the Desbuquois dysplasia type 1, *Cant1* knock-out mouse, the role of CANT1 in proteoglycan biosynthesis was recently demonstrated [117].
Due to the complexity of the animal model, in order to deeply investigate CANT1 function, an *in vitro* approach, using cell culture, represent a powerful tool to investigate specific aspects of cartilage biology. Primary chondrocyte cultures are a very well-defined system, however they have some limits since they undergo de-differentiation after few passages in culture, assuming pseudo-fibroblastoid morphology and a different pattern of gene expression [169, 192]. For this reason, cells cannot be expanded and several animals should be sacrificed to recover primary cells.
Due to the limitations of primary chondrocytes, it would be useful to generate immortalized cell lines, since they grow very rapidly for several passages compared to primary cultures, in order to reduce the number of sacrificed animals, according to the principle of the Three Rs, and the time for the experiments. However, during the immortalization process, cells might develop a different phenotype from the cells of origin; thus, it is important to deeply characterize them before their use [168, 184, 185].
Therefore, the aim of this work was the generation and phenotypic characterization of *Cant1* knock-out (*Cant1*$^{-/-}$) and wild-type chondrocytes immortalized using a plasmid vector expressing the SV40 small and large T antigen, in order to validate them as a model to get new insight on the role of CANT1 in the pathogenesis of DBQD1. For this purpose, after a morphological characterization of immortalized cells, the synthesis and deposition of the main cartilage ECM molecules, aggrecan and type II collagen, were analyzed.

These results were collected in a first-authored research paper entitled “Phenotypic characterization of immortalized chondrocytes from a Desbuquois dysplasia type 1 mouse model: a tool for studying defects in glycosaminoglycan biosynthesis”, which was published in *International journal of Molecular Sciences* in August 2021. The pdf of the published paper is provided below here.

International Journal of
Molecular Sciences

MDPI

Article

Phenotypic Characterization of Immortalized Chondrocytes from a Desbuquois Dysplasia Type 1 Mouse Model: A Tool for Studying Defects in Glycosaminoglycan Biosynthesis

Chiara Gramegna Tota, Beatrice Valenti †, Antonella Forlino, Antonio Rossi * and Chiara Paganini

Department of Molecular Medicine, Unit of Biochemistry, University of Pavia, 27100 Pavia, Italy; chiara.gramegnatota01@universitadipavia.it (C.G.T.); beatrice.valenti@cro.it (B.V.); antonella.forlino@unipv.it (A.F.); chiara.paganini@unipv.it (C.P.)

* Correspondence: antrossi@unipv.it; Tel.: +39-0382-987229

† Current affiliation: Oncogenetics and Functional Oncogenomics, Centro di Riferimento Oncologico di Aviano (CRO Aviano) IRCCS, National Cancer Institute, 33081 Aviano, Italy.

Abstract: The complexity of skeletal pathologies makes use of in vivo models essential to elucidate the pathogenesis of the diseases; nevertheless, chondrocyte and osteoblast cell lines provide relevant information on the underlying disease mechanisms. Due to the limitations of primary chondrocytes, immortalized cells represent a unique tool to overcome this problem since they grow very easily for several passages. However, in the immortalization procedure the cells might lose the original phenotype; thus, these cell lines should be deeply characterized before their use. We immortalized primary chondrocytes from a *Cant1* knock-out mouse, an animal model of Desbuquois dysplasia type 1, with a plasmid expressing the SV40 large and small T antigen. This cell line, based on morphological and biochemical parameters, showed preservation of the chondrocyte phenotype. In addition reduced proteoglycan synthesis and oversulfation of glycosaminoglycan chains were demonstrated, as already observed in primary chondrocytes from the *Cant1* knock-out mouse. In conclusion, immortalized *Cant1* knock-out chondrocytes maintained the disease phenotype observed in primary cells validating the in vitro model and providing an additional tool to further study the proteoglycan biosynthesis defect. The same approach might be extended to other cartilage disorders.

Keywords: proteoglycan; collagen; cartilage; extracellular matrix; in vitro model; immortalization; skeletal dysplasia

check for updates

Citation: Gramegna Tota, C.; Valenti, B.; Forlino, A.; Rossi, A.; Paganini, C. Phenotypic Characterization of Immortalized Chondrocytes from a Desbuquois Dysplasia Type 1 Mouse Model: A Tool for Studying Defects in Glycosaminoglycan Biosynthesis. *Int. J. Mol. Sci.* **2021**, *22*, 9304. https://doi.org/10.3390/ijms22179304

Academic Editors: Chiara Schiraldi, Donatella Cimini, Annalisa La Gatta and Yury A. Skorik

Received: 25 June 2021
Accepted: 11 August 2021
Published: 27 August 2021

Publisher's Note: MDPI stays neutral with regard to jurisdictional claims in published maps and institutional affiliations.

Copyright: © 2021 by the authors. Licensee MDPI, Basel, Switzerland. This article is an open access article distributed under the terms and conditions of the Creative Commons Attribution (CC BY) license (https://creativecommons.org/licenses/by/4.0/).

1. Introduction

Chondrocyte is the unique cell type in cartilage and is essential for cartilage formation and function. These cells are embedded in an extracellular matrix (ECM) consisting of complexes of aggrecan, hyaluronan, and link protein in a collagen fibril network [1]. In articular cartilage, the ECM synthesized by chondrocytes imparts to the tissue stiffness, wear resistance, and the ability to withstand compressive forces, allowing the joints to move smoothly and without pain [2]. The other major function of chondrocytes occurs in endochondral ossification, in which chondrocytes go through a process of maturation characterized by type X collagen expression, loss of aggrecan and type II collagen expression and cellular hypertrophy, leading to the formation of many skeletal elements and to longitudinal growth of long bones [3].

Chondrocytes maintain cartilage homeostasis by balanced anabolic and catabolic activities. This equilibrium is disrupted in osteoarthritis, the major degenerative pathology associated with chondrocytes. Osteoarthritis is characterized by the increased expression of ECM degrading enzymes resulting in cartilage destruction by degradation of the collagen and proteoglycan (PG) moieties [4]. Cartilage development and homeostasis is also altered in several genetic diseases that affect the skeleton. The updated nosology comprises

461 different disorders that range in severity from mild to severe and lethal forms; the gene defects have been characterized in 92% of these human syndromes [5].

Different in vivo and in vitro models have been developed in order to approach the complex biology of cartilage in normal and pathological conditions. Analysis of genetically modified mice provides a powerful method to study the role of gene products in vivo. Mouse models of osteoarthritis as well as of several skeletal dysplasias have been used to elucidate the effect of a single defect on the disease pathogenesis [6–8]. However, in vitro studies are a powerful tool to investigate specific aspects of cartilage biology that cannot be studied in the whole animal due to its complexity. Isolated primary chondrocytes present phenotype instability with increased time in culture providing an important limitation to chondrocyte use. The expression levels of major chondrocyte markers (i.e., type II and type IX collagen, COMP) significantly decrease with culture passages suggesting loss of the chondrocyte phenotype [9,10]. Thus, one of the main challenges to establish chondrocyte cell lines is to maintain the chondrocyte phenotype. To this purpose, high density aggregate culture methods [11] or co-cultures of chondrocytes with mesenchymal stem cells [12] have been described. In addition, approaches to re-differentiation of de-differentiated chondrocytes have been investigated in 3D culture using different gels containing alginate [13], agarose [14], hyaluronan [15], and a combination of collagen and alginate [16]. These culture systems maintain the chondrocyte phenotype, but since cells do not proliferate, they do not overcome the limitation in cell supply. Thus, investigators have generated immortalized chondrocyte cell lines from human controls and wild-type mice with different methods to preserve the phenotype and to provide a surrogate model system to study cartilage biology [17–27]. Most of these cell lines have been generated to study specific anabolic and catabolic pathways in order to provide additional information on the molecular mechanism of osteoarthritis development and progression [18,26]. To investigate the involvement of particular gene products in pathological mechanisms, these immortalized cells might be further modified by knocking down specific genes through RNA interference or gene editing. However, this approach, which have been reported in several cell lines such as ATDC5 [28] and Swarm rat chondrosarcoma cells [29], requires further subculturing to attain genetically modified clonal lines and, in addition, carries the risk of off-target effects. These problems can be overcome by the immortalization of chondrocytes from mouse models of genetic disorders of the skeleton to study putative disease pathways and/or ECM protein synthesis and assembly in simple and well-defined in vitro systems. Structural and biosynthetic defects in cartilage ECM proteins, including collagens, PGs, and glycoproteins (COMP, matrilin-3) result in several dominant and recessive skeletal dysplasias. Moreover, due to the relevance of the oligosaccharide part of PGs for their biological functions, different forms of skeletal disorders are caused by defects in glycosaminoglycan (GAG) biosynthesis, a complex process that involves several transporters and enzymes, most of them localized in the Golgi apparatus [30,31]. Thus, the use of in vitro systems [32] is ideal for a deep characterization of the biosynthetic defects.

We recently generated a *Cant1* knock-out mouse for the human Desbuquois dysplasia type 1 (DBQD1) [33]. This autosomal recessive chondrodysplasia is characterized by short stature, joint laxity, short extremities, typical hand anomalies, and progressive scoliosis. DBQD1 is caused by mutations in the calcium activated nucleotidase 1 (*CANT1*) gene encoding for an ER/Golgi nucleotidase that hydrolyses UDP [34,35]. We demonstrated that its impairment causes reduced synthesis, oversulfation, and reduced hydrodynamic size of GAGs [33], suggesting that CANT1 affects the whole biosynthetic process of GAGs occurring in the Golgi. For this reason, in vitro tools are necessary to dissect the complex pathway of GAG biosynthesis.

In this work we generated and characterized immortalized cell lines from a *Cant1* knock-out mouse [33]. These cell lines showed the defects in GAG biosynthesis already observed in primary chondrocytes from the same mouse model and they provide an in vitro tool for modeling the molecular mechanisms of skeletal defects caused by *Cant1* impairment.

2. Results

2.1. Immortalization of Murine Chondrocytes from Femoral Head Cartilage

Primary chondrocytes isolated from femoral head cartilage of *Cant1* knock-out and wild-type mice were transfected with the plasmid vector pZipSV766-1 expressing the large and small T antigen of SV40 and containing the neomycin resistance gene. Two days after transfection, neomycin resistant cells were selected by treatment with G418. The cells were passaged at high dilution and three colonies for each genotype were isolated. Cells from the selected clones showed a polygonal morphology characteristic of chondrocytes rather than fibroblasts (Figure 1), suggesting that cells maintained the chondrocyte phenotype. Thus, these cell lines were further characterized at the molecular level.

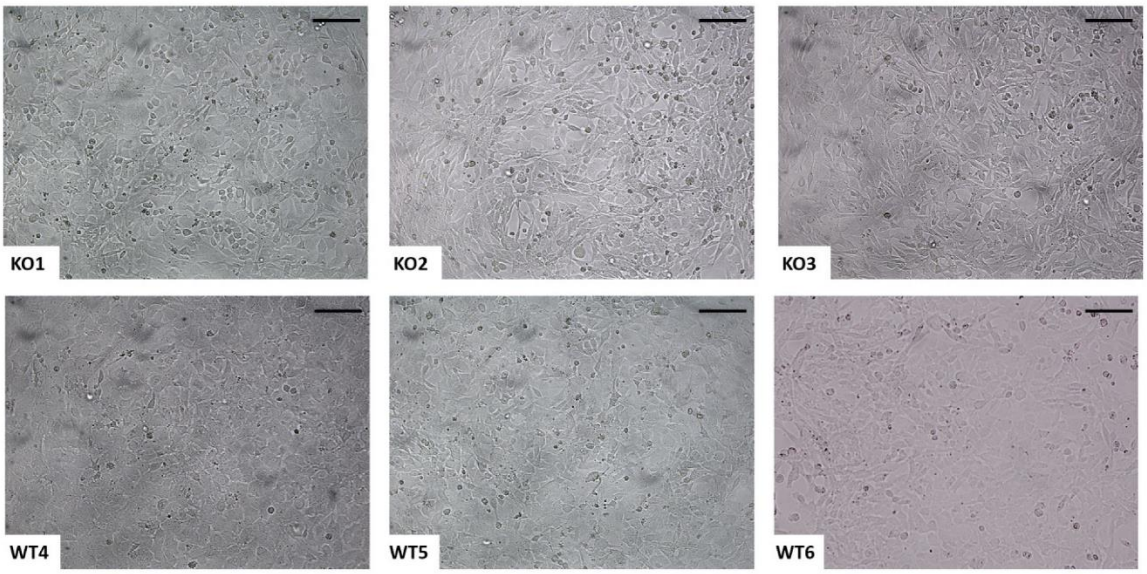

Figure 1. Morphology of immortalized chondrocytes. Representative images of immortalized cell lines at early confluence. Both *Cant1* knock-out (KO1, KO2, and KO3) and wild-type (WT4, WT5, and WT6) cells maintained the typical polygonal chondrocyte morphology after immortalization. Scale bar 100 μm.

2.2. Analysis of the Cartilage Phenotype in Immortalized Chondrocytes

We further characterized the phenotype of immortalized cell lines analyzing the expression level of the main ECM proteins synthesized by chondrocytes: type II collagen and aggrecan. It is well known that chondrocytes shift to a fibroblast-like phenotype when cultured in monolayer after several passages [9]. Since type II collagen is the typical differentiation marker of the chondrocyte phenotype, collagens secreted in the culture medium by immortalized cells were purified by pepsin digestion and analyzed by 6% SDS-PAGE (Figure 2a). Coomassie staining of the gel showed a single band in the type II collagen standard, corresponding to the α1 chain of type II collagen (α1(II)), and two bands in the standard of type I collagen, corresponding to the α1 and α2 chains of type I collagen (α1(I) and α2(I), respectively). Since the α1 chains of type I and type II collagen comigrate, the absence of the α2(I) band indicated that the α1 band consisted primarily of type II collagen. In all cell lines, both wild-type and knock-out, the α1(II) band was present indicating that the cells synthesized mainly type II collagen maintaining the chondrocyte phenotype. However, in several cell lines, both wild-type and knock-out, a faint α2(I) band was observed demonstrating that these cell lines synthesized very low levels of type I collagen. Among knock-out samples, the α2(I) band was not detected at all in KO1, while in WT6 the α2(I) band was negligible compared with the other wild-type cell lines (Figure 2a) and quantitated as less than 2% of the α1(I+II) collagen band by densitometric scanning

of stained gels. This observation suggested that KO1 and WT6 were the knock-out and wild-type cell lines, respectively, that better preserved the chondrocyte phenotype.

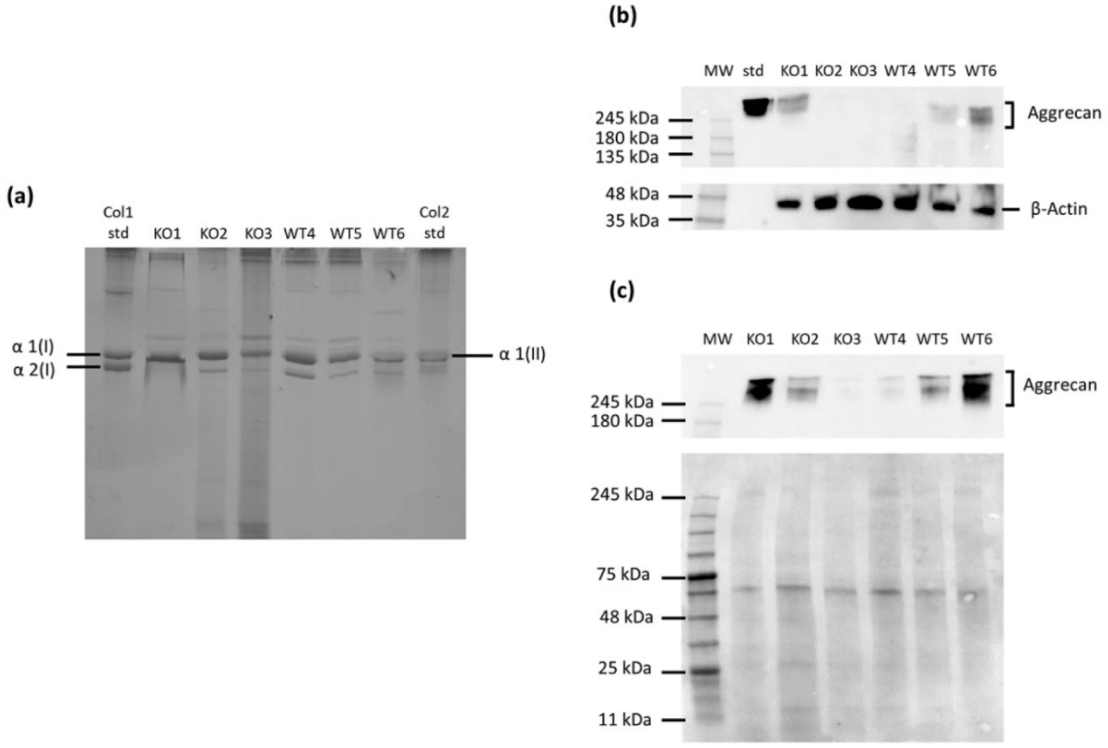

Figure 2. Synthesis of extracellular matrix proteins in immortalized chondrocytes. (**a**) 6% SDS-PAGE of collagen purified by pepsin digestion from the medium showed that all cell lines synthesized type II collagen, but a very small amount of type I collagen was present in wild-types and two *Cant1* knock-out samples. Col1 std = pepsin solubilized type I collagen standard and Col2 std = pepsin solubilized type II collagen standard. (**b**) Western blot of proteins extracted from cell layer of immortalized chondrocytes was performed with specific antibodies against aggrecan core protein and against β-Actin as internal control. The blot is representative of three independent experiments. MW = molecular weight and std = aggrecan core standard. (**c**) Western blot of proteins extracted from the medium was performed with a specific antibody against the aggrecan core protein; protein stain of the PVDF membrane with swift membrane stain was used as loading control. The blot is representative of two independent experiments. MW = molecular weight. Both cell layer and medium Western blots showed huge variability of aggrecan synthesis among immortalized chondrocytes; KO1 and WT6 were the *Cant1* knock-out and wild-type samples, respectively, that synthesized more aggrecan. The full original gel and Western blots are reported in Supplementary Materials Figure S1.

Immortalized cell lines were also screened for the expression of aggrecan, the main PG present in cartilage. For this purpose, aggrecan in the culture medium and the cell layer was analyzed by Western blot with a specific aggrecan antibody. An equal amount of proteins was loaded on gel for cell layer samples, while an equal volume was loaded on the gel for the culture medium. Western blot analysis showed a marked heterogeneous expression of aggrecan (Figure 2b,c). Among the different immortalized knock-out and wild-type cell lines, expression of this PG was quite evident in KO1 and WT6, respectively. This result confirmed that KO1 and WT6 cell lines had preserved the chondrocyte phenotype as already demonstrated by type II collagen analysis.

Type II collagen and aggrecan expression was also studied at the mRNA level by real-time PCR. The results confirmed that all immortalized cell lines expressed type II collagen and aggrecan, even if with huge variability (Figure 3). Among immortalized knock-out chondrocytes the highest type II collagen and aggrecan expression was in KO1

cell line, while in wild-type cell lines WT6 showed the highest expression level of type II collagen and aggrecan.

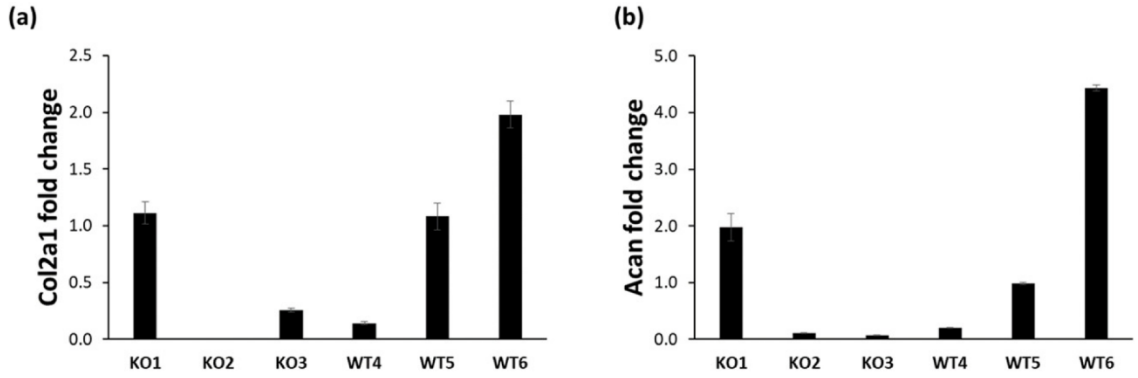

Figure 3. Expression of extracellular matrix proteins in immortalized chondrocytes. (**a**) The type II collagen (Col2a1) expression was assessed by real-time PCR. Fold change was calculated by ΔΔCt method using Gapdh as housekeeping gene and WT5 as reference sample random selected. Data are reported as mean ± standard deviation of three replicates. (**b**) The aggrecan (Acan) expression was assessed by real-time PCR. Fold change was calculated by ΔΔCt method using Gapdh as housekeeping gene and WT5 as reference sample random selected. Data are reported as mean ± standard deviation of three replicates. All samples expressed type II collagen and aggrecan, even if with a huge variability among cell lines.

Overall, these results demonstrated that the cell lines KO1 and WT6, obtained by the immortalization of *Cant1* knock-out and wild-type chondrocytes, respectively, maintained the chondrocyte phenotype based on expression at the protein and mRNA level of the two main cartilage ECM proteins. These cell lines were used to further investigate the cell phenotype at the biochemical level.

2.3. Glycosaminoglycan Synthesis and Sulfation in Immortalized Cant1 Knock-Out and Wild-Type Chondrocytes

In a previous work, we demonstrated that *Cant1* knock-out chondrocytes in primary culture synthesize reduced amount of GAGs which, in addition, were oversulfated [33].

PG synthesis in immortalized *Cant1* knock-out (KO1 cell line) and wild-type (WT6 cell line) chondrocytes was studied by metabolic labeling with ^{35}S-sulfate for 24 h. At the end of the labeling period, macromolecules were purified by ion exchange chromatography and GAGs were quantified by measuring the ^{35}S-activity and normalized to the protein content. In basal conditions, GAG synthesis was reduced in immortalized KO1 chondrocytes compared with immortalized WT6 cells (1629 ± 167 dpm/μg protein vs. 2505 ± 60 dpm/μg protein, respectively; $p = 0.020$) (Figure 4a). GAG synthesis was further studied by metabolic labeling in medium containing *p*-nitrophenyl β-D-xylopyranoside, a molecule that enhances GAG synthesis. In both cell lines, GAG synthesis was markedly increased compared to the basal condition. Moreover, GAG synthesis was significantly higher in WT6 chondrocytes compared with KO1 cells (16,116 ± 312 dpm/μg protein vs. 10,509 ± 596 dpm/μg protein, respectively; $p = 0.007$) (Figure 4b) as observed in the basal condition.

GAG synthesis was further characterized by sulfation analysis of chondroitin sulfate PGs secreted in the culture medium of immortalized chondrocytes. Purified GAGs were digested with chondroitinase ABC and ACII and released chondroitin sulfate disaccharides analyzed by HPLC after fluorescence derivatization. The percentage of monosulfated disaccharides (ΔDi-4S and ΔDi-6S) relative to the total amount of disaccharides (ΔDi-0S, ΔDi-4S, and ΔDi-6S) was increased in KO1 cells compared with WT6 ones (87.57 ± 0.82% vs. 79.42 ± 0.61% monosulfated disaccharides, respectively; $p = 0.008$) demonstrating GAG oversulfation in the *Cant1* knock-out cell line compared to the wild-type one (Figure 4c).

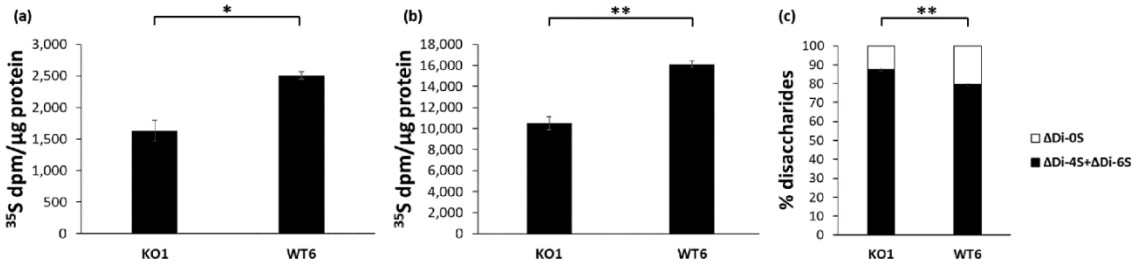

Figure 4. *Cant1* knock-out chondrocytes maintained the mutant phenotype after immortalization. (**a**) Immortalized chondrocytes were metabolically labeled with ^{35}S-sulfate for 24 h in basal medium. The amount of newly synthesized GAGs was determined normalizing the ^{35}S-activity to the protein content. Data are reported as mean ± standard deviation of three experiments. Significance between KO1 and WT6 samples was analyzed by Student's *t*-test; * $p < 0.05$. (**b**) Immortalized chondrocytes were metabolically labeled with ^{35}S-sulfate for 24 h in basal medium containing 1 mM *p*-nitrophenyl-β-D-xylopyranoside. The amount of newly synthesized GAGs was determined normalizing the ^{35}S-activity to the protein content. Data are reported as mean ± standard deviation of three experiments. Significance between KO1 and WT6 samples was analyzed by Student's *t*-test; ** $p < 0.01$. In both condition, basal medium with and without *p*-nitrophenyl-β-D-xylopyranoside, immortalized KO1 chondrocytes synthesized less GAGs compared with immortalized WT6 cells as demonstrated previously in primary chondrocytes [33]. (**c**) Sulfation of chondroitin sulfate PGs extracted from medium of immortalized chondrocytes was analyzed by HPLC after digestion with chondroitinases ABC and ACII. Data are reported as mean ± standard deviation of three replicates. Significance between KO1 and WT6 samples was analyzed by Student's *t*-test; ** $p < 0.01$. Immortalized KO1 chondrocytes showed a higher percentage of monosulfated disaccharides (ΔDi-4S + ΔDi-6S) compared with immortalized WT6 cells as demonstrated previously in primary chondrocytes [33].

In conclusion, the GAG synthesis and sulfation defects demonstrated in immortalized *Cant1* knock-out chondrocytes mimicked the defects previously described in primary cells from the same mouse model of DBQD1 [33].

2.4. Characterization of the Extracellular Matrix Produced by Immortalized Cells

One of the main features of chondrocytes is their ability to synthesize a huge amount of ECM. To analyze the synthesis and deposition of the ECM by immortalized *Cant1* knock-out and wild-type chondrocytes, KO1, and WT6 cells were incubated for 12 days in DMEM containing 5% FBS in presence or absence of ITS. Insulin, contained in this serum substitute (as in Nutridoma-SP) together with transferrin and sodium selenite, promotes chondrogenesis in ATDC5 cells and favors the differentiated phenotype in immortalized human chondrocytes [21,23,28]. The ECM produced over 12 days was analyzed by Alcian blue staining, aggrecan Western blot, and immunofluorescence.

Alcian blue staining, a cationic dye that stains sulfated GAGs, confirmed the deposition of sulfated PGs in the ECM in both cell lines either in presence or absence of ITS. When ITS was present, PG deposition in the cell layer was significantly increased demonstrating that both cell lines were responsive to ITS ($p = 0.028$ and $p = 0.00005$ in KO1 and WT6, respectively) (Figure 5a,b). Moreover, after ITS supplementation, PG deposition in the ECM was higher in WT6 compared with KO1 (1.970 ± 0.07 vs. 1.233 ± 0.20 absorbance units, respectively; $p = 0.004$) (Figure 5b) confirming the reduced capability of immortalized *Cant1* knock-out chondrocytes to synthesize ECM macromolecules.

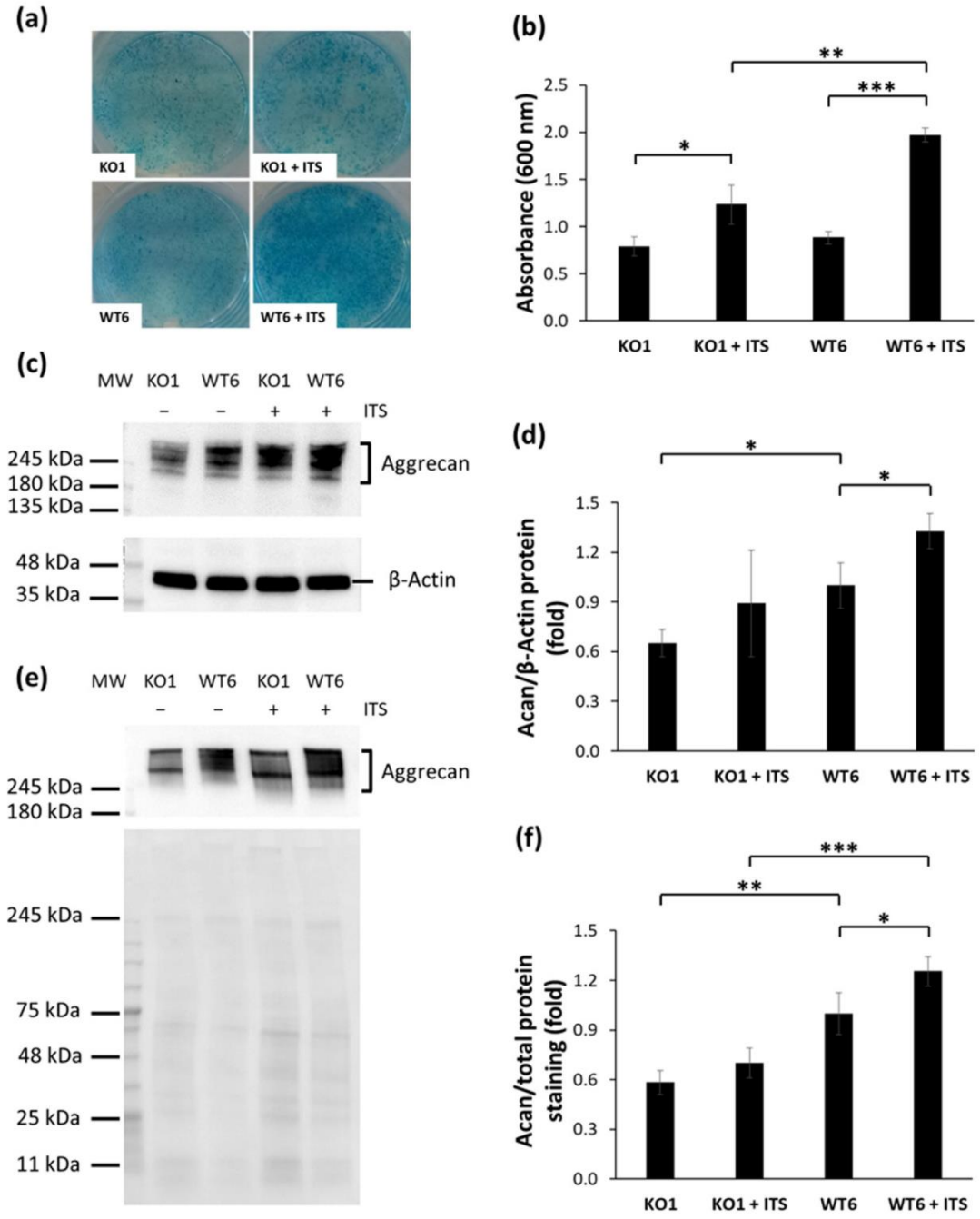

Figure 5. Synthesis and deposition of extracellular matrix proteins in immortalized chondrocytes. (**a**) Alcian blue staining of immortalized chondrocytes incubated with or without ITS for 12 days. (**b**) Spectrophotometric measurement after Alcian blue extraction. Data are reported as mean ± standard deviation of three replicates. Significance among samples was analyzed by Student's *t*-test; * $p < 0.05$; ** $p < 0.01$; *** $p < 0.001$. Alcian blue staining demonstrated that after 12 days of ITS incubation PG deposition was increased in both immortalized *Cant1* knock-out and wild-type chondrocytes and WT6 cells synthesized more PGs compared with KO1. (**c**) Western blot of proteins extracted from the cell layer of immortalized chondrocytes incubated with or without ITS for 12 days was performed with specific antibodies against aggrecan core protein and against β-Actin as internal control. MW = molecular weight. (**d**) Densitometric quantification of blots from cell

layer proteins. The aggrecan band was normalized to the β-Actin band. The intensity of WT6 band was set to one and the expression of other samples was expressed as fold change. Data are reported as mean ± standard deviation of three independent experiments. Significance among samples was analyzed by Student's *t*-test; * $p < 0.05$. (**e**) Western blot of proteins from the medium of immortalized chondrocytes incubated with or without ITS for 12 days was performed with an antibody against the aggrecan core protein; the protein stain of the PVDF membrane with swift membrane stain was used as loading control. MW = molecular weight. (**f**) Densitometric quantification of blots from medium proteins. The aggrecan band was normalized to total protein staining of the PVDF membrane. The intensity of WT6 band was set to one and the expression of other samples was expressed as fold change. Data are reported as mean ± standard deviation of four independent experiments. Significance among samples was analyzed by Student's *t*-test; * $p < 0.05$; ** $p < 0.01$; *** $p < 0.001$. Western blot of cell layer and medium proteins showed increased aggrecan synthesis in WT6 chondrocytes after ITS incubation and a higher aggrecan synthesis in WT6 cell line compared with immortalized KO1 chondrocytes. The full original Western blots are reported in Supplementary Materials Figure S2.

PG deposition in the cell layer was further studied by aggrecan Western blots (Figure 5c). Densitometric analysis demonstrated that aggrecan in the ECM was slightly increased when the KO1 cell line was incubated with ITS, while after ITS supplementation WT6 cell line showed a significant increase of aggrecan ($p = 0.03$). When cells were incubated in basal medium a significantly higher amount of aggrecan was detected in WT6 compared with KO1, while after ITS incubation WT6 showed an increase in aggrecan synthesis compared with KO1, even if not statistically relevant (Figure 5d). To further characterize aggrecan synthesis, the 24 h culture medium at the end of 12 days ITS incubation was analyzed by Western blot (Figure 5e). Aggrecan synthesis was increased after incubation with ITS in both cell lines, even if it was statistically significant only in WT6 cell line ($p = 0.017$). Either in the presence or in absence of ITS, aggrecan synthesis was significantly higher in WT6 compared with KO1 ($p = 0.0001$ and $p = 0.0013$ in presence and in absence of ITS, respectively) (Figure 5f).

The ECM produced after 12 days in presence or absence of ITS was also studied by immunofluorescence analysis with specific antibodies against aggrecan and type II collagen. Increased matrix deposition of both aggrecan and type II collagen was observed in immortalized *Cant1* knock-out and wild-type chondrocytes incubated with ITS compared with immortalized cells incubated in DMEM with 5% FBS. Moreover, in immortalized cells incubated with ITS a better-defined network of aggrecan and type II collagen was observed compared with cells grown in basal medium (Figure 6).

In conclusion, these data demonstrated that ECM is deposited in long term culture of immortalized chondrocytes, in particular when ITS was present in the culture medium. Moreover, immortalized KO1 chondrocytes showed a reduced deposition of ECM molecules compared with immortalized WT6 cells confirming the GAG synthesis defect described above and previously demonstrated in *Cant1* knock-out primary chondrocytes [33].

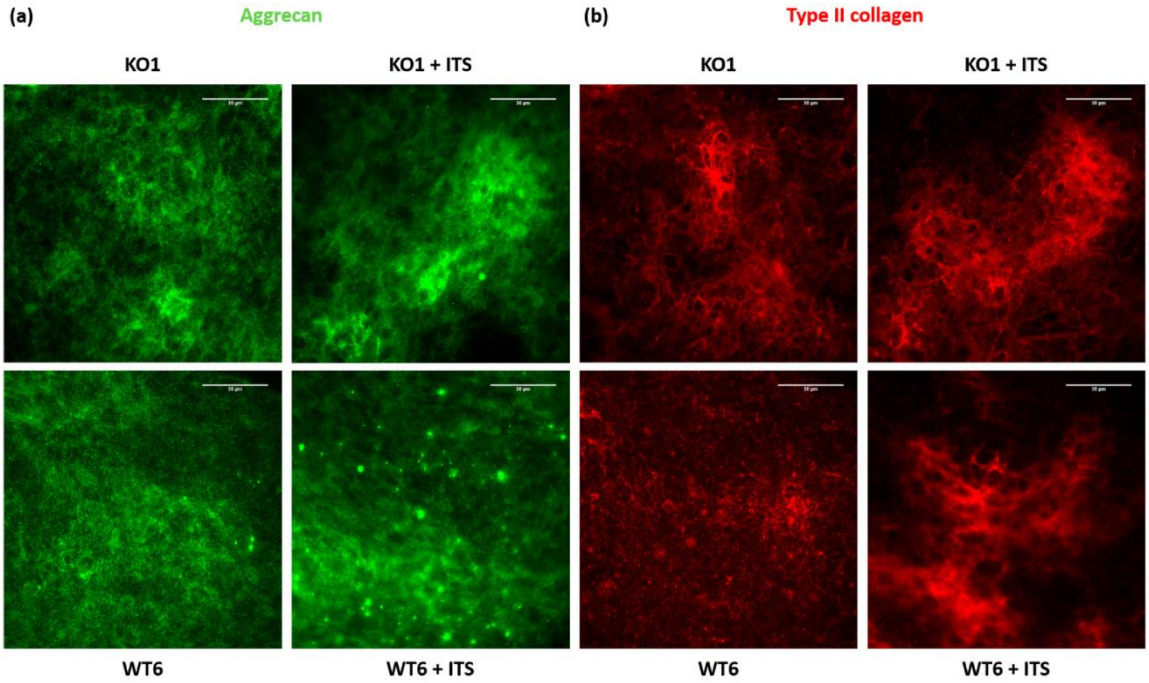

Figure 6. Immunofluorescence study of the extracellular matrix produced by immortalized chondrocytes incubated with or without ITS for 12 days. (**a**) Immunofluorescence analysis with a specific antibody against aggrecan. (**b**) Immunofluorescence analysis with a specific antibody against type II collagen. Both aggrecan and type II collagen showed an increased deposition and a better-defined network in immortalized chondrocytes, both *Cant1* knock-out (KO1) and wild-type (WT6), after incubation with ITS. Scale bar 50 μm.

3. Discussion

Chondrocytes are the sole cell type present in cartilage tissue; thus, they are the central player in the pathophysiology of cartilage disorders. Therefore, chondrocytes have been widely used to study the molecular and cellular regulation of the cells and their role in cartilage metabolism. However prolonged time in culture leads to the de-differentiation of chondrocytes characterized by loss of chondrogenic phenotype and decreased expression of ECM genes limiting their use in research [36]. To overcome these drawbacks chondrocyte cell lines with the ability to maintain or re-express their phenotype have been developed using different approaches: re-differentiation using 3D gels, establishment of chondrosarcoma cell lines and immortalization with viral infection or plasmid transfection [13–16].

The immortalized chondrocytes described so far include normal cells from different species that have been immortalized as an additional tool to study specific aspect of chondrocyte biology in normal condition or in osteoarthritis, the most common degenerative disorder of articular cartilage [25–27]. The functions of specific cartilage macromolecules have been studied also in vivo using different murine models of osteoarthritis as well as animal models of genetic disorders of the skeleton [6,8]. Cell lines established from genetically modified animals would also play important roles in the detailed understanding of the cartilage defects reflecting the genetic aberration and would ultimately reduce the use of transgenic animals for primary cells according to the principle of the Three Rs. In such investigations, cell lines that accurately reproduce the characteristics of primary cells in culture are important and can serve as appropriate model systems. In the last several years, in vitro testing has served as the primary testing model for drugs because it helps bringing new drugs to in vivo studies and then to clinical trials faster and with reduced costs [37].

However, there is a caveat: The in vitro preclinical tools should require a high amount of well-characterized cells, a condition that cannot be achieved with primary chondrocytes, but may be satisfied using immortalized chondrocyte cell lines.

In this work, we successfully established immortalized chondrocytes from *Cant1* knock-out and wild-type mice using a plasmid vector expressing the SV40 large and small T antigen which have been used for human, murine, and rabbit chondrocyte immortalization [17,18,21,26,27,38]. Our results demonstrated the generation of stable cell lines of immortalized murine chondrocytes that express the differentiated phenotype. Proliferation in monolayer culture in the presence of 10% FBS was quite fast and immortalized cells showed a morphology similar to primary chondrocytes. Since immortalization produces a continuous state of proliferation it is important to consider the maintenance of the chondrocyte phenotype. To assess the chondrocyte phenotype, the cell lines were characterized for type II collagen and aggrecan expression at the protein and mRNA level. Among the clones, KO1 and WT6 cell lines showed significantly higher type II collagen and aggrecan expression compared with other clones and for this reason they were further characterized. These observations suggest that SV40 large T antigen expression maintain chondrocytes in a proliferative state preserving the cartilage phenotype.

We previously demonstrated that *Cant1*, a calcium-activated nucleotidase of the Golgi, is important for GAG synthesis [33,35]. Mutations in this gene cause DBQD1 a skeletal disorder belonging to the multiple dislocation group and characterized by severe prenatal and postnatal growth retardation, joint laxity, short extremities, and progressive scoliosis [34]. The functional impairment of the enzyme causes reduced GAG synthesis, chondroitin sulfate oversulfation, reduced hydrodynamic size of GAGs and delayed PG secretion as demonstrated in primary chondrocyte cultures [33]. Thus, once we selected the immortalized cell lines with the chondrocyte phenotype, we checked whether immortalized *Cant1* knock-out cells maintain the phenotypic defects observed in primary chondrocytes. After metabolic labeling with ^{35}S-sulfate of immortalized cell lines, we observed reduced GAG synthesis either in basal medium or in medium containing *p*-nitrophenyl β-D-xylopyranoside in immortalized *Cant1* knock-out chondrocytes compared with immortalized wild-type cells. As already observed in primary culture, the defect was more enhanced in presence of *p*-nitrophenyl β-D-xylopyranoside, a molecule acting as a chain initiator for GAG synthesis. Furthermore, consistent with what observed in primary *Cant1* knock-out cells, chondroitin sulfate GAGs were oversulfated in immortalized *Cant1* knock-out chondrocytes compared with wild-type. Overall, these results confirmed the GAG synthesis defect in immortalized *Cant1* knock-out cells as already observed in primary cells validating the in vitro model.

Immortalized human chondrocytes have been proposed as a good surrogate model to study specific feature of chondrocytes by Hoffman et al.; they demonstrated that clones with a chondrocyte phenotype showed gene expression modulation to an anabolic and catabolic factor, BMP-7 and IL-1, respectively, similar to primary chondrocytes [27]. Correspondingly immortalized mouse chondrocytes either in monolayer or in alginate stimulated with BMP-2 resulted in increased expression of ECM molecules such as type II collagen and aggrecan, while treatment with the pro-inflammatory IL-1 caused increased gene expression of catabolic effectors mimicking primary chondrocytes [26].

PG production by immortalized human chondrocyte cell lines have been reported both in monolayer and alginate cultures since aggrecan, the large aggregating PG of cartilage, is not only a marker of differentiation, but also an essential constituent of the cartilage ECM. It has been reported that in T/C-28a2 and tsT/AC62 cell lines the expression of aggrecan is higher in monolayer compared with alginate cultures. Moreover, since alginate did not expand or remodel, clusters of cells were formed and this might affect cell survival [21]. In the same work it has been reported that FBS favors PG synthesis indicating that the growth factors present in serum were important for ECM synthesis. The capacity of insulin to stimulate PG synthesis has been well documented [18,39,40]. Furthermore, ITS, a serum substitute containing insulin, transferrin, and sodium selenite, increases

ECM deposition in long-term cultures as already observed in ATDC5 cells [28]. For this reason, the ECM produced by immortalized cells after long term culture (12 days) either in presence or absence of ITS was investigated by Alcian blue staining, Western blot, and immunofluorescence studies. All experiments demonstrated that in both cell lines ITS favored ECM synthesis suggesting its use to deeply study the synthesis and deposition of ECM molecules using immortalized chondrocytes. Moreover, the ECM deposition was higher in the wild-type compared with the *Cant1* knock-out cell line confirming the GAG synthesis defect in immortalized *Cant1* knock-out chondrocytes. Interestingly, these data demonstrated that a denser matrix was present in immortalized wild-type chondrocytes compared with immortalized *Cant1* knock-out cells as previously observed ex vivo by TEM studies in cartilage from the *Cant1* knock-out mouse [33].

In conclusion, we immortalized chondrocytes from our mouse model of DBQD1 and we demonstrated that the phenotype of immortalized cells was similar to the one of primary chondrocytes based on PG synthesis, sulfation, and ECM deposition. This cell line is a useful culture model for studying specific steps of PG synthesis, a complex and not well-characterized process. Moreover, since PGs are important components of the cartilage ECM, the model should provide additional information on how the defect in PG biosynthesis could affect the organization of the ECM. This successful immortalization procedure could be applied to cells from other animal models to increase the tools available for physiopathological studies and drug discovery.

4. Materials and Methods

4.1. Animal Model and Care

In this study, wild-type and homozygous *Cant1* knock-out mice with a C57Bl/6J × 129/SV background were used [33]. Animals were genotyped by polymerase chain reaction (PCR) using genomic DNA extracted from mouse tail clips.

Care and use of mice complied with relevant animal welfare institutional guidelines and protocols were approved by the Animal Care and Use Committee of the University of Pavia and the Ministry of Health (Licence n. 486/2019-PR released on 4 July 2019).

4.2. Chondrocyte Isolation and Immortalization

To establish primary chondrocyte cultures, femoral head cartilage of four-day-old mice was harvested and digested with 2 mg/mL of collagenase type II (Invitrogen, Thermo Fisher, Waltham, MA, USA) in Dulbecco's modified Eagle's medium (DMEM; Sigma–Aldrich, Milan, Italy) at 37 °C overnight. Released chondrocytes were plated and cultured in DMEM with 10% fetal bovine serum (FBS; EuroClone, Milan, Italy) at 37 °C in a humidified atmosphere containing 5% CO_2.

The day before transfection, primary chondrocytes were plated in a 24-well plate at 60 kcell/well in 1 mL of DMEM with 10% FBS. Cells were transfected in 0.5 mL of DMEM containing 10% FBS with the pZipSV766-1 plasmid [17,41,42] (kindly provided by Dr. Adriana Zingone, National Cancer Institute, Bethesda, USA) expressing the large and small T antigen of SV40 using the Lipofectamine® LTX & PLUS™ Reagent (Invitrogen, Thermo Fisher, Waltham, MA, USA) in accordance with the manufacturer's instruction. For stable transfection, two days after transfection cells were selected with 0.25 mg/mL G418 (Roche, Mannheim, Germany) in DMEM with 10% FBS for two weeks changing the medium every two days. Then cells were passaged to 10-cm^2 Petri dishes and the selection with 0.25 mg/mL G418 was maintained for another two weeks. For clonal isolation, diluted cells were plated in 10-cm^2 Petri dishes and clones were transferred to 96-well plates and on confluence expanded sequentially to culture dishes of increased cell culture area. Images of cells were acquired with a Leica DMIL LED microscope (Leica, Milan, Italy) connected to a Leica DFC480 camera at 20× magnification using the LAS 3.0.0 software (Leica, Milan, Italy). For all the experiments, cells were used from passage 10 to 20.

4.3. Collagen Analysis

Immortalized cells in a 75 cm^2 flask were incubated in DMEM without FBS supplemented with 100 µg/mL sodium ascorbate at 37 °C in 5% CO_2 for 48 h. After incubation, the medium was harvested, and protease inhibitors (10 mM of benzamidine, 2 mM of N-ethylmaleimide (NEM), 4 mM of ethylenediaminetetraacetic acid (EDTA), 1 mM of phenylmethylsulfonyl fluoride (PMSF) final concentration) were added. Then proteins were precipitated with 176 mg/mL of ammonium sulfate overnight at 4 °C. Collagens were purified by digestion with 100 µg/mL of pepsin (Sigma–Aldrich, Milan, Italy) in 0.5 M of acetic acid, pH 2.0, followed by precipitation with 2 M of NaCl in 0.5 M of acetic acid. Collagens were denatured in Laemmli buffer (62.5 mM of Tris-HCl, pH 6.8, 10% glycerol, 2% sodium dodecyl sulphate (SDS), 0.01% bromophenol blue) and analyzed by SDS-PAGE on 6% polyacrylamide gels in non-reducing condition. Gels were stained with Coomassie Brilliant Blue R-250 (Bio-Rad, Milan, Italy). Images were acquired using Chemidoc XRS apparatus (Bio-Rad, Milan, Italy). Densitometry analysis was performed using the Image-Quant TL v8.1.0.0 software (GE Healthcare Bio-Sciences, Piscataway, NJ, USA).

4.4. Real-Time PCR

Total RNA was extracted from a 10-cm^2 Petri dish of confluent immortalized chondrocytes by QIAzol® Lysis Reagent and miRNeasy Mini Kit (QIAGEN, Milan, Italy) in accordance with the manufacturer's instructions. Genomic DNA was removed by DNA digestion using RNase-Free DNase Set (QIAGEN, Milan, Italy). Then cDNA was obtained from 1 µg of purified RNA by SuperScript™ IV First-Strand Synthesis System (Invitrogen, Thermo Fisher, Waltham, MA, USA) in accordance with the manufacturer's protocol.

Quantitative real-time PCR experiments were performed using the QuantiFast SYBR Green PCR Kit (QIAGEN, Milan, Italy) with QuantiTect Primer Assay (QIAGEN, Milan, Italy) for type II collagen (Col2a1, QT01055523), aggrecan (Acan, QT00175364), and glyceraldehyde 3-phosphate dehydrogenase (Gapdh, QT01658692) as a housekeeping gene for expression normalization. Each sample was run in triplicate in 96-well plates with the QuantStudio 3 (Applied Biosystems, Thermo Fisher, Waltham, MA, USA) apparatus and relative gene expression was determined with the ΔΔCt method.

4.5. Analysis of Proteoglycan Synthesis by Metabolic Labeling

Immortalized chondrocytes were plated in six-well plates at 250 kcell/well in DMEM containing 10% FBS. After 48 h, cells were preincubated with or without 1 mM *p*-nitrophenyl β-D-xylopyranoside (Sigma–Aldrich, Milan, Italy) in minimal essential medium (MEM; Sigma–Aldrich, Milan, Italy) containing 250 µM cold Na_2SO_4 without FBS at 37 °C in 5% CO_2 for two hours. Then cells were labeled with 50 µCi/mL $Na_2[^{35}SO_4]$ (38.8–59.2 TBq/mmol, PerkinElmer, Waltham, MA, USA) in the same medium for 24 h as previously described [43]. Briefly, the medium was harvested with an equal volume of 100 mM sodium acetate buffer, pH 5.8, containing 8 M urea, 4% Triton X-100, 20 mM EDTA, 20 mM NEM, 0.1 M 6-aminocaproic acid and 1 mM PMSF, while the cell layer was lysed in 50 mM sodium acetate buffer, pH 5.8, containing 2 M urea and 2% Triton X-100. An aliquot of cell lysates was used to determine the protein content by the BCA Protein Assay (Thermo Fisher, Waltham, MA, USA) and the rest was added to the medium. PGs were then purified by DEAE Sephacel chromatography (GE Healthcare Bio-Sciences, Piscataway, NJ, USA) as previously described [33]. Then, PGs were quantified by measuring the ^{35}S-activity using a liquid scintillation counter (TRI-CARB 2300 TR, PerkinElmer, Waltham, MA, USA) and normalized to the protein content.

4.6. Proteoglycan Sulfation Analysis

For PG sulfation analysis, immortalized chondrocytes in a 25 cm^2 flask were incubated with DMEM without FBS at 37 °C in 5% CO_2 for 24 h. The medium was made 0.1 M of sodium acetate, pH 5.6, 5 mM of EDTA, and 5 mM of cysteine, and digested with 20 U of papain (Sigma–Aldrich, Milan, Italy) at 65 °C overnight. Then papain was inactivated

at 100 °C for 10 min and released GAGs were recovered by cetylpyridinium chloride precipitation as previously described [33]. Recovered GAGs were digested with 20 mU of chondroitinase ABC (AMSBIO, Abingdon, UK) and 20 mU of chondroitinase ACII (Sigma–Aldrich, Milan, Italy) in 0.1 M of ammonium acetate buffer, pH 7.35, and released chondroitin sulfate disaccharides analyzed by HPLC after 2-aminoacridone (Invitrogen, Thermo Fisher, Waltham, MA, USA) derivatization as previously described [44,45].

4.7. Western Blot Analysis

For Western blot analysis, 1.5×10^6 immortalized chondrocytes were plated in 60-mm-diameter culture dishes with DMEM and 10% FBS and incubated at 37 °C in 5% CO_2. After three days, cells were incubated in DMEM without FBS at 37 °C in 5% CO_2 for 24 h. For insulin–transferrin–selenium (ITS) incubation, 4.4×10^5 immortalized chondrocytes were plated in 60 mm culture dishes with DMEM and 10% FBS and incubated at 37 °C in 5% CO_2. When cells reached 50–70% confluency, the medium was changed with DMEM and 5% FBS with or without ITS (Gibco, Thermo Fisher, Waltham, MA, USA). The medium was changed every two or three days. After 12 days of ITS incubation, cells were incubated in DMEM without FBS at 37 °C in 5% CO_2 for 24 h. At the end of the incubation period, the medium was harvested, and the cell layer was scraped in PBS, centrifuged, and the pellets were lysed in RIPA buffer. Medium and lysed cells were ultrafiltered with Amicon Ultra centrifugal filter units (10 kDa cut-off, Merck Millipore, Milan, Italy) in 0.1 M of ammonium acetate, pH 7.35, and lyophilized. The lyophilizate was dissolved in 200 µL 0.1 M ammonium acetate, pH 7.35, and an aliquot of the cell layer fraction was used for protein quantitation by BCA Protein Assay (Thermo Fisher, Waltham, MA, USA). All samples were digested with 40 mU of chondroitinase ABC (Seikagaku Corporation, Tokyo, Japan) at 37 °C overnight to remove GAGs and unmask the epitope on the aggrecan core protein. Then samples were lyophilized and resuspended in Laemmli buffer. SDS-PAGE was performed on 4–15% polyacrylamide gradient gels (Bio-Rad, Milan, Italy) and proteins were transferred on polyvinylidene difluoride (PVDF) membrane (Amersham Biosciences, Amersham, UK). Membranes were blocked with 5% bovine serum albumin (BSA; Sigma–Aldrich, Milan, Italy) 0.05% Tween-20 (Sigma–Aldrich, Milan, Italy) in Tris-buffered saline (TBS), and incubated with primary antibodies against aggrecan (1:500, rabbit monoclonal antibody, Merck Millipore, Milan, Italy), β-actin (1:5000 mouse monoclonal antibody, Merck Millipore, Milan, Italy), and the appropriate HRP secondary antibody (1:2000, goat anti-rabbit antibody and horse anti-mouse antibody, Cell Signaling, Danvers, MA, USA). Aggrecan and β-actin bands were detected by Westar η C 2.0 (Cyanagen, Bologna, Italy) and images were acquired by ImageQuant LAS 4000 (GE Healthcare Bio-Sciences, Piscataway, NJ, USA). The ImageQuant TL v8.1.0.0 software (GE, Healthcare Bio-Sciences, Piscataway, NJ, USA) was used for densitometry analysis. For cell layer samples, the intensity of the aggrecan band was normalized to the intensity of the β-actin band as a loading control. For normalization of medium samples, before the blocking step, the membrane was stained with the swift membrane stain (G-Biosciences, St Louis, MO, USA) in accordance with the manufacturer's instructions and scanned with ImageQuant LAS 4000 (GE, Healthcare Bio-Sciences, Piscataway, NJ, USA); the intensity of the aggrecan band was normalized to the intensity of the lane after membrane staining. The intensity of the wild-type band was set to one and the expression of other samples was expressed as fold change.

4.8. Alcian Blue Staining

For Alcian blue staining, 40×10^3 immortalized chondrocytes were plated in 24-well plates in DMEM and 10% FBS and incubated at 37 °C in 5% CO_2. When cells reached 50–70% confluency, the medium was changed with DMEM and 5% FBS with or without ITS. The medium was changed every two or three days. After 12 days of ITS incubation, chondrocytes were fixed with 10% formalin in PBS (Sigma–Aldrich, Milan, Italy) for one hour at room temperature. Then, cells were incubated with 0.5% Alcian blue 8GX (Sigma–Aldrich, Milan, Italy) in 0.1 M HCl overnight at room temperature. After one wash with

0.1 M HCl and three with distilled water, the blue dye was solubilized with 4 M guanidine HCl overnight at 4 °C and the absorbance measured with a spectrophotometer at 600 nm.

4.9. Immunofluorescence Studies

To study deposition of ECM, 10×10^3 immortalized chondrocytes were plated on sterile glass coverslips (Marienfeld Superior, Lauda–Königshofen, Germany) in a 24-well plate in DMEM and 10% FBS and incubated at 37 °C in 5% CO_2. When cells reached 50–70% confluency, the medium was changed with DMEM, and 5% FBS supplemented with or without ITS. The medium was changed every two or three days. After 12 days of ITS incubation, cells were washed with PBS and the ECM was processed as previously described [46]. Briefly, samples were incubated three times for 10 min each with 0.5% sodium deoxycholate and 1 mM PMSF in 10 mM Tris-HCl, pH 8.0, at 4 °C followed by three washes 10 min each with 2 mM Tris-HCl, pH 8.0, containing 1 mM PMSF at 4 °C and fixation with 4% formaldehyde in PBS (Invitrogen, Thermo Fisher, Waltham, MA, USA) for 10 min at room temperature. Then samples were blocked with 1.5% BSA in PBS and incubated with a specific primary antibody against aggrecan (1:500, rabbit monoclonal antibody, Merck Millipore, Milan, Italy) and type II collagen (1:100, mouse monoclonal antibody, Merck Millipore, Milan, Italy) overnight at 4 °C. Then samples were incubated with appropriate secondary antibodies: anti-rabbit antibody conjugated with Alexa Fluor 488 (1:2000, Immunological Sciences, Rome, Italy) and anti-mouse antibody conjugated with Alexa Fluor 647 (1:1000, Cell Signaling, Danvers, MA, USA). Fluorescence images were acquired using a widefield Leica microscope (DM6B) driven by LasX software (Leica, Milan, Italy) and equipped with a Hamamatsu Orca-Flash 4.0 camera (Hamamatsu, Hamamatsu City, Japan) and a 63x oil immersion objective (Leica HC PL APO 63x, 1.4NA) (Leica, Milan, Italy).

4.10. Statistical Analysis

Statistical analysis was performed by Microsoft Excel software. All values are reported as mean ± standard deviation. Statistical difference between groups was evaluated using Student's *t*-test and a p-value < 0.05 was considered statistically significant.

Supplementary Materials: Supplementary materials are available online at https://www.mdpi.com/article/10.3390/ijms22179304/s1.

Author Contributions: Conceptualization: C.P.; funding acquisition: A.F. and A.R.; investigation: C.G.T. and B.V.; methodology: C.G.T., A.F., A.R. and C.P.; supervision: A.R. and C.P.; visualization: C.G.T.; writing original draft: A.R. and C.P.; writing—review and editing: all co-authors. All authors have read and agreed to the published version of the manuscript.

Funding: This work was supported by MIUR "Dipartimenti di Eccellenza 2018-2022" to Antonella Forlino and Antonio Rossi.

Institutional Review Board Statement: The study was previously approved by the Animal Care and Use Committee of the University of Pavia and the Ministry of Health (Licence n. 486/2019-PR released on 4 July 2019).

Data Availability Statement: Data are available within the article or Supplementary Materials.

Acknowledgments: We thank Patrizia Vaghi and Amanda Oldani, Centro Grandi Strumenti, University of Pavia, Italy, for fluorescence microscopy support and the animal facility "Centro di servizio per la gestione unificata delle attività di stabulazione e di radiobiologia" of the University of Pavia, Italy to host the animals.

Conflicts of Interest: The authors declare no conflict of interest.

Abbreviations

Acan	aggrecan
BCA	bicinchoninic acid
BMP	bone morphogenetic protein
BSA	bovine serum albumin
CANT1	calcium activated nucleotidase 1
Col2a1	α1 chain of type II collagen
COMP	cartilage oligomeric matrix protein
DBQD1	Desbuquois dysplasia type 1
DMEM	Dulbecco's modified Eagle's medium
ECM	extracellular matrix
EDTA	ethylenediaminetetraacetic acid
ER	endoplasmic reticulum
FBS	fetal bovine serum
GAG	glycosaminoglycan
Gapdh	glyceraldehyde 3-phosphate dehydrogenase
HPLC	high performance liquid chromatography
IL-1	interleukin-1
ITS	insulin-transferrin-selenium
MEM	minimal essential medium
NEM	N-ethylmaleimide
PBS	phosphate buffered saline
PCR	polymerase chain reaction
PG	proteoglycan
PMSF	phenylmethylsulfonyl fluoride
PVDF	polyvinylidene difluoride
SDS	sodium dodecyl sulfate
SDS-PAGE	sodium dodecyl sulfate-polyacrylamide gel electrophoresis
TBS	Tris buffered saline
TEM	transmission electron microscopy
ΔDi-0S	3-O-β(D-gluc-4-eneuronosyl)-N-acetylgalactosamine
ΔDi-4S and ΔDi-6S	derivatives of ΔDi-0S with a sulfate at the 4 or 6 position of hexosamine moiety respectively

References

1. Archer, C.W.; Francis-West, P. The chondrocyte. *Int. J. Biochem. Cell Biol.* **2003**, *35*, 401–404. [CrossRef]
2. Kiani, C.; Chen, L.; Wu, Y.J.; Yee, A.J.; Yang, B.B. Structure and function of aggrecan. *Cell Res.* **2002**, *12*, 19–32. [CrossRef] [PubMed]
3. Kozhemyakina, E.; Lassar, A.B.; Zelzer, E. A pathway to bone: Signaling molecules and transcription factors involved in chondrocyte development and maturation. *Development* **2015**, *142*, 817–831. [CrossRef] [PubMed]
4. Krishnan, Y.; Grodzinsky, A.J. Cartilage diseases. *Matrix Biol.* **2018**, *71*, 51–69. [CrossRef] [PubMed]
5. Mortier, G.R.; Cohn, D.H.; Cormier-Daire, V.; Hall, C.; Krakow, D.; Mundlos, S.; Nishimura, G.; Robertson, S.; Sangiorgi, L.; Savarirayan, R.; et al. Nosology and classification of genetic skeletal disorders: 2019 revision. *Am. J. Med. Genet. A* **2019**, *179*, 2393–2419. [CrossRef] [PubMed]
6. Briggs, M.D.; Bell, P.A.; Pirog, K.A. The utility of mouse models to provide information regarding the pathomolecular mechanisms in human genetic skeletal diseases: The emerging role of endoplasmic reticulum stress (Review). *Int. J. Mol. Med.* **2015**, *35*, 1483–1492. [CrossRef] [PubMed]
7. Serra, C.I.; Soler, C. Animal Models of Osteoarthritis in Small Mammals. *Vet. Clin. N. Am. Exot. Anim. Pract.* **2019**, *22*, 211–221. [CrossRef]
8. Hambright, W.S.; Niedernhofer, L.J.; Huard, J.; Robbins, P.D. Murine models of accelerated aging and musculoskeletal disease. *Bone* **2019**, *125*, 122–127. [CrossRef]
9. Zaucke, F.; Dinser, R.; Maurer, P.; Paulsson, M. Cartilage oligomeric matrix protein (COMP) and collagen IX are sensitive markers for the differentiation state of articular primary chondrocytes. *Biochem. J.* **2001**, *358*, 17–24. [CrossRef]
10. Goldring, M.B.; Sandell, L.J.; Stephenson, M.L.; Krane, S.M. Immune interferon suppresses levels of procollagen mRNA and type II collagen synthesis in cultured human articular and costal chondrocytes. *J. Biol. Chem.* **1986**, *261*, 9049–9055. [CrossRef]
11. Watt, F.M. Effect of seeding density on stability of the differentiated phenotype of pig articular chondrocytes in culture. *J. Cell Sci.* **1988**, *89 Pt 3*, 373–378. [CrossRef]
12. Meretoja, V.V.; Dahlin, R.L.; Kasper, F.K.; Mikos, A.G. Enhanced chondrogenesis in co-cultures with articular chondrocytes and mesenchymal stem cells. *Biomaterials* **2012**, *33*, 6362–6369. [CrossRef] [PubMed]

13. Mok, S.S.; Masuda, K.; Häuselmann, H.J.; Aydelotte, M.B.; Thonar, E.J. Aggrecan synthesized by mature bovine chondrocytes suspended in alginate. Identification of two distinct metabolic matrix pools. *J. Biol. Chem.* **1994**, *269*, 33021–33027. [CrossRef]
14. Benya, P.D.; Shaffer, J.D. Dedifferentiated chondrocytes reexpress the differentiated collagen phenotype when cultured in agarose gels. *Cell* **1982**, *30*, 215–224. [CrossRef]
15. Grigolo, B.; Lisignoli, G.; Piacentini, A.; Fiorini, M.; Gobbi, P.; Mazzotti, G.; Duca, M.; Pavesio, A.; Facchini, A. Evidence for redifferentiation of human chondrocytes grown on a hyaluronan-based biomaterial (HYAff 11): Molecular, immunohistochemical and ultrastructural analysis. *Biomaterials* **2002**, *23*, 1187–1195. [CrossRef]
16. Jin, G.Z.; Kim, H.W. Efficacy of collagen and alginate hydrogels for the prevention of rat chondrocyte dedifferentiation. *J. Tissue Eng.* **2018**, *9*, 1–9. [CrossRef]
17. Mallein-Gerin, F.; Olsen, B.R. Expression of simian virus 40 large T (tumor) oncogene in mouse chondrocytes induces cell proliferation without loss of the differentiated phenotype. *Proc. Natl. Acad. Sci. USA* **1993**, *90*, 3289–3293. [CrossRef]
18. Goldring, M.B.; Birkhead, J.R.; Suen, L.F.; Yamin, R.; Mizuno, S.; Glowacki, J.; Arbiser, J.L.; Apperley, J.F. Interleukin-1 beta-modulated gene expression in immortalized human chondrocytes. *J. Clin. Investig.* **1994**, *94*, 2307–2316. [CrossRef]
19. Mataga, N.; Tamura, M.; Yanai, N.; Shinomura, T.; Kimata, K.; Obinata, M.; Noda, M. Establishment of a novel chondrocyte-like cell line derived from transgenic mice harboring the temperature-sensitive simian virus 40 large T-antigen gene. *J. Bone Miner. Res.* **1996**, *11*, 1646–1654. [CrossRef]
20. Takazawa, Y.; Nifuji, A.; Mataga, N.; Yamauchi, Y.; Kurosawa, H.; Noda, M. Articular cartilage cells immortalized by a temperature sensitive mutant of SV40 large T antigen survive and form cartilage tissue in articular cartilage environment. *J. Cell Biochem.* **1999**, *75*, 338–345. [CrossRef]
21. Kokenyesi, R.; Tan, L.; Robbins, J.R.; Goldring, M.B. Proteoglycan production by immortalized human chondrocyte cell lines cultured under conditions that promote expression of the differentiated phenotype. *Arch. Biochem. Biophys.* **2000**, *383*, 79–90. [CrossRef] [PubMed]
22. Robbins, J.R.; Thomas, B.; Tan, L.; Choy, B.; Arbiser, J.L.; Berenbaum, F.; Goldring, M.B. Immortalized human adult articular chondrocytes maintain cartilage-specific phenotype and responses to interleukin-1beta. *Arthritis Rheum* **2000**, *43*, 2189–2201. [CrossRef]
23. Grigolo, B.; Roseti, L.; Neri, S.; Gobbi, P.; Jensen, P.; Major, E.O.; Facchini, A. Human articular chondrocytes immortalized by HPV-16 E6 and E7 genes: Maintenance of differentiated phenotype under defined culture conditions. *Osteoarthr. Cartil.* **2002**, *10*, 879–889. [CrossRef]
24. Chen, W.H.; Lai, W.F.; Deng, W.P.; Yang, W.K.; Lo, W.C.; Wu, C.C.; Yang, D.M.; Lai, M.T.; Lin, C.T.; Lin, T.W.; et al. Tissue engineered cartilage using human articular chondrocytes immortalized by HPV-16 E6 and E7 genes. *J. Biomed. Mater. Res. Part A* **2006**, *76*, 512–520. [CrossRef] [PubMed]
25. Majumdar, M.K.; Chockalingam, P.S.; Bhat, R.A.; Sheldon, R.; Keohan, C.; Blanchet, T.; Glasson, S.; Morris, E.A. Immortalized cell lines from mouse xiphisternum preserve chondrocyte phenotype. *J. Cell Physiol.* **2006**, *209*, 551–559. [CrossRef] [PubMed]
26. Majumdar, M.K.; Chockalingam, P.S.; Bhat, R.A.; Sheldon, R.; Keohan, C.; Blanchet, T.; Glasson, S.; Morris, E.A. Immortalized mouse articular cartilage cell lines retain chondrocyte phenotype and respond to both anabolic factor BMP-2 and pro-inflammatory factor IL-1. *J. Cell Physiol.* **2008**, *215*, 68–76. [CrossRef]
27. Hoffman, B.E.; Newman-Tarr, T.M.; Gibbard, A.; Wang, S.; Hanning, C.; Pratta, M.A.; Boyle, R.J.; Kumar, S.; Majumdar, M.K. Development and characterization of a human articular cartilage-derived chondrocyte cell line that retains chondrocyte phenotype. *J. Cell Physiol.* **2010**, *222*, 695–702. [CrossRef] [PubMed]
28. Hodax, J.K.; Quintos, J.B.; Gruppuso, P.A.; Chen, Q.; Desai, S.; Jayasuriya, C.T. Aggrecan is required for chondrocyte differentiation in ATDC5 chondroprogenitor cells. *PLoS ONE* **2019**, *14*, e0218399. [CrossRef]
29. Cinque, L.; De Leonibus, C.; Iavazzo, M.; Krahmer, N.; Intartaglia, D.; Salierno, F.G.; De Cegli, R.; Di Malta, C.; Svelto, M.; Lanzara, C.; et al. MiT/TFE factors control ER-phagy via transcriptional regulation of FAM134B. *EMBO J.* **2020**, *39*, 1–22. [CrossRef] [PubMed]
30. Paganini, C.; Costantini, R.; Superti-Furga, A.; Rossi, A. Bone and connective tissue disorders caused by defects in glycosaminoglycan biosynthesis: A panoramic view. *FEBS J.* **2019**, *286*, 3008–3032. [CrossRef]
31. Paganini, C.; Gramegna Tota, C.; Superti-Furga, A.; Rossi, A. Skeletal Dysplasias Caused by Sulfation Defects. *Int. J. Mol. Sci.* **2020**, *21*, 2710. [CrossRef]
32. Atsumi, T.; Miwa, Y.; Kimata, K.; Ikawa, Y. A chondrogenic cell line derived from a differentiating culture of AT805 teratocarcinoma cells. *Cell Differ. Dev.* **1990**, *30*, 109–116. [CrossRef]
33. Paganini, C.; Monti, L.; Costantini, R.; Besio, R.; Lecci, S.; Biggiogera, M.; Tian, K.; Schwartz, J.M.; Huber, C.; Cormier-Daire, V.; et al. Calcium activated nucleotidase 1 (CANT1) is critical for glycosaminoglycan biosynthesis in cartilage and endochondral ossification. *Matrix Biol.* **2019**, *81*, 70–90. [CrossRef]
34. Huber, C.; Oules, B.; Bertoli, M.; Chami, M.; Fradin, M.; Alanay, Y.; Al-Gazali, L.I.; Ausems, M.G.; Bitoun, P.; Cavalcanti, D.P.; et al. Identification of CANT1 mutations in Desbuquois dysplasia. *Am. J. Hum. Genet.* **2009**, *85*, 706–710. [CrossRef]
35. Nizon, M.; Huber, C.; De Leonardis, F.; Merrina, R.; Forlino, A.; Fradin, M.; Tuysuz, B.; Abu-Libdeh, B.Y.; Alanay, Y.; Albrecht, B.; et al. Further delineation of CANT1 phenotypic spectrum and demonstration of its role in proteoglycan synthesis. *Hum. Mutat.* **2012**, *33*, 1261–1266. [CrossRef]

36. Ma, B.; Leijten, J.C.; Wu, L.; Kip, M.; van Blitterswijk, C.A.; Post, J.N.; Karperien, M. Gene expression profiling of dedifferentiated human articular chondrocytes in monolayer culture. *Osteoarthr. Cartil.* **2013**, *21*, 599–603. [CrossRef]
37. Mullan, L.A.; Mularczyk, E.J.; Kung, L.H.; Forouhan, M.; Wragg, J.M.; Goodacre, R.; Bateman, J.F.; Swanton, E.; Briggs, M.D.; Boot-Handford, R.P. Increased intracellular proteolysis reduces disease severity in an ER stress-associated dwarfism. *J. Clin. Investig.* **2017**, *127*, 3861–3865. [CrossRef] [PubMed]
38. Steimberg, N.; Viengchareun, S.; Biehlmann, F.; Guénal, I.; Mignotte, B.; Adolphe, M.; Thenet, S. SV40 large T antigen expression driven by col2a1 regulatory sequences immortalizes articular chondrocytes but does not allow stabilization of type II collagen expression. *Exp. Cell Res.* **1999**, *249*, 248–259. [CrossRef] [PubMed]
39. Takigawa, M.; Pan, H.O.; Kinoshita, A.; Tajima, K.; Takano, Y. Establishment from a human chondrosarcoma of a new immortal cell line with high tumorigenicity in vivo, which is able to form proteoglycan-rich cartilage-like nodules and to respond to insulin in vitro. *Int. J. Cancer* **1991**, *48*, 717–725. [CrossRef]
40. Böhme, K.; Conscience-Egli, M.; Tschan, T.; Winterhalter, K.H.; Bruckner, P. Induction of proliferation or hypertrophy of chondrocytes in serum-free culture: The role of insulin-like growth factor-I, insulin, or thyroxine. *J. Cell Biol.* **1992**, *116*, 1035–1042. [CrossRef] [PubMed]
41. Cepko, C.L.; Roberts, B.E.; Mulligan, R.C. Construction and applications of a highly transmissible murine retrovirus shuttle vector. *Cell* **1984**, *37*, 1053–1062. [CrossRef]
42. Yagüe, E.; Arance, A.; Kubitza, L.; O'Hare, M.; Jat, P.; Ogilvie, C.M.; Hart, I.R.; Higgins, C.F.; Raguz, S. Ability to acquire drug resistance arises early during the tumorigenesis process. *Cancer Res.* **2007**, *67*, 1130–1137. [CrossRef] [PubMed]
43. Paganini, C.; Costantini, R.; Rossi, A. Analysis of Proteoglycan Synthesis and Secretion in Cell Culture Systems. *Methods Mol. Biol.* **2019**, *1952*, 71–80. [CrossRef] [PubMed]
44. Monti, L.; Paganini, C.; Lecci, S.; De Leonardis, F.; Hay, E.; Cohen-Solal, M.; Villani, S.; Superti-Furga, A.; Tenni, R.; Forlino, A.; et al. N-acetylcysteine treatment ameliorates the skeletal phenotype of a mouse model of diastrophic dysplasia. *Hum. Mol. Genet.* **2015**, *24*, 5570–5580. [CrossRef]
45. Paganini, C.; Gramegna Tota, C.; Monti, L.; Monti, I.; Maurizi, A.; Capulli, M.; Bourmaud, M.; Teti, A.; Cohen-Solal, M.; Villani, S.; et al. Improvement of the skeletal phenotype in a mouse model of diastrophic dysplasia after postnatal treatment with N-acetylcysteine. *Biochem. Pharmacol.* **2021**, *185*, 114452. [CrossRef] [PubMed]
46. Hedman, K.; Kurkinen, M.; Alitalo, K.; Vaheri, A.; Johansson, S.; Höök, M. Isolation of the pericellular matrix of human fibroblast cultures. *J. Cell Biol.* **1979**, *81*, 83–91. [CrossRef] [PubMed]

CHAPTER V: IMPROVEMENT OF THE SKELETAL PHENOTYPE IN A MOUSE MODEL OF DIASTROPHIC DYSPLASIA AFTER POSTNATAL TREATMENT WITH N-ACETYLCYSTEINE

1. Aim of the work

Diastrophic dysplasia is a severe chondrodysplasia caused by mutations in the *SLC26A2* gene that encodes for a sulfate/chloride antiporter on the cell membrane known as the diastrophic dysplasia sulfate transporter (DTDST or SLC26A2) [165]. Sulfate is essential for the sulfation of many macromolecules and in particular, of proteoglycans. For this reason, functional impairment of the SLC26A2 transporter causes the decrease of intracellular sulfate, leading to undersulfated PG synthesis.

In normal chondrocytes, the main source of intracellular sulfate is the extracellular uptake, but it has been demonstrated that a small fraction also comes from the catabolism of sulfur-containing amino acids such as cysteine, methionine and other thiols [151]. Interestingly, it has been shown *in vitro* that chondrocytes from a DTD patient in presence of cysteine or N-acetyl-L-cysteine (NAC), an acetylated derivative of cysteine, synthesise PGs that were more sulfated than in basal conditions, suggesting the potential use of sulfhydryl compounds as pharmacological treatment for DTD patients [193].

The dtd mouse, a *Slc26a2* knock-in mouse, reproduce the chondrodysplastic phenotype of DTD patients at the clinical, morphological and biochemical levels [145]; for this reason, it is a valuable *in vivo* model to study the pathogenesis of the disorder and develop potential therapeutic approaches.

In the first study suggesting the use of NAC as a possible alternative source of sulfate in chondrocytes, dtd mice were treated for the first 7 days of life, via daily hypodermic injections of NAC (1g/Kg of body weight). NAC treatment determined a weak but significant increase of PG sulfation in mutant mice compared with the placebo group, while, no skeletal improvement was observed. However, higher or more frequent administrations of the drug were not possible for long periods because of skin ulcers at the injection site. Pharmacokinetics of NAC showed a fast removal of the drug from the bloodstream, within 8 hours from the injection [194], despite its high concentration, suggesting that NAC treatment might be more effective if the plasma concentration of the drug would be stable during the day.

This hypothesis was confirmed in another work, by oral administration of NAC to pregnant females for the whole gestation period, in order to maintain a stable drug concentration in

foetuses. Mutant newborns from females treated with NAC showed a significantly increased cartilage PG sulfation and improved skeletal phenotype compared with mutant mice born from untreated females [195].

All these works demonstrated *in vivo* the effect of NAC as an alternative intracellular sulfate source through its catabolism, suggesting a potential pharmacological treatment for DTD patients. Despite these results, more evidences of its effect on a long-term postnatal period are needed. In fact, patients should be treated postnatally due to the progression of the skeletal phenotype; moreover, DTD is often diagnosed in childhood.

Thus, the aim of this work was to study the skeletal phenotype after a short postnatal treatment of 7 days with NAC, in order to evaluate the drug effect in the first period of life and a long-term postnatal NAC treatment of 21 days, to cover the main period of postnatal skeletal development and growth in mouse. Mice were treated with two daily hypodermic injections of NAC (250 mg/kg body weight), to maintain constant its blood concentration. At the end of the treatment, the effect of NAC at the biochemical and morphological level was evaluated by comparing treated mice with the placebo group. Cartilage PG sulfation was studied by HPLC (high performance liquid chromatography) analysis and skeletal morphology by X-rays, microCT, DEXA and histological analyses.

These results were collected in a research paper entitled “Improvement of the skeletal phenotype in a mouse model of diastrophic dysplasia after postnatal treatment with N acetylcysteine”, which was published in *Biochemical Pharmacology* in February 2021. The pdf of the published paper is provided below here.

Biochemical Pharmacology 185 (2021) 114452

Contents lists available at ScienceDirect

Biochemical Pharmacology

journal homepage: www.elsevier.com/locate/biochempharm

Improvement of the skeletal phenotype in a mouse model of diastrophic dysplasia after postnatal treatment with N-acetylcysteine

Chiara Paganini [a], Chiara Gramegna Tota [a], Luca Monti [a], Ilaria Monti [a], Antonio Maurizi [b], Mattia Capulli [b], Morgane Bourmaud [c], Anna Teti [b], Martine Cohen-Solal [c], Simona Villani [d], Antonella Forlino [a], Andrea Superti-Furga [e], Antonio Rossi [a,*]

[a] Department of Molecular Medicine, Unit of Biochemistry, University of Pavia, 27100 Pavia, Italy
[b] Department of Biotechnological and Applied Clinical Sciences, University of L'Aquila, 67100 L'Aquila, Italy
[c] Bioscar Inserm U1132 and Université de Paris, Hôpital Lariboisiere, 75010 Paris, France
[d] Department of Public Health, Experimental and Forensic Medicine, Unit of Biostatistics and Clinical Epidemiology, University of Pavia, 27100 Pavia, Italy
[e] Division of Genetic Medicine, Lausanne University Hospital and University of Lausanne, 1011 Lausanne, Switzerland

ARTICLE INFO

Keywords:
Cartilage
N-acetylcysteine
Proteoglycan
Skeletal dysplasia
Sulfation

ABSTRACT

Diastrophic dysplasia (DTD) is a recessive chondrodysplasia caused by mutations in the *SLC26A2* gene encoding for a sulfate/chloride transporter. When SLC26A2 is impaired intracellular level of sulfate is reduced leading to the synthesis of undersulfated proteoglycans. In normal chondrocytes, the main source of intracellular sulfate is the extracellular uptake through SLC26A2, but a small amount comes from the catabolism of sulfur-containing amino acids and other thiols. Here N-acetylcysteine (NAC), an extensively used drug, is proposed as alternative source of intracellular sulfate in an animal model of DTD (dtd mouse). Mutant and wild type mice were treated twice a day with hypodermic injections of 250 mg NAC/kg body weight for one week after birth. At the end of the treatment, an improvement trend in cartilage proteoglycan sulfation and in the skeletal phenotype of treated dtd mice were observed. Thus, a longer treatment lasted three weeks starting from birth was performed. Treated mutant mice showed a significant increase of cartilage proteoglycan sulfation and a relevant improvement of the skeletal phenotype based on measurements of several bony elements and bone quality by DEXA and micro CT. Moreover, the amelioration of the overall growth plate morphology in treated dtd mice suggested a partial rescue of the endochondral ossification process. Overall, the results prove that NAC is an effective source of intracellular sulfate for dtd mice in the postnatal period. This finding paves the way for a potential pharmacological treatment of DTD patients taking advantage from a drug repositioning strategy.

1. Introduction

Diastrophic dysplasia (DTD) is a rare autosomal recessive osteochondrodysplasia characterised by a severe form of dwarfism with shortened trunk, markedly shortened extremities, but a normal-size head [1]. Patients show growth retardation, kyphoscoliosis and typical hand and foot deformities, including hitchhiker thumb and clubfoot.

DTD belongs to the SLC26A2 family of disorders which are caused by mutations in the *SLC26A2* gene encoding for a sulfate/chloride antiporter of the cell membrane [2]. According to the clinical phenotypes, four different conditions have been described that in decreasing order of severity include achondrogenesis type 1B (ACG1B, MIM 600972), atelosteogenesis type 2 (AO2, MIM 256050), diastrophic dysplasia (DTD, MIM 222600) and recessive multiple epiphyseal dysplasia (EDM4, MIM 226900) [3]. Functional impairment of the SLC26A2 transporter causes reduced sulfate uptake leading to the synthesis of undersulfated

Abbreviations: ACG1B, achondrogenesis type 1B; AMAC, 2-aminoacridone; AO2, atelosteogenesis type 2; BMC, bone mineral content; CPC, cetylpyridinium chloride; DEXA, dual energy X-ray absorptiometry; DTD, diastrophic dysplasia; ΔDi-0S, 3-O-β-(D-gluc-4-ene-uronosyl)-N-acetylgalactosamine; ΔDi-4S, derivative of ΔDi-0S with a sulfate at the 4 position of the hexosamine moiety; ΔDi-6S, derivative of ΔDi-0S with a sulfate at the 6 position of the hexosamine moiety; ECM, extracellular matrix; EDM4, recessive multiple epiphyseal dysplasia; GAG, glycosaminoglycan; micro CT, micro computed tomography; NAC, N-acetyl-L-cysteine; PG, proteoglycan; SBD-F, 7-fluorobenzo-2-oxa-1,3-diazole-4-sulfonic acid ammonium salt; SLC26, solute carrier family 26.

* Corresponding author at: Dipartimento di Medicina Molecolare, Unità di Biochimica "Alessandro Castellani", Via Taramelli, 3/B, I-27100 Pavia, Italy.
E-mail address: antrossi@unipv.it (A. Rossi).

https://doi.org/10.1016/j.bcp.2021.114452
Received 30 October 2020; Received in revised form 22 January 2021; Accepted 25 January 2021
Available online 3 February 2021
0006-2952/© 2021 Elsevier Inc. All rights reserved.

proteoglycans (PGs). Sulfate is important for macromolecular sulfation, particularly in chondrocytes that synthesise a huge amount of sulfated PGs crucial for cartilage structure and function. The clinical severity has been related to the severity of the mutation, the residual activity of the sulfate transporter and the degree of cartilage PG undersulfation [4]. These results suggest that an amelioration of macromolecular sulfation might improve the skeletal phenotype.

Even if the intracellular sulfate needs are accomplished mainly by the sulfate transporter, it has been demonstrated that there are other pathways of sulfate recruitment (i.e. methionine, cysteine and other thiols) depending on the cell type [5,6]. Interestingly also chondrocytes from a DTD patient in the presence of cysteine or N-acetylcysteine (NAC), a derivative of cysteine, synthesise PGs that are more sulfated than in basal condition, suggesting a potential use of sulfhydryl compounds as pharmacological treatment for DTD patients [7].

The dtd mouse, a *Slc26a2* knock-in mouse, shows a chondrodysplastic phenotype reminiscent of human DTD with marked cartilage PG undersulfation making it an appropriate *in vivo* model to study the pathogenesis of the disorder and to develop potential therapeutic approaches [8]. Using the animal model we demonstrated that sulfate is recruited from the intracellular oxidation of thiols also *in vivo* [9]. Studies of NAC pharmacokinetic demonstrated a fast removal of the drug from the bloodstream within 8 hours from injection suggesting that NAC treatment might be more effective if the plasma concentration of NAC would be stable. This hypothesis was confirmed by administering NAC in drinking water to pregnant females for the whole pregnancy in order to allow a constant supply of the drug to foetuses. In dtd newborns from females treated with NAC, cartilage PG sulfation was increased compared with dtd mice from untreated females and the skeletal phenotype improved toward the normal bone morphology [10].

All these studies demonstrated *in vivo* the effect of NAC as an alternative intracellular sulfate source through its catabolism suggesting a potential pharmacological treatment for DTD patients. Despite these results, evidences of its effect on the postnatal period are needed; in fact, patients should be treated postnatally due to the progression of the skeletal phenotype; moreover, DTD is often diagnosed in childhood.

For this purpose, using the dtd mouse, we evaluated at the biochemical and morphological level the efficacy of a short and long term postnatal NAC treatment. The NAC blood concentration was maintained by injecting the drug twice a day. First, we performed a short NAC treatment of 7 days to evaluate the drug effect in the first period of life, and then a longer treatment of 21 days to cover the main period of mouse skeletal growth. At the end of the treatment, we evaluated the effect of NAC based on cartilage PG sulfation analysis, skeleton morphology by X-ray imaging and histological analysis of the cartilage growth plate.

2. Materials and methods

2.1. Animal model and drug treatment

The dtd mouse is a knock-in for a C1184T transition causing an A386V substitution in the Slc26a2, a mutation already found in patients with diastrophic dysplasia; homozygous mutant animals have been validated previously as animal models of human DTD [8]. In this study, wild type and homozygous mutant mice with a C57Bl/6J × 129/SV background were used. No gender difference has been observed in young animals; for this reason, only male mice were used. Animals were genotyped by polymerase chain reaction (PCR) using genomic DNA extracted from mouse tail clips to discriminate homozygous mutant (dtd) from heterozygous and wild type mice. Heterozygous animals were normal both at the skeletal and biochemical level as previously described [8]; thus, they were not used in the study.

Care and use of mice for this work were in compliance with relevant animal welfare institutional guidelines. Mice were bred with free access to water and standard pelleted food. Moreover, environmental parameters of the facility were controlled with 12:12 h light:dark cycle and constant temperature (24 °C). The drug treatment protocol was approved by the Animal Care and Use Committee of the University of Pavia and the Ministry of Health (licence n. 99/2018-PR).

Wild type and dtd mice were treated for 7 or 21 days starting from birth by twice a day hypodermic injections of 0.19 M N-acetylcysteine (NAC, Sigma-Aldrich, Milan, Italy) in water for injection, brought to pH 7.0–7.4 with NaOH, or placebo (physiological saline solution). Mouse handling and environmental conditions were carefully considered to avoid stress during the drug trial. In order to administer 250 mg NAC/kg body weight, 8 μl/g body weight of 0.19 M NAC solution were hypodermically injected in mice for each treatment session.

At the end of the drug treatment period, mice were sacrificed by CO_2 inhalation for skeletal, biochemical and histological studies.

2.2. Drug pharmacokinetic

A pharmacokinetic study was performed injecting 8 μl/g body weight of 0.19 M NAC solution in 5 days old wild type mice. At 0, 2, 4, 6 and 8 h after injection 3 mice for each time point were sacrificed and blood was collected with anticoagulant. Blood samples were centrifuged for 15 min at 3,000×*g* to collect plasma.

In order to measure the NAC concentration in plasma and in whole body homogenates 5 days old mice were injected with NAC as described above and 8 h from injection blood was collected and animals were sacrificed. The whole body was homogenised in PBS (Sigma-Aldrich, Milan, Italy) with an Ultra-Turrax T25 (IKA, Staufen, Germany). Since pups are sucking continuously, and therefore their intestine contains significant amounts of milk, the stomach and gut were excised from mice before homogenization to eliminate a possible dilution effect of milk. Body homogenates were clarified by centrifugation for 5 min at 13,000×*g* at 4 °C.

NAC concentration in plasma and homogenates was determined by high-performance liquid chromatography (HPLC) after 7-fluorobenzo-2-oxa-1,3-diazole-4-sulfonic acid ammonium salt (SBD-F, Sigma-Aldrich, Milan, Italy) derivatization. To measure the NAC plasma concentration, 35 pmol of cysteamine (Sigma-Aldrich, Milan, Italy) as internal standard were added to 50 μl of plasma, while for NAC homogenate concentration 70 pmol of cysteamine (Sigma-Aldrich, Milan, Italy) as internal standard were added to 100 μl of homogenate. Both samples were derivatized as previously reported [10,11].

A binary pump system (Binary HPLC Pump 1525μ, Waters, Milford, USA) coupled to a fluorescent detector (Multi λ Fluorescence detector 2475, Waters) set at λ_{ex} 385 nm and λ_{em} 515 nm was used for HPLC analysis. Chromatography was carried out with LiChroCART® 250–4 Superspher® 100 RP-18 endcapped column (Merck, Milan, Italy) and a LiChroCART® 25–4 LiChrospher® 100 RP-18 endcapped (5 μm) as precolumn (Merck, Milan, Italy). Mobile phases were 0.1 M KH_2PO_4 (Merck, Milan, Italy), pH 3.0 (buffer A) and 0.1 M KH_2PO_4, pH 3.0, in 50:50 (v/v) water and acetonitrile (Merck, Milan, Italy) (buffer B). Elution was carried out at room temperature with a linear gradient of 0–25% buffer B in 35 min at a flow rate of 0.8 ml/min.

2.3. Proteoglycan sulfation analysis

PG sulfation of femoral head cartilage was measured by HPLC disaccharide analysis after 2-aminoacridone (AMAC) derivatization.

At the end of the treatment periods, femoral head cartilage was carefully dissected under the dissection microscope and digested with 10 U of papain (Sigma-Aldrich, Milan, Italy) in 300 μl of 0.1 M sodium acetate, pH 5.6, 5 mM EDTA and 5 mM cysteine at 65 °C overnight. After papain inactivation at 100 °C for 10 min, released glycosaminoglycans (GAGs) were recovered by precipitation with 1% cetylpyridinium chloride (CPC) at room temperature overnight.

CPC precipitates were washed 3 times with 500 μl 10% potassium acetate in 96% ethanol and 3 times with 96% ethanol. Then pellets were

solubilised in 200 μl of 0.1 M ammonium acetate buffer, pH 7.35, containing 20 mU of chondroitinase ABC (AMSBIO, Abingdon, UK)) and 20 mU chondroitinase ACII (Sigma-Aldrich, Milan, Italy). After digestion at 37 °C overnight, samples were lyophilized and then derivatized with AMAC (Invitrogen, ThermoFisher, USA) as previously described [10].

HPLC analysis was performed using an HPLC binary pump system (Binary HPLC Pump 1525μ, Waters, Milford, USA) coupled to a fluorescent detector (Multi λ Fluorescence detector 2475, Waters, Milford, USA) set at λ_{ex} 425 nm and λ_{em} 525 nm. Chromatography was carried out with a LiChroCART® 250–4 Superspher® 100 RP-18 endcapped column (Merck, Milan, Italy) and a LiChroCART® 4–4 LiChrospher® 100 RP-18 endcapped (5 μm) as precolumn (Merck, Milan, Italy). Mobile phases were 0.1 M ammonium acetate (VWR, Milan, Italy), pH 7.00 (buffer A) and methanol (Merck, Milan, Italy) (buffer B), as previously reported [12]. Elution was performed at room temperature with a linear gradient of 0–20% buffer B in 2 min and 20–45% buffer B in 34 min at a flow rate of 0.7 ml/min.

2.4. X-ray analysis

X-ray analysis was performed with a Faxitron MX-20 cabinet X-ray system (Faxitron Bioptics, Marlborough, MA, USA), as previously described [13]. Briefly, X-rays of 1 week old mice was performed at 21 kV for 25 s with 3-fold magnification for whole body images and at 25 kV for 30 s with 4-fold magnification for limbs, while for 3 weeks old mice 27 kV for 19 s with 2-fold magnification for whole body and 30 kV for 30 s with 3-fold magnification for limbs were used. Kodak Direct-View Elite CR System (Kodak, Rochester, USA) was used to get digitalized X-ray images and K-PACS software (Kodak, Rochester, USA) for morphometric analysis. Bony elements were measured as shown in Fig. 1.

2.5. Histological staining and histomorphometric analysis.

Mouse hind limbs were dissected immediately after sacrifice, fixed with 10% formalin in PBS (Sigma-Adrich, Milan, Italy) and processed for light microscopy according to standard procedures. Briefly, samples were decalcified with Ion-Exchange Decal (I.E.D.) Unit (Biocare Medical, Pacheco, CA, USA) at room temperature. After washing with water, samples were dehydrated with increasing series of ethanol and embedded in paraffin (VWR, Milan, Italy). Six μm sections were cut parallel to the long axis of the tibia using a RM2265 microtome (Leica, Milan, Italy) and stained with haematoxylin and eosin according to standard protocols. Section images were acquired using a DM5500 B microscope (Leica, Milan, Italy) connected to a Leica DFC480 camera. All histomorphometric measurements were performed by LAS V4.5 software (Leica, Milan, Italy). To determine the height of the growth plate, 5 mice per group, 6 sections per animal and 5 measurements per section were performed. To determine the column height in the hypertrophic zone, 5 mice per group, 3 sections per animal and 20 columns per section were measured.

2.6. Micro CT analysis

Micro CT was performed using the SkyScan 1174 system (Bruker, Milan, Italy). The scans were carried out on tibia of wild type and dtd mice with a 6.7 μm slide resolution. Reconstruction of 2D serial images was performed by Skyscan NRecon software using a modified Feldkamp algorithm [14]. Three-dimensional (3D) analysis was carried out employing a Marching Cubes type model with a rendered surface [15]. The trabecular bone parameters were calculated in the secondary spongiosa on 300 consecutive slides starting 500 μm away from the growth plate [16]. Bone cortical analysis was performed on 150 consecutive slides in the tibia midshaft, starting 2500 μm below the growth plate. Threshold values were applied for segmenting trabecular bone using an adaptative median-c method. Bone trabecular and cortical variables were determined according to Bouxsein et al. [15]. All the micro CT analysis were adjusted to tibia length.

2.7. Dual energy X-ray absorptiometry (DEXA) analysis

Hind limbs were dissected from 21 day old mice and were fixed with 10% formalin in PBS (Sigma-Adrich, Milan, Italy). Then samples were analysed by Dual-energy X-ray absorptiometry (Faxitron UltraFocus^{DXA},

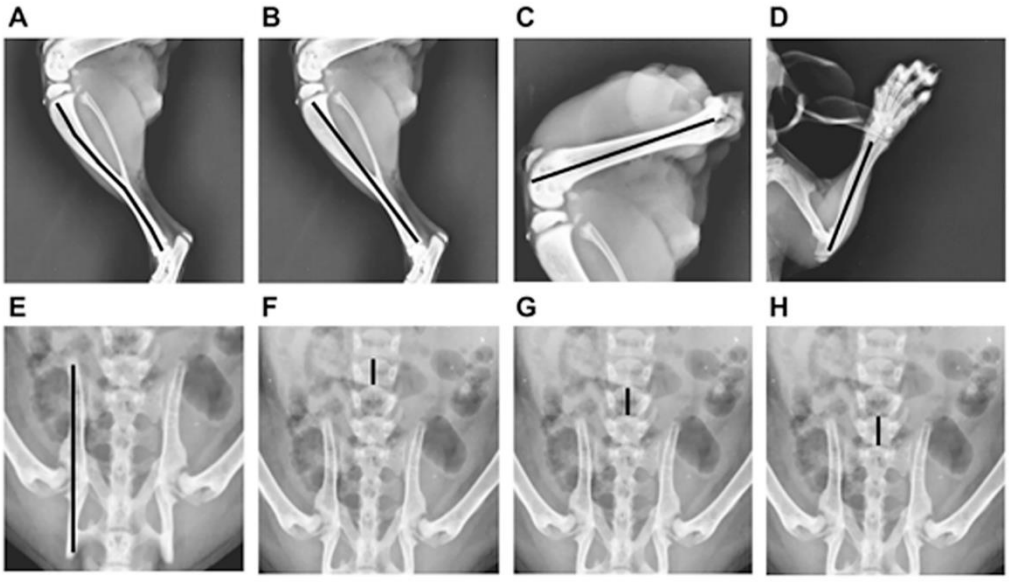

Fig. 1. Morphometric analysis of bony elements on X-ray images. Bony elements were measured on X-ray images as shown in the figure. Several long bones were considered measuring the tibia length (A), the distance between tibia metaphysis (B), the length of femur (C) and radius (D), while hip dysplasia was investigated analysing hip length (E). Moreover the height of L4 (F), L5 (G) and L6 (H) vertebrae was measured.

Marlborough, MA, USA). After calibration, the bone mineral content (BMC) in the femur and the tibia was measured using Faxitron software (Vision DXA, version 2.4.2U).

2.8. Statistical analysis

Data are reported as mean ± standard deviation (SD), if the normality was respected, or median with interquartile range (25th and 75th centiles) if not. The Shapiro-Wilk normality test was used.

To evaluate differences among groups, one-way analysis of variance (ANOVA) or the analogous non parametric test (Kruskal-Wallis test) was applied, followed by the appropriate post-hoc test if significant. The Bonferroni's correction for multiple comparison tests was applied. Mann-Whitney *U* test was used in the post-hoc analyses for Kruskal-Wallis test. A $P < 0.05$ was considered significant. In the multiple comparison test, $P < 0.0083$ was the marker of significant contrast, but the final p-values were reported at < 0.05. STATA 15® software was used for statistical analysis.

3. Results

3.1. Pharmacokinetics of hypodermic injections of N-acetylcysteine

Among the many routes of NAC administration, we considered hypodermic injection as the most reliable strategy to treat newborn mice since preliminary experiments demonstrated that the drug was not present in the milk of lactating females treated with NAC. To determine the plasma drug concentration over time we performed a pharmacokinetic study in 5 day old wild type mice; animals were injected with 250 mg NAC/kg body weight and plasma was collected at different time points from the injection: 0, 2, 4, 6 and 8 h. The plasma drug concentration was analysed by reverse-phase HPLC after derivatization with SBD-F.

In normal conditions, NAC was not present in plasma. After hypodermic injection of 250 mg NAC/kg body weight the drug plasma concentration reached a maximum after 2 h (39.52 ± 0.74 μg/ml) and then it rapidly dropped down to 0.76 ± 0.08 μg/ml 8 h after injection (Fig. 2).

In a further experiment, we measured the NAC concentration in plasma and in whole body homogenates of 5 day old wild type mice 8 h after NAC injection. The drug plasma concentration was 0.84 ± 0.11 μg NAC/ml, while in mouse homogenates we detected 0.64 ± 0.34 μg NAC/g body weight (n = 3).

In a previous work, we demonstrated that 0.7 ± 0.3 μg NAC/g foetus weight was effective to improve the skeletal phenotype of dtd newborns after treatment of pregnant females with NAC in drinking water [10]. Since the plasma and whole body homogenate drug concentration 8 h after hypodermic injection was similar to the one detected in NAC treatment of foetuses, wild type and dtd newborns were treated by hypodermic injection of 250 mg NAC/kg body weight twice a day. The placebo group received an equal amount of physiological solution. We set up two treatments that lasted 7 days (short term) and 21 days (long term) from birth, respectively.

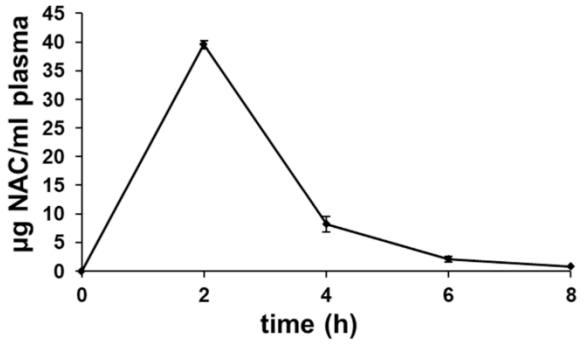

Fig. 2. Pharmacokinetic study of hypodermic injection of N-acetylcysteine. Five days old wild type mice were injected with an hypodermic injection of 250 mg NAC/kg body weight and the drug plasma concentration was analysed at different time points. Two hours from injection, NAC plasma concentration reached a maximum and then it rapidly dropped down. Eight hours after injection, NAC plasma concentration was 0.76 μg/ml, similar to the NAC concentration previously found in foetus treatment [10]. Data are reported as mean ± SD, n = 3.

3.2. Short term N-acetylcysteine treatment

3.2.1. Cartilage proteoglycan sulfation after 7 days N-acetylcysteine treatment

We treated newborn mice twice a day with hypodermic injections of 250 mg NAC/kg body weight for 7 days. At the end of the treatment period mice were sacrificed and femoral head cartilage was harvested for PG sulfation analysis by HPLC.

The percentage of monosulfated disaccharides (ΔDi-4S and ΔDi-6S) relative to the total amount of disaccharides (ΔDi-0S, ΔDi-4S and ΔDi-6S) was increased in dtd mice treated with hypodermic injections of NAC compared with the dtd placebo group (74.4% and 68.6%, respectively), but this improvement was not significant (Fig. 3). In accordance with this result, the percentage of monosulfated disaccharides in treated dtd mice was significantly reduced compared with treated and untreated wild type mice (85.7%, $P = 0.01$ and 84.9%, $P < 0.05$, respectively). Moreover, no difference was detected in the percentage of monosulfated disaccharides between treated and untreated wild type mice indicating no effect of NAC on PG sulfation in wild type animals (Fig. 3).

Overall, these data demonstrated that the 7 days NAC treatment did not significantly increase PG sulfation in mutant mice, even if an amelioration trend was observed.

3.2.2. Skeletal phenotype after 7 days N-acetylcysteine treatment

To investigate the NAC effect on the skeletal phenotype after 7 days treatment, the skeleton of wild type and dtd mice was studied by X-rays.

We performed morphometric analysis of the femur and tibia on X-ray

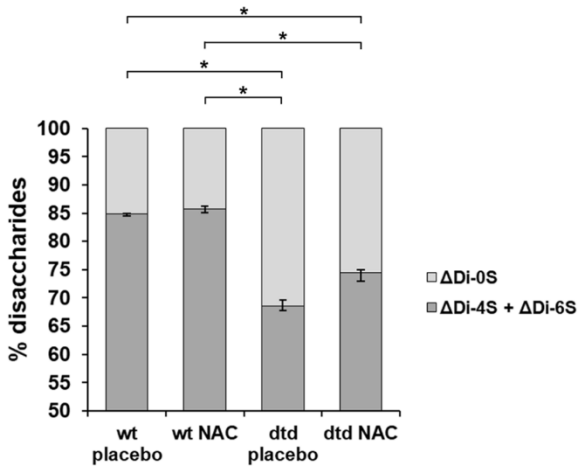

Fig. 3. Effect of 7 days N-acetylcysteine treatment on sulfation of cartilage proteoglycan. Wild type and dtd newborn mice were treated for 7 days from birth twice a day with hypodermic injections of 250 mg NAC/kg body weight or placebo. The percentage of sulfated disaccharides (ΔDi-4S + ΔDi-6S) was increased in treated dtd mice compared with untreated dtd ones, even if statistical significance was not reached. Data are reported as median, 25th and 75th percentile, n = 6. Significant differences among groups were found by Kruskal-Wallis test (KW = 21.49; $P = 0.0001$) and Mann-Whitney test was used as post-hoc analysis; $^*P < 0.05$.

images. In dtd mice after NAC treatment the femur length was slightly increased compared with the dtd placebo group, even if this improvement was not significant. The length and the distance between tibia metaphysis in NAC treated dtd mice showed an improvement compared with untreated dtd animals, but the difference was not statistically relevant. All these parameters in treated and untreated dtd mice were markedly reduced compared to wild type animals ($P < 0.001$), while no significant differences were found in wild type mice after the NAC treatment compared with the placebo group (Fig. 4).

In conclusion, these results demonstrated an amelioration trend not statistically relevant in the skeletal phenotype of dtd mice treated with NAC for 7 days. However, these data suggested that a long term treatment might be effective in improving the skeletal phenotype.

3.3. Long term N-acetylcysteine treatment

3.3.1. Cartilage proteoglycan sulfation after 21 days N-acetylcysteine treatment

To investigate if a longer NAC treatment could improve the mutant phenotype, we treated wild type and dtd mice with hypodermic injections of 250 mg NAC/kg body weight twice a day for 21 days from birth.

At the end of the drug treatment, mice were sacrificed and cartilage PG sulfation was studied by HPLC disaccharide analysis. Results demonstrated a significant increase in the percentage of monosulfated disaccharides (ΔDi-4S and ΔDi-6S) of dtd mice treated with NAC compared with the dtd placebo group (84.50% and 80.40%, respectively; $P < 0.05$), even though the monosulfated disaccharide percentage of treated dtd mice was reduced compared with wild type values ($P < 0.001$; Fig. 5). NAC had no effect on PG sulfation in wild type mice since no significant difference was observed between treated and untreated wild type animals (91.20% and 91.00%, respectively).

In summary, this result demonstrated that long term NAC treatment significantly increases PG sulfation in dtd mice, although wild type values were not reached.

3.3.2. Body weight and length after N-acetylcysteine treatment

To evaluate any potential adverse effect of NAC on mouse growth due to the dosage and administration route of the drug, we analysed the body weight of wild type and dtd mice in both NAC and placebo groups after the 21 days treatment.

Treated dtd mice showed a significant increase in body weight compared with the dtd placebo group (6.22 ± 0.75 g and 5.08 ± 0.75 g, respectively; $P < 0.01$), even though the weight of both dtd mouse groups was reduced compared with wild type mice ($P < 0.001$). Moreover, NAC treatment did not affect the body weight of wild type mice

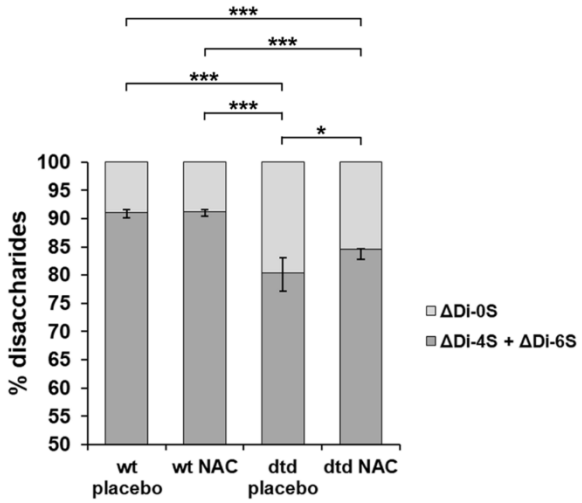

Fig. 5. Effect of 21 days N-acetylcysteine treatment on sulfation of cartilage proteoglycan. Wild type and dtd newborn mice were treated for 21 days twice a day with hypodermic injection of 250 mg NAC/kg body weight or placebo. The percentage of sulfated disaccharides (ΔDi-4S + ΔDi-6S) was significantly increased in treated dtd mice compared with untreated dtd ones. Data are reported as median, 25th and 75th percentile, n = 10. Significant differences among groups were found by Kruskal-Wallis test (KW = 31.49; $P = 0.0001$) and Mann-Whitney test was used as post-hoc analysis; *$P < 0.05$; ***$P < 0.001$.

since no difference was observed between wild types treated with the drug or the placebo (8.02 ± 0.87 g and 8.37 ± 0.48 g, respectively; Fig. 6A) suggesting no toxic effect of the drug on animal growth.

Drug toxicity on mouse growth was also excluded in the short term NAC treatment since no weight difference was observed between treated and untreated wild type animals (4.53 ± 0.60 g and 4.20 ± 0.46 g, respectively). Interestingly, dtd mice treated with NAC for 7 days showed body weight increase compared with untreated dtd ones (3.27 ± 0.48 g and 2.73 ± 0.45 g, respectively), although not statistically relevant supporting the amelioration trend of the mutant phenotype in the short term treatment.

Analysis of the body length of mice (from the tip of the nose to the 3rd caudal vertebra) at the end of the long term NAC treatment confirmed the normal growth of wild type mice during NAC administration since no relevant difference was observed in body length between treated and untreated wild type animals (58.67 ± 1.58 mm and 58.92 ± 1.83 mm, respectively). As already observed for the body

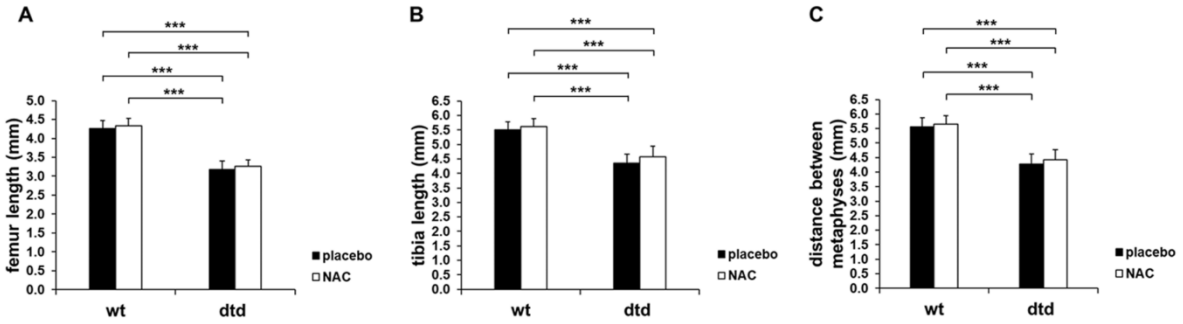

Fig. 4. Effect of 7 days N-acetylcysteine treatment on the skeletal phenotype. After treatment for 7 days from birth the long bones in the dtd group were significantly shorter compared with wild type group as demonstrated by the length of femur (A) and tibia (B) and by the distance between tibia metaphysis (C). In treated dtd mice an amelioration trend of these skeletal elements without significant relevance was observed. Data are reported as mean ± SD, n = 6. Significant differences among groups were found by ANOVA test (F = 130.511; $P < 0.001$ for femur length; F = 54.942; $P < 0.001$ for tibia length and F = 63.129; $P < 0.001$ for distance between tibia metaphysis) and Bonferroni's correction for multiple test was applied in the post-hoc analysis; ***$P < 0.001$.

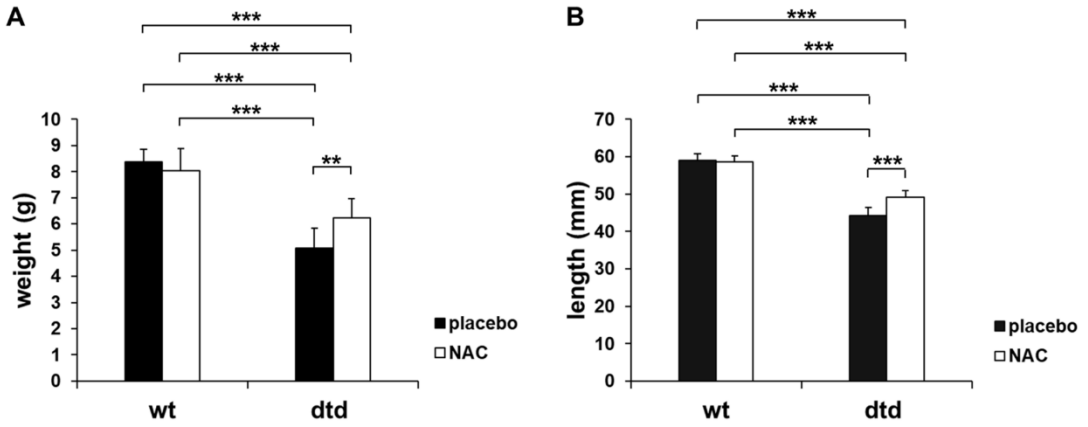

Fig. 6. Effect of 21 days N-acetylcysteine treatment on mice body weight and length. Wild type and dtd newborn mice were treated for 21 days twice a day with hypodermic injection of 250 mg NAC/kg body weight or placebo. Body weight (A) and length (B) of NAC treated dtd mice were significantly increased compared with untreated dtd animals and markedly reduced compared with treated and untreated wild type mice. No differences in body weight and length were observed in wild type group between treated and untreated animals suggesting that the drug had no toxic effect on body growth. Data are reported as mean ± SD, n = 9. Significant differences among groups were found by ANOVA test (F = 45.570; $P < 0.001$ and F = 143.389; $P < 0.001$ for body weight and length, respectively) with Bonferroni's correction for the post-hoc analysis; $^{**}P < 0.01$; $^{***}P < 0.001$.

weight, the body length of NAC treated dtd mice was significantly increased compared with the dtd placebo group (49.17 ± 1.73 mm and 44.23 ± 2.10 mm, respectively, $P < 0.001$), even if it was reduced compared with treated and untreated wild type animals ($P < 0.001$; Fig. 6B).

Overall, body weight and length analysis demonstrated that the drug dosage and administration route did not negatively affect animal growth.

3.3.3. Skeletal phenotype after 21 days N-acetylcysteine treatment

We performed X-ray analysis on wild type and dtd mice and morphometric measurement of several bony elements to investigate whether the skeletal phenotype improved in dtd mice after 21 days NAC treatment.

In dtd mice treated with NAC long bones improved compared with dtd untreated animals as demonstrated by the significant increase of the length and the distance between tibia metaphysis ($P < 0.001$). In addition, the length of the femur and radius was significantly increased in NAC treated dtd mice compared with untreated dtd animals ($P < 0.01$ and $P < 0.001$, respectively; Fig. 7).

Hip dysplasia, a typical skeletal deformity present in dtd mice, was studied by measuring the hip length and a significant amelioration in dtd mice treated with NAC compared with the dtd placebo group was observed ($P < 0.001$). Moreover, the height of three lumbar vertebrae (L4, L5 and L6) was significantly increased in NAC treated dtd mice compared with untreated dtd ones ($P < 0.01$, $P < 0.001$ and $P < 0.001$, respectively; Fig. 7). No significant differences for these skeletal elements were observed between treated and untreated wild type mice (Fig. 7).

In conclusion, morphometric analysis demonstrated a skeletal improvement in dtd mice after 21 days NAC treatment, although wild type values were not reached.

3.3.4. Bone phenotype after 21 days N-acetylcysteine treatment

To further characterize the improvement of the skeletal phenotype, we considered the bone quality by DEXA and micro CT studies.

DEXA analysis of tibiae revealed a significant reduction of the BMC in dtd mice treated with placebo compared with treated and untreated wild type animals (1.25 ± 0.91 mg, 5.96 ± 1.10 mg and 6.06 ± 0.91 mg, respectively; $P < 0.001$). After 21 days of NAC treatment, tibia BMC of treated dtd mice was significantly increased compared with untreated dtd ones (3.56 ± 0.61 mg; $P < 0.001$), even if it did not reach wild type values ($P < 0.001$; Fig. 8B). DEXA analysis of femur confirmed tibia results. A significant improvement of femur BMC was found in NAC treated dtd mice compared with dtd placebo group (3.04 ± 0.66 mg and 1.32 ± 0.43 mg, respectively; $P = 0.01$), even if it did not reach the value of treated and untreated wild type animals (5.54 ± 1.54 mg and 5.93 ± 1.05 mg, respectively; $P < 0.001$; Fig. 8C). In wild type groups no differences in BMC of tibia and femur were observed after administration of the drug or placebo.

Micro CT analysis showed a significant increase of trabecular bone mass in NAC treated dtd mice compared with dtd placebo group (Fig. 9), confirmed by the measurement of trabecular Bone Volume over total Tissue Volume (BV/TV) (10.63 ± 1.86% and 5.96 ± 1.56%, respectively; $P < 0.001$; Fig. 9B) and trabecular number (2.92 ± 0.58 mm^{-1} and 1.68 ± 0.56 mm^{-1}, respectively; $P < 0.001$; Fig. 9C), while trabecular thickness remained unchanged after the treatment (Fig. 9D). Consistently, trabecular separation was significantly increased in NAC treated dtd mice compared with dtd placebo group (286.68 ± 66.04 μm and 375.88 ± 69.84 μm, respectively; $P < 0.01$; Fig. 9E). On the contrary, a higher bone volume, trabecular number along with a lower trabecular separation were observed in wild type mice compared with the dtd group, while no significant differences were found in wild type mice upon NAC treatment (Fig. 9). Furthermore, the analysis of cortical bone revealed a trend of increase of the cortical volume and cortical thickness in NAC treated dtd mice compared with dtd placebo group (Fig. 9F, G). In wild type mice cortical bone parameters were significantly higher compared with the dtd group, but no differences were found after NAC treatment (Fig. 9F, G).

Overall these results demonstrated the improvement of the bone quality in dtd mice after 21 days NAC treatment, although wild type values were not reached.

3.3.5. Cartilage growth plate after 21 days N-acetylcysteine treatment

The significant increase of long bone length in dtd mice after 21 days of NAC treatment suggested an improvement of the endochondral ossification process. For this reason, we studied the growth plate morphology by haematoxylin and eosin staining of tibia paraffin sections from wild type and dtd mice treated with NAC or placebo.

The overall architecture of the growth plate with the resting, proliferative and hypertrophic zones was preserved in dtd mice treated with the placebo. However in dtd mice, chondrocyte columns were more

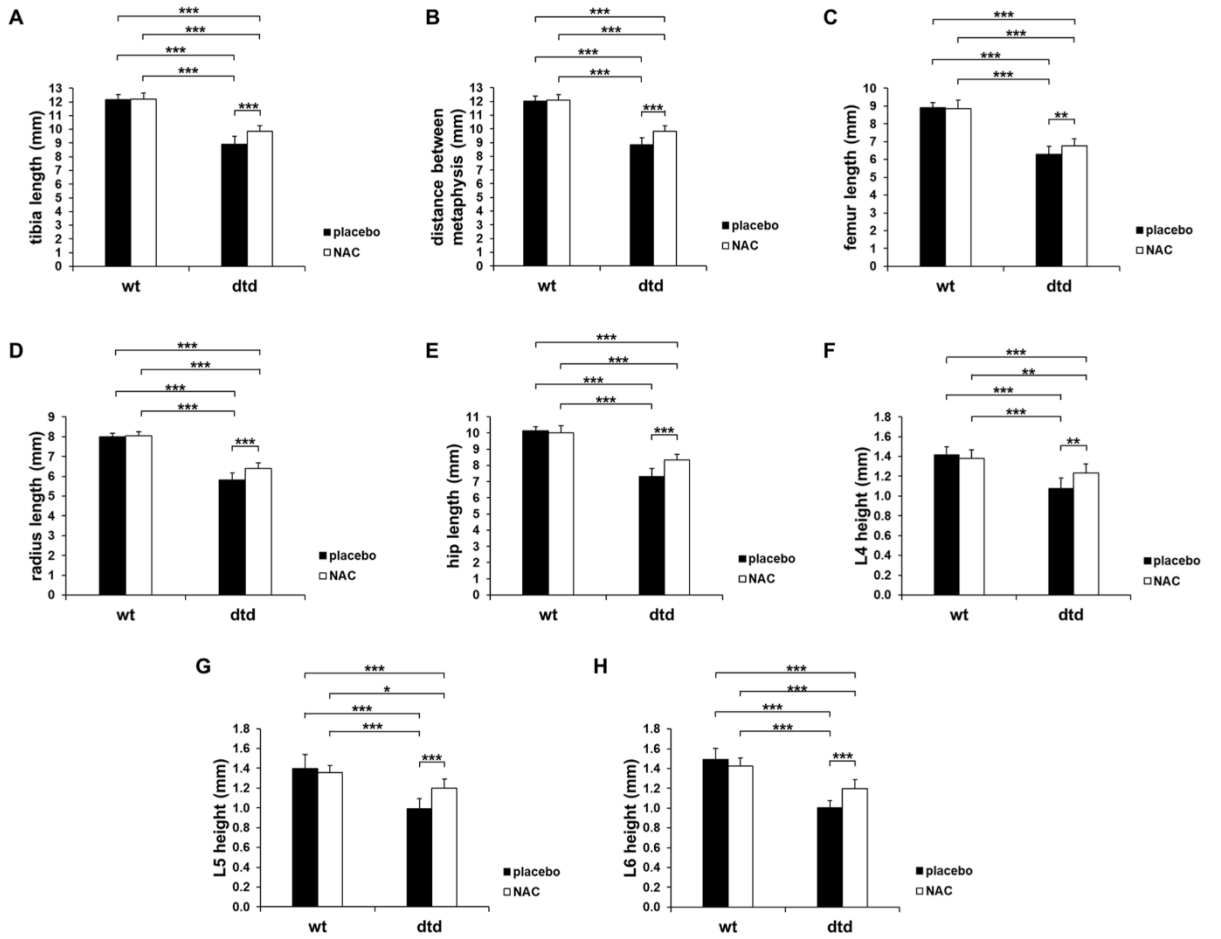

Fig. 7. Effect of 21 days N-acetylcysteine treatment on the skeletal phenotype. After treatment for 21 days from birth with twice a day hypodermic injection of 250 mg NAC/kg body weight or placebo, dtd mice treated with NAC showed a significant increase of the tibia length (A), distance between tibia metaphysis (B), length of femur (C) and radius (D) compared with untreated dtd animals. The hip dysplasia improved in treated dtd mice compared with untreated dtd ones as demonstrated by the increase of its length (E). Moreover, the height of the lumbar vertebrae L4 (F), L5 (G) and L6 (H) ameliorated in NAC treated dtd mice compared with untreated dtd animals. Skeletal elements from NAC treated dtd mice did not reach wild type values. No differences between treated and untreated wild type mice were observed. Data are reported as mean ± SD, n = 9. Significant differences among groups were found by ANOVA test ($F = 277.000$; $P < 0.001$ for tibia length; $F = 277.608$; $P < 0.001$ for distance between tibia metaphysis; $F = 228.502$; $P < 0.001$ for femur length; $F = 313.447$; $P < 0.001$ for radius length; $F = 226.584$; $P < 0.001$ for hip length; $F = 28.107$; $P < 0.001$ for L4 height; $F = 29.464$; $P < 0.001$ for L5 height and $F = 60.367$; $P < 0.001$ for L6 height) with Bonferroni's correction for multiple comparison test in the post-hoc analysis; $^{*}P < 0.05$; $^{**}P < 0.01$; $^{***}P < 0.001$.

spread within the extracellular matrix (ECM) compared with wild types and the dtd growth plate was smaller than the wild type one. After 21 days of NAC treatment, dtd mice showed a well conserved growth plate with defined zones. Interestingly, chondrocyte columns appeared less spread in the ECM compared with untreated dtd mice showing a growth plate morphology more similar to wild type (Fig. 10A).

Histomorphometric measurements were performed to quantify the growth plate improvement. Dtd mice treated with placebo showed a significant reduction of the total growth plate height compared with treated and untreated wild type animals (263.58 μm, 303.44 μm, $P < 0.001$ and 279.55 μm, $P < 0.05$, respectively). After 21 days of NAC treatment, the total growth plate height of treated dtd mice (271.44 μm) was similar to wild type animals, but this height increase was not significant compared with the dtd placebo group (Fig. 10B). Moreover, in the hypertrophic zone of dtd mice treated with the placebo the column height was significantly reduced compared with treated and untreated wild type animals (101.36 μm, 125.12 μm and 127.24 μm, respectively; $P < 0.001$) confirming the reduced growth plate height. Interestingly, the column height in the hypertrophic zone of NAC treated dtd mice was significantly increased compared with the untreated dtd group (112.58 μm; $P < 0.05$) and no differences were found with wild type ones (Fig. 10C). Wild type mice did not show significant differences between treated and untreated animals for both considered parameters of the growth plate morphology.

In conclusion, histological analysis demonstrated an improvement of growth plate morphology in dtd mice after NAC treatment suggesting a recovery of the endochondral ossification process and thus supporting long bone amelioration.

4. Discussion

In mammals sulfate is important for several biochemical processes such as metabolism of xenobiotics and drugs, inactivation of steroids and neurotransmitters and sulfation of macromolecules. The intracellular sulfate pool is maintained by extracellular sulfate uptake and by the catabolism of sulfur-containing amino acids or other thiols

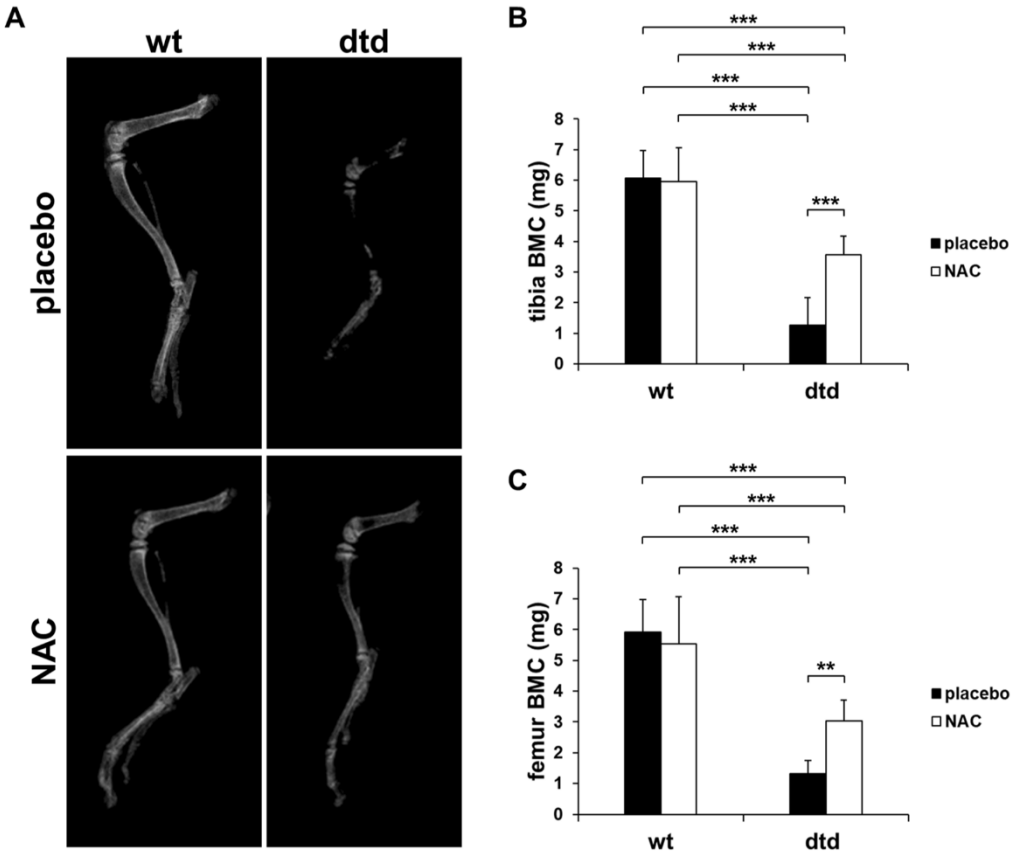

Fig. 8. Effect of 21 days N-acetylcysteine treatment on bone mineral content. Hind limb X-ray of wild type and dtd mice treated twice a day with hypodermic injection of 250 mg NAC/kg body weight or placebo for 21 days starting from birth (A). The tibia BMC (B) was significantly increased in NAC treated dtd mice compared with untreated dtd ones. In addition the femur BMC (C) was significantly improved in the dtd group after NAC treatment. For both parameters, NAC treated dtd mice did not reach wild type values; no differences were observed in wild type group between treated and untreated mice. Data are reported as mean ± SD, n = 10 for tibia BMC and n = 9 for femur BMC. Significant differences among groups were found by ANOVA test ($F = 64.608$; $P < 0.001$ and $F = 39.828$; $P < 0.001$ for tibia and femur BMC, respectively) with Bonferroni's correction for multiple comparison in the post-hoc analysis; $^{**}P < 0.01$; $^{***}P < 0.001$.

depending on the cell type [5,17]. In chondrocytes the main source of sulfate is the extracellular uptake through the SLC26A2 transporter. Indeed when SLC26A2 is impaired, the intracellular level of sulfate is reduced leading to the synthesis of undersulfated PGs and causing a spectrum of chondrodysplasias with clinical phenotypes ranging from mild to lethal. Among these conditions diastrophic dysplasia is compatible with life, even if patients have several physical problems; due to pain and skeletal abnormalities, their everyday life activities and movements are hampered. Nowadays patients are treated by corrective orthopaedic surgery and physiotherapy, but no pharmacological treatment is available.

Since a correlation between the severity of the clinical phenotype and cartilage PG undersulfation was demonstrated in SLC26A2 chondrodysplasias [4], a pharmacological strategy targeted at increasing cartilage PG sulfation would likely result in an improvement of the skeletal phenotype.

In chondrocytes, beyond extracellular sulfate uptake, a small amount of sulfate may come from the catabolism of sulfur-containing amino acids such as methionine and cysteine. The increase of PG sulfation in chondrocytes from a DTD patient was demonstrated after addition of cysteine or NAC to the medium [7]. This finding suggested the use of NAC as alternative source of intracellular sulfate through its catabolism in order to bypass the sulfate uptake defect.

The effect of NAC on the diastrophic dysplasia phenotype has already been investigated in the dtd mouse. In a previous work we demonstrated a significant improvement of PG sulfation and skeletal phenotype in dtd mice born from females treated with an oral solution of NAC compared with dtd newborns from females treated with the placebo [10]. Since NAC efficacy on foetal skeletal development of mutant mice was proved, it is importent to evaluate the NAC effect in the postnatal period, when most DTD patients would be treated. While limb shortening can be observed prenatally, the precise diagnosis of diastrophic dysplasia in humans is usually made only after birth, at least for the first case in a family. Thus, it is crucial to check if the drug is effective when administered after birth. In the future, it will be interesting to perform and evaluate a combined pre- and postnatal treatment. This type of protocol might be applicable in pregnancies known to be at risk or diagnosed.

Mice were treated in the first 3 weeks after birth when skeletal growth is enhanced. However, in this period mice are fed only by mother's milk, thus hypodermic injection was the unique treatment strategy. To identify the correct time interval for drug administration, a pharmacokinetic study was performed in wild type mice. The clearance of the drug was fast: NAC reached the highest plasma concentration in 2 h from injection and then quickly dropped down. At 8 h from injection the plasma NAC concentration was similar to the effective NAC concentration found in foetuses from pregnant females treated with the drug [10]. Comparison of the drug concentration in the plasma and in whole body homogenates of 5 day old mice 8 h from injection confirmed

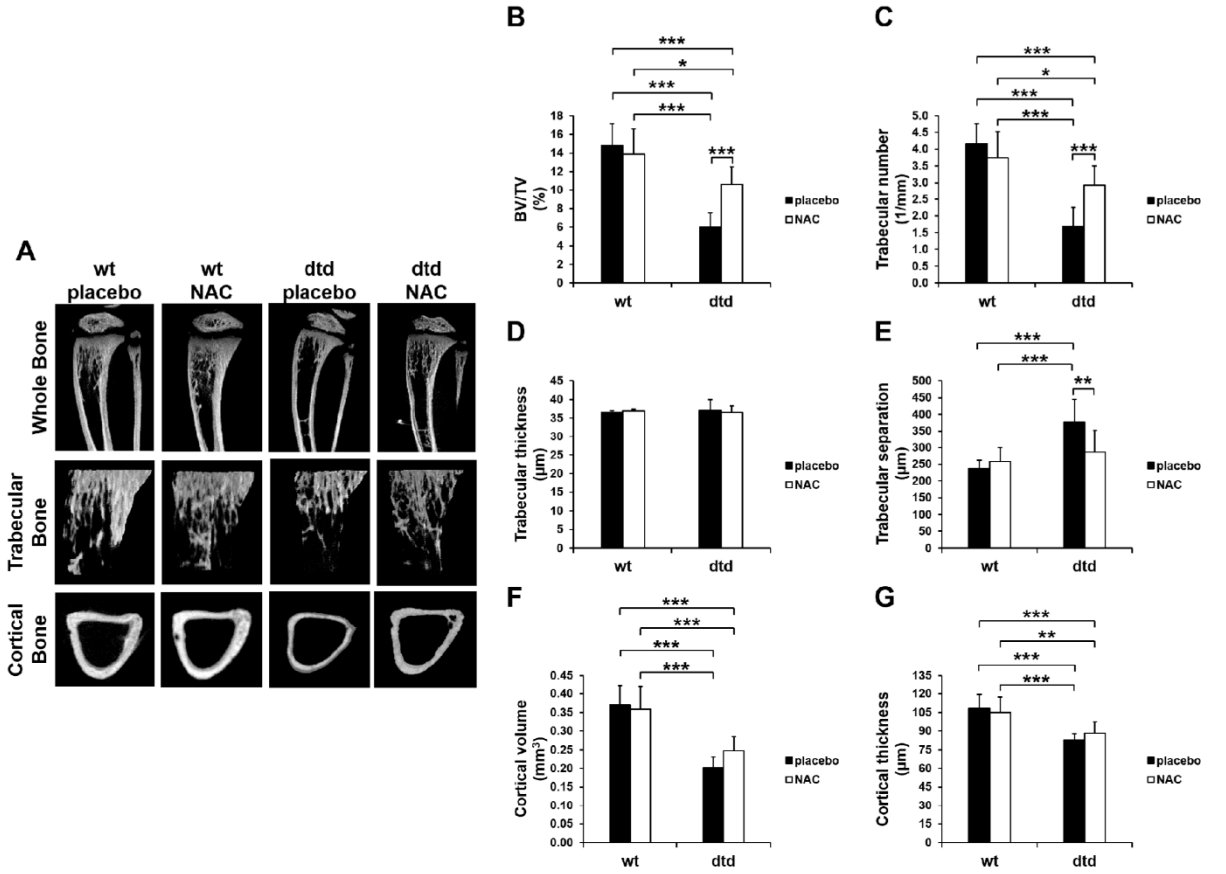

Fig. 9. Effect of 21 days N-acetylcysteine treatment on trabecular and cortical bone. Micro CT images of proximal tibia, trabecular and cortical bone from wild type and dtd mice treated twice a day with hydopermic injection of 250 mg NAC/kg body weight or placebo for 21 days starting from birth (A). In treated dtd mice a significant increase of BV/TV (B) and of trabecular number (C) compared with untreated dtd animals was demonstrated. No differences among groups were observed in trabecular thickness (D), while trabecular separation (E) showed a significant reduction in NAC treated dtd mice compared with dtd placebo group and no significant differences between treated dtd mice and wild type ones were found. Regarding the cortical bone, only a trend of improvement of the cortical volume (F) and thickness (G) was observed in treated dtd mice compared with untreated ones. Trabecular and cortical parameters of NAC treated dtd mice did not reach wild type values and no differences were found between treated and untreated wild type animals. Data are reported as mean ± SD, n = 10. Significant differences among groups were found by ANOVA test ($F = 34.732$; $P < 0.001$ for BV/TV; $F = 30.124$; $P < 0.001$ for trabecular number; $F = 12.790$; $P < 0.001$ for trabecular separation; $F = 31.572$; $P < 0.001$ for cortical volume; $F = 15.219$; $P < 0.001$ for cortical thickness) with Bonferroni's correction for multiple comparison in the post-hoc analysis; for trabecular thickness data are reported as median, 25th and 75th percentile, n = 10 and differences among groups were analysed by Kruskal-Wallis test ($KW = 1.428$; $P = 0.699$); $^{*}P < 0.05$; $^{**}P < 0.01$; $^{***}P < 0.001$.

that the NAC concentration used in the postnatal treatment was similar to the drug concentration of the previous foetal treatment. Based on these observations, mice were treated postnatally twice a day with hypodermic injections of 250 mg NAC/kg body weight.

At first mice were treated with NAC for 7 days starting from birth. At the end of treatment cartilage PG sulfation was slightly increased in dtd mice treated with NAC compared with the dtd placebo group, although the increase was not significant. Moreover, the skeletal phenotype showed an amelioration trend in treated dtd mice without any statistical relevance, as demonstrated by morphometric analysis of tibia and femur length. Overall, these results demonstrated an amelioration trend and suggested that a longer NAC treatment might be effective.

To investigate this hypothesis, a second treatment lasted 3 weeks after birth was set up with the same administration protocol. During the treatment period, wild type mice grew normally as demonstrated by no significant differences in body weight and length between treated and untreated animals. This observation revealed that NAC had no toxic effect on mouse growth, notwithstanding the high dosage and the long term administration.

The increase of body weight and length observed in treated dtd mice was the first evidence that the drug improved the skeletal phenotype in the postnatal period. This observation was further confirmed by morphometric analysis of several bony elements: tibia, femur, radius, hip and lumbar vertebrae. NAC treatment improved the mutant phenotype also at the biochemical level since HPLC analysis demonstrated a significant increase of cartilage PG sulfation in treated dtd mice. Furthermore, histological analysis of tibia sections from treated dtd mice showed that the overall growth plate morphology was more similar to wild type animals supporting the skeletal phenotype improvement of long bones in dtd mice treated with NAC.

Functional impairment of the Slc26a2 transporter affects sulfate uptake in chondrocytes and also in osteoblasts with a primary effect on bone homeostasis. Indeed an osteopenic phenotype due to altered bone ECM organisation was demonstrated in dtd growing mice [8,16]. The increase of tibia and femur BMC in dtd mice treated with NAC for 21 days showed an improvement of the bone quality and a partial rescue of the osteopenic phenotype. Moreover, the increase of the trabecular BV/TV and trabecular number with the reduction of trabecular separation

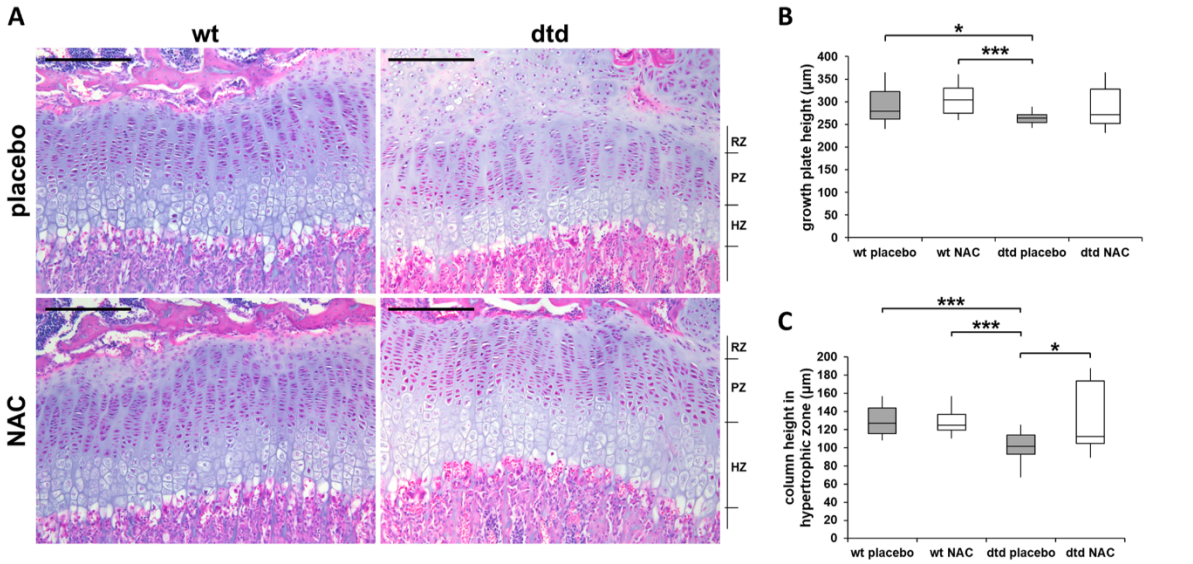

Fig. 10. Effect of 21 days N-acetylcysteine treatment on growth plate morphology. Wild type and dtd newborn mice were treated for 21 days from birth twice a day with hypodermic injection of 250 mg NAC/kg body weight or placebo. Haematoxylin and eosin staining of tibia sections (A) showed that the overall architecture of the growth plate was maintained in dtd mice, even if it appeared smaller compared with wild types. The growth plate of NAC treated dtd mice presented a morphology more similar to wild type animals. The growth plate height (B) was significantly reduced in untreated dtd mice compared with wild types, while no difference was found between NAC treated dtd and wild type animals. The column height in the hypertrophic zone (C) was significantly increased in NAC treated dtd mice compared with untreated dtd ones and no significant differences were found compared with treated and untreated wild type mice. Conversely, the column height in the hypertrophic zone of the dtd placebo group was markedly reduced compared with wild type animals. Data are reported as a box plot where the median as well as the 25th and 75th percentile are indicated, n = 5 for growth plate height and column height. Significant differences among groups were found by Kruskal-Wallis test (KW = 21.342; $P < 0.001$ for total growth plate height and KW = 24.987; $P < 0.001$ for column height) and Mann-Whitney test was used as post-hoc analysis; $^{*}P < 0.05$; $^{***}P < 0.001$. RZ = resting zone; PZ = proliferative zone; HZ = hypertrophic zone; scale bar 200 µm.

confirmed the amelioration of the bone phenotype in dtd mice treated with NAC for 21 days. Interestingly, these data are in agreement with a previous study demonstrating that NAC enhances osteoblast differentiation and matrix mineralization [18].

Neither of the two postnatal treatment can reach wild type values in mutant mice; this could be due to the fast removal of NAC from the bloodstream as demonstrated by the pharmacokinetic study. A strategy to improve the effect of NAC treatment could be the maintenance of the NAC plasma concentration as stable as possible; in order to reach this goal new administration methods should be developed. Recently a pharmacokinetic study of polyethylene glycol-poly-lactide-co-glycolide block copolymer (PLGA-PEG) nanoparticles loaded with NAC showed the maximal plasma concentration of NAC after 24 h from nanoparticle injection, while after 48 h NAC was present only in trace amount [19].

Our interest on NAC as a specific thiol compound for pharmacological treatment of DTD comes from its wide use in clinical settings and since it is considered a safe and well-tolerated drug [20]. Starting from early 1960's, NAC has been used as mucolytic agent in the treatment of cystic fibrosis [21] and as antidote against paracetamol and paraquat intoxication [22]. NAC has important antioxidant properties acting directly as a scavenger of free radicals and indirectly providing cysteine for glutathione synthesis, the major cellular antioxidant molecule [23,24]. For these properties it is used in many diseases eliciting oxidative stress such as neurodegenerative disorders [24], psychiatric disorders [25], contrast-induced nephropathy [26] and cancer [23]. Moreover, NAC has also anti-inflammatory effect decreasing NF-kB activity and modulating cytokines release [23,24]. The use of NAC as alternative intracellular source of sulfate when extracellular sulfate uptake is impaired, as proposed in this work, represents a novel therapeutic effect of the drug. The same property has been tested recently in a specific postnatal period of brain development in heterozygous knockout mice for *Slc13a4*, a sulfate transporter present in placenta and brain; in these animals the drug prevented the development of deficits in social interaction and in long-term memory [27].

The administration of NAC to increase the intracellular sulfate levels represents a new application of the drug and an example of drug repositioning. Drug repositioning is an exciting alternative approach to drug development that allows to treat a disease with a drug already on the market for a different disorder [28]. This strategy dramatically reduces the time and costs for drug development since the use of an approved drug allows to skip the early phases of development and clinical testing [28–30]. Thus, drug repositioning is a promising strategy for patients affected by rare diseases [30,31]. In the last few years, thanks to the deeper understanding of disease pathogenesis, new treatments and repositioned drugs have been suggested for several skeletal dysplasias [32]. Recently, it has been demonstrated that 4-phenylbutyrate, an FDA-approved drug for urea cycle disorders, had an effect on bone mineralization and skeletal defects in a zebrafish model of osteogenesis imperfecta [33]. Moreover, preclinical studies demonstrated the efficacy of carbamazepine, a drug already on the market for epilepsy and bipolar disorders, in the treatment of metaphyseal chondrodysplasia type Schmid [34] and a clinical trial in affected children is ongoing.

In conclusion, we have demonstrated the beneficial effect of NAC in dtd mice in the postnatal period at the biochemical level increasing cartilage PG sulfation and at the morphological level ameliorating the skeletal phenotype. Furthermore, NAC improved not only cartilage development, but also the bone quality. These findings are a further step forward to a possible pharmacological treatment of patients affected by diastrophic dysplasia.

CRediT authorship contribution statement

Chiara Paganini: Investigation, Writing - review & editing. **Chiara Gramegna Tota:** Investigation, Visualization. **Luca Monti:**

Investigation. **Ilaria Monti:** Investigation. **Antonio Maurizi:** Investigation. **Mattia Capulli:** Investigation. **Morgane Bourmaud:** Investigation. **Anna Teti:** Writing - review & editing, Funding acquisition. **Martine Cohen-Solal:** Writing - review & editing, Funding acquisition. **Simona Villani:** Formal analysis. **Antonella Forlino:** Writing - review & editing, Funding acquisition. **Andrea Superti-Furga:** Conceptualization, Writing - review & editing. **Antonio Rossi:** Conceptualization, Supervision, Writing - review & editing, Funding acquisition.

Declaration of Competing Interest

The authors declare that they have no known competing financial interests or personal relationships that could have appeared to influence the work reported in this paper.

Acknowledgements

This work was supported by the European Community's Seventh Framework Programme under grant agreement n. 602300 (SYBIL) (to AT, MCS, AF and AR), Ministero dell'Istruzione, Università e Ricerca (MIUR), Italy "Dipartimenti di Eccellenza 2018-2022" (to AF and AR) and MIUR "Progetti di ricerca di rilevante interesse nazionale" (PRIN) grant n. 2015F3JHMB (to AT and AR).

References

[1] O. Makitie, I. Kaitila, Growth in diastrophic dysplasia, J. Pediatr. 130 (4) (1997) 641–646.
[2] J. Hästbacka, A. de la Chapelle, M.M. Mahtani, G. Clines, M.P. Reeve Daly, M. Daly, B.A. Hamilton, K. Kusumi, B. Trivedi, A. Weaver, A. Coloma, M. Lovett, A. Buckler, I. Kaitila, E.S. Lander, The diastrophic dysplasia gene encodes a novel sulfate transporter: positional cloning by fine-structure linkage disequilibrium mapping, Cell 78 (6) (1994) 1073–1087.
[3] A. Rossi, A. Superti-Furga, Mutations in the diastrophic dysplasia sulfate transporter (DTDST) gene (SLC26A2): 22 Novel mutations, mutation review, associated skeletal phenotypes, and diagnostic relevance, Hum. Mutat. 17 (3) (2001) 159–171.
[4] A. Rossi, I. Kaitila, W.R. Wilcox, D.L. Rimoin, B. Steinmann, G. Cetta, A. Superti-Furga, Proteoglycan sulfation in cartilage and cell cultures from patients with sulfate transporter chondrodysplasias: Relationship to clinical severity and indications on the role of intracellular sulfate production, Matrix Biol. 17 (5) (1998) 361–369.
[5] C. Paganini, C. Gramegna Tota, A. Superti-Furga, A. Rossi, Skeletal dysplasias caused by sulfation defects, Int. J. Mol. Sci. 21 (8) (2020).
[6] A. Rossi, J. Bonaventure, A.L. Delezoide, A. SupertiFurga, G. Cetta, Undersulfation of cartilage proteoglycans ex vivo and increased contribution of amino acid sulfur to sulfation in vitro in McAlister dysplasia atelosteogenesis type 2, Eur. J. Biochem. 248 (3) (1997) 741–747.
[7] A. Rossi, A. Cetta, R. Piazza, J. Bonaventure, B. Steinmann, A. Superti-Furga, In vitro proteoglycan sulfation derived from sulfhydryl compounds in sulfate transporter chondrodysplasias, Pediatr. Pathol. Molec. Med. 22 (2003) 311–321.
[8] A. Forlino, R. Piazza, C. Tiveron, S. Della Torre, L. Tatangelo, L. Bonafe, B. Gualeni, A. Romano, F. Pecora, A. Superti-Furga, G. Cetta, A. Rossi, A diastrophic dysplasia sulfate transporter (SLC26A2) mutant mouse: morphological and biochemical characterization of the resulting chondrodysplasia phenotype, Hum. Mol. Genet. 14 (6) (2005) 859–871.
[9] F. Pecora, B. Gualeni, A. Forlino, A. Superti-Furga, R. Tenni, G. Cetta, A. Rossi, In vivo contribution of amino acid sulfur to cartilage proteoglycan sulfation, Biochem. J. 398 (3) (2006) 509–514.
[10] L. Monti, C. Paganini, S. Lecci, F. De Leonardis, E. Hay, M. Cohen-Solal, S. Villani, A. Superti-Furga, R. Tenni, A. Forlino, A. Rossi, N-acetylcysteine treatment ameliorates the skeletal phenotype of a mouse model of diastrophic dysplasia, Hum. Mol. Genet. 24 (19) (2015) 5570–5580.
[11] R. Ferin, M.L. Pavao, J. Baptista, Methodology for a rapid and simultaneous determination of total cysteine, homocysteine, cysteinylglycine and glutathione in plasma by isocratic RP-HPLC, J. Chromatogr. B Analyt. Technol. Biomed. Life Sci. 911 (2012) 15–20.
[12] J.A. Deakin, M. Lyon, A simplified and sensitive fluorescent method for disaccharide analysis of both heparan sulfate and chondroitin/dermatan sulfates from biological samples, Glycobiology 18 (6) (2008) 483–491.
[13] C. Paganini, L. Monti, R. Costantini, R. Besio, S. Lecci, M. Biggiogera, K. Tian, J. M. Schwartz, C. Huber, V. Cormier-Daire, B.G. Gibson, K.A. Pirog, A. Forlino, A. Rossi, Calcium activated nucleotidase 1 (CANT1) is critical for glycosaminoglycan biosynthesis in cartilage and endochondral ossification, Matrix Biol. (2018).
[14] W.E. Lorensen, H.E. Cline, Marching cubes: A high resolution 3D surface construction algorithm, ACM SIGGRAPH Comput. Graph. 21 (1987) 163–169.
[15] M.L. Bouxsein, S.K. Boyd, B.A. Christiansen, R.E. Guldberg, K.J. Jepsen, R. Muller, Guidelines for assessment of bone microstructure in rodents using micro-computed tomography, J. Bone Miner. Res. 25 (7) (2010) 1468–1486.
[16] B. Gualeni, M.C. de Vernejoul, C. Marty-Morieux, F. De Leonardis, M. Franchi, L. Monti, A. Forlino, P. Houillier, A. Rossi, V. Geoffroy, Alteration of proteoglycan sulfation affects bone growth and remodeling, Bone 54 (1) (2013) 83–91.
[17] P.A. Dawson, Sulfate in fetal development, Semin. Cell Dev. Biol. 22 (6) (2011) 653–659.
[18] M. Yamada, N. Tsukimura, T. Ikeda, Y. Sugita, W. Att, N. Kojima, K. Kubo, T. Ueno, K. Sakurai, T. Ogawa, N-acetyl cysteine as an osteogenesis-enhancing molecule for bone regeneration, Biomaterials 34 (26) (2013) 6147–6156.
[19] E. Chiesa, L. Monti, C. Paganini, R. Dorati, B. Conti, T. Modena, A. Rossi, I. Genta, Polyethylene glycol-poly-lactide-co-glycolide block copolymer-based nanoparticles as a potential tool for off-label use of N-acetylcysteine in the treatment of diastrophic dysplasia, J. Pharm. Sci. 106 (12) (2017) 3631–3641.
[20] I. Elbini Dhouib, M. Jallouli, A. Annabi, N. Gharbi, S. Elfazaa, M.M. Lasram, A minireview on N-acetylcysteine: An old drug with new approaches, Life Sci. 151 (2016) 359–363.
[21] G.F. Rushworth, I.L. Megson, Existing and potential therapeutic uses for N-acetylcysteine: the need for conversion to intracellular glutathione for antioxidant benefits, Pharmacol. Ther. 141 (2) (2014) 150–159.
[22] Y. Samuni, S. Goldstein, O.M. Dean, M. Berk, The chemistry and biological activities of N-acetylcysteine, Biochim. Biophys. Acta, Mol. Cell. Biol. Lipids 1830 (8) (2013) 4117–4129.
[23] Y. Pei, H. Liu, Y. Yang, Y. Jiao, F.R. Tay, J. Chen, Biological activities and potential oral applications of N-acetylcysteine: progress and prospects, Oxid. Med. Cell. Longev. 2018 (2018) 2835787.
[24] G. Tardiolo, P. Bramanti, E. Mazzon, Overview on the effects of N-acetylcysteine in neurodegenerative diseases, Molecules 23 (12) (2018).
[25] A. Minarini, S. Ferrari, M. Galletti, N. Giambalvo, D. Perrone, G. Rioli, G. M. Galeazzi, N-acetylcysteine in the treatment of psychiatric disorders: current status and future prospects, Expert Opin. Drug Metab. Toxicol. 13 (3) (2017) 279–292.
[26] N. Wang, P. Qian, S. Kumar, T.D. Yan, K. Phan, The effect of N-acetylcysteine on the incidence of contrast-induced kidney injury: A systematic review and trial sequential analysis, Int. J. Cardiol. 209 (2016) 319–327.
[27] Z. Zhang, P.A. Dawson, M. Piper, D.G. Simmons, Postnatal N-acetylcysteine administration rescues impaired social behaviors and neurogenesis in Slc13a4 haploinsufficient mice, EBioMedicine 43 (2019) 435–446.
[28] J.P. Jourdan, R. Bureau, C. Rochais, P. Dallemagne, Drug repositioning: a brief overview, J. Pharm. Pharmacol. (2020).
[29] N. Nosengo, Can you teach old drugs new tricks? Nature 534 (7607) (2016) 314–316.
[30] M. Lotfi Shahreza, N. Ghadiri, J.R. Green, A computational drug repositioning method applied to rare diseases: Adrenocortical carcinoma, Sci. Rep. 10 (1) (2020) 8846.
[31] B. Delavan, R. Roberts, R. Huang, W. Bao, W. Tong, Z. Liu, Computational drug repositioning for rare diseases in the era of precision medicine, Drug Discov. Today 23 (2) (2018) 382–394.
[32] P. Marzin, V. Cormier-Daire, New perspectives on the treatment of skeletal dysplasia, Ther. Adv. Endocrinol. Metab. 11 (2020), 2042018820904016.
[33] R. Gioia, F. Tonelli, I. Ceppi, M. Biggiogera, S. Leikin, S. Fisher, E. Tenedini, T. A. Yorgan, T. Schinke, K. Tian, J.M. Schwartz, F. Forte, R. Wagener, S. Villani, A. Rossi, A. Forlino, The chaperone activity of 4PBA ameliorates the skeletal phenotype of Chihuahua, a zebrafish model for dominant osteogenesis imperfecta, Hum. Mol. Genet. 26 (15) (2017) 2897–2911.
[34] L.A. Mullan, E.J. Mularczyk, L.H. Kung, M. Forouhan, J.M. Wragg, R. Goodacre, J. F. Bateman, E. Swanton, M.D. Briggs, R.P. Boot-Handford, Increased intracellular proteolysis reduces disease severity in an ER stress-associated dwarfism, J Clin Invest 127 (10) (2017) 3861–3865.

CHAPTER VI

Conclusions

Skeletal dysplasias are a huge heterogeneous group of rare genetic diseases that mainly affect cartilage and bone. Although rare, the study of these diseases is important in order to: i) elucidate the pathogenetic mechanism(s) causing the disease, ii) identify among different disorders common disease pathways that might be targeted by the same drug, iii) develop new potential therapeutic approaches and iv) increase our knowledge about skeletal biology in normal and pathological conditions.

Due to the small number of patient samples and to ethical problems, different *in vivo* and *in vitro* models have been developed in order to achieve the objectives described above. Analysis of genetically modified mice and/or zebrafishes provides a strong approach to elucidate the role of gene products *in vivo*. However, due to the complexity of the animal model, *in vitro* studies represent a powerful tool to investigate specific aspects of skeletal biology. Moreover, the use of *in vitro* models allows to reduce the number of sacrificed animals, according to the principle of the Three Rs.

The work presented in this thesis is paradigmatic of the efforts being made nowadays in the field of genetic disorders: deep phenotyping of *in vivo* and *in vitro* models to identify the molecular mechanisms causing the disorder and the validation of potential therapeutic approaches.

The first work has been focused on Desbuquois dysplasia type 1, a chondrodysplasia caused by mutations in *CANT1* gene whose molecular basis are far from complete. In this work, using the animal model, the role of CANT1 in PG processing and organelle homeostasis was investigated. In particular, reduced PG secretion in *Cant1*$^{-/-}$ chondrocytes, also confirmed by the accumulation of aggrecan inside mutant cells, has been demonstrated. However, delayed PG secretion was not associated with an overall delay in protein secretion, suggesting that it was probably related to impaired PG glycosylation in the Golgi.

Despite the defect in GAG synthesis, it has been demonstrated that only glycanated aggrecan is secreted by *Cant1*$^{-/-}$ chondrocytes, as in wild-type cells. Alteration in the structure of the ER, without activation of ER stress, suggested that the ER enlargement might be due to GAG synthesis impairment in the Golgi. In fact, Golgi studies demonstrated an increase of cis and trans Golgi dimensions and an overexpression of Golgi structural proteins GM130 and Golgin-97 in mutant chondrocytes, suggesting alteration in Golgi homeostasis. Indeed, TFE3 nuclear

localization demonstrated the activation of one of the three putative Golgi stress response pathways. To date, Golgi stress represents a still partially unexplored field. The study of molecular pathways underlying Golgi stress could lead to increasing knowledge of the molecular basis of many diseases, including Desbuquois dysplasia type 1, and might lead to the development of new therapies.

Moreover, in this work, an *in vitro* model to further study Desbuquois dysplasia type 1 has been proposed; primary chondrocytes from the mouse model of DBQD1 were immortalized with a plasmid vector expressing the SV40 large and small T antigen. In fact, even if primary chondrocyte culture is a well-defined system, it has some limits since cells undergo de-differentiation after few passages in culture [169, 192]. For this reason, immortalized cell lines are a useful tool, but since during the immortalization process they might develop a different phenotype from the cells of origin, it is important to deeply characterize them before use [168, 184, 185]. Thus, in this work immortalized chondrocytes were characterized and validated as an additional *in vitro* model for DBDQ1. Results demonstrated the generation of stable cell lines of immortalized murine chondrocytes that express the differentiated phenotype similar to the one of primary chondrocytes based on PG synthesis, sulfation, and ECM deposition. Thus, the model should provide additional information on how the defect in PG biosynthesis could affect the organization of the ECM. This successful immortalization procedure could be applied to cells from other animal models to increase the tools available for physiopathological studies and drug discovery.

The other skeletal dysplasia studied in this work is diastrophic dysplasia, which is caused by mutations in the *SLC26A2* gene encoding for a sulfate/chloride antiporter on the cell membrane. Deep phenotyping of the *dtd* mouse, an animal model of the disorder, and molecular and biochemical studies in cartilage and cells from the patients [152] lead to the hypothesis that cysteine and other thiols might increase, through their catabolism, proteoglycan sulfation. In this thesis, the *dtd* mouse has been used to evaluate *in vivo* a potential pharmacological treatment for the disease with NAC that, through its catabolism, provides an alternative source of intracellular sulfate, improving PG sulfation [193] and ameliorating the skeletal phenotype [194, 196]. A long-term treatment with NAC of mutant mice after birth has been considered; in particular, mice were treated for the first 3 weeks of life, the key period for postnatal skeletal development and growth in mice. Biochemical and morphological analysis demonstrated an amelioration of PG sulfation and of the skeletal phenotype in *dtd* mice treated with NAC, compared with the placebo group. These results suggested that a potential pharmacological

treatment with NAC should be considered for diastrophic dysplasia, in order to increase the patients quality of life since, up to now, surgery and physiotherapy are the only available therapeutic approaches.

In past decades, NAC has been widely used in many different clinical settings demonstrating that it is a well-tolerated and safe drug with mild side effects [197]. It is on the World Health Organization's List of Essential Medicines for adults (https://www.who.int/publications/i/item/WHO-MHP-HPS-EML-2021.02) and children (https://www.who.int/publications/i/item/WHO-MHP-HPS-EML-2021.03).

The novel use of NAC to treat diastrophic dysplasia would be an example of drug repositioning, an alternative approach to drug development that allows to treat a disease with drugs already on the market for a different disorder [198]. This strategy reduces the time and costs required for drug development, allowing to skip the early phases of development. They can potentially win the approval in less than half the time and at one quarter of the cost compared to new molecules [199]. Moreover, these drugs are appealing for Pharma companies because they are already on the market and so they are easy and cheap to get, their safety profiles are well known and new formulations or applications to new disorders can be patented. Thus, drug repositioning is a promising strategy for patients affected by rare diseases including skeletal dysplasias.

BIBLIOGRAPHY

1. Adamo S., C.P., Molinaro M., Siracusa G., Stefanini M., Ziparo E., *Istologia di V. Monesi*. 5 edizione ed. 2013.
2. Junqueira Luis C., C.J., *Compendio di istologia*. 5 ed. 2006.
3. Sophia Fox, A.J., A. Bedi, and S.A. Rodeo, *The basic science of articular cartilage: structure, composition, and function.* Sports Health, 2009. 1(6): p. 461-8.
4. Poole, A.R., et al., *Composition and structure of articular cartilage: a template for tissue repair.* Clin Orthop Relat Res, 2001(391 Suppl): p. S26-33.
5. Carballo, C.B., et al., *Basic Science of Articular Cartilage.* Clin Sports Med, 2017. 36(3): p. 413-425.
6. Lowe, J. and A.J. Almarza, *A review of in-vitro fibrocartilage tissue engineered therapies with a focus on the temporomandibular joint.* Arch Oral Biol, 2017. 83: p. 193-201.
7. Clarke, B., *Normal bone anatomy and physiology.* Clin J Am Soc Nephrol, 2008. 3 Suppl 3: p. S131-9.
8. Usami, Y., et al., *Wnt signaling in cartilage development and diseases: lessons from animal studies.* Lab Invest, 2016. 96(2): p. 186-96.
9. Breeland, G., M.A. Sinkler, and L.G. Menezes, *Embriology, Bone ossification*, StatPearls, Editor. 2022, StatPearls.
10. Percival, C.J. and J.T. Richtsmeier, *Angiogenesis and intramembranous osteogenesis.* Dev Dyn, 2013. 242(8): p. 909-22.
11. Kanczler, J.M. and R.O. Oreffo, *Osteogenesis and angiogenesis: the potential for engineering bone.* Eur Cell Mater, 2008. 15: p. 100-14.
12. Brannigan, K. and M. Griffin, *An Update into the Application of Nanotechnology in Bone Healing.* Open Orthop J, 2016. 10: p. 808-823.
13. Kronenberg, H.M., *Developmental regulation of the growth plate.* Nature, 2003. 423(6937): p. 332-6.
14. Karsenty, G. and E.F. Wagner, *Reaching a genetic and molecular understanding of skeletal development.* Dev Cell, 2002. 2(4): p. 389-406.
15. Gerber, H.P., et al., *VEGF couples hypertrophic cartilage remodeling, ossification and angiogenesis during endochondral bone formation.* Nat Med, 1999. 5(6): p. 623-8.
16. Nilsson, O., et al., *Endocrine regulation of the growth plate.* Horm Res, 2005. 64(4): p. 157-65.
17. Hunziker, E.B., *Mechanism of longitudinal bone growth and its regulation by growth plate chondrocytes.* Microsc Res Tech, 1994. 28(6): p. 505-19.
18. Hallett, S.A., W. Ono, and N. Ono, *Growth Plate Chondrocytes: Skeletal Development, Growth and Beyond.* Int J Mol Sci, 2019. 20(23).
19. Vanky, P., et al., *Kinetic studies on epiphyseal growth cartilage in the normal mouse.* Bone, 1998. 22(4): p. 331-9.
20. Samsa, W.E., X. Zhou, and G. Zhou, *Signaling pathways regulating cartilage growth plate formation and activity.* Semin Cell Dev Biol, 2017. 62: p. 3-15.
21. Yang, G., et al., *Osteogenic fate of hypertrophic chondrocytes.* Cell Res, 2014. 24(10): p. 1266-9.

22. Mackie, E.J., et al., *Endochondral ossification: how cartilage is converted into bone in the developing skeleton.* Int J Biochem Cell Biol, 2008. 40(1): p. 46-62.
23. Kobayashi, T., et al., *Indian hedgehog stimulates periarticular chondrocyte differentiation to regulate growth plate length independently of PTHrP.* J Clin Invest, 2005. 115(7): p. 1734-42.
24. Ahmed, Y.A., et al., *Physiological death of hypertrophic chondrocytes.* Osteoarthritis Cartilage, 2007. 15(5): p. 575-86.
25. Moore, E.R. and C.R. Jacobs, *The primary cilium as a signaling nexus for growth plate function and subsequent skeletal development.* J Orthop Res, 2017.
26. Liu, Z., et al., *FGF18 is required for early chondrocyte proliferation, hypertrophy and vascular invasion of the growth plate.* Dev Biol, 2007. 302(1): p. 80-91.
27. Long, F. and D.M. Ornitz, *Development of the endochondral skeleton.* Cold Spring Harb Perspect Biol, 2013. 5(1): p. a008334.
28. Archer, C.W. and P. Francis-West, *The chondrocyte.* Int J Biochem Cell Biol, 2003. 35(4): p. 401-4.
29. Saha, A.K. and S.S. Kohles, *A cell-matrix model of anabolic and catabolic dynamics during cartilage biomolecule regulation.* Int J Comput Healthc, 2012. 1(3): p. 214-228.
30. DeLise, A.M., L. Fischer, and R.S. Tuan, *Cellular interactions and signaling in cartilage development.* Osteoarthritis Cartilage, 2000. 8(5): p. 309-34.
31. Kozhemyakina, E., A.B. Lassar, and E. Zelzer, *A pathway to bone: signaling molecules and transcription factors involved in chondrocyte development and maturation.* Development, 2015. 142(5): p. 817-31.
32. Komori, T., *Runx2, an inducer of osteoblast and chondrocyte differentiation.* Histochem Cell Biol, 2018. 149(4): p. 313-323.
33. Theocharis, A.D., et al., *Extracellular matrix structure.* Adv Drug Deliv Rev, 2016. 97: p. 4-27.
34. Karamanos, N.K., *Extracellular Matrix: Pathobiology and Signaling*. 2012.
35. Eyre, D., *Collagen of articular cartilage.* Arthritis Res, 2002. 4(1): p. 30-5.
36. van der Rest, M. and R. Mayne, *Type IX collagen proteoglycan from cartilage is covalently cross-linked to type II collagen.* J Biol Chem, 1988. 263(4): p. 1615-8.
37. Heinegård, D., *Fell-Muir Lecture: Proteoglycans and more--from molecules to biology.* Int J Exp Pathol, 2009. 90(6): p. 575-86.
38. Vynios, D.H., *Metabolism of cartilage proteoglycans in health and disease.* Biomed Res Int, 2014. 2014: p. 452315.
39. Paganini, C., et al., *Bone and connective tissue disorders caused by defects in glycosaminoglycan biosynthesis: a panoramic view.* FEBS J, 2019. 286(15): p. 3008-3032.
40. Taylor, K.R. and R.L. Gallo, *Glycosaminoglycans and their proteoglycans: host-associated molecular patterns for initiation and modulation of inflammation.* FASEB J, 2006. 20(1): p. 9-22.
41. Iozzo, R.V. and L. Schaefer, *Proteoglycan form and function: A comprehensive nomenclature of proteoglycans.* Matrix Biol, 2015. 42: p. 11-55.
42. Liliana, S., *introduction*, in *Extracellular matrix: pathobiology and signaling*, K.N. K., Editor. 2012, De Gruyter: Göttingen (D). p. 135-140.

43. Ulf, L., et al., *Proteoglycans and Sulfated Glycosaminoglycans*, in *Essentials of Glycobiology*, V. A, C. RD, and E. JD, Editors. 2017, Cold Spring Harbor.
44. Iozzo, R.V. and A.D. Murdoch, *Proteoglycans of the extracellular environment: clues from the gene and protein side offer novel perspectives in molecular diversity and function.* FASEB J, 1996. 10(5): p. 598-614.
45. Izumikawa, T., et al., *Involvement of chondroitin sulfate synthase-3 (chondroitin synthase-2) in chondroitin polymerization through its interaction with chondroitin synthase-1 or chondroitin-polymerizing factor.* Biochem J, 2007. 403(3): p. 545-52.
46. Mizumoto, S. and K. Sugahara, *Bone and skin disorders caused by a disturbance in the biosynthesis of chondroitin sulfate and dermatan sulfate*, in *Extracellular Matrix: Pathobiology and Signaling*, K. Nikos, Editor. 2012, Walter de Gruyter: Berlin, Germany. p. 97-118.
47. Sugahara, K. and T. Mikami, *Chondroitin/dermatan sulfate in the central nervous system.* Curr Opin Struct Biol, 2007. 17(5): p. 536-45.
48. Ledin, J., et al., *Heparan sulfate structure in mice with genetically modified heparan sulfate production.* J Biol Chem, 2004. 279(41): p. 42732-41.
49. Antonsson, P., D. Heinegård, and A. Oldberg, *The keratan sulfate-enriched region of bovine cartilage proteoglycan consists of a consecutively repeated hexapeptide motif.* J Biol Chem, 1989. 264(27): p. 16170-3.
50. A., P., et al., *Metabolic control of hyaluronan synthesis*, in *Extracellular matrix: pathobiology and signaling*, K.N. K., Editor. 2012, De Gruyter: Göttingen (D). p. 26-38.
51. Nicholls, M.A., et al., *The Disease-Modifying Effects of Hyaluronan in the Osteoarthritic Disease State.* Clin Med Insights Arthritis Musculoskelet Disord, 2017. 10: p. 1179544117723611.
52. Rilla, K., et al., *Pericellular hyaluronan coat visualized in live cells with a fluorescent probe is scaffolded by plasma membrane protrusions.* J Histochem Cytochem, 2008. 56(10): p. 901-10.
53. Jiang, D., J. Liang, and P.W. Noble, *Hyaluronan as an immune regulator in human diseases.* Physiol Rev, 2011. 91(1): p. 221-64.
54. Tavana, S., et al., *Hyaluronic acid-based hydrogel scaffold without angiogenic growth factors enhances ovarian tissue function after autotransplantation in rats.* Biomed Mater, 2016. 11(5): p. 055006.
55. Maeshima, N., et al., *Hyaluronan binding identifies the most proliferative activated and memory T cells.* Eur J Immunol, 2011. 41(4): p. 1108-19.
56. Vincent, H. and E.J. D., *Hyaluronan*, in *Essentials of Glycobiology*, V. A, C. RD, and E. JD, Editors. 2017, Cold Spring Harbor: New York (USA).
57. Kitagawa, H., et al., *Molecular cloning of a chondroitin polymerizing factor that cooperates with chondroitin synthase for chondroitin polymerization.* J Biol Chem, 2003. 278(26): p. 23666-71.
58. Götting, C., et al., *Molecular cloning and expression of human UDP-d-Xylose:proteoglycan core protein beta-d-xylosyltransferase and its first isoform XT-II.* J Mol Biol, 2000. 304(4): p. 517-28.

59. Mizumoto, S., S. Yamada, and K. Sugahara, *Human genetic disorders and knockout mice deficient in glycosaminoglycan.* Biomed Res Int, 2014. 2014(495764): p. 495764.
60. Mizumoto, S., S. Yamada, and K. Sugahara, *Mutations in Biosynthetic Enzymes for the Protein Linker Region of Chondroitin/Dermatan/Heparan Sulfate Cause Skeletal and Skin Dysplasias.* Biomed Res Int, 2015. 2015: p. 861752.
61. Mizumoto, S., S. Ikegawa, and K. Sugahara, *Human genetic disorders caused by mutations in genes encoding biosynthetic enzymes for sulfated glycosaminoglycans.* J Biol Chem, 2014. 288(16): p. 10953-61.
62. Izumikawa, T., et al., *Identification of chondroitin sulfate glucuronyltransferase as chondroitin synthase-3 involved in chondroitin polymerization: chondroitin polymerization is achieved by multiple enzyme complexes consisting of chondroitin synthase family members.* J Biol Chem, 2008. 283(17): p. 11396-406.
63. Kitagawa, H., T. Uyama, and K. Sugahara, *Molecular cloning and expression of a human chondroitin synthase.* J Biol Chem, 2001. 276(42): p. 38721-6.
64. Mikami, T. and H. Kitagawa, *Biosynthesis and function of chondroitin sulfate.* Biochim Biophys Acta, 2013. 1830(10): p. 4719-33.
65. Morimoto-Tomita, M., et al., *Cloning and characterization of two extracellular heparin-degrading endosulfatases in mice and humans.* J Biol Chem, 2002. 277(51): p. 49175-85.
66. Paganini, C., et al., *Skeletal Dysplasias Caused by Sulfation Defects.* Int J Mol Sci, 2020. 21(8).
67. Hastbacka, J., et al., *Diastrophic dysplasia gene maps to the distal long arm of chromosome 5.* Proc Natl Acad Sci U S A, 1990. 87(20): p. 8056-9.
68. Schroder, E., et al., *Human PAPS Synthase Isoforms Are Dynamically Regulated Enzymes with Access to Nucleus and Cytoplasm.* PLoS One, 2012. 7(1): p. e29559.
69. Venkatachalam, K.V., *Human 3'-phosphoadenosine 5'-phosphosulfate (PAPS) synthase: biochemistry, molecular biology and genetic deficiency.* IUBMB Life, 2003. 55(1): p. 1-11.
70. Fuda, H., et al., *Characterization and expression of human bifunctional 3'-phosphoadenosine 5'-phosphosulphate synthase isoforms.* Biochem J, 2002. 365(Pt 2): p. 497-504.
71. Kamiyama, S., et al., *Molecular cloning and characterization of a novel 3'-phosphoadenosine 5'-phosphosulfate transporter, PAPST2.* J Biol Chem, 2006. 281(16): p. 10945-53.
72. Frederick, J.P., et al., *A role for a lithium-inhibited Golgi nucleotidase in skeletal development and sulfation.* Proc Natl Acad Sci U S A, 2008. 105(33): p. 11605-12.
73. Mihov, D. and M. Spiess, *Glycosaminoglycans: Sorting determinants in intracellular protein traffic.* Int J Biochem Cell Biol, 2015. 68: p. 87-91.
74. Prydz, K., *Determinants of Glycosaminoglycan (GAG) Structure.* Biomolecules, 2015. 5(3): p. 2003-22.
75. Kiani, C., et al., *Structure and function of aggrecan.* Cell Res, 2002. 12(1): p. 19-32.
76. Sivan, S.S., E. Wachtel, and P. Roughley, *Structure, function, aging and turnover of aggrecan in the intervertebral disc.* Biochim Biophys Acta, 2014. 1840(10): p. 3181-9.

77. Barry, F.P., et al., *N- and O-linked keratan sulfate on the hyaluronan binding region of aggrecan from mature and immature bovine cartilage.* J Biol Chem, 1995. 270(35): p. 20516-24.
78. Roughley, P.J. and J.S. Mort, *The role of aggrecan in normal and osteoarthritic cartilage.* J Exp Orthop, 2014. 1(1): p. 8.
79. Tim, H., *Proteoglycans and Glycosaminoglycans*, in *Dynamics of bone and cartilage metabolism.Principles and clinical applications*, S.M. J., R.S. P., and B.J. P., Editors. 2006, Academic Press: San Diego (USA). p. 85-98.
80. Bayliss, M.T., et al., *Sulfation of chondroitin sulfate in human articular cartilage. The effect of age, topographical position, and zone of cartilage on tissue composition.* J Biol Chem, 1999. 274(22): p. 15892-15900.
81. Chakravarti, S., *Functions of lumican and fibromodulin: lessons from knockout mice.* Glycoconj J, 2002. 19(4-5): p. 287-93.
82. Shoulders, M.D. and R.T. Raines, *Collagen structure and stability.* Annu Rev Biochem, 2009. 78: p. 929-58.
83. Manka, S.W., et al., *Structural insights into triple-helical collagen cleavage by matrix metalloproteinase 1.* Proc Natl Acad Sci U S A, 2012. 109(31): p. 12461-6.
84. Myllyharju, J., *Extracellular matrix and developing growth plate.* Curr Osteoporos Rep, 2014. 12(4): p. 439-45.
85. Alcaide-Ruggiero, L., et al., *Main and Minor Types of Collagens in the Articular Cartilage: The Role of Collagens in Repair Tissue Evaluation in Chondral Defects.* Int J Mol Sci, 2021. 22(24).
86. Melrose, J., et al., *The cartilage extracellular matrix as a transient developmental scaffold for growth plate maturation.* Matrix Biol, 2016. 52-54: p. 363-383.
87. Vaughan-Thomas, A., et al., *Characterization of type XI collagen-glycosaminoglycan interactions.* J Biol Chem, 2001. 276(7): p. 5303-9.
88. Alexopoulos, L.G., et al., *Developmental and osteoarthritic changes in Col6a1-knockout mice: biomechanics of type VI collagen in the cartilage pericellular matrix.* Arthritis Rheum, 2009. 60(3): p. 771-9.
89. Veidal, S.S., et al., *MMP mediated degradation of type VI collagen is highly associated with liver fibrosis--identification and validation of a novel biochemical marker assay.* PLoS One, 2011. 6(9): p. e24753.
90. Warman, M.L., et al., *A type X collagen mutation causes Schmid metaphyseal chondrodysplasia.* Nat Genet, 1993. 5(1): p. 79-82.
91. Gelse, K., E. Pöschl, and T. Aigner, *Collagens--structure, function, and biosynthesis.* Adv Drug Deliv Rev, 2003. 55(12): p. 1531-46.
92. Halász, K., et al., *COMP acts as a catalyst in collagen fibrillogenesis.* J Biol Chem, 2007. 282(43): p. 31166-73.
93. Burton-Wurster, N., G. Lust, and J.N. Macleod, *Cartilage fibronectin isoforms: in search of functions for a special population of matrix glycoproteins.* Matrix Biol, 1997. 15(7): p. 441-54.
94. Chevalier, X., *Fibronectin, cartilage, and osteoarthritis.* Semin Arthritis Rheum, 1993. 22(5): p. 307-18.

95. Rellmann, Y., E. Eidhof, and R. Dreier, *Review: ER stress-induced cell death in osteoarthritic cartilage.* Cell Signal, 2021. 78: p. 109880.
96. Briggs, M.D., et al., *New developments in chondrocyte ER stress and related diseases.* F1000Res, 2020. 9.
97. Sasaki, K. and H. Yoshida, *Organelle autoregulation-stress responses in the ER, Golgi, mitochondria and lysosome.* J Biochem, 2015. 157(4): p. 185-95.
98. Flamment, M., et al., *New insights into ER stress-induced insulin resistance.* Trends Endocrinol Metab, 2012. 23(8): p. 381-90.
99. Sim, H.J., et al., *Augmented ERAD (ER-associated degradation) activity in chondrocytes is necessary for cartilage development and maintenance.* Sci Adv, 2022. 8(3): p. eabl4222.
100. Sun, Z. and J.L. Brodsky, *Protein quality control in the secretory pathway.* J Cell Biol, 2019. 218(10): p. 3171-3187.
101. Settembre, C., et al., *Defective collagen proteostasis and matrix formation in the pathogenesis of lysosomal storage disorders.* Matrix Biol, 2018. 71-72: p. 283-293.
102. Hellicar, J., et al., *Supply chain logistics - the role of the Golgi complex in extracellular matrix production and maintenance.* J Cell Sci, 2022. 135(1).
103. Smits, P., et al., *Lethal skeletal dysplasia in mice and humans lacking the golgin GMAP-210.* N Engl J Med, 2010. 362(3): p. 206-16.
104. Chan, W.L., et al., *Impaired proteoglycan glycosylation, elevated TGF-β signaling, and abnormal osteoblast differentiation as the basis for bone fragility in a mouse model for gerodermia osteodysplastica.* PLoS Genet, 2018. 14(3): p. e1007242.
105. Osipovich, A.B., et al., *Dyggve-Melchior-Clausen syndrome: chondrodysplasia resulting from defects in intracellular vesicle traffic.* Proc Natl Acad Sci U S A, 2008. 105(42): p. 16171-6.
106. Ferreira, C.R., et al., *A Recurrent De Novo Heterozygous COG4 Substitution Leads to Saul-Wilson Syndrome, Disrupted Vesicular Trafficking, and Altered Proteoglycan Glycosylation.* Am J Hum Genet, 2018. 103(4): p. 553-567.
107. Choi, W., S. Kang, and J. Kim, *New insights into the role of the Golgi apparatus in the pathogenesis and therapeutics of human diseases.* Arch Pharm Res, 2022. 45(10): p. 671-692.
108. Lakpa, K.L., et al., *Lysosomal Stress Response (LSR): Physiological Importance and Pathological Relevance.* J Neuroimmune Pharmacol, 2021. 16(2): p. 219-237.
109. Zhu, S.Y., et al., *Lysosomal quality control of cell fate: a novel therapeutic target for human diseases.* Cell Death Dis, 2020. 11(9): p. 817.
110. Raben, N. and R. Puertollano, *TFEB and TFE3: Linking Lysosomes to Cellular Adaptation to Stress.* Annu Rev Cell Dev Biol, 2016. 32: p. 255-278.
111. Sardiello, M., et al., *A gene network regulating lysosomal biogenesis and function.* Science, 2009. 325(5939): p. 473-7.
112. Krakow, D. and D.L. Rimoin, *The skeletal dysplasias.* Genet Med, 2010. 12(6): p. 327-41.
113. Mortier, G.R., et al., *Nosology and classification of genetic skeletal disorders: 2019 revision.* Am J Med Genet A, 2019. 179(12): p. 2393-2419.

114. Desbuquois, G., et al., *Nanisme chondrodystrophique avec ossification anarchique et polymalformations chez deux soeurs.* Arch Fr Pediatr, 1966. 23: p. 573-587.
115. Laccone, F., et al., *Desbuquois dysplasia type I and fetal hydrops due to novel mutations in the CANT1 gene.* Eur J Hum Genet, 2011. 19(11): p. 1133-7.
116. Faivre, L., et al., *Desbuquois dysplasia, a reevaluation with abnormal and "normal" hands: radiographic manifestations.* Am J Med Genet A, 2004. 124A(1): p. 48-53.
117. Paganini, C., et al., *Calcium activated nucleotidase 1 (CANT1) is critical for glycosaminoglycan biosynthesis in cartilage and endochondral ossification.* Matrix Biol, 2018.
118. Kim, O.H., et al., *A variant of Desbuquois dysplasia characterized by advanced carpal bone age, short metacarpals, and elongated phalanges: report of seven cases.* Am J Med Genet A, 2010. 152A(4): p. 875-85.
119. Nizon, M., et al., *Further delineation of CANT1 phenotypic spectrum and demonstration of its role in proteoglycan synthesis.* Hum Mutat, 2012. 33(8): p. 1261-6.
120. Furuichi, T., et al., *CANT1 mutation is also responsible for Desbuquois dysplasia, type 2 and Kim variant.* J Med Genet, 2010. 48(1): p. 32-7.
121. Faden, M., et al., *Mutation of CANT1 causes Desbuquois dysplasia.* Am J Med Genet A, 2010. 152A(5): p. 1157-60.
122. Huber, C., et al., *Identification of CANT1 mutations in Desbuquois dysplasia.* Am J Hum Genet, 2009. 85(5): p. 706-10.
123. Bui, C., et al., *XYLT1 mutations in Desbuquois dysplasia type 2.* Am J Hum Genet, 2014. 94(3): p. 405-14.
124. Failer, B.U., N. Braun, and H. Zimmermann, *Cloning, expression, and functional characterization of a Ca(2+)-dependent endoplasmic reticulum nucleoside diphosphatase.* J Biol Chem, 2002. 277(40): p. 36978-86.
125. Smith, T.M., et al., *Cloning, expression, and characterization of a soluble calcium-activated nucleotidase, a human enzyme belonging to a new family of extracellular nucleotidases.* Arch Biochem Biophys, 2002. 406(1): p. 105-15.
126. Smith, T.M. and T.L. Kirley, *The calcium activated nucleotidases: A diverse family of soluble and membrane associated nucleotide hydrolyzing enzymes.* Purinergic Signal, 2006. 2(2): p. 327-33.
127. Yang, M., et al., *Calcium-dependent dimerization of human soluble calcium activated nucleotidase: characterization of the dimer interface.* J Biol Chem, 2006. 281(38): p. 28307-17.
128. Cali, T., et al., *Ca2+-activated nucleotidase 1, a novel target gene for the transcriptional repressor DREAM (downstream regulatory element antagonist modulator), is involved in protein folding and degradation.* J Biol Chem, 2012. 287(22): p. 18478-91.
129. Harden, T.K., et al., *Signalling and pharmacological properties of the P2Y receptor.* Acta Physiol (Oxf), 2010. 199(2): p. 149-60.
130. Bonafe, L., et al., *A novel mutation in the sulfate transporter gene SLC26A2 (DTDST) specific to the Finnish population causes de la Chapelle dysplasia.* J Med Genet, 2008. 45(12): p. 827-31.

131. Lamy, M. and P. Maroteaux, *[Diastrophic nanism]*. Presse Med, 1960. 68: p. 1977-80.
132. Makitie, O. and I. Kaitila, *Growth in diastrophic dysplasia.* J Pediatr, 1997. 130(4): p. 641-6.
133. Remes, V., et al., *Walking ability in patients with diastrophic dysplasia: a clinical, electroneurophysiological, treadmill, and MRI analysis.* J Pediatr Orthop, 2004. 24(5): p. 546-51.
134. Gollop, T.R. and A. Eigier, *Prenatal ultrasound diagnosis of diastrophic dysplasia at 16 weeks.* Am J Med Genet, 1987. 27(2): p. 321-4.
135. Peltonen, J., V. Remes, and P. Tervahartiala, *Early degeneration of the knee in diastrophic dysplasia: an MRI study.* J Pediatr Orthop, 2003. 23(6): p. 722-6.
136. Vaara, P., et al., *Development of the hip in diastrophic dysplasia.* J Bone Joint Surg Br, 1998. 80(2): p. 315-20.
137. Remes, V., et al., *Cervical spine in diastrophic dysplasia: an MRI analysis.* J Pediatr Orthop, 2000. 20(1): p. 48-53.
138. Griffin, J.R., et al., *Optometric screening in achondroplasia, diastrophic dysplasia, and spondyloepiphyseal dysplasia congenita.* Am J Optom Physiol Opt, 1980. 57(2): p. 118-23.
139. Krecak, J. and R.J. Starshak, *Cervical kyphosis in diastrophic dwarfism: CT and MR findings.* Pediatr Radiol, 1987. 17(4): p. 321-2.
140. Tunkel, D., et al., *Hearing loss in skeletal dysplasia patients.* Am J Med Genet A, 2012. 158A(7): p. 1551-5.
141. Lachman, R., et al., *Diastrophic dysplasia: the death of a variant.* Radiology, 1981. 140(1): p. 79-86.
142. Vaara, P., et al., *Health-related quality of life in patients with diastrophic dysplasia.* Scand J Public Health, 1999. 27(1): p. 38-42.
143. Honório, J.C., et al., *Diastrophic dysplasia: prenatal diagnosis and review of the literature.* Sao Paulo Med J, 2013. 131(2): p. 127-32.
144. Rossi, A. and A. Superti-Furga, *Mutations in the diastrophic dysplasia sulfate transporter (DTDST) gene (SLC26A2): 22 Novel mutations, mutation review, associated skeletal phenotypes, and diagnostic relevance.* Human Mutation, 2001. 17(3): p. 159-171.
145. Forlino, A., et al., *A diastrophic dysplasia sulfate transporter (SLC26A2) mutant mouse: morphological and biochemical characterization of the resulting chondrodysplasia phenotype.* Hum Mol Genet, 2005. 14(6): p. 859-71.
146. Superti-Furga, A., *A defect in the metabolic activation of sulfate in a patient with achondrogenesis type IB.* Am J Hum Genet, 1994. 55(6): p. 1137-1145.
147. Newbury-Ecob, R., *Atelosteogenesis type 2.* J Med Genet, 1998. 35(1): p. 49-53.
148. Sillence, D., et al., *Atelosteogenesis syndromes: a review, with comments on their pathogenesis.* Pediatr Radiol, 1997. 27(5): p. 388-96.
149. Gustavson, K.H., et al., *Lethal and non-lethal diastrophic dysplasia. A study of 14 Swedish cases.* Clin Genet, 1985. 28(4): p. 321-34.
150. Superti-Furga, A., et al., *Recessively inherited multiple epiphyseal dysplasia with normal stature, club foot, and double layered patella caused by a DTDST mutation.* J Med Genet, 1999. 36(8): p. 621-624.

151. Dawson, P.A., *Sulfate in fetal development.* Semin Cell Dev Biol, 2011. 22(6): p. 653-9.
152. Rossi, A., et al., *Proteoglycan sulfation in cartilage and cell cultures from patients with sulfate transporter chondrodysplasias: Relationship to clinical severity and indications on the role of intracellular sulfate production.* Matrix Biology, 1998. 17(5): p. 361-369.
153. Alper, S.L. and A.K. Sharma, *The SLC26 gene family of anion transporters and channels.* Mol Aspects Med, 2013. 34(2-3): p. 494-515.
154. Langford, R., E. Hurrion, and P.A. Dawson, *Genetics and pathophysiology of mammalian sulfate biology.* J Genet Genomics, 2017. 44(1): p. 7-20.
155. Jennings, M.L., *Proton fluxes associated with erythrocyte membrane anion exchange.* J Membr Biol, 1976. 28(2-3): p. 187-205.
156. Dawson, P.A., et al., *Review: Nutrient sulfate supply from mother to fetus: Placental adaptive responses during human and animal gestation.* Placenta, 2017. 54: p. 45-51.
157. Cole, D.E. and C.R. Scriver, *Age-dependent serum sulfate levels in children and adolescents.* Clin Chim Acta, 1980. 107(1-2): p. 135-9.
158. Bradley, H., et al., *Sulfate metabolism is abnormal in patients with rheumatoid arthritis. Confirmation by in vivo biochemical findings.* J Rheumatol, 1994. 21(7): p. 1192-6.
159. Cole, D.E., L.S. Baldwin, and L.J. Stirk, *Increased serum sulfate in pregnancy: relationship to gestational age.* Clin Chem, 1985. 31(6): p. 866-7.
160. Heafield, M.T., et al., *Plasma cysteine and sulphate levels in patients with motor neurone, Parkinson's and Alzheimer's disease.* Neurosci Lett, 1990. 110(1-2): p. 216-20.
161. Forlino, A., et al., *A diastrophic dysplasia sulfate transporter (SLC26A2) mutant mouse: morphological and biochemical characterization of the resulting chondrodysplasia phenotype.* Human Molecular Genetics, 2005. 14(6): p. 859-871.
162. Schwartz, N.B., et al., *Sulfate activation and transport in mammals: system components and mechanisms.* Chem Biol Interact, 1998. 109(1-3): p. 143-51.
163. Karniski, L.P., *Functional expression and cellular distribution of diastrophic dysplasia sulfate transporter (DTDST) gene mutations in HEK cells.* Hum Mol Genet, 2004. 13(19): p. 2165-71.
164. Bissig, M., et al., *Functional expression cloning of the canalicular sulfate transport system of rat hepatocytes.* J Biol Chem, 1994. 269(4): p. 3017-3021.
165. Hästbacka, J., et al., *The diastrophic dysplasia gene encodes a novel sulfate transporter: positional cloning by fine-structure linkage disequilibrium mapping.* Cell, 1994. 78(6): p. 1073-1087.
166. Kere, J., *Overview of the SLC26 family and associated diseases.* Novartis Found Symp, 2006. 273: p. 2-11; discussion 11-8, 261-4.
167. Gualeni, B., et al., *Alteration of proteoglycan sulfation affects bone growth and remodeling.* Bone, 2013. 54(1): p. 83-91.
168. Hoffman, B.E., et al., *Development and characterization of a human articular cartilage-derived chondrocyte cell line that retains chondrocyte phenotype.* J Cell Physiol, 2010. 222(3): p. 695-702.

169. Zaucke, F., et al., *Cartilage oligomeric matrix protein (COMP) and collagen IX are sensitive markers for the differentiation state of articular primary chondrocytes.* Biochem J, 2001. 358(Pt 1): p. 17-24.
170. Watt, F.M., *Effect of seeding density on stability of the differentiated phenotype of pig articular chondrocytes in culture.* J Cell Sci, 1988. 89 (Pt 3): p. 373-8.
171. Meretoja, V.V., et al., *Enhanced chondrogenesis in co-cultures with articular chondrocytes and mesenchymal stem cells.* Biomaterials, 2012. 33(27): p. 6362-9.
172. Gramegna Tota, C., et al., *Phenotypic Characterization of Immortalized Chondrocytes from a Desbuquois Dysplasia Type 1 Mouse Model: A Tool for Studying Defects in Glycosaminoglycan Biosynthesis.* Int J Mol Sci, 2021. 22(17).
173. Yao, Y. and Y. Wang, *ATDC5: an excellent in vitro model cell line for skeletal development.* J Cell Biochem, 2013. 114(6): p. 1223-9.
174. Altaf, F.M., et al., *Ascorbate-enhanced chondrogenesis of ATDC5 cells.* Eur Cell Mater, 2006. 12: p. 64-9; discussion 69-70.
175. Hodax, J.K., et al., *Aggrecan is required for chondrocyte differentiation in ATDC5 chondroprogenitor cells.* PLoS One, 2019. 14(6): p. e0218399.
176. Stevens, J.W., *Swarm chondrosarcoma: a continued resource for chondroblastic-like extracellular matrix and chondrosarcoma biology research.* Connect Tissue Res, 2013. 54(4-5): p. 252-9.
177. King, K.B. and J.H. Kimura, *The establishment and characterization of an immortal cell line with a stable chondrocytic phenotype.* J Cell Biochem, 2003. 89(5): p. 992-1004.
178. Moses, M.A. and Y. Shing, *Production of matrix metalloproteinases and a metalloproteinase inhibitor by swarm rat chondrosarcoma.* Biochem Biophys Res Commun, 1994. 199(1): p. 418-24.
179. Bosserhoff, A.K., et al., *Mouse CD-RAP/MIA gene: structure, chromosomal localization, and expression in cartilage and chondrosarcoma.* Dev Dyn, 1997. 208(4): p. 516-25.
180. Wang, Y., et al., *A prospect of cell immortalization combined with matrix microenvironmental optimization strategy for tissue engineering and regeneration.* Cell Biosci, 2019. 9: p. 7.
181. Goldring, M.B., *Culture of immortalized chondrocytes and their use as models of chondrocyte function.* Methods Mol Med, 2004. 100: p. 37-52.
182. Ramboer, E., et al., *Strategies for immortalization of primary hepatocytes.* J Hepatol, 2014. 61(4): p. 925-43.
183. Yang, J., et al., *Establishment and characterization of an immortalized human chondrocyte cell line.* Biotechnol Lett, 2020. 42(5): p. 707-716.
184. Takazawa, Y., et al., *Articular cartilage cells immortalized by a temperature sensitive mutant of SV40 large T antigen survive and form cartilage tissue in articular cartilage environment.* J Cell Biochem, 1999. 75(2): p. 338-45.
185. Kokenyesi, R., et al., *Proteoglycan production by immortalized human chondrocyte cell lines cultured under conditions that promote expression of the differentiated phenotype.* Arch Biochem Biophys, 2000. 383(1): p. 79-90.

186. Quentin, E., et al., *A genetic defect in the biosynthesis of dermatan sulfate proteoglycan: galactosyltransferase I deficiency in fibroblasts from a patient with a progeroid syndrome.* Proc Natl Acad Sci U S A, 1990. 87(4): p. 1342-6.
187. Sasaki, K. and H. Yoshida, *Golgi stress response and organelle zones.* FEBS Lett, 2019. 593(17): p. 2330-2340.
188. Taniguchi, M. and H. Yoshida, *TFE3, HSP47, and CREB3 Pathways of the Mammalian Golgi Stress Response.* Cell Struct Funct, 2017. 42(1): p. 27-36.
189. Martina, J.A., et al., *The nutrient-responsive transcription factor TFE3 promotes autophagy, lysosomal biogenesis, and clearance of cellular debris.* Sci Signal, 2014. 7(309): p. ra9.
190. Martina, J.A., et al., *TFEB and TFE3 are novel components of the integrated stress response.* EMBO J, 2016. 35(5): p. 479-95.
191. Pacifici, M., *Independent secretion of proteoglycans and collagens in chick chondrocyte cultures during acute ascorbic acid treatment.* Biochem J, 1990. 272(1): p. 193-9.
192. Goldring, M.B., et al., *Immune interferon suppresses levels of procollagen mRNA and type II collagen synthesis in cultured human articular and costal chondrocytes.* J Biol Chem, 1986. 261(19): p. 9049-55.
193. Rossi, A., et al., *In vitro proteoglycan sulfation derived from sulfhydryl compounds in sulfate transporter chondrodysplasias.* Pediatr Pathol Molec Med, 2003. 22: p. 311-321.
194. Pecora, F., et al., *In vivo contribution of amino acid sulfur to cartilage proteoglycan sulfation.* Biochem J, 2006. 398(3): p. 509-14.
195. Monti, L., et al., *N-acetylcysteine treatment ameliorates the skeletal phenotype of a mouse model of diastrophic dysplasia.* Human Molecular Genetics, 2015. 24(19): p. 5570-5580.
196. Monti, L., et al., *N-acetylcysteine treatment ameliorates the skeletal phenotype of a mouse model of diastrophic dysplasia.* Hum Mol Genet, 2015. 24(19): p. 5570-80.
197. Samuni, Y., et al., *The chemistry and biological activities of N-acetylcysteine.* Biochim Biophys Acta, 2013. 1830(8): p. 4117-29.
198. Jourdan, J.P., et al., *Drug repositioning: a brief overview.* J Pharm Pharmacol, 2020.
199. Nosengo, N., *Can you teach old drugs new tricks?* Nature, 2016. 534(7607): p. 314-6.

APPENDIX: Further publications

International Journal of
Molecular Sciences

MDPI

Review

Skeletal Dysplasias Caused by Sulfation Defects

Chiara Paganini [1], Chiara Gramegna Tota [1], Andrea Superti-Furga [2] and Antonio Rossi [1,*]

[1] Department of Molecular Medicine, Unit of Biochemistry, University of Pavia, 27100 Pavia, Italy; chiara.paganini01@universitadipavia.it (C.P.); chiara.gramegnatota01@universitadipavia.it (C.G.T.)
[2] Division of Genetic Medicine, Lausanne University Hospital, University of Lausanne, 1011 Lausanne, Switzerland; asuperti@unil.ch
* Correspondence: antrossi@unipv.it

Received: 25 February 2020; Accepted: 10 April 2020; Published: 14 April 2020

Abstract: Proteoglycans (PGs) are macromolecules present on the cell surface and in the extracellular matrix that confer specific mechanical, biochemical, and physical properties to tissues. Sulfate groups present on glycosaminoglycans, linear polysaccharide chains attached to PG core proteins, are fundamental for correct PG functions. Indeed, through the negative charge of sulfate groups, PGs interact with extracellular matrix molecules and bind growth factors regulating tissue structure and cell behavior. The maintenance of correct sulfate metabolism is important in tissue development and function, particularly in cartilage where PGs are fundamental and abundant components of the extracellular matrix. In chondrocytes, the main sulfate source is the extracellular space, then sulfate is taken up and activated in the cytosol to the universal sulfate donor to be used in sulfotransferase reactions. Alteration in each step of sulfate metabolism can affect macromolecular sulfation, leading to the onset of diseases that affect mainly cartilage and bone. This review presents a panoramic view of skeletal dysplasias caused by mutations in genes encoding for transporters or enzymes involved in macromolecular sulfation. Future research in this field will contribute to the understanding of the disease pathogenesis, allowing the development of targeted therapies aimed at alleviating, preventing, or modifying the disease progression.

Keywords: sulfate metabolism; sulfotransferase; glycosaminoglycan; proteoglycan; cartilage; genotype phenotype correlation; skeletal disorders

1. Introduction

Sulfated compounds include a wide array of substances, ranging in molecular weight from less than 10^3 Da to greater than 10^6 Da, that undergo striking changes in their physicochemical properties upon the addition of the negatively charged sulfated groups. Sulfation increases electrostatic interactions, water solubility, converts lipophilic molecules to amphiphiles, and can lead to conformational changes both in low and high-molecular-weight molecules. Whereas phosphorylation is central to intracellular signal transduction, sulfation modulates cell–cell and cell–matrix communication.

The highest density of sulfate groups is found in proteoglycans (PGs), a broad category of macromolecules characterized by a core protein to which one to over one hundred glycosaminoglycan (GAG) chains are attached [1]. PGs are present in the cell nucleus, in cytoplasm, and at the cell membranes, but they are particularly abundant in the extracellular matrix (ECM) of connective tissues. The highly acidic and hydrophilic properties of GAGs have a major influence on tissue hydration, elasticity, and cation composition. Furthermore, they bind with high-affinity ECM proteins, growth factors, enzymes, and cell surface receptors [2–4].

Aside from PGs, many other molecules can be sulfated showing different effects; for instance, sulfate moieties added to hormones influence their biological activity [5]. Sulfoglycolipids such as sphingolipids and galactoglycerolipids are abundant in myelin as well as spermatozoa, kidney, and small intestine [6]. Sulfation of tyrosine residues represents the prevalent posttranslational modification of many secretory and membrane proteins and peptides that may significantly influence their function [7]. Sulfation also has a significant role in the biotransformation of many endogenous low-molecular-weight compounds including catecholamines and iodothyronines [8], cholesterol, bile acids, and steroids [9–11].

These examples highlight that proper sulfation of endogenous molecules is a widespread phenomenon so far poorly explored, although it is essential for growth and development. Indeed several heritable disorders caused by defects in the biosynthesis and catabolism of sulfated compounds are associated mainly with abnormal development of the skeleton [12].

Skeletal dysplasias are a huge and heterogeneous group of genetic disorders that affect mainly, but not exclusively, cartilage and bone. Beyond orthopedic complications, neurological, auditory, visual, cardiac, pulmonary, and renal problems could be present because the causative genes might also have functional roles in tissues other than the skeleton [13,14]. Nowadays 461 disorders have been characterized based on clinical, radiographic and molecular observations and 437 disease genes have been identified [15]. Skeletal dysplasias show a wide range of severity from very mild phenotypes compatible with life to fetal and neonatal lethality. Interestingly, mutations in different genes may cause the same skeletal dysplasia or mutations in the same gene are related to different skeletal disorders [14]. Genes involved in skeletal dysplasias encode for different protein products including ECM proteins, enzymes, cellular transporters, transcription factors, signal transducers, channel proteins, chaperones, cytoplasmic proteins, cilia, proteins involved in cell cycle, and chromatin modifying enzymes [13,14].

This review deals with disorders of the biosynthesis of sulfated macromolecules, which are associated mainly with abnormal development of the skeleton.

2. The Cellular Metabolism of Sulfate

Sulfation is mechanistically analogous to phosphorylation: in analogy to ATP, the phosphate donor used by several kinases, there is a “universal” sulfate donor for different substrate specific sulfotransferases. Studies in prokaryotes, yeast, liver, and cartilage tissue have demonstrated that the universal sulfate donor for sulfotransferase reactions is 3′-phosphoadenosine 5′-phosphosulfate (PAPS) [16–18]. Thus, in all mammalian tissues, intracellular sulfate is activated to PAPS through the sulfate activation pathway in order to be used in sulfation reactions catalyzed by sulfotransferases (Figure 1) [19,20].

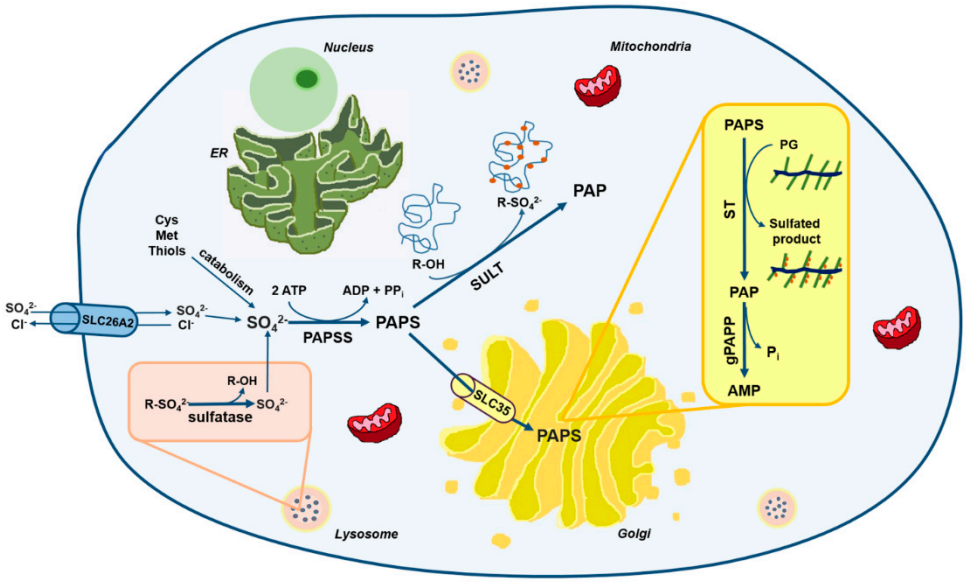

Figure 1. Schematic view of sulfate metabolism in cells. Intracellular level of sulfate depends mainly on extracellular uptake through membrane transporters such as the solute carrier family 26 member 2 (SLC26A2). A small amount of sulfate comes also from the catabolism of sulfur-containing amino acids and thiols or from sulfatase reactions in lysosomes. Once in cell, sulfate is activated to 3′-phosphoadenosine 5′-phosphosulfate (PAPS) by PAPS synthetase (PAPSS). PAPS represents the universal sulfate donor and is used by cytosolic sulfotransferases (SULTs) for hormone and xenobiotics sulfation or by Golgi sulfotransferases (STs) for the sulfation of macromolecules such as PGs. The solute carrier family 35 member B2 (SLC35B2) and SLC35B3 transporters allow Golgi uptake of PAPS. During sulfotransferase reactions, phosphoadenosine phosphate (PAP) is produced as a by-product and is hydrolyzed to AMP and phosphate by a Golgi resident phosphoadenosine phosphate phosphatase (gPAPP, also known as IMPAD1 or BPNT2).

2.1. The Origin of Intracellular Sulfate

Endogenous sulfate is essential for PAPS synthesis. The cytoplasmic sulfate pool may be either derived from the extracellular fluids or from the catabolism of sulphur containing amino acids and other thiols with production of sulfite, which is then oxidized to sulfate. Intracellular sulfate can also come from the degradation of sulfated molecules through sulfatases [21].

In healthy adults, one third of sulfate is provided from the diet [22]; sulfate is adsorbed in the small intestine and the plasma level, that in humans span a broad range (250–400 μM), is maintained by renal reabsorption in proximal tubule through SLC13A1 and SLC26A1 transporters [21,23]. Age [24], gestational period [25] and diseases [26] alter sulfate homeostasis affecting sulfate concentrations in body fluids [22].

The transport of sulfate ions across cell membranes and epithelial tissues is mediated by carrier proteins. Sulfate transporters function either as sulfate/chloride antiporters or sodium/sulfate symporters [21,27–29]. Human sulfate transporters belong to different solute linked carrier families such as SLC4, SLC13 and SLC26. Transporters of the same family, such as the SLC26 transporter family, show similar structure and sequence, but mutations in each gene cause different phenotypes due to different tissue distribution and exchanged anion [30]. For instance, SLC26A1 and SLC26A2 are both present in kidney and intestine, but the former is primarily expressed in hepatocytes, while the latter in chondrocytes [31]. In the SLC13 family, SLC13A1 is mainly expressed in renal tissue [32], while SLC13A4 in placenta [33].

Among sulfate transporters, SLC26A2 is also known as the diastrophic dysplasia sulfate transporter (DTDST). The identification of this sulfate/chloride antiporter was the end result of a long-term project aimed at elucidating the molecular basis of diastrophic dysplasia (DTD), a skeletal dysplasia particularly

frequent in the Finnish population [34]. The hypothesis that DTD was associated with impaired sulfate transport was confirmed by the reduced sulfate uptake in cultured fibroblasts from patients and by the identification of mutations in the candidate gene in these individuals [34].

Despite the wide distribution of sulfate transporters in different organs, not all tissues use inorganic sulfate as the main sulfate source. Kidney cells also use cysteine, N-acetylcysteine, and glutathione, whereas in lung cells cysteine is the most efficient source of sulfate [35]. In human fibroblast cultures, at less than physiological extracellular sulfate concentrations, cysteine is a major contributor to the intracellular sulfate pool [36].

A small fraction of intracellular sulfate can come from lysosomal degradation of the carbohydrate moiety of glycoproteins and GAGs that produces monosaccharides and sulfate which must efflux from the lysosomes before re-entering biosynthetic pathways [37].

In conclusion, based on our knowledge it is likely that, the three distinct sources of sulfate work together to maintain the intracellular sulfate pool, but with different prevalence in different cell types.

2.2. The Sulfate Activation Pathway

Sulfation reactions require PAPS as universal sulfate donor. Its concentration differs among tissues and species; in humans it ranges between 3.6–22.6 nmol/g tissue [16].

The activation of sulfate to PAPS results from the concerted action of two enzymes ATP sulfurylase and adenosine 5′-phosphosulfate (APS) kinase which are located on separate polypeptide chains in bacteria, fungi, yeast, and plants, while in animals they are present in a bifunctional protein named PAPS synthetase (PAPSS) [38]. The catalytic domain of APS kinase is located in the amino-terminal region, whereas the ATP sulfurylase domain is in the carboxy-terminal part. The first step is catalyzed by ATP sulfurylase and involves the activation of inorganic sulfate with ATP to form APS and pyrophosphate. The second step, the conversion of APS and another molecule of ATP in PAPS and ADP, is catalyzed by APS kinase. The first reaction is not energetically favoured and it is the rate limiting step in PAPS formation; however, subsequent hydrolysis of pyrophosphate and the rapid utilization of APS in the second reaction relieve the energy constraint of the overall reaction. PAPSS exists as two isozymes encoded by genes located on separate chromosomes. The human gene for PAPS synthetase 1 (PAPSS1) is located on chromosome 4q25–26 [39]; while the gene for human PAPS synthetase 2 (PAPSS2) has been localized to chromosome 10q23–24 [40]. Interestingly the mouse and human PAPSS2 isozymes were discovered through investigation of specific developmental dwarfism disorders, i.e., brachymorphism in mice and a form of spondyloepimetaphyseal dysplasia in humans [40,41]. More recently, PAPSS2 has also been implicated in steroid metabolism [42], while mutations in PAPSS1 have not been linked to any human pathology suggesting embryonic lethality since PAPSS1 is the main isoform in developing nervous system [21,43].

In both human and mouse species, PAPSS1 and 2 are 76% identical [20], but the catalytic activity of the PAPSS2 variant is 10- to 15-fold higher than that of PAPSS1 [44]. The two isoforms have different cellular localization: PAPSS1 localizes mainly to the nucleus, while PAPSS2 to the cytosol [45]. Moreover the two isoenzymes differ also for tissue localization, since PAPSS1 is expressed in skin and brain, whereas PAPSS2 in liver and cartilage [20].

PAPS is the universal sulfate donor for sulfation either in the cytosol or in the Golgi. In the cytosol PAPS is used for sulfation of a wide variety of endogenous compounds including hormones and neurotransmitters as well as drugs and xenobiotics. On the other hand, sulfation of carbohydrates, peptides and proteins occurs in the Golgi; for this purpose PAPS is transported to the Golgi by specific PAPS transporters (PAPSTs). Two different PAPST isoforms have been cloned, PAPST1 and PAPST2 [46,47], also known as SLC35B2 and SLC35B3, respectively [48,49]. The two transporters are closely related and show similar transport activity; they are both widely expressed among tissues, in particular PAPST2 is highly expressed in colon [46]. Kinetic studies of PAPSTs have suggested that PAPS transport occurs through an antiport mechanism that might involve phosphoadenosine phosphate (PAP) or AMP [49]. So far, no human genetic disorders have been linked to mutations

in *SLC35B2* and *SLC35B3* genes, but cartilage defects have been reported in *slc35b2* null zebrafish mutants [21,50].

2.3. The Sulfation Pathway

The transfer of sulfate from the activated donor, PAPS, to a variety of molecules is catalyzed by sulfotransferases. Two classes of sulfotransferases are present in eukaryotes: cytosolic sulfotransferases, that sulfate small molecules such as hormones, amines and xenobiotics including drugs, and Golgi resident sulfotransferases that sulfate larger substrates involved in the secretory pathway [43,51].

In human genome 13 genes for cytosolic sulfotransferases (SULTs) exist and these enzymes are classified in four families (SULT1, SULT2, SULT4 and SULT6) based on distribution and substrate preference, even if SULTs may show overlapping substrate specificity [52]. SULT enzymes, with the exception of SULT6, are soluble cytosolic proteins that form dimers thank to a 10 amino acid sequence at the C-terminal end named KTVE motif [48,53].

Carbohydrate sulfotransferases (STs) are membrane bound enzymes present in the Golgi; up to now, 37 genes have been identified in humans [21]. STs are stereoselective and exhibit strict substrate specificity [2]; the addition of a sulfate group can convert a common carbohydrate structural motif into a unique recognition site for a specific receptor. Members of ST families show similar primary structure and identical substrate specificity, but they are differently distributed [2].

In the Golgi also specific tyrosine residues of secreted proteins and peptides are sulfated by tyrosylprotein sulfotransferases (TPST1 and TPST2) [54]. These two enzymes show 67% amino acid identity and use PAPS as obligate sulfate donor. Tyrosine sulfation can determine the bioactivity of several neuropeptides or expand the functions of some proteins. Moreover, sulfated tyrosines are important to boost protein-protein or protein-biopolymer interactions [48,55].

PAPS-dependent sulfotransferase reactions produce PAP as by-product that can inhibit, via negative feedback, sulfotransferases [48]. To prevent their inhibition, rapid degradation of PAP in AMP and phosphate by a PAP phosphatase is important as demonstrated in chondrodysplasia with joint dislocations gPAPP type caused by mutations in the *IMPAD1* gene (recently renamed *BPNT2*, 3′(2′), 5′-bisphosphate nucleotidase 2), encoding for a Golgi resident PAP phosphatase (gPAPP) or in the gene trap knock-out mice for the same gene [56–58].

Sulfatases, hydrolytic enzymes belonging to the alkaline phosphatase superfamily [48], play an opposite role to that of sulfotransferases. Indeed, these enzymes are a highly conserved family of proteins that catalyze the hydrolysis of sulfate ester bonds from a wide variety of substrates including GAGs, sulfolipids and steroid sulfates [59]. Seventeen genes have been identified in the human genome [21] encoding sulfatase enzymes, that share similar size, high glycosylation level, sequence homology and similar active site. Based on their subcellular localization, sulfatases are grouped in two main categories: those expressed in lysosomes, that act at acidic pH and are involved in catabolism, and those present in the endoplasmic reticulum, Golgi apparatus and at the cell surface acting at neutral pH and more likely involved in biosynthetic, rather than catabolic, pathways [59].

3. Sulfate Metabolism and Genetic Diseases

Genetic defects have been identified in several steps of PG biosynthesis, leading to a huge number of diseases that primarily affect cartilage and endochondral bone [12]. The cartilage phenotype might be explained by the high amount of sulfated PGs that are synthesized and deposited in the cartilage ECM. Among these disorders, diseases involving sulfate uptake, metabolic activation, and sulfation of GAGs are discussed in this review (Figure 2).

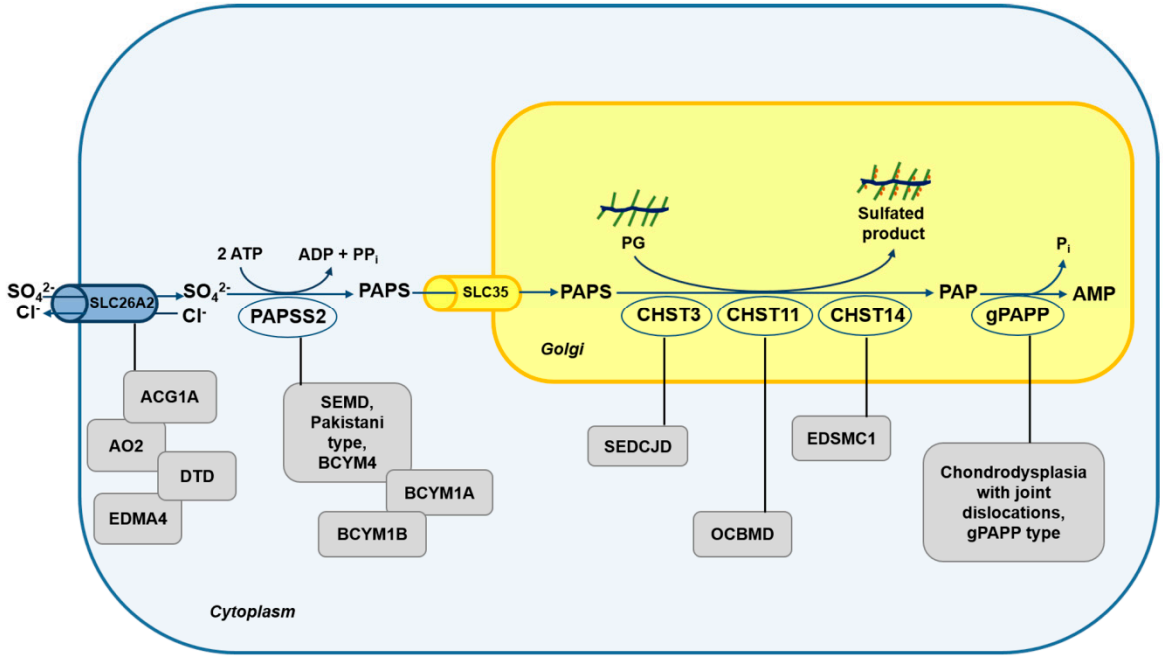

Figure 2. Schematic diagram of the defects in the sulfation pathway causing skeletal dysplasias. Mutations in genes encoding for transporter and enzymes involved in sulfate metabolism cause several skeletal dysplasias (grey box). ACG1B, achondrogenesis type 1B; AO2, atelosteogenesis type 2; DTD, diastrophic dysplasia; EDM4, recessive multiple epiphyseal dysplasia; SEMD, spondyloepimetaphyseal dysplasia; BCYM4, brachyolmia type 4; BCYM1A, brachyolmia type 1, Hobaek form; BCYM1B, brachyolmia type 1, Toledo form; SEDCJD, spondyloepiphyseal dysplasia with congenital joint dislocations; EDSMC1, Ehlers–Danlos syndrome musculocontractural type 1 and OCBMD, osteochondrodysplasia, brachydactyly and overlapping malformed digits.

3.1. Skeletal Dysplasias Linked to Proteins Involved in Sulfate Metabolism

SLC26A2 linked chondrodysplasias represent a heterogeneous group of skeletal diseases caused by mutations in the *SLC26A2* gene encoding for a sulfate transporter present on the cell membrane, also known as diastrophic dysplasia sulfate transporter. There are currently four distinct phenotypes associated to *SLC26A2* mutations; this division is useful for differential diagnosis and prognosis, but has no biological basis since the spectrum of diseases based on clinical and radiological criteria is continuous. The four different conditions described in decreasing order of severity include: achondrogenesis type 1B (ACG1B, MIM 600972), atelosteogenesis type 2 (AO2, MIM 256050), diastrophic dysplasia (DTD, MIM 222600) and recessive multiple epiphyseal dysplasia (EDM4, MIM 226900) [60]. Key clinical features comprise lethality in the fetal period or immediately after birth (ACG1B and AO2), shortened limbs (all but not EDM4), joint pain, joint contractures, "hitchhiker" thumb (AO2 and DTD), cystic swelling of the external ear (DTD), cleft palate (DTD and AO2), scoliosis, clubfoot and double-layered patellae (EDM4). Two other conditions originally described as distinct lethal skeletal dysplasias based on radiographic findings, namely de la Chapelle dysplasia and McAllister dysplasia [61,62], were proven to be related to AO2 based on biochemical and molecular data [63,64].

In these disorders the different clinical phenotypes have been linked to the mutation severity, the residual activity of the sulfate transporter and the undersulfation level of cartilage PGs [60,65,66], but it appears that the nature of the *SLC26A2* mutations is not the only factor determining phenotypic severity. Phenotypic differences have been observed between unrelated and even first-degree relatives with the same mutation. In the dtd mouse, an animal model of human DTD, the skeletal phenotype has been confirmed by the presence of reduced skeletal growth, deformities of long bones, reduced toluidine blue staining of cartilage, chondrocytes of irregular size and delay in the formation of the secondary ossification center. Interestingly impaired sulfate uptake was demonstrated in chondrocytes,

osteoblasts, and fibroblasts, but significant PG undersulfation was detected only in cartilage, despite the generalized sulfate uptake defect [67]. Studies on the growth plate of the animal model demonstrated reduced chondrocyte proliferation due to altered Indian hedgehog (Ihh) signalling [68] and reduced phosphorylation of the pocket protein p130 that inhibits transcription factors of the E2F family leading to the block in the G1 phase of cell cycle progression [69]. Even if sulfate uptake from the extracellular environment is crucial for PG sulfation in chondrocytes, an alternative source of sulfate, namely intracellular thiol compounds, has been reported in the dtd mouse suggesting potential pharmacological approaches to DTD [70]. Recently an over activation of fibroblast growth factor receptor 3 (FGFR3) signalling has been described in a *Slc26a2* knock-out mouse, an animal model of ACG1B and AO2. This finding suggests the involvement of altered FGFR3 pathway in the pathogenic mechanism contributing to the lethal phenotype [71].

Spondyloepimetaphyseal dysplasia (SEMD), Pakistani type has been described in a large family from Pakistan by Ahmad et al. in 1998 [72]. The clinical phenotype includes short stature, short and bowed lower limbs with enlarged knee joints, kyphoscoliosis, mild brachydactyly, delayed ossification of the epiphyses and osteoarthritis [72]. In these patients mutations in the *PAPSS2* gene, encoding for the 3′-phosphoadenosine-5′-phosphosulfate synthetase 2, have been identified [40,73]. PAPSS2 impairment causes reduced intracellular synthesis of PAPS leading to reduced macromolecular sulfation. SMED Pakistani type has been defined in OMIM as *Brachyolmia type 4* (BCYM4, MIM 612847), even if this name is obsolete and rarely used. Compound heterozygous mutations in *PAPSS2* have been identified in a girl with alteration of steroid metabolism as demonstrated by premature pubarche, hyperandrogenic anovulation, very low dehydroepiandrosterone sulfate ester (DHEAS) levels, and increased androgen levels [42]. This phenotype can be explained by the observation that PAPS is the sulfate donor not only for macromolecular sulfation, but also for steroid hormones as androgens. Indeed PAPS is required for the conversion of the androgen hormone precursor, dehydroepiandrosterone (DHEA), to its inactive sulfate ester (DHEAS), reducing its conversion to an active androgen. Interestingly, the bone phenotype does not present long bone epiphyseal or metaphyseal changes demonstrating that it is milder in this patient compared to SEMD Pakistani type.

Brachyolmia type 1 including *Hobaek* and *Toledo forms* (BCYM1A and 1B, MIM 271530 and 271630, respectively) is characterised by short trunk, platyspondyly, irregular and narrow intervertebral spaces, scoliosis, precocious calcification of the costal cartilage and in some cases corneal opacities [74]. In the Toledo form of brachyolmia abnormal chondroitin sulfation has been described as demonstrated by chondroitin sulfate (CS) undersulfation in urine [74] and low activity of PAPS-chondroitin sulfate sulfotransferase in serum [75]. In 2012, *PAPSS2* mutations have been identified in brachyolmia type 1 patients [73], making this disorder allelic to the SEMD Pakistani type. Further studies involving 13 patients from 10 families identified *PAPSS2* mutations in brachyolmia type 1 and confirmed that brachyolmia type 1A, 1B and 4 are indeed the same disorder [76]. Despite PAPS involvement in androgen metabolism, only a minority of these patients showed signs of androgen excess or increased serum DHEA.

Chondrodysplasia with joint dislocations, gPAPP type (MIM 614078) is characterised by short stature, chondrodysplasia with brachydactyly, congenital joint dislocations, micrognathia, cleft palate and facial dysmorphism. It is caused by mutations in the *IMPAD1* gene recently renamed *BPNT2* encoding for gPAPP [56]. BPNT2 impairment reduces the hydrolysis of PAP, the by-product of the sulfotransferase reactions, leading to its accumulation in the Golgi and to the inhibition of sulfotransferase reactions via negative feedback. The final consequence of BPNT2 impairment is the undersulfation of macromolecules. Unfortunately, cells or cartilage biopsies from patients were not available, but through a gene trap approach two *Impad1* knock-out mice have been generated and are characterised by severe dwarfism, skeletal defects and abnormal joint formation. Even if they showed a perinatal lethal phenotype, the impaired CS and heparan sulfate (HS) proteoglycan sulfation confirmed that this condition is associated with defective synthesis of sulfated PGs. [57,58]. The overlapping features of chondrodysplasia with joint dislocations, gPAPP type with Catel-Manzke syndrome and

Desbuquois dysplasia type 1, other skeletal dysplasias caused by altered PG synthesis [12], represent the complexity of specifically identify the different conditions in patients. For instance, *BPNT2* gene mutations have been detected in two patients previously described as Catel-Manzke syndrome [77].

3.2. Skeletal Dysplasias Linked to Proteins Involved in GAG Sulfation

Spondyloepiphyseal dysplasia with congenital joint dislocations, CHST3 type (SEDCJD, MIM 143095), also named *recessive Larsen syndrome*, is due to biallelic variants in the *CHST3* gene, encoding for carbohydrate sulfotransferase-3, also known as chondroitin 6-sulfotransferase 1 (C6ST-1). Individuals with CHST3 deficiency have dislocation of the knees and/or hips at birth, clubfoot, elbow joint dysplasia with subluxation and limited extension, short stature, and progressive kyphosis developing in late childhood with marked flattening of intervertebral spaces [78]. Since patients affected by this disorder show knee dislocations at birth, the disorder is initially recognised as *Larsen syndrome* (MIM 245600). During childhood, features of spondyloepiphyseal dysplasia become more apparent and the dislocations improve, both spontaneously and with surgical treatment, causing arthritis of the hips and spine with intervertebral disc degeneration, rigid kyphoscoliosis and trunk shortening by late childhood. At this stage, the clinical features are those previously identified as the *Spondyloepiphyseal dysplasia, Omani type* [79]. In conclusion disorders previously designated as *Spondyloepiphyseal dysplasia, Omani type*, *Humerospinal dysostosis* and *recessive Larsen syndrome* represent different age-related descriptions of the same condition. The clinical spectrum underlies the wide mutational spectrum in the *CHST3* gene [78–82]; the gene defects lead to functional impairment of C6ST1 that catalyzes sulfate transfer from PAPS to C6 of N-acetylgalactosamine (GalNAc) residues. This biochemical defect is confirmed by the almost complete depletion of 6-O-sulfated GalNAc residues in CS chains from patients' fibroblasts and urine [79–81]. In some patients, cardiac involvement with systolic murmur, and mitral, tricuspid and aortic regurgitation has been reported [82–84]. This issue has not been well studied, but it seems likely that involvement of the cardiac connective tissue may be a genuine, if not constant, feature of CHST3 deficiency, and more attention should be payed to this aspect in the future.

Ehlers-Danlos syndrome (EDS) musculocontractural type 1 (EDSMC1, MIM 601776), formerly *EDS type VIB* or *adducted thumb-clubfoot syndrome,* include distinctive craniofacial dysmorphism, congenital contractures of thumbs and fingers, clubfeet, severe kyphoscoliosis, muscular hypotonia, hyperextensible thin skin with easy bruisability and atrophic scarring, wrinkled palms, joint hypermobility, atrial septal defects and ocular involvement [85,86]. The causative gene of this disorder is *CHST14* encoding for carbohydrate sulfotransferase-14 (also named dermatan-4-sulfotransferase-1, D4ST1), that catalyzes the 4-O-sulfation of GalNAc residues in dermatan sulfate (DS) [85–87]. In patients' fibroblasts, reduced 4-O-sulfation in GalNAc residues of DS chains, decreased DS and increased CS chain synthesis was demonstrated. The CS increased synthesis is due to the conversion of DS to CS, since the lack of 4-O-sulfation in GalNAc residues allows the reverse epimerization of iduronic acid present in DS chains into glucuronic acid [87]. Thus, decorin DS chains are completely replaced by CS chains leading to reduction of GAG chain flexibility, that in turn affects collagen fibril assembly [88,89]. The presence of congenital contractures in a disorder called "Ehlers-Danlos syndrome" appears to be inappropriate, but the important role of PGs in the development of the skeletal-muscular function unit may account for the phenotype.

Osteochondrodysplasia, brachydactyly and overlapping malformed digits (OCBMD, MIM 618167) has been recently described in a Pakistani family and it is characterised by bilateral and symmetrical skeletal defects affecting mainly the limbs and by hand and foot malformations such as short and adducted thumbs, overriding fingers and broad halluces. Moreover, scoliosis, dislocated patellae and fibulae, pectus excavatum and mild osteoarthritis have been reported. In this family a deletion in the *CHST11* gene encoding for carbohydrate sulfotransferase 11 has been detected [90]. The enzyme also known as chondroitin-4-sulfotrasferase 1 (C4ST1) is a Golgi sulfotransferase responsible for sulfate transfer to C4 of the GalNAc residues in CS chain. Three years earlier, a deletion spanning exon 2 of *CHST11* gene and embedded microRNA MIR3922 was reported in a woman with short stature,

brachydactyly with disproportionately short index finger and congenital malformations of hand and feet digits and malignant lymphoproliferative disease [91]. Since combined skeletal phenotype and lymphoproliferative diseases are rare, the involvement in tumour progression of CHST11 is not clear, but it is likely that concomitant loss of MIR3922 or additional genetic and environmental factors may be required [91]. The *Chst11* knock-out mouse confirms the involvement of *CHST11* gene in the chondrodysplasia phenotype [92]. Indeed, homozygous mutant mice die within hours after birth and show severe chondrodysplasia restricted to endochondral bones. Detailed analysis of the cartilage growth plate demonstrated that loss of C4st1 disturbs the balance of CS and causes abnormal CS localization leading to robust up-regulation of transforming growth factor β (TGF-β) signalling with concomitant down-regulation of bone morphogenetic protein (BMP) signalling. These defects result in abnormal chondrocyte differentiation and orientation within the growth plate causing severe disturbances in growth plate morphogenesis [92].

The skeletal disorders which have been discussed in this session are summarized in Table 1.

Table 1. Skeletal dysplasias caused by defects in sulfate metabolism.

Pathology	MIM/Inheritance	Causative Gene	Protein Product and Function	Biochemical Phenotype	References
Achondrogenesis type 1B (ACG1B)	600972/AR	*SLC26A2*	Sulfate/chloride antiporter present on cell membrane.	Severe cartilage PG undersulfation; reduced sulfate uptake in fibroblasts.	[60,65,66,71,93]
Atelosteogenesis type 2 (AO2)	256050/AR	*SLC26A2*	Sulfate/chloride antiporter present on cell membrane.	Severe cartilage PG undersulfation; reduced sulfate uptake in fibroblasts.	[60,65,66,94]
Diastrophic dysplasia (DTD)	222600/AR	*SLC26A2*	Sulfate/chloride antiporter present on cell membrane.	Cartilage PG undersulfation; reduced sulfate uptake in fibroblasts; in mice altered sulfate uptake in chondrocytes, and osteoblasts; altered Ihh signaling; reduced chondrocytes proliferation.	[34,60,65–70]
Recessive multiple epiphyseal dysplasia (EDM4)	226900/AR	*SLC26A2*	Sulfate/chloride antiporter present on cell membrane.	Reduced sulfate uptake.	[60,65,95]
Spondyloepimetaphyseal dysplasia, SEMD, Pakistani type or Brachyolmia type 4 (BCYM4)	612847/AR	*PAPSS2*	PAPS synthetase 2, enzyme that synthesizes the universal sulfate donor (PAPS).	Macromolecular undersulfation; signs of androgen excess (in a minority of patients); very low DHEAS levels and increased androgen levels (in one patient).	[40,42,72,73,76]
Brachyolmia type 1 (includes Hobaek form and Toledo form, BCYM1A and 1B respectively)	271530/AR 271630/AR	*PAPSS2*	PAPS synthetase 2, enzyme that synthesizes the universal sulfate donor (PAPS).	Undersulfation of CS; low activity of PAPS-CS sulfotransferase; signs of androgen excess (in a minority of patients).	[73–76]
Chondrodysplasia with joint dislocations, gPAPP type	614078/AR	*BPNT2*	Golgi resident PAP phosphatase, enzyme that hydrolyzes PAP to AMP and phosphate.	In mice impaired CS and HS sulfation.	[56–58,77]
Spondyloepiphyseal dysplasia with congenital joint dislocations (SEDCJD or SED Omani type)	143095/AR	*CHST3*	Carbohydrate sulfotransferase-3, enzyme that transfers sulfate to GalNAc residues of CS.	Depletion of 6-O-sulfated GalNAc residues in CS chains in fibroblasts and urine.	[78–84]

Table 1. *Cont.*

Pathology	MIM/Inheritance	Causative Gene	Protein Product and Function	Biochemical Phenotype	References
Ehlers-Danlos syndrome musculocontractural type 1 (EDSMC1)	601776/AR	*CHST14*	Carbohydrate sulfotransferase-14, enzyme that transfers sulfate to GalNAc residues of DS.	Reduction of 4-O-sulfation in GalNAc residues in DS chains; decrease of DS and increase of CS chain synthesis.	[85–89]
Osteochondrodysplasia, brachydactyly and overlapping malformed digits (OCBMD)	618167/AR	*CHST11*	Carbohydrate sulfotransferase-11, enzyme that transfers sulfate to GalNAc residues of CS.	In mice abnormal CS localization; strong up-regulation of TGF-β signaling and down-regulation of BMP signaling; altered morphology of the growth plate.	[90–92]

4. Alterations of Extracellular Matrix and Cell Homeostasis Due to Defects in PG Sulfation

PGs are fundamental components of ECMs and affect the biochemical, physical, and mechanical properties of tissues. In particular, PGs are the most abundant ECM proteins in cartilage and they play a pivotal role in the maintenance of cartilage homeostasis. Recent studies underline how altered PG synthesis affects cartilage structure and development, leading to disorders that primarily affect the skeleton [12].

Defects in the metabolism of sulfate and mutations in genes encoding for enzymes and transporters involved in the sulfate activation pathway or in sulfotransferase reactions cause altered PG sulfation, affecting PG synthesis and the cartilage ECM properties. The first evidence of impaired sulfate metabolism due to reduced sulfate uptake, decreased PAPS synthesis, or reduced sulfotransferase activity is the synthesis of undersulfated PGs. This condition may affect cartilage homeostasis at different levels impairing the synthesis of whole GAG chains, altering the ECM structure, or the cell behavior.

In DS biosynthesis, the 4-O-sulfation of GalNAc residue is important to prevent the reconversion of DS chain in CS. CHST14 sulfotransferase impairment reduces the sulfation of GAG chains leading to GAG biosynthetic defects as demonstrated by the complete replacement of DS chain with CS on decorin core protein in fibroblasts from patients affected by EDSMC1 [86–88].

In the extracellular environment, PGs are fundamental for interactions with ions, small molecules and proteins and for the organisation of the complex ECM network. For instance, the flexible DS chain of decorin and biglycan allows the correct formation of collagen fibres. TEM analysis of a healthy skin sample shows that the majority of GAG chains are curved and in close contact with the outer of collagen fibres. Conversely, in skin biopsies of patients affected by EDSMC1, collagen fibres are dispersed and GAG chains appear to be straight since DS is converted to CS [86,88,89]. In the bone trabeculae of the animal model of diastrophic dysplasia, the dtd mouse, collagen fibres present a smaller diameter and are less organised in the matrix compared with wild type animals. The undersulfation of CS-PGs, due to impairment of SLC26A2 transporter, could cause defects in collagen fibres organisation leading to an altered bone matrix [96].

PGs in ECM and on the cell membrane interact also with signalling molecules through the high negative charge of their GAG chains. Among GAGs, HS is mainly present on the cell surface and it works as co-receptor binding growth factors and making them closer to their receptors. On the other hand, CS in the ECM binds growth factors protecting them from proteases and regulating their diffusion in the matrix. For instance, Ihh signalling, a fundamental pathway for cartilage development, relies on sulfated PGs for its activity as confirmed by the altered Ihh distribution in cartilage ECM of animal models with *PAPPS2* and *SLC26A2* mutations, that causes reduced chondrocyte proliferation [68,97]. Moreover, alteration in Ihh distribution and expression of its downstream targets has been observed also in the *Impad1* knock-out mouse confirming the important link between sulfated PGs and Ihh [58].

Defects in PG sulfation disrupt not only Ihh signalling, but may perturb also other signalling pathways important for regulation of chondrocyte proliferation and differentiation. The downstream effector of BMP signalling is reduced, while the TGF-β effector is increased in growth plate chondrocytes of *Chst11* knock-out mice demonstrating an altered balance between the BMP and TGF-β pathway when PG sulfation is impaired [92].

5. Conclusions and Perspectives

Over the last few years, there have been significant advances in the skeletal dysplasia field leading to the identification of the underlying genetic defects in more than 400 different skeletal disorders [15]. The above synopsis highlights the complexity of skeletal defects caused by mutations in genes encoding for enzymes and transporters involved in sulfate metabolism. Progress in this field has been allowed by next-generation genomic technologies, that are a first-line diagnostic resource. In this complex scenario, patient derived biopsies, cell cultures, and animal models are fundamental to investigate the pathogenesis and to analyze new aspects of the role of GAG in connective tissue biology.

Despite the great step forward in the identification of causative genes, genotype-phenotype correlations are lacking and we are still far from a comprehensive view of the disease molecular mechanisms. First, it is unclear how the tissue specificity and the redundancy of genes can determine the phenotype. Defects in PG sulfation mainly affect cartilage and bone, but other tissues can be involved as cardiac tissue in SEDCJD [82,84] or lymphoid tissue leading to tumour progression in OCBMD [91]. The involvement of different tissues and its implications on the disease phenotype should be carefully studied in the future. Moreover, mutations in different genes cause skeletal dysplasias with overlapping features that may be wrongly diagnosed as occurs in condrodysplasia with joint dislocation, gPAPP type, Catel-Manzke syndrome and Desbuquois dysplasia type 1. Nowadays we cannot provide a full explanation why some classes of sulfated PGs are more affected by enzyme deficiency than others. Even if the GAGs role depends on their physicochemical properties, it is difficult to molecularly dissect the function of sulfated GAGs when they interact in the complex ECM network. Lastly, the variability in the clinical phenotypes caused by mutations in the same gene suggests that also environmental and epigenetic factors might play a role.

A deep understanding of the molecular mechanisms of these disorders is crucial to ultimately pave the way for innovative therapies. Recently, significant advances in the development of therapeutic approaches for some disorders have been achieved with the aim of alleviating, preventing or modifying the disease progression [70,98–101]. This progress has been made thank to deep phenotyping of in vitro and/or in vivo models that has allowed the identification of new molecules or already existing ones through a drug repositioning approach. Moreover, molecular studies in different disorders could lead to the identification of common pathogenic mechanisms resulting in common therapeutic strategies that might be targeted to a range of individual phenotypes.

Author Contributions: C.P., C.G.T., A.S.-F., and A.R. analyzed the literature and co-wrote the review. C.G.T. prepared the figures. All authors have read and agreed to the published version of the manuscript.

Funding: This work was supported by the European Community's Seventh Framework Program under grant agreement n. 602300 (SYBIL), MIUR "Progetti di ricerca di rilevante interesse nazionale" (PRIN 2015F3JHMB) and MIUR "Dipartimenti di Eccellenza 2018–2022".

Conflicts of Interest: The authors declare no conflicts of interest.

Abbreviations

ACG1B	achondrogenesis type 1B
AO2	atelosteogenesis type 2
APS	adenosine 5′-phosphosulfate
BCYM1A	brachyolmia type 1 Hobaek form
BCYM1B	brachyolmia type 1 Toledo form
BCYM4	brachyolmia type 4
BPNT2	3′(2′) 5′-bisphosphate nucleotidase 2
C4ST	chondroitin-4-O-sulfotransferase
C6ST	chondroitin-6-O-sulfotransferase
CS	chondroitin sulfate
D4ST	dermatan-4-O-sulfotransferase
DHEA	dehydroepiandrosterone
DHEAS	dehydroepiandrosterone sulfate ester
DS	dermatan sulfate
DTD	diastrophic dysplasia
DTDST	diastrophic dysplasia sulfate transporter
ECM	extracellular matrix
EDM4	recessive multiple epiphyseal dysplasia
EDSMC1	Ehlers-Danlos syndrome musculocontractural type 1
GAG	glycosaminoglycan
GalNAc	N-acetylgalactosamine
gPAPP	Golgi resident phosphoadenosine phosphate phosphatase
HS	heparan sulfate
IMPAD1	inositol monophosphatase domain-containing protein 1
OCBMD	osteochondrodysplasia brachydactyly and overlapping malformed digits
PAP	phosphoadenosine phosphate
PAPS	3′-phosphoadenosine 5′-phosphosulfate
PAPSS	PAPS synthetase
PAPST	PAPS transporter
PG	proteoglycan
SEDCJD	spondyloepiphyseal dysplasia with congenital joint dislocations
ST	carbohydrate sulfotransferase
SULT	cytosolic sulfotransferase
TPST	tyrosylprotein sulfotransferase

References

1. Iozzo, R.V. Matrix proteoglycans: From molecular design to cellular function. *Annu. Rev. Biochem.* **1998**, *67*, 609–652. [CrossRef] [PubMed]
2. Honke, K.; Taniguchi, N. Sulfotransferases and sulfated oligosaccharides. *Med. Res. Rev.* **2002**, *22*, 637–654. [CrossRef] [PubMed]
3. Bowman, K.G.; Bertozzi, C.R. Carbohydrate sulfotransferases: Mediators of extracellular communication. *Chem. Biol.* **1999**, *6*, R9–R22. [CrossRef]
4. Gallagher, J.T. Heparan sulphates as membrane receptors for the fibroblast growth factors. *Eur. J. Clin. Chem. Clin. Biochem.* **1994**, *32*, 239–247.
5. Pacifici, G.M. Sulfation of drugs and hormones in mid-gestation human fetus. *Early Hum. Dev.* **2005**, *81*, 573–581. [CrossRef]
6. Farooqui, A.A.; Horrocks, L.A. On the role of sulfolipids in mammalian metabolism. *Mol. Cell. Biochem.* **1985**, *66*, 87–95. [CrossRef]
7. Stone, M.J.; Chuang, S.; Hou, X.; Shoham, M.; Zhu, J.Z. Tyrosine sulfation: An increasingly recognised post-translational modification of secreted proteins. *Nat. Biotechnol.* **2009**, *25*, 299–317. [CrossRef]

8. Richard, K.; Hume, R.; Kaptein, E.; Stanley, E.L.; Visser, T.J.; Coughtrie, M.W. Sulfation of thyroid hormone and dopamine during human development: Ontogeny of phenol sulfotransferases and arylsulfatase in liver, lung, and brain. *J. Clin. Endocrinol. Metab.* **2001**, *86*, 2734–2742. [CrossRef]
9. Aksoy, I.A.; Otterness, D.M.; Weinshilboum, R.M. Cholesterol sulfation in human liver. Catalysis by dehydroepiandrosterone sulfotransferase. *Drug Metab. Dispos.* **1993**, *21*, 268–276.
10. Alnouti, Y. Bile Acid sulfation: A pathway of bile acid elimination and detoxification. *Toxicol. Sci.* **2009**, *108*, 225–246. [CrossRef]
11. Falany, C.N.; Wheeler, J.; Oh, T.S.; Falany, J.L. Steroid sulfation by expressed human cytosolic sulfotransferases. *J. Steroid Biochem. Mol. Biol.* **1994**, *48*, 369–375. [CrossRef]
12. Paganini, C.; Costantini, R.; Superti-Furga, A.; Rossi, A. Bone and connective tissue disorders caused by defects in glycosaminoglycan biosynthesis: A panoramic view. *FEBS J.* **2019**, *286*, 3008–3032. [CrossRef]
13. Krakow, D.; Rimoin, D.L. The skeletal dysplasias. *Genet. Med.* **2010**, *12*, 327–341. [CrossRef]
14. Geister, K.A.; Camper, S.A. Advances in Skeletal Dysplasia Genetics. *Annu. Rev. Genom. Hum. Genet.* **2015**, *16*, 199–227. [CrossRef]
15. Mortier, G.R.; Cohn, D.H.; Cormier-Daire, V.; Hall, C.; Krakow, D.; Mundlos, S.; Nishimura, G.; Robertson, S.; Sangiorgi, L.; Savarirayan, R.; et al. Nosology and classification of genetic skeletal disorders: 2019 revision. *Am. J. Med. Genet. A* **2019**, *179*, 2393–2419. [CrossRef]
16. Klaassen, C.D.; Boles, J.W. Sulfation and sulfotransferases 5: The importance of 3′- phosphoadenosine 5′-phosphosulfate (PAPS) in the regulation of sulfation. *FASEB J.* **1997**, *11*, 404–418. [CrossRef]
17. Leyh, T.S. The physical biochemistry and molecular genetics of sulfate activation. *Crit. Rev. Biochem. Mol. Biol.* **1993**, *28*, 515–542. [CrossRef]
18. Lipmann, F. Biological sulfate activation and transfer. *Science* **1958**, *128*, 575–580. [CrossRef]
19. Farooqui, A.A. 3′-phosphoadenosine 5′-phosphosulphate metabolism in mammalian tissues. *Int. J. Biochem.* **1980**, *12*, 529–536. [CrossRef]
20. Venkatachalam, K.V. Human 3′-phosphoadenosine 5′-phosphosulfate (PAPS) synthase: Biochemistry, molecular biology and genetic deficiency. *Iubmb Life* **2003**, *55*, 1–11. [CrossRef]
21. Langford, R.; Hurrion, E.; Dawson, P.A. Genetics and pathophysiology of mammalian sulfate biology. *J. Genet. Genom.* **2017**, *44*, 7–20. [CrossRef]
22. Dawson, P.A. Sulfate in fetal development. *Semin. Cell Dev. Biol.* **2011**, *22*, 653–659. [CrossRef]
23. Dawson, P.A.; Richard, K.; Perkins, A.; Zhang, Z.; Simmons, D.G. Review: Nutrient sulfate supply from mother to fetus: Placental adaptive responses during human and animal gestation. *Placenta* **2017**, *54*, 45–51. [CrossRef]
24. Cole, D.E.; Scriver, C.R. Age-dependent serum sulfate levels in children and adolescents. *Clin. Chim. Acta* **1980**, *107*, 135–139. [CrossRef]
25. Cole, D.E.; Baldwin, L.S.; Stirk, L.J. Increased serum sulfate in pregnancy: Relationship to gestational age. *Clin. Chem.* **1985**, *31*, 866–867. [CrossRef]
26. Bradley, H.; Gough, A.; Sokhi, R.S.; Hassell, A.; Waring, R.; Emery, P. Sulfate metabolism is abnormal in patients with rheumatoid arthritis. Confirmation by in vivo biochemical findings. *J. Rheumatol.* **1994**, *21*, 1192–1196.
27. Jennings, M.L. Proton fluxes associated with erythrocyte membrane anion exchange. *J. Membr. Biol.* **1976**, *28*, 187–205. [CrossRef]
28. Lötscher, M.; Custer, M.; Quabius, E.S.; Kaissling, B.; Murer, H.; Biber, J. Immunolocalization of Na/SO4-cotransport (NaSi-1) in rat kidney. *Pflug. Arch.* **1996**, *432*, 373–378. [CrossRef]
29. Simmons, D.G.; Rakoczy, J.; Jefferis, J.; Lourie, R.; McIntyre, H.D.; Dawson, P.A. Human placental sulfate transporter mRNA profiling from term pregnancies identifies abundant SLC13A4 in syncytiotrophoblasts and SLC26A2 in cytotrophoblasts. *Placenta* **2013**, *34*, 381–384. [CrossRef]
30. Dawson, P.A.; Markovich, D. Pathogenetics of the human SLC26 transporters. *Curr. Med. Chem.* **2005**, *12*, 385–396. [CrossRef]
31. Alper, S.L.; Sharma, A.K. The SLC26 gene family of anion transporters and channels. *Mol. Asp. Med.* **2013**, *34*, 494–515. [CrossRef]
32. Markovich, D. Na+-sulfate cotransporter SLC13A1. *Pflug. Arch.* **2014**, *466*, 131–137. [CrossRef]
33. Zhang, Z.; Aung, Z.T.; Simmons, D.G.; Dawson, P.A. Molecular analysis of sequence and splice variants of the human SLC13A4 sulfate transporter. *Mol. Genet. Metab.* **2017**, *121*, 35–42. [CrossRef]

34. Hästbacka, J.; de la Chapelle, A.; Mahtani, M.M.; Clines, G.; Reeve Daly, M.P.; Daly, M.; Hamilton, B.A.; Kusumi, K.; Trivedi, B.; Weaver, A.; et al. The diastrophic dysplasia gene encodes a novel sulfate transporter: Positional cloning by fine-structure linkage disequilibrium mapping. *Cell* **1994**, *78*, 1073–1087. [CrossRef]
35. Dawson, J.R.; Norbeck, K.; Moldeus, P. The effectiveness of different sulfate precursors in supporting extrahepatic sulfate conjugation. *Biochem. Pharm.* **1983**, *32*, 1789–1791. [CrossRef]
36. Elgavish, A.; Meezan, E. Sulfation by human lung fibroblasts: SO4(2-) and sulfur- containing amino acids as sources for macromolecular sulfation. *Am. J. Physiol.* **1991**, *260*, L450–L456. [CrossRef]
37. Rome, L.H.; Hill, D.F. Lysosomal degradation of glycoproteins and glycosaminoglycans. Efflux and recycling of sulphate and N-acetylhexosamines. *Biochem. J.* **1986**, *235*, 707–713. [CrossRef]
38. Lyle, S.; Stanczak, J.; Ng, K.; Schwartz, N.B. Rat chondrosarcoma ATP sulfurylase and adenosine 5′-phosphosulfate kinase reside on a single bifunctional protein. *Biochemistry* **1994**, *33*, 5920–5925. [CrossRef]
39. Xu, Z.H.; Otterness, D.M.; Freimuth, R.R.; Carlini, E.J.; Wood, T.C.; Mitchell, S.; Moon, E.; Kim, U.J.; Xu, J.P.; Siciliano, M.J.; et al. Human 3′-phosphoadenosine 5′-phosphosulfate synthetase 1 (PAPSS1) and PAPSS2: Gene cloning, characterization and chromosomal localization. *Biochem. Biophys. Res. Commun.* **2000**, *268*, 437–444. [CrossRef]
40. ul Haque, M.F.; King, L.M.; Krakow, D.; Cantor, R.M.; Rusiniak, M.E.; Swank, R.T.; Superti-Furga, A.; Haque, S.; Abbas, H.; Ahmad, W.; et al. Mutations in orthologous genes in human spondyloepimetaphyseal dysplasia and the brachymorphic mouse. *Nat. Genet.* **1998**, *20*, 157–162. [CrossRef]
41. Kurima, K.; Warman, M.L.; Krishnan, S.; Domowicz, M.; Krueger, R.C., Jr.; Deyrup, A.; Schwartz, N.B. A member of a family of sulfate-activating enzymes causes murine brachymorphism. *Proc. Natl. Acad. Sci. USA* **1998**, *95*, 8681–8685, Erratum in **1998**, *95*, 12071. [CrossRef] [PubMed]
42. Noordam, C.; Dhir, V.; McNelis, J.C.; Schlereth, F.; Hanley, N.A.; Krone, N.; Smeitink, J.A.; Smeets, R.; Sweep, F.C.; Claahsen-van der Grinten, H.L.; et al. Inactivating PAPSS2 mutations in a patient with premature pubarche. *N. Engl. J. Med.* **2009**, *360*, 2310–2318. [CrossRef] [PubMed]
43. Strott, C.A. Sulfonation and molecular action. *Endocr. Rev.* **2002**, *23*, 703–732. [CrossRef] [PubMed]
44. Fuda, H.; Shimizu, C.; Lee, Y.C.; Akita, H.; Strott, C.A. Characterization and expression of human bifunctional 3′-phosphoadenosine 5′-phosphosulphate synthase isoforms. *Biochem. J.* **2002**, *365*, 497–504. [CrossRef]
45. Schroder, E.; Gebel, L.; Eremeev, A.A.; Morgner, J.; Grum, D.; Knauer, S.K.; Bayer, P.; Mueller, J.W. Human PAPS Synthase Isoforms Are Dynamically Regulated Enzymes with Access to Nucleus and Cytoplasm. *PLoS ONE* **2012**, *7*, e29559. [CrossRef]
46. Kamiyama, S.; Sasaki, N.; Goda, E.; Ui-Tei, K.; Saigo, K.; Narimatsu, H.; Jigami, Y.; Kannagi, R.; Irimura, T.; Nishihara, S. Molecular cloning and characterization of a novel 3′-phosphoadenosine 5′-phosphosulfate transporter, PAPST2. *J. Biol. Chem.* **2006**, *281*, 10945–10953. [CrossRef]
47. Kamiyama, S.; Suda, T.; Ueda, R.; Suzuki, M.; Okubo, R.; Kikuchi, N.; Chiba, Y.; Goto, S.; Toyoda, H.; Saigo, K.; et al. Molecular cloning and identification of 3′-phosphoadenosine 5′-phosphosulfate transporter. *J. Biol. Chem.* **2003**, *278*, 25958–25963. [CrossRef]
48. Günal, S.; Hardman, R.; Kopriva, S.; Mueller, J.W. Sulfation pathways from red to green. *J. Biol. Chem.* **2019**, *294*, 12293–12312. [CrossRef]
49. Parker, J.L.; Newstead, S. Gateway to the Golgi: Molecular mechanisms of nucleotide sugar transporters. *Curr. Opin. Struct. Biol.* **2019**, *57*, 127–134. [CrossRef]
50. Wiweger, M.I.; Avramut, C.M.; de Andrea, C.E.; Prins, F.A.; Koster, A.J.; Ravelli, R.B.; Hogendoorn, P.C. Cartilage ultrastructure in proteoglycan-deficient zebrafish mutants brings to light new candidate genes for human skeletal disorders. *J. Pathol.* **2011**, *223*, 531–542. [CrossRef]
51. Bojarova, P.; Williams, S.J. Sulfotransferases, sulfatases and formylglycine-generating enzymes: A sulfation fascination. *Curr. Opin. Chem. Biol.* **2008**, *12*, 573–581. [CrossRef]
52. Coughtrie, M.W.H. Function and organization of the human cytosolic sulfotransferase (SULT) family. *Chem. Biol. Interact.* **2016**, *259*, 2–7. [CrossRef]
53. Petrotchenko, E.V.; Pedersen, L.C.; Borchers, C.H.; Tomer, K.B.; Negishi, M. The dimerization motif of cytosolic sulfotransferases. *FEBS Lett.* **2001**, *490*, 39–43. [CrossRef]
54. Hartmann-Fatu, C.; Trusch, F.; Moll, C.N.; Michin, I.; Hassinen, A.; Kellokumpu, S.; Bayer, P. Heterodimers of tyrosylprotein sulfotransferases suggest existence of a higher organization level of transferases in the membrane of the trans-Golgi apparatus. *J. Mol. Biol.* **2015**, *427*, 1404–1412. [CrossRef]

55. Leung, A.W.; Backstrom, I.; Bally, M.B. Sulfonation, an underexploited area: From skeletal development to infectious diseases and cancer. *Oncotarget* **2016**, *7*, 55811–55827. [CrossRef]
56. Vissers, L.E.; Lausch, E.; Unger, S.; Campos-Xavier, A.B.; Gilissen, C.; Rossi, A.; Del Rosario, M.; Venselaar, H.; Knoll, U.; Nampoothiri, S.; et al. Chondrodysplasia and abnormal joint development associated with mutations in IMPAD1, encoding the Golgi-resident nucleotide phosphatase, gPAPP. *Am. J. Hum. Genet.* **2011**, *88*, 608–615. [CrossRef]
57. Frederick, J.P.; Tafari, A.T.; Wu, S.M.; Megosh, L.C.; Chiou, S.T.; Irving, R.P.; York, J.D. A role for a lithium-inhibited Golgi nucleotidase in skeletal development and sulfation. *Proc. Natl. Acad. Sci. USA* **2008**, *105*, 11605–11612. [CrossRef]
58. Sohaskey, M.L.; Yu, J.; Diaz, M.A.; Plaas, A.H.; Harland, R.M. JAWS coordinates chondrogenesis and synovial joint positioning. *Development* **2008**, *135*, 2215–2220. [CrossRef]
59. Diez-Roux, G.; Ballabio, A. Sulfatases and human disease. *Annu. Rev. Genom. Hum. Genet.* **2005**, *6*, 355–379. [CrossRef]
60. Rossi, A.; Superti-Furga, A. Mutations in the diastrophic dysplasia sulfate transporter (DTDST) gene (SLC26A2): 22 Novel mutations, mutation review, associated skeletal phenotypes, and diagnostic relevance. *Hum. Mutat.* **2001**, *17*, 159–171. [CrossRef]
61. De la Chapelle, A.; Maroteaux, P.; Havu, N.; Granroth, G. A rare lethal bone dysplasia with recessive autosomic transmission. *Arch. Fr. Pediatr.* **1972**, *29*, 759–770.
62. McAlister, W.H.; Crane, J.P.; Bucy, R.P.; Craig, R.B. A new neonatal short limbed dwarfism. *Skelet. Radiol.* **1985**, *13*, 271–275. [CrossRef]
63. Bonafe, L.; Hastbacka, J.; de la Chapelle, A.; Campos-Xavier, A.B.; Chiesa, C.; Forlino, A.; Superti-Furga, A.; Rossi, A. A novel mutation in the sulfate transporter gene SLC26A2 (DTDST) specific to the Finnish population causes de la Chapelle dysplasia. *J. Med. Genet.* **2008**, *45*, 827–831. [CrossRef]
64. Rossi, A.; Bonaventure, J.; Delezoide, A.L.; SupertiFurga, A.; Cetta, G. Undersulfation of cartilage proteoglycans ex vivo and increased contribution of amino acid sulfur to sulfation in vitro in McAlister dysplasia atelosteogenesis type 2. *Eur. J. Biochem.* **1997**, *248*, 741–747. [CrossRef]
65. Karniski, L.P. Mutations in the diastrophic dysplasia sulfate transporter (DTDST) gene: Correlation between sulfate transport activity and chondrodysplasia phenotype. *Hum. Mol. Genet.* **2001**, *10*, 1485–1490. [CrossRef]
66. Rossi, A.; Kaitila, I.; Wilcox, W.R.; Rimoin, D.L.; Steinmann, B.; Cetta, G.; Superti-Furga, A. Proteoglycan sulfation in cartilage and cell cultures from patients with sulfate transporter chondrodysplasias: Relationship to clinical severity and indications on the role of intracellular sulfate production. *Matrix Biol.* **1998**, *17*, 361–369. [CrossRef]
67. Forlino, A.; Piazza, R.; Tiveron, C.; Della Torre, S.; Tatangelo, L.; Bonafe, L.; Gualeni, B.; Romano, A.; Pecora, F.; Superti-Furga, A.; et al. A diastrophic dysplasia sulfate transporter (SLC26A2) mutant mouse: Morphological and biochemical characterization of the resulting chondrodysplasia phenotype. *Hum. Mol. Genet.* **2005**, *14*, 859–871. [CrossRef]
68. Gualeni, B.; Facchini, M.; De Leonardis, F.; Tenni, R.; Cetta, G.; Viola, M.; Passi, A.; Superti-Furga, A.; Forlino, A.; Rossi, A. Defective proteoglycan sulfation of the growth plate zones causes reduced chondrocyte proliferation via an altered Indian hedgehog signalling. *Matrix Biol.* **2010**, *29*, 453–460. [CrossRef]
69. De Leonardis, F.; Monti, L.; Gualeni, B.; Tenni, R.; Forlino, A.; Rossi, A. Altered signaling in the G1 phase deregulates chondrocyte growth in a mouse model with proteoglycan undersulfation. *J. Cell. Biochem.* **2014**, *115*, 1779–1786. [CrossRef]
70. Monti, L.; Paganini, C.; Lecci, S.; De Leonardis, F.; Hay, E.; Cohen-Solal, M.; Villani, S.; Superti-Furga, A.; Tenni, R.; Forlino, A.; et al. N-acetylcysteine treatment ameliorates the skeletal phenotype of a mouse model of diastrophic dysplasia. *Hum. Mol. Genet.* **2015**, *24*, 5570–5580. [CrossRef]
71. Zheng, C.; Lin, X.; Xu, X.; Wang, C.; Zhou, J.; Gao, B.; Fan, J.; Lu, W.; Hu, Y.; Jie, Q.; et al. Suppressing UPR-dependent overactivation of FGFR3 signaling ameliorates SLC26A2-deficient chondrodysplasias. *EBioMedicine* **2019**, *40*, 695–709. [CrossRef] [PubMed]
72. Ahmad, M.; Haque, M.F.; Ahmad, W.; Abbas, H.; Haque, S.; Krakow, D.; Rimoin, D.L.; Lachman, R.S.; Cohn, D.H. Distinct, autosomal recessive form of spondyloepimetaphyseal dysplasia segregating in an inbred Pakistani kindred. *Am. J. Med. Genet.* **1998**, *78*, 468–473. [CrossRef]

73. Miyake, N.; Elcioglu, N.H.; Iida, A.; Isguven, P.; Dai, J.; Murakami, N.; Takamura, K.; Cho, T.J.; Kim, O.H.; Hasegawa, T.; et al. PAPSS2 mutations cause autosomal recessive brachyolmia. *J. Med. Genet.* **2012**, *49*, 533–538. [CrossRef] [PubMed]
74. Toledo, S.P.; Mourao, P.A.; Lamego, C.; Alves, C.A.; Dietrich, C.P.; Assis, L.M.; Mattar, E. Recessively inherited, late onset spondylar dysplasia and peripheral corneal opacity with anomalies in urinary mucopolysaccharides: A possible error of chondroitin-6-sulfate synthesis. *Am. J. Med. Genet.* **1978**, *2*, 385–395. [CrossRef] [PubMed]
75. Mourao, P.A.; Kato, S.; Donnelly, P.V. Spondyloepiphyseal dysplasia, chondroitin sulfate type: A possible defect of PAPS–chondroitin sulfate sulfotransferase in humans. *Biochem. Biophys. Res. Commun.* **1981**, *98*, 388–396. [CrossRef]
76. Iida, A.; Simsek-Kiper, P.O.; Mizumoto, S.; Hoshino, T.; Elcioglu, N.; Horemuzova, E.; Geiberger, S.; Yesil, G.; Kayserili, H.; Utine, G.E.; et al. Clinical and radiographic features of the autosomal recessive form of brachyolmia caused by PAPSS2 mutations. *Hum. Mutat.* **2013**, *34*, 1381–1386. [CrossRef]
77. Nizon, M.; Alanay, Y.; Tuysuz, B.; Kiper, P.O.; Genevieve, D.; Sillence, D.; Huber, C.; Munnich, A.; Cormier-Daire, V. IMPAD1 mutations in two Catel-Manzke like patients. *Am. J. Med. Genet. A* **2012**, *158A*, 2183–2187. [CrossRef]
78. Unger, S.; Lausch, E.; Rossi, A.; Megarbane, A.; Sillence, D.; Alcausin, M.; Aytes, A.; Mendoza-Londono, R.; Nampoothiri, S.; Afroze, B.; et al. Phenotypic features of carbohydrate sulfotransferase 3 (CHST3) deficiency in 24 patients: Congenital dislocations and vertebral changes as principal diagnostic features. *Am. J. Med. Genet. A* **2010**, *152A*, 2543–2549. [CrossRef]
79. Thiele, H.; Sakano, M.; Kitagawa, H.; Sugahara, K.; Rajab, A.; Hohne, W.; Ritter, H.; Leschik, G.; Nurnberg, P.; Mundlos, S. Loss of chondroitin 6-O-sulfotransferase-1 function results in severe human chondrodysplasia with progressive spinal involvement. *Proc. Natl. Acad. Sci. USA* **2004**, *101*, 10155–10160. [CrossRef]
80. Hermanns, P.; Unger, S.; Rossi, A.; Perez-Aytes, A.; Cortina, H.; Bonafe, L.; Boccone, L.; Setzu, V.; Dutoit, M.; Sangiorgi, L.; et al. Congenital joint dislocations caused by carbohydrate sulfotransferase 3 deficiency in recessive Larsen syndrome and humero-spinal dysostosis. *Am. J. Hum. Genet.* **2008**, *82*, 1368–1374. [CrossRef]
81. van Roij, M.H.; Mizumoto, S.; Yamada, S.; Morgan, T.; Tan-Sindhunata, M.B.; Meijers-Heijboer, H.; Verbeke, J.I.; Markie, D.; Sugahara, K.; Robertson, S.P. Spondyloepiphyseal dysplasia, Omani type: Further definition of the phenotype. *Am. J. Med. Genet. A* **2008**, *146A*, 2376–2384. [CrossRef] [PubMed]
82. Tuysuz, B.; Mizumoto, S.; Sugahara, K.; Celebi, A.; Mundlos, S.; Turkmen, S. Omani-type spondyloepiphyseal dysplasia with cardiac involvement caused by a missense mutation in CHST3. *Clin. Genet.* **2009**, *75*, 375–383. [CrossRef] [PubMed]
83. Kozlowski, K.S.; Celermajer, J.M.; Tink, A.R. Humero-spinal dysostosis with congenital heart disease. *Am. J. Dis. Child.* **1974**, *127*, 407–410. [CrossRef] [PubMed]
84. Hall, B.D. Humero-spinal dysostosis: Report of the fourth case with emphasis on generalized skeletal involvement, abnormal craniofacial features, and mitral valve thickening. *J. Pediatr. Orthop. B* **1997**, *6*, 11–14. [CrossRef] [PubMed]
85. Malfait, F.; Syx, D.; Vlummens, P.; Symoens, S.; Nampoothiri, S.; Hermanns-Le, T.; Van Laer, L.; De Paepe, A. Musculocontractural Ehlers-Danlos Syndrome (former EDS type VIB) and adducted thumb clubfoot syndrome (ATCS) represent a single clinical entity caused by mutations in the dermatan-4-sulfotransferase 1 encoding CHST14 gene. *Hum. Mutat.* **2010**, *31*, 1233–1239. [CrossRef]
86. Janecke, A.R.; Li, B.; Boehm, M.; Krabichler, B.; Rohrbach, M.; Muller, T.; Fuchs, I.; Golas, G.; Katagiri, Y.; Ziegler, S.G.; et al. The phenotype of the musculocontractural type of Ehlers-Danlos syndrome due to CHST14 mutations. *Am. J. Med. Genet. A* **2016**, *170*, 103–115. [CrossRef]
87. Dundar, M.; Muller, T.; Zhang, Q.; Pan, J.; Steinmann, B.; Vodopiutz, J.; Gruber, R.; Sonoda, T.; Krabichler, B.; Utermann, G.; et al. Loss of dermatan-4-sulfotransferase 1 function results in adducted thumb-clubfoot syndrome. *Am. J. Hum. Genet.* **2009**, *85*, 873–882. [CrossRef]
88. Miyake, N.; Kosho, T.; Mizumoto, S.; Furuichi, T.; Hatamochi, A.; Nagashima, Y.; Arai, E.; Takahashi, K.; Kawamura, R.; Wakui, K.; et al. Loss-of-function mutations of CHST14 in a new type of Ehlers-Danlos syndrome. *Hum. Mutat.* **2010**, *31*, 966–974. [CrossRef]

89. Hirose, T.; Takahashi, N.; Tangkawattana, P.; Minaguchi, J.; Mizumoto, S.; Yamada, S.; Miyake, N.; Hayashi, S.; Hatamochi, A.; Nakayama, J.; et al. Structural alteration of glycosaminoglycan side chains and spatial disorganization of collagen networks in the skin of patients with mcEDS-CHST14. *Biochim. Biophys. Acta Gen. Subj.* **2018**. [CrossRef]
90. Shabbir, R.M.K.; Nalbant, G.; Ahmad, N.; Malik, S.; Tolun, A. Homozygous *CHST11* mutation in chondrodysplasia, brachydactyly, overriding digits, clino-symphalangism and synpolydactyly. *J. Med. Genet.* **2018**, *55*, 489–496. [CrossRef]
91. Chopra, S.S.; Leshchiner, I.; Duzkale, H.; McLaughlin, H.; Giovanni, M.; Zhang, C.; Stitziel, N.; Fingeroth, J.; Joyce, R.M.; Lebo, M.; et al. Inherited CHST11/MIR3922 deletion is associated with a novel recessive syndrome presenting with skeletal malformation and malignant lymphoproliferative disease. *Mol. Genet. Genom. Med.* **2015**, *3*, 413–423. [CrossRef] [PubMed]
92. Kluppel, M.; Wight, T.N.; Chan, C.; Hinek, A.; Wrana, J.L. Maintenance of chondroitin sulfation balance by chondroitin-4-sulfotransferase 1 is required for chondrocyte development and growth factor signaling during cartilage morphogenesis. *Development* **2005**, *132*, 3989–4003. [CrossRef] [PubMed]
93. SupertiFurga, A.; Hastbacka, J.; Wilcox, W.R.; Cohn, D.H.; vanderHarten, H.J.; Rossi, A.; Blau, N.; Rimoin, D.L.; Steinmann, B.; Lander, E.S.; et al. Achondrogenesis type IB is caused by mutations in the diastrophic dysplasia sulphate transporter gene. *Nat. Genet.* **1996**, *12*, 100–102. [CrossRef] [PubMed]
94. Hästbacka, J.; Superti-Furga, A.; Wilcox, W.R.; Rimoin, D.L.; Cohn, D.H.; Lander, E.S. Atelosteogenesis type II is caused by mutations in the diastrophic dysplasia sulfate-transporter gene (DTDST): Evidence for a phenotypic series involving three chondrodysplasias. *Am. J. Hum. Genet.* **1996**, *58*, 255–262.
95. Superti-Furga, A.; Neumann, L.; Riebel, T.; Eich, G.; Steinmann, B.; Spranger, J.; Kunze, J. Recessively inherited multiple epiphyseal dysplasia with normal stature, club foot, and double layered patella caused by a DTDST mutation. *J. Med. Genet.* **1999**, *36*, 621–624.
96. Gualeni, B.; de Vernejoul, M.C.; Marty-Morieux, C.; De Leonardis, F.; Franchi, M.; Monti, L.; Forlino, A.; Houillier, P.; Rossi, A.; Geoffroy, V. Alteration of proteoglycan sulfation affects bone growth and remodeling. *Bone* **2013**, *54*, 83–91. [CrossRef]
97. Cortes, M.; Baria, A.T.; Schwartz, N.B. Sulfation of chondroitin sulfate proteoglycans is necessary for proper Indian hedgehog signaling in the developing growth plate. *Development* **2009**, *136*, 1697–1706. [CrossRef]
98. Besio, R.; Antonella, F. Treatment options for osteogenesis imperfecta. *Expert Opin. Orphan Drugs* **2015**, *3*, 165–181. [CrossRef]
99. Briggs, M.D.; Bell, P.A.; Wright, M.J.; Pirog, K.A. New therapeutic targets in rare genetic skeletal diseases. *Expert Opin. Orphan Drugs* **2015**, *3*, 1137–1154. [CrossRef]
100. Ornitz, D.M.; Legeai-Mallet, L. Achondroplasia: Development, pathogenesis, and therapy. *Dev. Dyn.* **2017**, *246*, 291–309. [CrossRef]
101. Marzin, P.; Cormier-Daire, V. New perspectives on the treatment of skeletal dysplasia. *Adv. Endocrinol. Metab.* **2020**, *11*. [CrossRef] [PubMed]

© 2020 by the authors. Licensee MDPI, Basel, Switzerland. This article is an open access article distributed under the terms and conditions of the Creative Commons Attribution (CC BY) license (http://creativecommons.org/licenses/by/4.0/).

Chapter 11

Analysis of Aggrecan Glycanation by Western Blot in Cell Culture

Chiara Gramegna Tota, Alessandra Leone, Antonio Rossi, and Chiara Paganini

Abstract

Several experimental protocols are available to study the synthesis and secretion of proteoglycans in health and diseases, but there are few methods to analyse the intracellular processing of these macromolecules. We report a western blot analysis on medium and cell layer of primary chondrocyte culture to determine the glycanation status of aggrecan. Using a specific antibody against the aggrecan core protein and digesting an aliquot of sample with chondroitinase ABC, it is possible to analyse the whole aggrecan macromolecule and the core protein in order to evaluate defects in aggrecan glycanation.

Key words Aggrecan, Proteoglycan, Glycosaminoglycan, Western blot, Cell processing, Secretion, Chondrocyte

1 Introduction

Proteoglycans (PGs) are among the most abundant macromolecules of the extracellular matrix (ECM) in many tissues. They are composed of a core protein to which glycosaminoglycans (GAGs), linear polysaccharide chains, are attached. GAGs are constituted of repeated disaccharide units that can be sulphated, and they vary in size and composition [1]. PGs can bind many other ECM components forming a matrix network and interact with growth factors and cell surface receptors regulating cell behaviour [2]. Among different types of PGs, aggrecan is the major PG of cartilage, but it is also present in intervertebral disks and brain [2]. It represents the most glycanated PG since the aggrecan core is bound to over 100 GAGs, in particular chondroitin sulphate and keratan sulphate chains. In cartilage aggrecan is fundamental to confer load-bearing properties to the tissue forming a hydrated gel with hyaluronan and link proteins and attracting water [3, 4].

Nikos K. Karamanos (ed.), *Proteoglycans: Methods and Protocols*,
Methods in Molecular Biology, vol. 2619, https://doi.org/10.1007/978-1-0716-2946-8_11,
© The Author(s), under exclusive license to Springer Science+Business Media, LLC, part of Springer Nature 2023

The synthesis of PGs is a complex process composed of several steps. First, the core protein is synthetised by ribosomes of the endoplasmic reticulum. Then, the core protein moves to the Golgi apparatus where GAG chain synthesis and sulphation occur, and finally newly synthetised PGs are secreted in the extracellular space. Since PGs are fundamental in cartilage and bone development, alterations in their metabolism cause several skeletal dysplasias [5, 6].

Due to the important role of PGs in health and diseases, several experimental protocols are available to study the synthesis and secretion of PGs. The 1,9-dimethylmethylene blue or safranin O colorimetric assays allow the PG content measurement in tissues and in cell cultures [7, 8]. When few cells from patients or animal models are available, more sensitive methods using radioactive labelling with ^{35}S-sulphate could be used [9]. However, little is known about intracellular PG processing and their quality control.

Here we describe an innovative method to study the processing of aggrecan in cell cultures. The level of aggrecan glycanation is determined in medium and cell layer by western blot using an antibody against the aggrecan core protein. By analysing the sample without and with chondroitinase ABC digestion to remove GAGs, we can observe the aggrecan core protein (not glycanated form) or total aggrecan (glycanated and not glycanated forms), respectively. For this analysis an aggrecan antibody that binds only the core protein is mandatory. Thus, differences in the aggrecan glycanation process could be observed. The method has been set up in primary murine chondrocytes, but it could be extended to other cell types and cell lines.

2 Materials

Prepare all solutions using Milli-Q water and analytical grade reagents. Follow waste disposal regulations for all waste materials. Protect yourself wearing gloves and personal safety devices when necessary.

2.1 Cell Culture

1. Dulbecco's Modified Eagle Medium (DMEM): 13.5 g/L DMEM, 3.7 g/L sodium bicarbonate ($NaHCO_3$), 1× antibiotic solution (penicillin/streptomycin 100×) and 10% foetal bovine serum (FBS) heat inactivated. Weight 13.5 g DMEM and 3.7 g $NaHCO_3$ and transfer in a cylinder. Add water and dissolve powder. Make up to 900 mL and filter to sterilise the solution. Under the laminar flow hood, add 10 mL of sterile penicillin/streptomycin 100× solution and 100 mL FBS. Store at 4 °C.

2. 1× phosphate buffer saline (PBS): 137 mM NaCl, 2.7 mM KCl, 8.1 mM Na_2HPO_4, 1.5 mM KH_2PO_4, pH 7.4. Weight 8 g NaCl, 0.2 g KCl, 1.15 g Na_2HPO_4 and 0.2 g KH_2PO_4. Add water and dissolve the powder. Adjust the pH to 7.4 adding diluted phosphoric acid or NaOH and make up to 1 L. Filter to sterilise the solution and store at 4 °C.

2.2 Cell Layer and Medium Processing

1. RIPA buffer: 150 mM NaCl, 1% IGEPAL CA-630, 0.5% sodium deoxycholate, 0.1% sodium dodecyl sulphate (SDS), 50 mM Tris(hydroxymethyl)aminomethane hydrochloride (Tris-HCl), pH 8.00. Weight 0.30 g Tris-HCl, 0.44 g NaCl and 0.25 g sodium deoxycholate. Add water and dissolve the powders. Adjust the pH to 8.00 adding diluted HCl or NaOH. Then, add 0.5 mL IGEPAL CA-630 and 0.5 mL 10% SDS. Mix well and make up to 50 mL. Aliquot the solution in Eppendorf tubes and store at −20 °C.
2. Protein inhibitors 10×: 0.1 M benzamidine, 19.98 mM N-ethylmaleimide (NEM) and 40 mM ethylenediaminetetraacetic acid (EDTA). Weight 1.20 g benzamidine, 2.5 g NEM and 1.17 g EDTA and dissolve the powders in water. Make up to 100 mL and split the protein inhibitor solution in 10 mL aliquots. Store at −20 °C.
3. 0.2 M phenylmethylsulfonyl fluoride (PMSF) in 96% ethanol. Weight 0.70 g PMSF and add 96% ethanol. Dissolve the powder and make up to 20 mL. Store at −20 °C (*see* **Note 1**).
4. 0.1 M ammonium acetate pH 7.35. Weight 0.77 g ammonium acetate and add water. When the powder is dissolved, adjust the pH to 7.35 with diluted acetic acid or ammonia. Make up to 100 mL and store at −20 °C.
5. Pierce bicinchoninic acid (BCA) protein assay kit.
6. Amicon Ultra 0.5 mL centrifugal filter unit 10 K (Millipore) and Amicon Ultra 4 mL centrifugal filter unit 10 K (Millipore).
7. Chondroitinase ABC (AMSBIO) (*see* **Note 2**).
8. Sample buffer: 62.5 mM Tris-HCl, 2% SDS, 10% glycerol, 0.01% bromophenol blue and 5% β-mercaptoethanol, pH 6.8. Weight 5 mg bromophenol blue and add 6.25 mL Tris-HCl 0.5 M pH 6.8 and 10 mL 10% SDS. Dissolve the powder and add 5 g glycerol. Mix well and add 2.5 mL β-mercaptoethanol. Make up to 50 mL and aliquot in 1 mL Eppendorf tube; store at −20 °C.

2.3 Western Blot Analysis

1. 4–15% Mini-PROTEAN TGX Stain-Free Protein Gel.
2. Running Buffer 10×: 250 mM Tris-HCl, 1.92 M glycine and 1% SDS. Weight 15.14 g Tris-HCl, 72.07 g glycine and 5 g SDS. Add water and dissolve the powders. Make up to 500 mL and store at 4 °C.

3. Transfer buffer 10×: 200 mM Tris-HCl and 1.5 M glycine. Weight 12.11 g Tris-HCl and 56.30 g glycine. Add water and dissolve the powders. Make up to 500 mL and store at 4 °C (*see* **Note 3**).
4. Tris-buffered saline (TBS) 5×: 100 mM Tris-HCl and 2.5 M NaCl, pH 7.5. Weight 12.11 g Tris-HCl, 146.10 g NaCl and add water. When the powders are dissolved, adjust the pH to 7.5 with diluted HCl or NaOH. Make up to 1 L and store at 4 °C.
5. TBS 1×: 20 mM Tris-HCl and 500 mM NaCl, pH 7.5. Dilute TBS 5× by adding 800 mL water to 200 mL TBS 5×. Store at 4 °C.
6. TBS-T: 20 mM Tris-HCl, 500 mM NaCl and 0.1% Tween-20, pH 7.5. Add 0.5 mL Tween-20 to 500 mL TBS 1× (*see* **Note 4**). Store at 4 °C.
7. Blocking solution: 5% bovine serum albumin (BSA) and 0.05% Tween-20 in TBS 1×. Weight 2.5 g BSA and add TBS 1×. When the powder is dissolved, make up to 50 mL with TBS 1× and add 25 μL Tween-20 mixing vigorously. Store at 4 °C (*see* **Note 5**).
8. Polyvinylidene difluoride (PVDF) membrane.
9. Protein ladder Sharpmass VI.
10. Swift Membrane Stain.
11. Anti-aggrecan polyclonal antibody (Millipore).
12. Anti-actin monoclonal antibody.
13. Anti-rabbit IgG, HRP-linked antibody.
14. Anti-mouse IgG, HRP-linked antibody.

3 Methods

3.1 Cell Culture and Sample Harvest

1. Plate 1.5×10^6 cells in a 60 mm diameter petri dish in 5 mL of DMEM with 10% FBS and incubate at 37 °C in 5% CO_2.
2. After 48 h, wash the cells once with 4 mL PBS and once with 4 mL DMEM without FBS (*see* **Note 6**).
3. Incubate cells in 5 mL DMEM without FBS at 37 °C in 5% CO_2 for 24 h (*see* **Note 7**).
4. Harvest the medium in a 15 mL Falcon tube and centrifuge at 2000 rpm for 10 min (*see* **Note 8**).
5. Transfer the supernatant in a new tube and freeze immediately the medium at −20 °C.
6. Wash the cell layer twice with 5 mL PBS (*see* **Note 9**).
7. Scrape the cells in 1 mL PBS.

8. Harvest the cell solution in a 2 mL Eppendorf tube.
9. Wash the petri dish with 700 μL of PBS and transfer in the same tube of the cell solution.

3.2 Cell Layer Processing

1. Centrifuge the cell layer sample at 12,000×*g* for 5 min at 4 °C.
2. Remove the supernatant.
3. Resuspend the pellet in 100 μL RIPA buffer with protein inhibitors (*see* **Note 10**) and lyse the cells with three cycles of freezing and thawing (*see* **Note 11**).
4. Centrifuge the cell lysate at 12,000×*g* for 5 min at 4 °C.
5. Harvest the supernatant in a new tube (*see* **Note 12**).
6. Collect an aliquot of 10 μL to determine the protein content by the BCA protein assay (*see* **Note 13**).
7. Dilute the cell layer sample with 200 μL of 0.1 M ammonium acetate, pH 7.35, and load the samples on Amicon Ultra 0.5 mL centrifugal filter unit 10 K previously washed with water (*see* **Note 14**).
8. Centrifuge the sample in Amicon Ultra 0.5 mL unit at 9000×*g* for 5 min and discard the flow through.
9. Wash twice the Amicon Ultra 0.5 mL unit with 400 μL of 0.1 M ammonium acetate, pH 7.35, and centrifuge at 9000×*g* for 4 min each time discarding the flow through.
10. To recover the concentrated sample, remove the Amicon Ultra 0.5 mL filter device, place it upside down in a new collection tube and centrifuge at 10,000×*g* for 5 min.
11. Wash twice the filter unit with 200 μL of 0.1 M ammonium acetate, pH 7.35, and centrifuge each time the filter unit upside down at 10,000×*g* for 5 min in the same collection tube.
12. The cell layer sample with an approximate volume of 550 μL is lyophilised.

3.3 Medium Processing

1. Thaw the medium on ice.
2. Load 3 mL of medium sample on Amicon Ultra 4 mL centrifugal filter unit 10 K previously washed with water (*see* **Note 15**).
3. Centrifuge the Amicon Ultra 4 mL filter unit at 4200×*g* for about 11 min and discard the flow through.
4. Add the remaining 2 mL of medium sample on Amicon Ultra 4 mL filter unit and centrifuge the columns at 4200×*g* for about 10 min.
5. Discard the flow through.

6. Wash twice the Amicon Ultra 4 mL filter unit with 2 mL of 0.1 M ammonium acetate, pH 7.35, centrifuge at 4200×*g* for 10 min each time and discard the flow through.
7. Transfer the concentrated sample (approximately 250 μL) in a new Eppendorf tube.
8. Wash twice the filter membrane with 200 μL of 0.1 M ammonium acetate, pH 7.35, and recover the solution with a Pasteur pipette in the same tube of the medium sample.
9. The medium sample with an approximate volume of 650 μL is lyophilised.

3.4 Chondroitinase Digestion and Sample Preparation

1. Lyophilise cell layer and medium samples in order to concentrate proteins.
2. Resuspend the lyophilised samples (both the medium and the cell layer) in 400 μL of 0.1 M ammonium acetate, pH 7.35.
3. Divide each sample in two aliquots 200 μL each.
4. Digest one aliquot with chondroitinase ABC adding 40 mU of chondroitinase ABC in 45 μL of 0.1 M ammonium acetate, pH 7.35 (*see* **Note 16**).
5. The second aliquot is not digested with chondroitinase ABC; thus add 45 μL of 0.1 M ammonium acetate, pH 7.35.
6. Incubate both aliquots (with and without chondroitinase ABC) at 37 °C overnight (*see* **Note 17**).
7. After overnight incubation, lyophilise both aliquots.
8. Resuspend samples with 150 μL of sample buffer (*see* **Note 18**).
9. Denature all samples at 90 °C for 10 min.
10. Cool samples at room temperature, vortex and rapidly spin them (*see* **Note 19**).
11. Store samples at −20 °C until western blot analysis.

3.5 Western Blot Analysis

1. Load denatured samples on 4–15% acrylamide gel (*see* **Notes 20** and **21**).
2. Carry out electrophoresis in running buffer 1× (*see* **Note 22**) at 80 V at room temperature (*see* **Note 23**).
3. At the end of electrophoresis, turn off the power supply, recover the gel and equilibrate in transfer buffer 1× (*see* **Note 24**).
4. Activate the PVDF membrane in methanol for 10 s by constant shaking. Then, wash it twice in Milli-Q water and equilibrate in transfer buffer 1×.

5. Wet two foam pads and some pieces of Whatman N. 3 MM paper in transfer buffer 1×.
6. Assemble the gel-membrane sandwich laying a wet foam pad, two or three sheets of Whatman paper, the gel, the PVDF membrane, two or three sheets of Whatman paper and wet foam pad (*see* **Note 25**).
7. Place the gel-membrane sandwich in the blotting apparatus placing the gel side at the negative electrode of the apparatus. Fill the apparatus with transfer buffer 1×.
8. Transfer the proteins from the gel to the PVDF membrane at 100 V for 2 h at 4 °C (*see* **Note 26**).
9. After blotting rapidly rinse the membrane in TBS-T (*see* **Note 27**).
10. Incubate the membrane with the blocking solution at constant shaking for 2 h at room temperature (*see* **Note 28**).
11. Then, incubate the membrane with primary antibody against aggrecan core protein diluted 1:500 in blocking solution in constant shaking at 4 °C overnight (*see* **Note 29**).
12. Remove the antibody solution and wash the membrane three times, 5 min each, in TBS-T at constant shaking at room temperature.
13. Incubate the membrane with the secondary anti-rabbit antibody diluted 1:2000 in 5% milk in TBS at constant shaking at room temperature for 1 h (*see* **Note 29**).
14. Remove the antibody solution and wash the membrane five times, 5 min each, in TBS-T at constant shaking at room temperature.
15. Incubate the membrane with appropriate volume of ECL chemiluminescent reagent to develop the blot and get the image with an imaging system (i.e. ImageQuant LAS 4000) (Fig. 1).
16. Wash rapidly the membrane with TBS-T.
17. For cell layer samples, incubate the membrane with primary antibody against actin diluted 1:1000 in blocking solution in constant shaking at 4 °C overnight (*see* **Notes 29** and **30**).
18. Remove the antibody solution and wash the membrane three times, 5 min each, in TBS-T in constant shaking at room temperature.
19. Incubate the membrane with secondary anti-mouse antibody diluted 1:2000 in blocking solution in constant shaking at room temperature for 1 h (*see* **Note 29**).

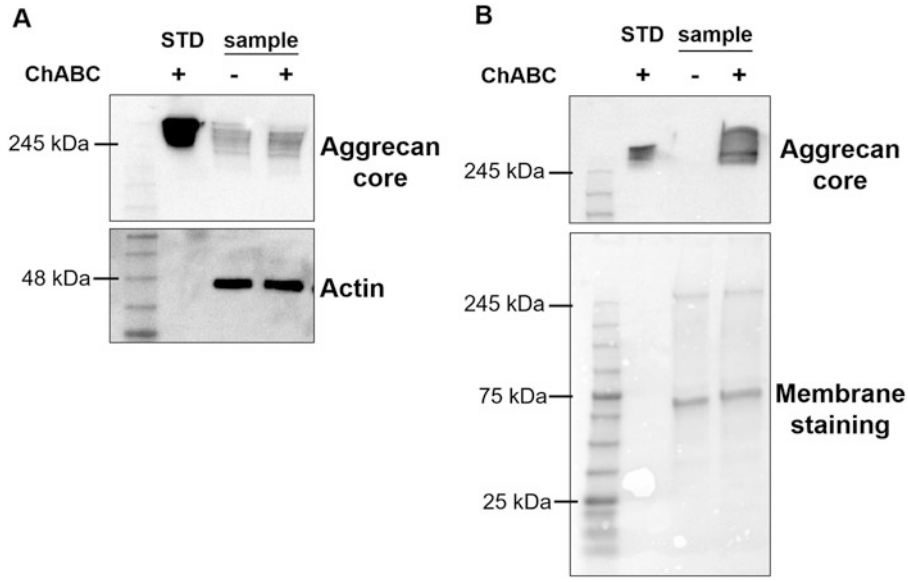

Fig. 1 Western blot analysis of aggrecan from murine chondrocytes. (**a**) The cell layer sample was divided in two aliquots to study the glycanated status of aggrecan. Using a specific antibody against the aggrecan core protein, a band of total aggrecan (glycanated form and core protein) is observed in the aliquot digested with chondroitinase ABC (ChABC), while in the not digested aliquot, the band represents only the core protein without any GAGs (non-glycanated form). Densitometric analysis of the two lanes (not digested and digested with ChABC) demonstrates that the bands show the same intensity. This data suggests that the aggrecan inside the cell is mainly present in the non-glycanated form (core protein) and, probably, once glycanated it is immediately secreted. The aggrecan band is normalised to the actin band. (**b**) The medium sample was divided in two aliquots to study the glycanated status of secreted aggrecan using a specific antibody against the core protein. In the aliquot digested with chondroitinase ABC (ChABC), a band is observed, while the not digested aliquot does not show any band. This result demonstrated that normal chondrocytes secrete in the medium only glycanated aggrecan and not the core protein since without chondroitinase digestion no aggrecan band is observed. Aggrecan band is normalised to membrane staining with Swift Membrane Stain. STD = cartilage aggrecan standard digested with chondroitinase ABC

20. Remove the antibody solution and wash the membrane five times, 5 min each, in TBS-T in constant shaking at room temperature.
21. Incubate the membrane with appropriate volume of ECL chemiluminescent reagent to develop the blot and get the image with an imaging system (i.e. ImageQuant LAS 4000) (Fig. 1).
22. Wash rapidly the membrane with TBS-T and store in TBS 1× at 4 °C for further experiments, if necessary.
23. Perform densitometric analysis by ImageJ software. In medium samples, the aggrecan band is normalised to total protein gel staining, while in cell layer samples, the aggrecan band is normalised to the actin band.

4 Notes

1. At −20 °C PMSF solution does not freeze, but PMSF precipitates. Before using it, thaw the PMSF solution at room temperature and be sure that it is completely dissolved. Vortex the solution to allow PMSF resuspension.
2. Chondroitinase ABC is lyophilised. The enzyme is resuspended in Milli-Q water and split in appropriate aliquots. The aliquots are immediately lyophilised and stored at −80 °C. This step is necessary because the enzyme is not stable if stored in solution.
3. When transfer buffer 10× is diluted to 1×, it is necessary to add methanol up to 20%. Thus, mix 100 mL transfer buffer 10×, 200 mL methanol and 700 mL water.
4. Tween-20 is a detergent with high viscosity. Thus, pay attention adding it to TBS and vigorously mix the solution to completely resuspend the detergent.
5. While BSA is dissolving, the volume of the solution could increase. Thus, add a small volume of TBS 1× to dissolve BSA powder and then make up to the final volume.
6. This step is necessary to remove all residual serum from the petri dish.
7. The incubation of cells in DMEM without FBS is necessary to remove all serum proteins from the medium sample to avoid western blot overloading.
8. Centrifugation is useful to remove all cell debris, if any, present in the medium before going on with the experiment. This step is important since the cell debris in the medium could clog the centrifugal filter unit.
9. The wash of the cell layer with PBS is necessary to remove all medium traces in order to avoid contamination between medium and cell layer.
10. Thaw an aliquot of RIPA buffer and add the protein inhibitors diluting the protein inhibitors 10× in order to reach a final concentration of 10 mM benzamidine, 1.998 mM NEM, 4 mM EDTA and 1 mM PMSF. For example, to prepare 1 mL RIPA buffer with protein inhibitors, add 100 μL protein inhibitors 10× and 5 μL 0.2 M PMSF to 900 μL RIPA buffer.
11. Freeze and thaw cycles lyse the cells. To make the freezing step faster, it is possible to use dry ice. Once the cell sample is thawed, it is vortexed and refrozen immediately.
12. At this step, if necessary, cell layer samples can be frozen at −20 °C, and it is possible to go on in the following days.

13. Collect 10 μL of cell layer and measure the protein content by BCA protein assay using bovine serum albumin (BSA) as standard in the working range 5–250 μg/mL.
14. Before use, Amicon Ultra 0.5 mL centrifugal filter units are washed with 400 μL of Milli-Q water and centrifuged at 9000×*g* for 4 min. Then the flow through is discarded.
15. Before use, Amicon Ultra 4 mL centrifugal filter units 10 K are washed with 2 mL of Milli-Q water and centrifuged at 4200×*g* for approximately 9 min. Then the flow through is discarded. It is important that the filter membrane stays wet. If the filter units are not used immediately, they can be stored in Milli-Q water to cover the filter membrane.
16. The digestion with chondroitinase ABC is necessary to remove the chondroitin/dermatan sulphate GAGs linked to the PG core protein. This step is necessary to unmask the epitope on the aggrecan core protein for the aggrecan antibody. In western blot analysis, the aggrecan band in samples digested with chondroitinase ABC points to total aggrecan, while the presence of an aggrecan core band in the aliquots that are not digested with chondroitinase ABC points to the not glycanated aggrecan (core protein without GAGs).
17. To examine if the chondroitinase ABC enzyme works properly, it is useful to check its activity. Two samples, negative and positive controls, are prepared. The positive control is made by 500 μL of 1 mg/mL chondroitin sulphate C, 455 μL of 0.1 M ammonium acetate, pH 7.35, and 45 μL chondroitinase ABC (40 mU) in 0.1 M ammonium acetate, pH 7.35. The negative control is made of 500 μL 1 mg/ml chondroitin sulphate C and 500 μL 0.1 M ammonium acetate, pH 7.35. The two samples are immediately read in a spectrophotometer. The absorbance is recorded at 232 nm. The rise of absorbance within few minutes in the positive control points out that the enzyme works properly and digests GAGs to disaccharides.
18. The volume of sample buffer used to resuspend cell layer samples is determined based on results from the BCA protein assay. The optimum protein concentration for western blot analysis is approximately 1 μg/μL. For medium samples the volume of sample buffer is fixed at 150 μL.
19. The centrifuge is necessary to mix the bubbles on the cap of tubes with whole sample.
20. Load the aliquot digested with chondroitinase ABC and the aliquot not digested in adjacent wells. Load 5 μL of protein ladder in the first well of the gel.
21. If possible, 20 μg of proteins are loaded for each sample in a maximum volume of 20–25 μL.

22. Running buffer 1× is obtained by diluting running buffer 10×. Add 100 mL of running buffer 10× to 900 mL of Milli-Q water and mix well.
23. The electrophoresis is performed until the dye front reaches the bottom of the gel. It takes approximately 2 h.
24. Transfer buffer 1× is obtained by diluting transfer buffer 10× and adding methanol. Thus, mix 100 mL of transfer buffer 10×, 200 mL of methanol and 700 mL of Milli-Q water. After blotting, the transfer buffer can be recovered and reused twice.
25. Once the sandwich is obtained, press with a serological pipette to remove all air bubbles present between the different sandwich layers. The presence of air bubbles between gel and PVDF membrane does not allow protein transfer and compromises the analysis.
26. To maintain 4 °C during transfer, the blotting apparatus is dipped in an ice tray.
27. The coloured protein ladder on membrane points to correct protein transfer from the gel to the membrane.
28. For medium samples it is necessary to perform a membrane staining by Swift Membrane Stain following the manufacturer's instructions to reveal total proteins and use them for normalisation. This step is performed before blocking the membrane with blocking solution.
29. It is necessary to optimise the antibody dilutions for all specific antibodies.
30. The actin is used in cell layer samples as housekeeping protein for normalisation.

References

1. Vynios DH (2014) Metabolism of cartilage proteoglycans in health and disease. Biomed Res Int 2014:452315
2. Theocharis AD, Skandalis SS, Gialeli C et al (2016) Extracellular matrix structure. Adv Drug Deliv Rev 97:4–27
3. Kiani C, Chen L, Wu YJ et al (2002) Structure and function of aggrecan. Cell Res 12:19–32
4. Sivan SS, Wachtel E, Roughley P (2014) Structure, function, aging and turnover of aggrecan in the intervertebral disc. Biochim Biophys Acta 1840:3181–3189
5. Paganini C, Costantini R, Superti-Furga A et al (2019) Bone and connective tissue disorders caused by defects in glycosaminoglycan biosynthesis: a panoramic view. FEBS J 286:3008–3032
6. Dubail J, Cormier-Daire V (2021) Chondrodysplasias with multiple dislocations caused by defects in glycosaminoglycan synthesis. Front Genet 12:12
7. Farndale RW, Buttle DJ, Barrett AJ (1986) Improved quantitation and discrimination of sulphated glycosaminoglycans by use of dimethylmethylene blue. Biochim Biophys Acta 883:173–177
8. Carrino DA, Arias JL, Caplan AI (1991) A spectrophotometric modification of a sensitive densitometric safranin O assay for glycosaminoglycans. Biochem Int 24:485–495
9. Paganini C, Costantini R, Rossi A (2019) Analysis of proteoglycan synthesis and secretion in cell culture systems. Methods Mol Biol 1952: 71–80